

DIRECT LIQUEFACTION: WHERE WE STAND
AND WHERE WE ARE SUPPOSED TO GO - AN OVERVIEW

Eneo C. Moroni
U.S. Department of Energy
FE-231 GTN
Washington, D.C. 20545

Keywords: Coal, Liquefaction, Program Planning/Coordination.

INTRODUCTION

The U.S. Department of Energy (DOE) precommercial activities in the 1970's and early 1980's established the commercial viability of direct coal liquefaction from a technical point of view. In the early 1980's, the direct liquefaction program was reoriented toward longer range process research and development activities with the objective of developing improved, lower cost technology. The DOE development program since then has made substantial and significant improvements in the process technology. Liquid yields have been improved by over 30 percent. On a balanced commercial plant basis, this translates to a production of about 3.3 barrels of liquids per ton of coal for the improved technology compared to 2.5 barrels for the technologies developed in the 1970's. The quality of the coal-derived distillates produced by the current technology has been substantially improved, but at the expenses of increased consumption of the upgrading catalyst. As a result, the currently produced liquids are of much higher quality than petroleum crudes in general. Other technology improvements include less severe operating conditions which favorably impact construction costs, operability and maintenance; and improved product slate flexibility, which allows greater freedom in producing products for specific market applications.

As a consequence of these improvements in technology, substantial cost reduction has been achieved. Current two-stage technology demonstrated at the Wilsonville, Alabama proof-of-concept (POC) facility gave estimated product costs at about \$38-40 per barrel. Because of improved quality, these products would be competitive with crude oil at about \$33-35 per barrel.

Supporting and exploratory research made critical contributions in some area of process development, e.g. by providing process analysis data leading to improved process operation and performance. F. Burke and coworkers at the Consolidation Coal R&D Division have done an excellent analytical and process evaluation work in this area. Similarly, D. Gray and the MITRE Corporation team provided valuable process economic information for comparative processes evaluation. To be noted, both activities are crosscutting in that they contribute to all DOE-supported processes under development. In addition, both supporting activities, through many years of experience and close cooperation between them and with the contractors working in process development, have reached a high degree of sophistication in various aspects of process evaluation so that, presently, they are capable of offering valuable research

guidance for the evaluation of novel research activities in coal liquefaction.

For more than a decade DOE has encouraged the generation of an extensive analytical and economic data bank on coal liquefaction processes and on related research activities, with the specific provision that the data and the ensuing process evaluation would be developed by competent sources independently from the actual process developers and from individual researchers. Presently, we continue to pursue this endeavor by expanding the "teaming arrangement" promoted by Consolidation Coal and MITRE, and to support a similar "teaming" effort by A. Davis at Penn State University to establish an analytical data bank in support of the determination of the mechanisms and the kinetics of the rapid changes occurring in dispersed catalyst composition during the initial stages of liquefaction.

Consequently, we appear on the way to being prepared organizationally for the challenge presented to us in integrating into the current processing schemes the discoveries of present and future research and development studies.

PROGRAM OBJECTIVES/DIRECTION

In line with the current environmental and energy shortage concerns and with the effort to sustain coal as a viable option in competition with other energy sources, the main objective of the DOE's direct coal liquefaction current program is to develop the technology for the production of specification liquid fuels at a cost competitive with crude oil, within the next 5 to 7 years.

More specifically, the program calls for a proof-of concept demonstration, by 1997, of a system capable of producing liquid fuels from coal which complies with environmental requirements at cost of less than \$30 per barrel of oil equivalent and with lower greenhouse gas emissions than those from 1980 state-of-the-art coal liquefaction technology, or comparable to petroleum-based systems, and are suitable to be blended with petroleum stocks to produce and, perhaps, enhance the quality of reformulated gasoline, jet fuel and other high quality liquid transportation fuels.

The key issue is the integration of coal-derived liquids into existing petroleum refining systems which would require no major modifications to the fuel distribution and storage infrastructure which currently exists.

In the evaluation and planning of present and future research and development activities, we need to provide answers to two important questions: How should the present activities in the fundamental and applied research at the university and national laboratory level be changed in order that the remaining scientific and technical challenges can be addressed? And, what are the most important feedback information that the process developers and process evaluation teams can provide to the scientific community in order to evidence the most compelling research and development needs to

overcome the current challenges and provide a better understanding of the reactions involved in coal liquefaction?

The first step is the recognition that all of the knowledge in this field does not and cannot reside in a single discipline. We need to support in a substantive way a policy of multi-disciplinary research teamwork and to further encourage cooperative efforts between the fundamental and applied research and bench scale development of integrated process activities.

The excellent study done by a panel group on research needs assessment for coal liquefaction (COLIRN), headed by H.D. Schindler, and sponsored by the DOE Office of Energy Research, Office of Program Analysis, resulted in a publication which provided important recommendations to be implemented by the fundamental and applied researchers in this field. The recommendations were reviewed and approved by the representatives of DOE Office of Fossil Energy, with some reservations about the usefulness of chemical pretreatments in the overall liquefaction processing scheme and the use of novel catalysts prior to gain a better understanding of the mechanism and the kinetics involved in the initial stages of coal liquefaction.

We agree with the conclusion of the COLIRN panel which has challenged the conventional view of the chemistry and the mechanisms of direct liquefaction--that the initial reactions of liquefaction involve thermal homolytic bond cleavage with stabilization of the free radicals formed-- and is being replaced by the recent work on a deeper understanding of bond-breaking and bond-forming processes via hydrogen transfer. This new model of coal depolymerization may explain the cleavage of bonds which are too strong to be broken thermally at liquefaction conditions.

The COLIRN panel agreed that these new understandings of structure and mechanisms are expected to lead to more efficient liquefaction processes, which, eventually, need to be developed before coal liquefaction can be commercialized.

In particular, the panel placed the highest priority on identifying the coal structures responsible for retrograde reactions and the reaction mechanisms and kinetics of these reactions. The panel also placed high priority on developing a coal structure-reactivity relationship, develop kinetic models of liquefaction, and develop intrinsic quantitative rate expressions as a basis for understanding initial reaction paths during coal dissolution.

Among the remaining recommendations the panel scored lower priority for the study on catalytic hydrogenation and cracking functions mechanism to establish their interaction and to determine the effects of thermal reaction on these functions. However, current data from the Wilsonville POC unit indicate that the thermal/catalytic staged liquefaction mode gives substantially higher coal conversion than the catalytic/thermal mode, and this fact is mistifying process evaluators and, as a consequence, a better understanding of the contribution and of the reaction

mechanisms attributed to the thermal and catalytic functions would certainly require a much higher research priority because it is quite evident that our knowledge in this important area is indeed insufficient.

CONCLUSIVE REMARKS

The current advanced research program needs to be reoriented to follow more closely the recommendations of the COLIRN panel and the direction suggested by the process development program, which require a clearer understanding of the initial reaction paths, particularly the reactions involved in the preconversion step and those of the attendant catalyst deactivation mechanism. The acquisition of this knowledge should lead to substantially more efficient liquefaction processes.

According to J. Larsen³ there are three areas which are crucial to our state of knowledge in coal processing: coal structure, coal as reaction environment, and which reactions are actually occurring in coals.

We agree with J. Larsen that our knowledge in all three areas is sufficiently uncertain to make extrapolation from routine model compound studies to coals quite unreliable. And we need to add that similar extrapolation unreliabilities exist for the current catalyst studies and applications, solvent extraction, alkylation, pyrolysis, chemical pretreatment, water supported reactions and many other approaches fashionable in past and present advanced research activities because they suffer from the same lack of fundamental knowledge of coal structure, reaction mechanisms and kinetics to make them viable for further scaleup consideration.

The process development activities is also at crucial turning point because we are finding that coal derived materials, such as resids and the quality of the solvent, which are used in the recycle stream, exhibit larger beneficial effects in coal liquefaction than the comparison of novel catalyst formulation versus existing commercial catalysts.

Consequently, the commitment of DOE to develop the technology for the production of specification liquid fuels from coal, at a cost competitive with crude oil, within the next 5 to 7 years, will require a reorientation of the advanced research program, increases in both scope and pace of the fundamental and applied research effort, perhaps by teaming arrangements with the process development and process evaluation programs, to produce a timely resolution of the technical issues in order to meet the requirements dictated by the current and perhaps more restrictive future environmental and economic constrains for coal derived liquid fuels.

If a strong and clear message should be given to the participants of this "Symposium on Coal Reaction Mechanism", from the content of this brief overview, it would sound like a mimic of the famous message contained in the inaugural address of the late president of the U.S., J.F. Kennedy:

"Ask not what you can do for coal processing",
"Ask, first, what coal structure/reactions can do for you".

REFERENCES

- (1) Coal Liquefaction. A Research Needs Assessment. February 1989. Prepared for U.S. Dept. of Energy, Office of Energy Research, Office of Program Analysis, Contract DE-AC01-87ER30110.
- (2) Unpublished current work at the Wilsonville POC unit.
- (3) Larsen, J. W., Am.Chem.Soc., Div.Fuel Chem. Preprints, 1990, 35(2), 376.

LIQUEFACTION PATHWAYS OF U.S. COALS

Robert A. Keogh and Burtron H. Davis
Center for Applied Energy Research
University of Kentucky
3572 Iron Works Pike
Lexington, KY 40511

Keywords: coal liquefaction, thermal and catalytic pathways

ABSTRACT

The solubility classes obtained from the thermal liquefaction of 69 high volatile bituminous U.S. coals using a single residence time and three reaction temperatures were combined into the following lumped parameters for examination of the data: (a) oils plus gases, (b) asphaltenes plus preasphaltenes, and (c) IOM (insoluble organic matter). The lumped parameters were plotted on a Wei-Prater diagram and the resulting graph suggested a common liquefaction pathway for these coals. The thermal pathway was verified using a single Western Kentucky #6 coal and a number of residence times and reaction temperatures. The utilization of a number of catalysts and solvents with different hydrogen donor abilities did not change the pathway observed thermally. The effect of coal rank was studied using a Wyodak subbituminous coal. The thermal pathway defined by the liquefaction of the Wyodak coal was substantially different from the pathway defined by the bituminous coals. Addition of a catalyst did not alter the observed pathway defined thermally for this coal.

INTRODUCTION

Historically, lumped parameter kinetic models have been used successfully to describe industrially significant complex processes such as catalytic cracking¹, catalytic reforming¹, addition polymerization², and condensation polymerization³. Not surprisingly, the same approach has been used in the description of the various liquefaction processes^{4,5}. A physically realistic and technically viable lumped parameter kinetic model for liquefaction would be of considerable value in the development of pathways, mechanisms and the scale-up of liquefaction processes.

In this work, the typical solubility classes obtained from the liquefaction products were lumped into the following parameters: (a) oils plus gases (O+G), (b) asphaltenes plus preasphaltenes (A+P), and (c) IOM (insoluble organic matter). The three lumped parameters were plotted on a Wei-Prater diagram (triangle graph) for interpretation. The resulting data suggested a common thermal liquefaction pathway. The effects of catalyst, solvent quality and coal rank are discussed.

EXPERIMENTAL

The description and range of values of the key coal properties of the 69 high volatile bituminous coals used in the initial work are given in Table 1. It should be noted that all of these coals have ≥ 80 vol. % vitrinite (dmmf) concentrations. The analyses of the three coals (W.Ky. #6, W.Ky. #9 and Wyodak) which were extensively studied are given in Table 2.

All of the liquefaction experiments were performed in 50 mL batch microautoclaves using a hydrogen atmosphere. Details of the liquefaction procedure and solubility class analysis of the products are given in detail elsewhere⁶.

The quantity of catalyst added to the 5g of dry coal were as follows: (a) Shell 324 (1g), (b) molybdenum naphthenate (1g), (c) Fe_2O_3 (.1g), (d) $\text{Fe}_2\text{O}_3 \cdot \text{SO}_4$ (.1g), (e) $\text{SnCl}_2 \cdot 2\text{H}_2\text{O}$ (.25g), and (f) ZnCl_2 (.25g). All of the catalysts, with the exception of Shell 324, were sulfided in-situ by adding twice the stoichiometric amount of dimethyldisulfide required to sulfide the metal to the reactor. The Shell 324 catalyst was presulfided with dimethyldisulfide prior to the addition of coal and liquefaction solvent.

RESULTS AND DISCUSSION

The thermal liquefaction data obtained for the 69 high volatile bituminous coals using a 15 minute residence time and three reaction temperatures (385°C, 427°C, 445°C) are shown in Figure 1. The data suggest a common liquefaction pathway for these coals. A single bituminous coal (W.Ky. #6) was selected to verify the suggested pathway. Liquefaction conditions were selected to produce a series of conversion levels which would define the pathway of the coal from a minimum conversion level to a maximum conversion level. The results of these experiments are shown in Figure 2.

As can be seen in Figure 2, the thermal pathway of the Western Kentucky #6 coal over the entire range of conversions is identical to that suggested in Figure 1 for the diverse set of coals. In the initial stage of dissolution, the primary reaction is the conversion of coal (IOM) to the A+P intermediate. In this region of the pathway, the conversions show a positive linear correlation with the A+P yields. It is also observed in this region of the pathway that the O+G yields remain relatively constant. The pathway changes in the region of maximum conversion (and A+P yield). In this section of the pathway, the primary reaction taking place is in the conversion of the intermediate, A+P, to the final product O+G. During this stage of the liquefaction pathway, conversion remains relatively constant. At the highest reaction temperature (445°C) and long residence times (> 15 min.), the pathway appears to change. In this region, conversion, A+P and O+G yields concurrently decrease, indicating the possibility that retrograde reactions are predominant. The results of these experiments suggest that the high volatile bituminous coals studied in this work have a common thermal liquefaction pathway.

The liquefaction pathway defined by these coals indicates that a maximum in the intermediate yields (A+P) must be achieved prior to an increase in the O+G yields. It is desirable to alter the pathway in such a manner that the O+G yields increases with increase in coal conversion. A number of catalysts were studied to determine if the added catalyst effect the selectivity defined by these reactions and thus change the pathway. The catalytic pathway is compared to the thermal pathway using the Western Kentucky #6 coal and two iron based catalysts in Figure 3. As can be seen, the addition of these catalysts had no effect on the observed thermal pathway. Identical experiments employing a supported catalyst (Shell 324), an oil soluble catalyst precursor (molybdenum naphthenate) and two acid catalysts (ZnCl_2 and $\text{SnCl}_2 \cdot 2\text{H}_2\text{O}$) also produced the same pathway that was observed for the thermal experiments. Therefore, the effect of catalyst addition is to increase the rate of production of the intermediate, A+P. The addition of catalysts has no effect on the selectivity defined by the solubility classes.

The effectiveness of a catalyst may be influenced by the quality of the liquefaction solvent. To determine the effect of solvent quality, as measured by hydrogen donor ability, a series of experiments (catalytic and thermal) were conducted using a Western Kentucky #9 coal and a donor (tetralin) and a non-donor (1-methylnaphthalene). The results of these experiments are shown in Figure 4. As can be seen, these data show that no change was observed in the liquefaction pathway. Additional experiments which used a mixture of phenanthrene and hydrogenated phenanthrenes as the liquefaction solvent defined the same pathway described above.

The next task in this investigation was to determine if the catalytic and thermal pathways of low rank coals were the same as that defined by the high volatile bituminous coals. A Wyodak subbituminous coal was chosen for the initial thermal and catalytic (Fe_2O_3 , molybdenum naphthenate) experiments. The pathways obtained from the liquefaction of the Wyodak coal are shown in Figure 5. Clearly, the thermal and catalytic pathway are also identical for this coal. However, the pathway for the subbituminous coal is substantially different from the pathway defined by the bituminous coals. Similar to the pathway of the bituminous coal, there are two regions in the pathway of the subbituminous coal. During the initial coal dissolution stage, both the A+P and O+G yield increase with increasing coal conversion. The second region of this pathway is similar to that of the bituminous coal. Here the coal conversion increases minimally and the major reaction is the conversion of A+P to O+G. On the basis of these solubility class data, the subbituminous coal has an improved catalytic and thermal pathway when compared to that of the bituminous coals studied due to the concurrent increase in O+G yields with coal conversion.

CONCLUSIONS

The utilization of lumped solubility class parameters and the Wei-Prater diagram have shown that the bituminous coals studied have a common thermal liquefaction pathway. Attempts to change the observed pathway using a number of catalysts and liquefaction solvents were not successful. The role of the catalyst in this work is to increase the rates of the defined reactions. The catalyst provided no selectivity to the production of the final products, O+G.

The pathway defined by a subbituminous Wyodak coal was substantially different from the pathway of the bituminous coals. The major difference was the parallel increase in A+P and O+G yields with the increase in coal conversion. Similar to the bituminous coal data, addition of catalysts had no effect on the Wyodak thermally defined pathway.

ACKNOWLEDGMENT

This work was supported by the Commonwealth of Kentucky and DOE contract no. DE-FC88PC8806 as part of the Consortium for Fossil Fuel Liquefaction Science (administered by the University of Kentucky).

REFERENCES

1. Weekman, V. W., *AIChE Monograph Series*, No. 11, Vol. 75, 1979.
2. Platzler, N., *Ind. & Eng. Chem.*, 62 (1), 1970.

3. Flory, P. J., "Principles of Polymer Chemistry", Cornell University Press, New York, NY, 1953.
4. Weller, S., Pelipetz, M. G., and Friedman, S., *Ind. Eng. Chem.*, **43** (7), (1951) 1575.
5. Cronauer, D. C., Shah, Y.T., and Ruberto, R.G., *Ind. Eng. Chem., Process Des. Div.*, **17**, (1978) 281.
6. Keogh, R. A., Chawla, B., Tsai, K. J., and Davis, B. H., *Preprints, Div. Fuel Chem., Am. Chem. Soc.*, **33** (3), (1988).
7. Derbyshire, F. J., *Energy and Fuels*, **3** (3), (1989).

Table 1

Make-up of Sample Set and Range of Key Properties

A. Distribution of Samples by State:

Kentucky	36
Indiana	22
Ohio	10
West Virginia	1

B. Distribution by ASTM Rank Classification:

High volatile bituminous A, B, C

C. Ranges of Key Properties

	Wt.% V.M.(daf)	Wt.% C(daf)	Wt.% Total S.(daf)	Wt.% Org.S.(daf)	Wt.% Pyr.S.(daf)	Vol.% Vitrinite(dmmf)	R _o max
Minimum	34.27	76.04	.70	.55	.03	80.06	.388
Maximum	48.34	86.48	13.78	4.72	8.87	92.70	.984
Mean	43.15	80.67	4.15	2.25	1.70	86.78	.606

Table 2

Coal Analyses

	W.Ky. #6	W.Ky. #9	Wyodak
<u>Ultimate (wt.%, daf)</u>			
Carbon	82.87	76.80	71.02
Hydrogen	5.42	5.41	5.42
Nitrogen	1.72	1.90	1.37
Sulfur	5.15	8.41	1.00
Oxygen ¹	4.84	7.40	21.29
Reflectance (R _o max)	.77	.54	----

1 By difference

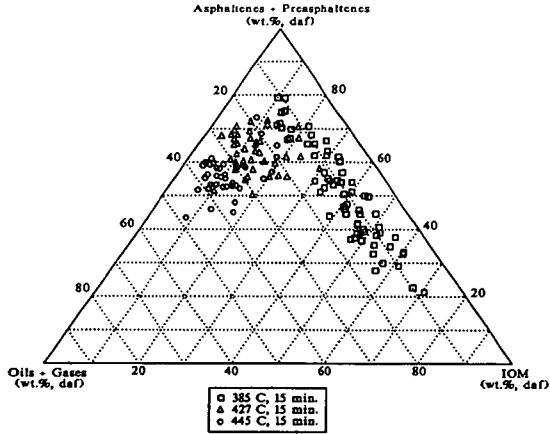


Figure 1. Solubility class distributions of 69 U.S. bituminous Coals

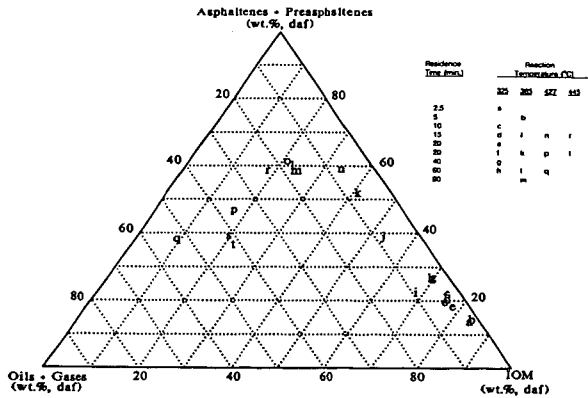


Figure 2. Thermal liquefaction pathway of a W.Ky.#6 bituminous coal.

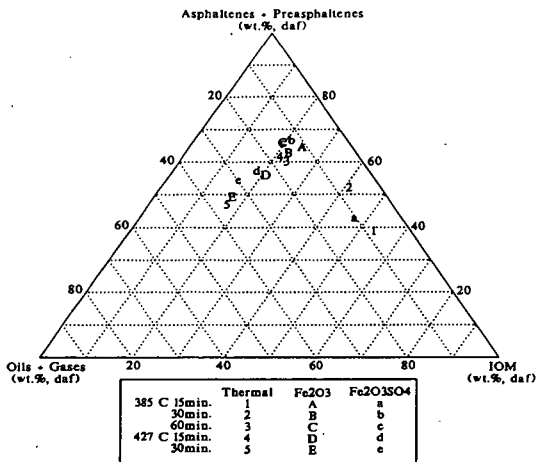


Figure 3. Catalytic pathway of a W.K.v. #6 bituminous coal.

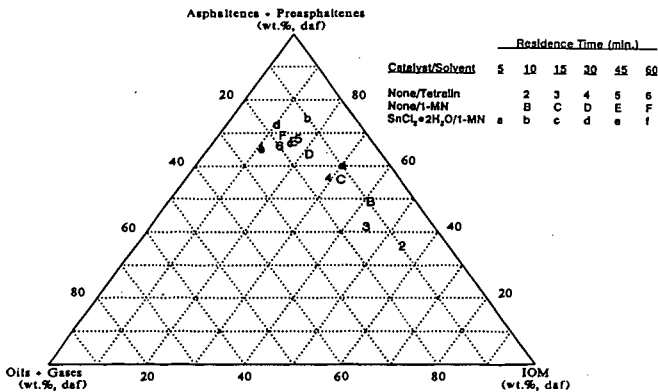


Figure 4. The effect of solvent quality on the pathway of a W.K.v. #9 coal.

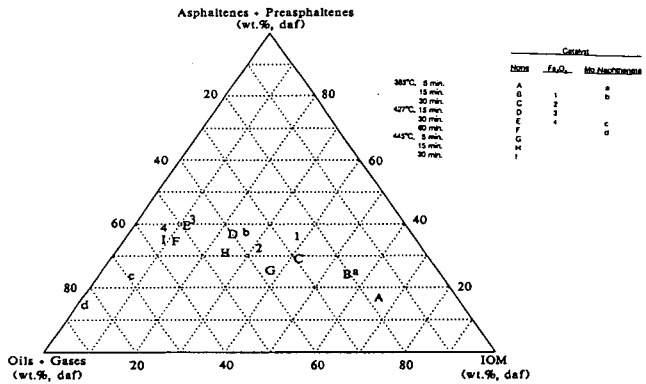


Figure 5. Thermal and catalytic pathway of a Wyodak subbituminous coal.

MICROSCOPIC EVIDENCE OF COMPETING HYDROGENATION AND
CONDENSATION REACTIONS DURING COAL LIQUEFACTION

Alan Davis, G.D. Mitchell, F.J. Derbyshire¹, H.H. Schobert, and Rui Lin²

Energy and Fuels Research Center
Penn State University
University Park, PA 16802

¹University of Kentucky, KY, USA
²UNOCAL Corp., CA, USA

Keywords: liquefaction, residue microscopy, catalysis

INTRODUCTION

Reflectance characteristics of vitrinite-derived residues from coal liquefaction provide a measure of the response of coals to reaction conditions (1-3). The presence of a low-reflecting primary vitroplast (4,5), an isotropic pitch-like material formed by simple melting of vitrinite, indicates that depolymerization reactions were incomplete. Low-reflecting secondary vitroplast (5), formed by precipitation from the solubilized products, suggests that the coal had been at least partially hydrogenated. High-reflecting vitroplast or vitrinite residue indicates that condensation reactions had predominated. The presence together of the last two of these residue types indicates that hydrogenation and condensation have been locally competing reactions following thermolysis.

This paper discusses the use of residue microscopy in evaluating the influence of a dispersed molybdenum catalyst, of reactor atmosphere, of a pretreatment stage and of coal rank in bench-scale liquefaction experiments.

EXPERIMENTAL

The four coals used in this study (1ig, subB, hvC and hvA bituminous) were obtained from the Penn State Coal Sample Bank. Some of their relevant properties are listed in Table 1.

Hydrogenation reactions were performed, mostly without a solvent vehicle (i.e., dry), in batch stainless-steel tube reactors (approx. 25 cm³ capacity) (6, 7). Approximately 5 g of coal (-60 mesh U.S. sieve size) were charged to the reactor for the dry runs. For hydrogenations conducted with added solvent, 2.5 g of coal and 5 g of solvent were used. If catalyst was present (as 1% sulfided Mo on dmmf coal), a stoichiometric amount of CS₂ was added to ensure that enough available sulfur was present to convert the metal to its sulfide form. The assumption was made that ammonium tetrathiomolybdate (ATM) would convert entirely to MoS₂. The procedure employed for preparing the ATM and dispersing it on the coal, and reference to the metastability of this catalyst precursor are described elsewhere (8, 9).

The loaded reactor was purged of air with nitrogen and then purged three times with the desired gas (hydrogen or nitrogen) before finally being pressurized

to 7 MPa cold pressure. The reactor contents were agitated vertically through 2.5 cm at about 200 cycles per minute by an electrically driven cam system while the reactor was immersed in a preheated, fluidized sandbath. After reaction for the desired time, the reactor was removed from the sandbath and quenched to room temperature by immersion in cold water. First-stage reactions were conducted at 275°C, and the second stage at 425°C, both for 30 min.

In between the steps of the temperature-staged liquefaction experiments, the reactor was quenched and the gaseous products vented. The reactor was then repressurized with 7 MPa hydrogen and reaction was continued at the higher temperature. This procedure was adopted to circumvent the possibility of limiting the hydrogen partial pressure.

Liquefaction experiments were done in duplicate. The products of one of the reactors were used for microscopy. The second reactor was vented and the remaining liquefaction products washed out and extracted with tetrahydrofuran (THF) to determine percent conversion.

RESULTS AND DISCUSSION

Non-Catalytic Reactions

Preceding a coal liquefaction reaction with a low-temperature pretreatment stage has been shown to have a profound effect on conversion and product selectivity, particularly where catalysts are employed in the reaction (1). Consequently, some detailed microscopy was performed on residues that represent pretreatment conditions alone. Three of the coals which had been reacted at 275°C (PSOC-1482, 1401 and 1504) under different atmospheres were evaluated to determine whether there had been any discernible changes in the structure of the reacted coal.

Following pretreatment (first stage) conditions the lignite and subbituminous coals showed almost no microscopic evidence of change in the coal structure other than some separation of coal particles along bedding planes. It is important to note that the vitrinite/huminite macerals showed no rims of low reflectance that would signify that hydrogenation has proceeded via a shell progressive mechanism. Also, there was no evidence of maceral devolatilization or the onset of fluidity that would help to explain the improved conversion and product selectivity that occurs when a low-temperature pretreatment is employed prior to reaction under full liquefaction conditions. Maximum reflectance values were measured for a selection of residues from pretreated coals and are presented in Figure 1. Compared to the reflectance of the feed coal, little change was observed following pretreatment. Only in the case of the subbituminous coal was there a significant increase. These general relationships are consistent whether a hydrogen or a nitrogen atmosphere was employed during the reaction (Table 2).

The same similarity between reflectances of residues from runs in nitrogen and hydrogen was found for the higher temperature and temperature-staged experiments (Table 2). This is somewhat surprising given the fact that the best conversion was observed for the temperature-staged reaction of the bituminous coal in a hydrogen environment. These observations suggest that the reflectance

increase of vitrinite-derived residual material from runs made in the absence of a solvent may be more related to the maximum temperature employed in the reaction than to the reactant gas.

Major changes in the appearance and optical properties of residues were observed following the high-temperature (425°C) and temperature-staged reactions. For the most part the liptinite macerals had been converted and were no longer present in the residues. Huminite/vitrinite remnants and vitroplast were the predominant components found in residues of the lignite (PSOC-1482) and subbituminous (PSOC-1401) coals, whereas vitroplast was the dominant component found in residues from the hvCb (PSOC-1498) and hvAb (PSOC-1504) coals. The maximum reflectances of these residue components were greatly increased over those of the original coal. Fig. 1 compares the trends in reflectance for the different hydrogenation conditions and coals used during this project. For lower coal ranks, temperature-staged residues have a higher reflectance than the single-stage high-temperature liquefaction residues. Reflectance is lower for temperature-staged compared to high-temperature reactions for the hvC and A bituminous coals. If higher reflectance is indicative of a greater degree of molecular condensation, then these data suggest that the lower rank coals have a greater tendency to condense under temperature-staged, dry, non-catalytic liquefaction than the conventional high-temperature liquefaction. The reversal of this tendency, and therefore a lower degree of molecular condensation under temperature-staged conditions, is seen in the residues from the higher rank coals. Finally, the reflectance values measured for both the temperature-staged and high-temperature residues of PSOC-1498 are somewhat low compared to the other coals (Fig. 1). We suspect that the maximum temperature (425°C) used for liquefaction of this hvCb coal may be too low to be optimal. Conversion yield for this coal (PSOC-1498) also supports this conclusion, averaging 21% compared to 34% conversion for the other coals.

Analysis of Extracted Residues to Determine Effects of Molybdenum Sulfide Catalyst

The general relationship in the reflectance of vitrinite-derived residues between non-catalytic and catalytic (1% Mo) temperature-staged hydrogenation experiments is provided in Fig. 2. This figure shows that the residual materials from the catalytic runs generally have higher reflectances than those from non-catalytic runs. The higher volumetric conversion of each coal in the presence of the molybdenum catalyst means that there is much less of the original coal material remaining; therefore, the residues will be of higher molecular weight and more highly condensed than from runs which achieve significantly lower levels of conversion. Another possible contribution to the higher reflectances would result from the catalyst promoting dehydrogenation reactions.

The significance of the foregoing is that a reflectance measurement made on residual material, considered in isolation from all pertinent information, may not be a good indication of the conversion of coal to a soluble product. In particular, low molecular weight products generated as a result of efficient hydrogenation are presumed to have had a relatively low reflectance; however, these materials will have dissolved in the solvent (THF) used to separate the soluble products from the insoluble residues. Because of this problem, a series of experiments was undertaken specifically to study the reflectance distribution

of the whole products (without extraction), as well as the insoluble residues of catalytic and non-catalytic temperature-staged hydrogenation. The results, are summarized in the section entitled "Analyses of Whole Products".

Reflectance analyses also were performed on just the THF-insoluble residues of dry catalytic and non-catalytic, single- and two-staged liquefaction of the subbituminous coal (PSOC-1401) reacted under N_2 and H_2 atmospheres and a combination of the two gases. This series of runs has enabled the influence of atmosphere, catalyst and pretreatment to be evaluated. Table 3 shows that, for both catalytic and non-catalytic runs, vitrinite reflectance values of the residues of pretreatment are low whether generated in a nitrogen or a hydrogen atmosphere. The influence of atmosphere and catalyst becomes more evident as a result of high-temperature and temperature-staged reactions (425°C). The vitrinite was subject to significant changes as shown by a large increase in maximum reflectance and by the qualitative descriptions provided in Table 3. In this table, "reacted" vitrinite (or vitroplast) refers to those vitrinite particles which had undergone thermoplastic deformation and might have developed a granular anisotropy; "unreacted" vitrinite refers to those showing no evidence of the thermoplasticity, for the most part retaining their original morphology.

In the presence of the molybdenum catalyst and hydrogen atmosphere, most of the vitrinite particles became plastic in the reactor and were partially subject to condensation leading to the development of a granular anisotropy. In comparison, the other three high-temperature residues processed in a nitrogen atmosphere are composed mainly of "unreacted" vitrinite particles. This demonstrates that the presence of a catalyst and hydrogen gas play an important role in promoting vitrinite reactivity during liquefaction of the subbituminous coal. Although the "unreacted" vitrinite particles may possess a lower reflectance than the "reacted" particles, the latter were associated with a higher volumetric conversion.

During the temperature-staged reactions (275°C + 425°C), the effect of the first stage is negligible when a nitrogen atmosphere was used during the second stage. It was found, for residues of reactions at 425°C, N_2 ; 275°C, N_2 + 425°C, N_2 ; and 275°C, H_2 + 425°C, N_2 , that the reflectance values were very similar for residues of the catalytic runs and again for those from the non-catalytic runs (Table 3). This suggests that first-stage reactions did not play an important role in liquefaction if an inert atmosphere was used in the second stage. This is further supported by the conversion data for these groups of three reactions (Table 3).

The impact of first-stage reaction became important when a hydrogen atmosphere was employed. In all residues after two-stage reactions with a hydrogen atmosphere, no granular anisotropic carbons were formed from the subbituminous coal (PSOC-1401), whereas this material is present in the residue of the corresponding single, high-temperature stage reaction. Also, the reflectance of the "reacted" vitrinite only is lowest when a hydrogen atmosphere was used in both stages with the catalyst, representing the conditions which gave rise to the highest conversion. This implies that first-stage reaction may have created products or molecular structures which are not as likely to undergo the condensation reactions that would otherwise take place during the second stage.

During the temperature-staged reactions, the presence of the catalyst minimized retrogressive reactions in the subbituminous coal. The reflectance values of the residues from the non-catalytic runs are consistently higher than those of the catalytic ones in the temperature-staged reactions even though there may have been considerably lower conversion (Table 3).

In brief, the influence of different parameters on dry liquefaction are interrelated. The effects of atmosphere and catalysis are manifested during the second stage, whereas they have relatively little apparent effect during the first stage. The presence of a hydrogen gas and catalyst promotes the thermoplastic development of vitrinite in the tubing bomb reactor, in turn favoring liquid conversion as a consequence of enhanced hydrogen transfer and catalyst dispersion.

Analyses of Whole Products, Catalytic and Non-Catalytic

The advantage of performing reflectance analysis upon the whole products of reaction is that a better opportunity is provided for evaluating the efficiency of hydrogenation. As noted above, some of the products of hydrogenation which would be dissolved by the extraction solvent are available for study in addition to undissolved coal and any products of retrogressive condensation reactions. This type of analyses is possible only with the products of dry hydrogenation; when a vehicle solvent is used, the products have a tarry consistency and cannot be formed into a pellet or polished without prior extraction. Published work (2) on the experimental hydrogenation of an hvA bituminous coal has shown that thermal reactions produced only higher reflecting vitrinite-derived materials, but where a dispersed catalyst was employed the reflectance distribution was extended downwards to significantly lower levels. The lower reflecting population, in the latter case, was THF soluble and highly fluorescing under blue-light irradiation. This contrasted with the THF-insoluble and non-fluorescent nature of the higher reflecting population. It was concluded that the low-reflecting material generated under catalytic hydrogenation in these experiments probably was asphaltenic in nature.

Subsequent work (3) showed that although similar reflectance distributions were obtained for the vitrinite-derived materials in the whole products from the hydrogenation of hvA and C bituminous coals, the anisotropic textures of these materials were quite different. A fine-grained anisotropy was apparent in the product of the first of these coals, possibly because of the large size of molecules generated during catalytic liquefaction (the residue of the corresponding thermal run was isotropic). It is supposed that locally, in the absence of hydrogen, the molecular fragments would align and stack to give an anisotropic texture. The same coal catalytically hydrogenated in the presence of a distillate process solvent fraction (220-500°C-boiling H-coal fractionator bottoms from Consolidation Coal Company) produced only negligible anisotropic semicoke; apparently the solvent must aid the dispersal of free radicals so that there is a greater likelihood of hydrogenation. In the case of the hvC bituminous coal, no anisotropic semicoke was produced during the dry hydrogenation under either thermal or catalytic conditions. It was concluded that the aromatic fragments formed during catalytic hydroprocessing of this coal must be less planar than those from the hvA bituminous coal. The reported difference in conversion levels between coals of hvC and A bituminous rank (Figs 1 & 2), and the optical

textures of their respective residues appear to be manifestations of known differences in molecular structure between coals of these ranks. These results, then, illustrate how geochemistry affects coal structure, and the significant effect this can have upon reaction chemistry.

Acknowledgment

The research was conducted with the financial support of a grant from the U.S. Department of Energy (DE-FG22-86PC90910).

REFERENCES

1. Derbyshire, F., Davis, A., Epstein, M. and Stansberry, P., 1986, *Fuel*, 65, 1233-1239.
2. Derbyshire, F.J., Davis, A. and Lin, R., 1989, *Energy & Fuels*, 3, 431-437.
3. Davis, A., et al., Optical properties of coals and liquefaction residues as indicators of reactivity, *Fuel*, in press.
4. Mitchell, G.D., Davis, A. and Spackman, W., in *Liquid Fuels from Coal* (Ed. R.T. Ellington), Academic Press, 1977, pp. 245-270.
5. Shibaoka, M., 1981, *Fuel*, 60, 240-246.
6. Yarzab, R.F., Given, P.H., Spackman, W. and Davis, A., 1980, *Fuel*, 59, 81-92.
7. Szladow, A.J. and Given, P.H., 1981, *Ind. Eng. Chem. Proc. Res. Dev.*, 20, 27.
8. Derbyshire, F., Davis, A., Schobert, H. and Stansberry, P., 1990, *American Chemical Society, Division of Fuel Chemistry, Preprints*, 35(1), 51-57.
9. Mitchell, G.D., Davis, A. and Derbyshire, F.J., 1989, *Proceedings International Coal Science Conference, Tokyo, Japan, International Energy Agency, Vol. II*, 751-754.

Table 1. Coal Properties

Penn State Sample Number	PSOC-1482	PSOC-1401	PSOC-1498	PSOC-1504
Seam	Hage1	Lower Hyodak	Madge	Upper Sunnyside
State	North Dakota	Wyoming	Colorado	Utah
ASTM Rank	1-g	subB	hvc	hVA
Mean-Maximum Reflectance of Vitrinite (R _{max} , %)	0.39	0.42	0.60	0.80
Ultimate Analysis (% daf)				
Carbon	72.3	74.3	77.5	82.0
Hydrogen	2.3	5.2	5.5	5.8
Oxygen (by difference)	23.5+	19.3	14.7+	9.7+
Nitrogen	1.0	1.1	1.8	1.8
Organic Sulfur	0.9	0.2	0.6	0.8
Proximate Analysis (a.r.%)				
Moisture	34.7	16.3	9.5	3.4
Volatile Matter	28.1	37.7	38.0	37.5
Fixed Carbon	31.4	41.1	46.1	51.8
Ash	5.9	6.6	6.4	7.3
Petrographic Composition (vol %, mineral-free)				
Vitrinite	88	85	89	87
Liptinite	2	2	2	3
Inertinite	10	13	9	10
Chloroform-soluble extract (% dmmf)	1.76	NA	1.31	1.06

Table 2. Maximum Reflectance Measurements on Vitritite-Derived THF-Insoluble Residue Material From Dry, Non-catalytic Liquefaction

Raw	275°C, H ₂	275°C, N ₂	425°C, H ₂	425°C, N ₂	275°C, H ₂ + 425°C, H ₂	275°C, N ₂ + 425°C, N ₂
PSOC-1482	0.39	0.38	1.40	1.42	1.43	1.42
PSOC-1401	0.42	0.56	1.25	1.41	1.41	1.40
PSOC-1504	0.80	0.73	1.38	1.36	1.35	1.37

Table 3. Maximum Reflectance of Vitritite-Derived Residue Material (THF insolubles) from Liquefaction of PSOC-1401

Sample Identification	Dry, catalytic (1% MoS ₂)			Dry, non-catalytic		
	Reflectance, %	Vitrinite Type	Conversion, %	Reflectance, %	Vitrinite Type	Conversion, %
Raw	0.42	(unreacted)	--	0.42	(unreacted)	--
275°C, N ₂	0.62	(unreacted)	4.5	0.56	(unreacted)	7.7
275°C, H ₂	0.60	(unreacted)	4.1	0.57	(unreacted)	9.0
425°C, N ₂	1.25	(unreacted)	25.9	1.41	(unreacted)	32.0
425°C, H ₂	1.58	(reacted)	60.3	1.25	(unreacted)	33.7
275°C, N ₂ + 425°C, H ₂	1.46	(reacted)	58.7	1.62	(reacted)	41.0
275°C, H ₂ + 425°C, N ₂	1.24	(unreacted)	25.7	1.43	(unreacted)	32.0
275°C, N ₂ + 425°C, N ₂	1.19	(unreacted)	24.8	1.40	(unreacted)	32.2
275°C, H ₂ + 425°C, H ₂	1.40	(reacted)	67.4	1.41	(reacted)	40.4

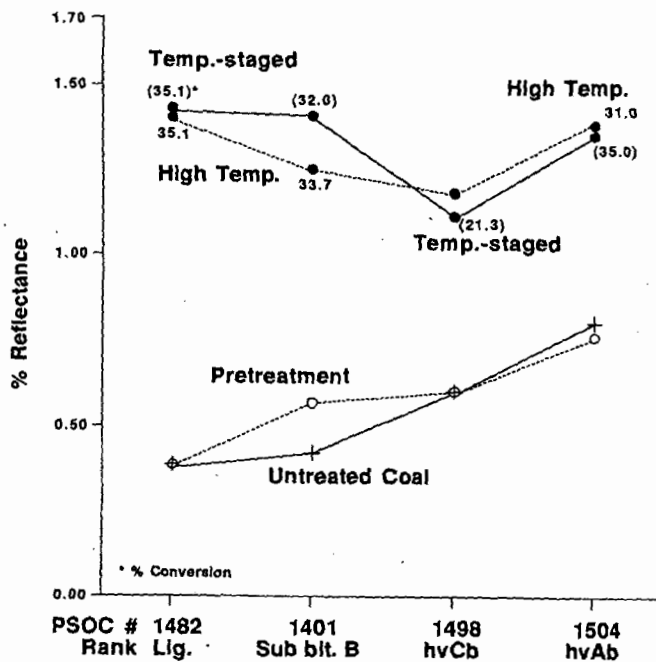


Figure 1. Mean Reflectance of Vitrinite-Derived Materials as a Function of Reaction Conditions; Dry, Non-catalytic Hydrogenation Residues

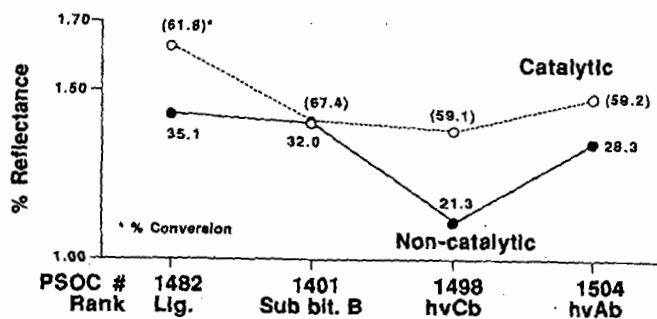


Figure 2. Mean Reflectance of Vitrinite-Derived Materials; Temp.-staged Dry, Catalytic (Mo) and Non-catalytic Hydrogenation Residues

LINKS BETWEEN HYDROGENATION BEHAVIOR OF COALS AND THEIR GIESELER-SOLIDIFICATION

Anna Marzec and Hans-Rolf Schulten*
Institute of Coal Chemistry, Polish Academy of Sciences, 44-100
Gliwice, 1 Maja 62, Poland
*Fachhochschule Fresenius, 6200 Wiesbaden, Dambachtal 20, Germany

INTRODUCTION

The present study aims at better understanding of links that were found between hydrogen acceptor abilities of coals and their solidification temperatures (1) in search for means of prediction of the development of anisotropic texture in coking coal blends (1).

Our approach is based on the four methodological steps applied to a set of twenty coals that represent a wide range of thermoplastic properties. The steps are: (1) determination of hydrogen acceptor abilities of the coals in reaction with tetralin; (2) determination of Gieseler-solidification temperatures of the coals; (3) characterization of the coals by pyrolysis /Py/-field ionization /FI/ mass spectrometry /MS/ of the coals; and (4) multivariate chemometric evaluation of these three data sets. Specific role of Py-FIMS of coals lies in that the technique displays chemical composition of a part of coal material that is able to diffuse and penetrate coal grains on heating during coal processing; it has been found that this movable part influences coal reactivity in reaction with H-donor (2,3) and in low-temperature pyrolysis (4).

The present paper is aimed at search for structural units of coal material that are active in hydrogen transfer and units that are active in reactions resulting in coal solidification on heating. It is believed that the results can contribute to identification of structures active in liquefaction retrogressive reactions.

EXPERIMENTAL

Coal Samples. Twenty carboniferous coals from Poland were studied. Their basic properties (wt.% daf) are: carbon 85-91; hydrogen 4.3-5.3; oxygen 0.8-7.0; sulfur 0.5-3.8. The petrographic composition (wt.% dmmf) is: vitrinite 63-88; exinite 0.-11; inertinite 7-30. Solidification temperatures of the coals (Table 1) are in the 417-490°C range.

Reaction of Coals with Tetralin. The reaction was carried out at 400°C; 60 min; for coal-tetralin mixture 1:2 w/w. The amount of hydrogen transferred from tetralin to coal material /HTr/ was calculated on the basis of GC determination of unreacted tetralin/naphthalene ratio. Other details were reported earlier (3) except for thermal decomposition of tetralin at 400°C. Tetralin was heated in the autoclave at 400°C/60 min and GC analysed. The result of analysis: 97.8 % tetralin; 1.4 % naphthalene; and compounds of lower and higher retention times 0.5 % and 0.3 %, respectively, were used for calculation of corrected HTr values /shown in Table 1/. The same procedure was

applied in determination of HTr for pyridine /Py/- extractables and Py-residues of the coals.

Py-FI MS and Chemometric Techniques. Both have been previously described in details (2-4).

RESULTS

Hydrogen Transfer to Coal Material. The data in Table 1 show that organic material of Py-extractables as well as of Py-residues react with tetralin. Amount of hydrogen transferred to Py-extractables and to the residues is in the same range from 0.4 to 1.0 grams of H / 100 grams of org. material. If one compares HTr values for a coal, its extracted material and residue, one can say, all cases are observed: some coal samples show the highest HTr; in other coals the highest HTr is found for their extractables or for residues.

The correlation coefficient found between HTr values for the coals and their solidification temperatures is very significant / $r = 0.87$ /. Lower r values were found for the products of extraction.

Hydrogen Transfer and FI Difference Mass Spectrum of Selected Coals. Four most reactive coals /HTr in the range from 0.8 to 1.2/ were selected; their FI mass spectra were normalized and summed. Next, four least reactive coals /HTr in 0.1 - 0.4 range/ were chosen and their spectra were normalized and summed. Figure shows the difference spectrum for the two groups of coals. The upper part of Figure shows FI mass signals whose intensities are higher in the high reactive coals. The lower part shows signals whose intensities are higher in the least reactive coals. Hence, it has been concluded that the composition of the volatilized, in the mass spectrometer, material of coals can supply information about components that are active in hydrogen transfer as well as about unreactive species.

FI Mass Signals Correlated with Hydrogen Transfer. Results of correlation analysis carried out for two sets of data: (a) FI mass signals in the range 158-400 a.m.u. and (b) amounts of hydrogen transferred to the samples of coals, are shown in Table 2. Seventy seven FI mass signals were found to be significantly correlated with the HTr values. A vast majority of the coefficients are highly significant ($r > |0.68|$). This indicates that there is a causative link between structures represented by the correlated signals and reactivity of the coals in hydrogen transfer.

Out of all the correlated signals, forty seven signals are correlated with positive sign /Table 2; upper/ i.e., the higher the intensities of these signals the higher amount of hydrogen is transferred to the coals. All these signals can be found in the upper part of the difference spectrum /Figure/.

Thirty signals are correlated with negative sign /Table 2; lower/ which means: the higher the intensities of the signals the lower amount of hydrogen is transferred to the coals. All the signals can be found in the lower part of the difference spectrum.

Proposed structures for all correlated signals are shown in Table 3. The structures represent only one of all possible isomers for example, pyrene / m/z 202/ is displayed, although there are three other four-ring aromatic hydrocarbons, all with the same

accurate mass as for pyrene. Isomers not presented in the Table can be found in reference 5.

Structures Active in Hydrogen Transfer /Table 3; upper/. In general, there are two types of compounds that are positively correlated with hydrogen transfer. They are aromatic hydrocarbons and hydroxycompounds. Hydroaromatics seem to be of minor importance for the reactivity of the studied coals, compared with lower rank coals (3,4), since they are represented by a few hydropyrenes.

Aromatic hydrocarbons are represented by 12 classes with respect of number of aromatic rings and mode of their arrangement. They are: 3-aromatic ring hydrocarbon (m/z 190); 4-aromatic ring (m/z 202; 226; 240; 254); 5-aromatic ring (m/z 252; 264; 276; 278); 6-aromatic ring (m/z 302; 328) and 7-aromatic ring hydrocarbon (m/z 300). With respect of alkyl substituents, majority of the hydrocarbons are present as unsubstituted and containing one methyl group. A few hydrocarbons may have C2 and C3 alkyl substituents for example, accurate masses related to signals m/z 328 and 342 may represent either C2 and C3- coronenes or C0-C1-dibenzochrysenes.

Hydroxycompounds are represented by /OH/- and /OH/2-benzenes;/OH/ and /OH/2-indenes; and /OH/ -naphthalenes, -acenaphthenes, -anthracenes, -fluorenes. No doubt, at least some of the compounds have phenolic OH (m/z 94; 110; 134).

Structures Inactive in Hydrogen Transfer /Table 3; lower/. In contrast to the positively correlated mass signals, the negatively correlated signals represent entirely different structures. None of them can be assigned to unsubstituted aromatic hydrocarbons. Instead of that, the signals represent short alkyl derivatives of naphthalene, fluorene, acenaphthene, anthracene and chrysene, the five classes of aromatic hydrocarbons that are not present at all in the set of active structures. The other aromatics are alkylated, C2-C5, pyrene, perylene, cyclopentachrysene and dibenzopyrene; these aromatics in the positively correlated set are entirely unsubstituted. A few hydroxycompounds i.e., C4-C7-dihydroxybenzenes were also found to be inactive in hydrogen transfer.

Comparing the present results with results obtained for another set of twenty coals of lower rank (2-4), the major difference is, that in high rank coals much more correlated signals are related to aromatic structures. This refers to the positively as well as negatively correlated signals.

FI Mass Signals and Structures Correlated with Solidification Temperatures. Results of correlation analysis carried out for two sets of data i.e., FI mass signals and temperatures of solidification of coals, T_s , are presented in Table 2. It has been stated that all signals, significantly correlated with T_s , are also significantly correlated with hydrogen transfer, however with opposite sign (Table 2). This means, the higher the content in a coal of structures shown in upper part of Table 3, the lower is its temperature of solidification and the higher its hydrogen transfer. It clearly indicates a strong link between reactivities of the structures in reactions resulting in solidification and in hydrogen transfer

reactions.

Next, the results of correlation analysis also show: the higher the content in a coal of structures presented in lower part of Table 3, the higher is its temperature of solidification and the lower its hydrogen transfer. Thus, the structures are inactive in solidification as well as hydrogen transfer reactions.

Summing up the results:

- The same structures are reactive in hydrogen transfer from the hydrogen donor and in reactions that result in solidification of coal on its heating. They are: (a) numerous unsubstituted and C1-aromatic hydrocarbons that contain from 3 up to 7 aromatic rings /except for the hydrocarbons quoted in the next para/; a few may have also C2 and C3 alkyls; and (b) C0-C7-alkylated hydroxyaromatic compounds that contain from 1 to 3 aromatic rings.

- Structures that are inactive in hydrogen transfer as well as in solidification reactions, are: alkyl-, up to C3, naphthalenes, fluorenes, acenaphthenes, anthracenes and chrysenes as well as alkyl-, up to C5, aromatic hydrocarbons that have 4 rings (pyrene, perylene, cyclopentachrysene) and 6 rings (dibenzopyrene).

DISCUSSION

The link between H-acceptor capability of coals in reaction with H-donor and their temperature-induced solidification (1) lies in the fact that the same structures that are active in H-transfer from H-donor are also active in thermal reactions resulting in solidification. Hence, these structures during liquefaction can react via two pathways: they can either react with H-donor or participate in condensation/polymerization reactions. The pathway by which the structure reacts depends on the availability of H-donor molecule or a molecule with which it can condensate or polymerize.

H-transfer activity of the shown aromatic hydrocarbons (Table 3; upper) can be explained on the basis of mechanism worked out by McMillen, Malhotra et al. (6); the aromatics react with hydroaromatic H-donor and give rise to cyclohexadienyl radicals which in turn, lead to cleavage of single bonds in coal material. The mechanism of solidification reactions of the aromatics can be deduced from studies of carbonization at 430-450°C of model aromatic hydrocarbons (7) showing that they undergo condensation reactions. Hence, it is concluded that the shown aromatic hydrocarbons undergo such condensation during liquefaction and that this constitutes a part of retrogressive reactions in liquefaction.

Assuming that the hydroxycompounds (Table 3; upper) are phenolic compounds, one can explain their activity in H-transfer by several hypotheses (8,9). More obscure is mechanism by which they contribute to solidification, except for dihydroxybenzenes (10). It has been stated that they readily polymerize at 400°C; ionic mechanism was suggested (10). Thus, it is concluded that the hydroxycompounds polymerize in liquefaction and give rise to retrogressive reactions in this way, if H-donor is not available on molecular level.

The inactive structures (Table 3; lower) dilute the concentration

of active species. Hence, the higher the content of inactive ones the longer time is needed for solidification. This has been manifested in the Gieseler-plastometer as the increase of solidification temperature.

REFERENCES

- (1) S. Iyama, T. Yokono and Y. Sanada, Carbon 1986, 24, 423; and references therein
- (2) H-R. Schulten, N. Simmleit and A. Marzec, Fuel 1988, 67, 619
- (3) A. Marzec, S. Czajkowska, N. Simmleit and H-R. Schulten, Fuel Processing Technology, 1990, 26, 53
- (4) H-R. Schulten, A. Marzec, P. Dyla, N. Simmleit and R. Mueller Energy & Fuels 1989, 3, 481
- (5) M.L. Lee, V. Novotny and K.D. Bartle, "Analytical Chemistry of Polycyclic Hydrocarbons". Academic Press, 1981, pp.363-386
- (6) D.F. McMillen, R. Malhotra, G.P. Hum and S-J. Chang, Energy & Fuels 1987, 1, 193; and references therein
- (7) M. Zander, ACS Fuel Chem. Div., Preprints 1989, 34/4/, 1218; and references therein
- (8) D.D. Whitehurst, Th.O. Mitchell and M. Farcasiu, "Coal Liquefaction", Academic Press, 1980, Ch. 8 and 9.
- (9) L.M. Stock, in: "Chemistry of Coal Conversion", Ed. R.H. Schlosberg. Plenum Press, 1985, pp. 253-313.
- (10) F.M. Wang, V.P. Senthilnathan and S.E. Stein, Proceedings of the 1989 Coal Science Conference, Tokyo, vol. 1, p. 165.

ACKNOWLEDGEMENTS. This work was supported by the Deutsche Forschungsgemeinschaft, Bonn-Bad Godesberg /Project Schu 416/15-1/ and by the Polish Academy of Sciences.

Table 1
BASIC CHARACTERISTICS OF THE STUDIED COALS

COAL No	Wt % daf		SOLIDIFTN* Ts; oC	HYDROGEN TRANSFER, HTr g of H /100 g org.mat.		
	C	O		COAL	RESIDUE	EXTRACT
100	85.0	6.9	433	0.78	0.77	0.68
102	87.3	4.6	417	1.06	0.84	0.83
103	85.9	6.6	428	1.20	0.95	0.85
104	85.3	6.9	451	0.71	0.70	0.86
105	85.7	6.9	440	0.68	0.67	0.91
106	85.7	6.6	451	0.76	0.61	1.01
107	86.4	2.8	464	0.74	0.51	0.95
109	88.4	3.8	471	0.63	0.69	0.61
110	88.3	3.6	458	0.55	0.71	0.55
111	86.7	5.2	465	0.42	0.73	0.60
112	90.6	1.9	478	0.49	0.77	0.49
113	91.9	0.8	487	0.32	0.71	0.47
114	89.4	3.2	490	0.12	0.42	0.44
117	84.5	7.5	454	0.76	1.03	0.81
118	85.7	5.3	448	0.61	0.95	0.72
119	89.5	2.7	479	0.27	0.47	0.41
120	84.5	7.7	430	0.83	1.00	0.72
121	91.4	0.8	488	0.41	0.42	0.50
122	88.7	1.7	490	0.36	0.46	0.97
124	85.1	6.8	430	0.73	1.02	0.62

Range: 85-91 | 0.8-7.7 | 417-490 | 0.1-1.2 | 0.4-1.0 | 0.4-1.0

*/ Gieseler plastometer; standard method PN-62/G-04536.

Table 2
 FI MASS SIGNALS CORRELATED WITH HYDROGEN TRANSFER VALUES /HTr/
 AND WITH SOLIDIFICATION TEMPERATURES /Ts/ OF THE COALS

m/z	Corrln coeffnt		m/z	Corrln coeffnt	
	HTr	Ts		HTr	Ts
	Upper Part			Upper Part	
158	.85	-.82	374	.67	-.76
160	.59	-.56	376	.80	-.86
162	.81	-.75	378	.88	-.90
164	.82	-.74	380	.59	-.55
172	.85	-.83	388	.74	-.84
174	.69	-.63	390	.87	-.83
176	.76	-.71	392	.84	-.88
188	.79	-.70		Lower Part	
190	.53	-.59	166	-.70	.70
200	.70	-.67	168	-.58	.70
202	.54	-.60	180	-.80	.87
212	.91	-.85	182	-.71	.80
214	.80	-.83	192	-.78	.85
224	.50	-.60	194	-.83	.85
226	.93	-.91	196	-.62	.55
238	.82	-.88	206	-.91	.90
240	.91	-.94	208	-.71	.77
250	.82	-.81	218	-.72	.74
252	.81	-.84	220	-.80	.59
254	.77	-.75	230	-.86	.90
260	.57	-.64	244	-.90	.90
262	.72	-.75	256	-.69	.74
264	.85	-.90	258	-.90	.85
274	.73	-.73	280	-.75	.85
276	.76	-.76	284	-.74	.71
278	.88	-.79	294	-.86	.91
288	.69	-.70	298	-.72	.71
290	.68	-.55	306	-.75	.79
300	.62	-.65	308	-.87	.84
302	.87	-.85	318	-.81	.85
314	.86	-.86	320	-.88	.95
328	.79	-.83	322	-.59	.62
338	.81	-.77	330	-.57	.70
340	.64	-.48	332	-.83	.87
342	.83	-.77	334	-.87	.79
350	.71	-.72	344	-.83	.79
352	.90	-.92	346	-.87	.85
364	.85	-.88	358	-.72	.68
366	.88	-.83			

Table 3
STRUCTURES IN THE CORRELATED FI MASS SIGNALS

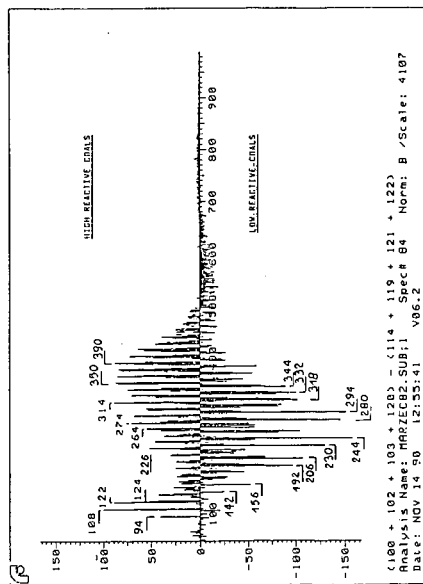
Upper: FI signals positively correlated with H-transfer and negatively correlated with solidification temperatures
Lower: FI signals negatively correlated with H-transfer and positively correlated with solidification temperatures

		m/z		PROPOSED STRUCTURES	
Upper; ACTIVE STRUCTURES					
108	122	136	150	164	C ₀ - C ₅ -hydroxybenzenes*
110	124	138	174		C ₀ - C ₂ -dihydroxybenzenes*
146	160	174	188		C ₁ - C ₄ -hydroxyindenes*
134	148	162	176	190	C ₀ , C ₁ , C ₂ , C ₃ , C ₅ -dihydroxyindenes
158	172		200	214	C ₁ - C ₂ and C ₄ - C ₅ -hydroxynaphthalenes*
198	212				C ₂ - C ₃ -hydroxyacenaphthenes*
224	238				C ₃ - C ₄ -hydroxyfluorenes* and
					C ₁ - C ₂ -octahydroxyrenes*
190					4H-cyclopentadeflphenanthrene*
202					pyrene*
250	and	262			C ₃ -hexahydroxyrene* and C ₄ -tetrahydroxyrene*
226	240	254			C ₀ - C ₂ -benzolghlfluoranthenes*; C ₀ - C ₁ -cyclo
					pentadeflchrysenes*; C ₀ -cyclohexa[def]chrysene*
					perylene*
252					C ₀ H ₂₀ - 20, N 22*
260	274	288			C ₀ - C ₁ -11H-cyclopenta[ghl]chrysene*; C ₀ -picene*;
264	278				C ₀ - C ₆ -hydroxyanthracenes*
					C ₀ - C ₁ -anthanthrenes*
276	290				C ₀ -dibenzopyrene*; C ₀ - hydroxypyrene*
302	314	328	342		C ₀ , C ₁ , C ₂ , C ₃ -coronenes;
300					C ₀ * - C ₁ -dibenzochrysenes
340					C ₁ -dibenzocyclopenta[cd]pyrene
350	364	378	392		C ₀ - C ₃ -benzocoronenes; C ₀ - C ₁ -tribenzochrysenes
352	366	380			C ₀ - C ₂ -tribenzopyrenes
374	388	and	376	390	?

Lower; INACTIVE STRUCTURES

142	156		C ₁ - C ₂ - naphthalenes *	
166	180	194	208	C ₄ - C ₇ - dihydroxybenzenes * a. C ₁ - C ₂ - fluorenes *
192	206	220		C ₁ - C ₂ - anthracenes *
218		176		C ₂ - 4H-cyclopenta[def]phenanthrene
168		258		C ₁ ; C ₃ - acenaphthenes * and C _{1,2} H _{1,2} N *
230	244	284	298	C ₂ - C ₄ - pyrenes
256		324		C ₂ ; C ₄ * ; C ₅ - chrysenes
280	294	308	322	C ₂ ; C ₃ ; C ₄ ; C ₅ - perylenes
306	320	334		C ₃ ; C ₄ ; C ₅ * -11H-cyclopenta[ghi]chrysenes
304	318	332	346	C ₂ - C ₃ - anthanthrenes
330	344	358		C ₂ ; C ₃ ; C ₄ - dibenzopyrenes

* the assignments have been confirmed by high res. and accurate mass measurements



(100 + 102 + 103 + 120) - (114 + 119 + 121 + 122)
 Analysis Name: MPR1EG62.SUB;1 Spec# 64 Norm: B /Scale: 4107
 Date: NOV 14 '90 12:55:41

Figure.
 FI Difference Mass Spectrum
 of Selected Coals showing high and low
 reactivity towards the H-donor.
 See Table 1 for coals No. 100, 102, 103,
 120 and 114, 119, 121, 122.

EFFECT OF MOLYBDENUM SULFIDE CATALYST ON THE MECHANISM OF COAL LIQUEFACTION

Caroline E. Burgess, Levent Artok, and Harold H. Schobert
Fuel Science Program
Department of Materials Science and Engineering
The Pennsylvania State University
University Park, PA 16802

Keywords: molybdenum sulfide catalyst, liquefaction mechanism, low severity liquefaction

INTRODUCTION

Molybdenum sulfide catalyst has been used to improve liquefaction yield and to refine coal oils for the last 60 to 70 years [1]. It was an important step in coal liquefaction that these catalysts were developed because before that time known catalysts were poisoned by sulfur [1], an element all coals contain. In 1923, M. Pier found selective, oxidic catalysts used in methanol synthesis that were less sensitive to sulfur than the metallic catalyst that was developed from ammonia synthesis [1]. In 1924, M. Pier prepared sulfur resistant coal hydrogenation catalysts: sulfides and oxides of molybdenum, tungsten, and the iron group metals [1].

Weller and Pelipetz [2] used ammonium heptamolybdate (AHM) to liquefy Rock Springs subbituminous B coal (Table 1) and found a remarkable increase in coal conversion when using a catalyst (92.7%) relative to an uncatalyzed reaction (33.7%). Their work shows that both oils and asphaltenes increase in yield. The reaction conditions of 450°C for 1 h at 1000 psig were such that asphaltenes initially produced could easily crack to oils. However, with a change in the oil-to-asphaltene (O/A) ratio from 3.71 for the uncatalyzed reaction to 1.51 for the catalyzed reaction, it appears the catalyst functions mainly to form asphaltenes. With the use of only one coal, there is not enough data to substantiate this trend. Table 2 contains data from Garg and Givens [3] showing AHM catalyst to have virtually no effect on total conversion, but a substantial increase in the O/A ratio from 0.19 to 0.38. At their reaction conditions (825°F for 35 min at 2000 psig), molybdenum catalyst appears to function to hydrogenate asphaltenes to oils. Since these data are in contradiction to those of Weller and Pelipetz, experimental work with more coals is necessary to see how coal rank and structure relate to the mechanism of molybdenum sulfide catalyst behavior in coal liquefaction. If these data are compared to liquefaction work done in our laboratory with molybdenum sulfide catalysts at low severity reaction conditions, the beginning of an understanding of the role molybdenum catalysts play in the coal liquefaction can be developed.

EXPERIMENTAL

Three different catalyst precursors were used. Sulfided ammonium molybdate (SAM) was prepared, as described in several publications [4-6], by bubbling H₂S into a solution of ammonium heptamolybdate. Sulfided tetrahydroquinolinium molybdate (STM) of the chemical formula (THQH)₆Mo₈S₂₂O₅·H₂O (where THQH represents protonated tetrahydroquinoline) was prepared as described by Burgess and Schobert [7]. Ammonium tetrathiomolybdate (ATM) was prepared in a similar manner to SAM, except the addition of NH₄OH provided sufficient additional ammonium ions to drive the reaction to completion [8].

The coal was impregnated in the same manner as reported previously [4-6]. Coal was slurried with catalyst precursor solutions for 2 hours and vacuum freeze dried to less than 1% moisture. Although several molybdenum sulfide precursors were used, previous data have shown that the predominant active catalyst species is MoS₂ [4-9], and relative comparisons can be made about the effect of molybdenum catalysts on coal liquefaction. However, it should be recognized that the degree of dispersion of the catalyst precursors on coal could be different because three different molybdenum sulfide catalyst precursors were used.

Five coals were used. Data on the elemental composition of each coal are contained in Tables 3-8. All reactions were carried out in 25 ml microautoclave (tubing bomb) reactors, and heating was accomplished in a temperature controlled fluidized sandbath. The catalyst loading was 1% expressed as weight of molybdenum (not of molybdenum compound) on a daf basis. The reactor was flushed three times with hydrogen, with the final addition pressurized to 6.9 MPa (cold). The reactor was vertically oscillated 2.5 cm at 200 cycles per minute. Two subbituminous B coals and a hvA bituminous coal used a single stage reaction at 425°C for 10 min and a temperature-staged reaction (350°C for 1 h followed by 425°C for 10 min). The solvent used was naphthalene at a 2/1 solvent-to-coal ratio, and the mass of the coal reacted was 2.5g. A Texas lignite and a hvB bituminous coal used the following reaction conditions: a phenanthrene solvent at a 1/1 solvent-to-coal ratio, with the coal mass 5g, and the reaction temperature was 275°C for 30 min.

For the first three coals (PSOC 1266, 1401, and 1488), the cooled reactor was vented into a glass expansion bulb, and the contents were analyzed by gas chromatography using a Varian model 3700. The contents of the reactor were then rinsed with tetrahydrofuran (THF) into a dried Soxhlet thimble and extracted for about 12 h under nitrogen. The THF was removed by rotary evaporation. The solid residue was dried at 100°C for 12 h before weighing. Conversion was calculated by subtracting the weight of the residue from the weight of the coal and dividing by the dmmf weight of the coal. Liquids were further separated into asphaltenes and oils by adding hexane to the THF-soluble portion. This mixture was refluxed for 12 h under nitrogen, followed by filtration into hexane-solubles and insolubles. The hexane was removed by rotary evaporation, and the samples were dried at 100°C for 1 h before weighing. The oil (hexane-soluble) yield was calculated by difference from the conversion percentages of the gas yield, THF solubles, and the THF insolubles.

For the last two coals (DECS-1 and DECS-6), the work-up procedure was changed slightly. Gas percentages were not determined, so the calculated difference for the oils includes the gas yield as well. Once the pressure was vented from the reactor, the contents of the tubing bomb were rinsed with toluene into a dried, weighed ceramic thimble and Soxhlet extracted for about 12 h under nitrogen. The toluene was removed from the extract by rotary evaporation. Toluene-solubles were further separated into asphaltenes and oils by adding about 400 ml of hexane to the extract. The mixture was stirred for 1 h and asphaltenes were allowed to settle overnight, with solids separated by vacuum filtration. The toluene-insoluble residue was then Soxhlet extracted with THF to separate preasphaltenes from the residue. THF was removed from the extract by rotary evaporation. Preasphaltenes, asphaltenes, and residue were dried overnight under vacuum at 110°C. Conversion was calculated by subtracting the weight of the residue from the weight of the coal and dividing by the daf weight of the coal.

RESULTS AND DISCUSSION

Conversion data for coals PSOC 1266 and 1401 at 425°C for 10 min are contained in Table 3, and conversion data for these two coals at 350°C for 1h followed by 425°C for 10 min are contained in Table 4. These data were obtained by M. Epstein [2]. For the single stage at 425°C, the bituminous coal (PSOC 1266) and the subbituminous coal (PSOC 1401) reacted in a similar manner. When comparing catalyzed experiments to uncatalyzed experiments, the change in total conversion was ~25% for both coals, with oil yields decreasing and asphaltene yields increasing substantially. The O/A for PSOC 1266 was 0.32 for the uncatalyzed experiment and 0.07 for the catalyzed experiment. A similar trend was noticed with PSOC 1401 with an O/A 6.1 for the uncatalyzed experiment and 0.42 for the catalyzed experiment.

Temperature-staging had a substantial effect on conversion of both coals. For PSOC 1266, when comparing catalyzed experiments to uncatalyzed experiments, the change in total conversion was about the same, ~28%, but the increase was substantial for the oil yield, while the asphaltene yield decreased. The O/A changed from 0.22 for the uncatalyzed experiment to 1.33 for the catalyzed experiment. However, for the subbituminous coal PSOC 1401, when comparing catalyzed experiments to uncatalyzed experiments, the conversion increased ~50%, with increases in both oil and asphaltene yields. The greatest increase occurred in the asphaltene yield, with O/A for the uncatalyzed experiments 1.46 and for the catalyzed experiments 0.60.

PSOC 1488 liquefaction data using two different molybdenum sulfide catalyst precursors are located in Tables 5-7. Table 5 contains data at 425°C for 10 min, Table 6 contains data at 350°C for 1 h followed by 425°C for 10 min, and Table 7 contains data for 350°C for 1 h. At 425°C for 10 min, total conversion for the uncatalyzed experiment is low, at 25%. The experiment using SAM has a total conversion of 66%. There is little change in the oil yield (~14%), but there is a large increase in asphaltene production, from 10% for no catalyst to 46% for the SAM-catalyzed experiment. At this temperature, STM-catalyzed experiments showed poor yields, with oil yield about the same (14%) and asphaltene yield at 20%. The O/A ratio reflects this behavior by decreasing from 1.25 for the uncatalyzed experiment to 0.73 for the STM-catalyzed experiment and 0.29 for the SAM-catalyzed experiment.

Temperature-staging also had a significant effect on the catalyzed experiments. When using no catalyst, total conversion was 31%, with low oil yield (12%) and low asphaltene yield (14%). However, when comparing experiments using SAM and STM, total conversion increased to ~80%. The predominant increase for both catalytic experiments was in asphaltene yield, from 14% to 58% for SAM-catalyzed experiments and 50% for STM-catalyzed experiments. Although the STM experiment showed a lower asphaltene yield, a high oil yield (~25%) was observed compared to SAM-catalyzed experiments (~16%). STM seems to be more effective for hydrogenating asphaltenes to oils, as discussed elsewhere [9]. The O/A of the uncatalyzed experiment is 0.84, and similar to the 425°C experiments, the O/A decreased for the STM-catalyzed experiment to 0.52 and to 0.28 for the SAM-catalyzed experiment.

Data for experiments at 350°C for 1 h are located in Table 7. However, although the yields are lower than the temperature-staged experiments, the catalytic experiments showed an increase primarily in the asphaltene yields compared to uncatalyzed experiments, as in the previous results for PSOC 1488. At low severity, an indication of the coal's liquefaction ability can be readily seen, although the liquid yields are not high. The next set of data to be discussed is at even lower severity reaction conditions, but can be used to indicate a trend in how the coal will liquefy at higher reaction conditions.

Liquefaction data at 275°C for 30 min for a Texas subbituminous C coal (DECS-1) and a hvB bituminous coal (DECS-6) are located in Table 8. Conversion for DECS-1 is low at 275°C, but when comparing catalyzed experiments to uncatalyzed experiments, the predominant increase occurs in the preasphaltenes and asphaltenes and not in the oil fraction. The O/A (here A represents the sum of preasphaltenes and asphaltenes) changes from 0.32 for the uncatalyzed experiments to 0.2 for ATM-catalyzed experiments. The bituminous coal has a higher initial conversion (18% versus 6% for uncatalyzed). Although the total conversion increases in the ATM-catalyzed experiments (25%) compared to uncatalyzed experiments for DECS-6, the O/A remains constant at 0.38.

Despite the facts that different reaction conditions and different molybdenum catalyst precursors were used, there are some trends that can be seen in this whole body of work [2-9]. In the Penn State experimental work, two bituminous coals were reacted. PSOC 1266 (temperature-staged reaction) liquefaction yields (Tables 4) increased when comparing catalyzed experiments to uncatalyzed experiments, with the increased conversion being predominantly oils. DECS-6 liquefaction yields (Table 8) increased when comparing catalyzed experiments to uncatalyzed experiments, where liquefaction yield increases were equal between oils and asphaltenes. DECS-6 was reacted at very low severity reaction conditions (275°C), however, and cracking asphaltenes to oils at 275°C may be difficult. If these data are compared to Garg and Given's data (Table 2) [3], in which they used a hvC bituminous coal, a similar trend is noticed. They obtained a very high liquefaction conversion without catalyst (85%), and although in the catalytic experiment the total conversion did not increase much (87%), the O/A increased from 0.19 to 0.38. The molybdenum catalyst appears to function predominantly to hydrogenate asphaltenes to oils because, in all of these cases, initial conversion to asphaltenes even without catalyst is usually high. There was one exception with PSOC 1266 for the 425°C/10 min experiment (Table 3). The O/A ratio decreased when comparing the catalyzed experiment to the uncatalyzed experiment from 0.32 to 0.07. This phenomenon may be because the reaction conditions do not allow enough time for asphaltenes to be hydrogenated to oils. PSOC 1488, a subbituminous coal, (Table 5) at 425°C/10 min shows a similar occurrence. However, for

experiments using STM, reaction yields are very low, and may be due to poisoning of MoS₂ by products of THQ decomposition [9].

Three subbituminous coals were reacted. Liquefaction yields for all three (Tables 3-8) were substantially increased by the use of catalyst. For PSOC 1401, for the temperature-staged experiment, total conversion (Table 4) increased from 42% to 91%, where the increase in conversion was predominantly in the asphaltenes. The O/A ratio changed from 1.46 for the uncatalyzed experiment to 0.60 for the SAM-catalyzed experiment. For PSOC 1488, for all reaction conditions and both catalyst precursors (Tables 5-7), the catalytic experiments showed an increase in total conversion compared to uncatalyzed experiments, where the predominant increase was in the asphaltenes. DECS-1 (Table 8) showed a similar trend. Weller and Pelipetz [2] also show a similar trend (Table 1). The catalyst appears to first function to break apart the macromolecular network, and then, function to hydrogenate some of the asphaltenes to oils if conditions are conducive to do so. So why is the molybdenum catalyst functioning differently in bituminous and subbituminous coals?

Subbituminous coals contain more oxygen and are thought to be more highly crosslinked than bituminous coals. Hirsch describes low-rank coals with an open structure where there are many crosslinks (heteroatoms and hydrocarbon chains) connected to small aromatic systems (3 rings or less) [10]. Bituminous coals (85-91% C) tend to have a liquid structure, where there are fewer crosslinks, larger aromatic systems, and overall more order in structure [10]. Without catalyst or hydrogen donor solvent, little atomic hydrogen is available externally because hydrogen radicals generated from H₂ tend to react with each other before being able to react with radicals as the crosslinks break apart. Since ether, thioether, and some carbon-carbon bonds are relatively weak [11-13], if catalyst provides atomic hydrogen at the milder reaction conditions ($\leq 350^{\circ}\text{C}$ or temperature-staging), radicals can be generated more slowly and capped more efficiently to form asphaltenes. Since subbituminous coals in general contain more crosslinks to break apart, the catalyst functions mainly to provide hydrogen for capping generated radicals. Hence the large asphaltene yields and relatively large conversions for subbituminous coals when using molybdenum catalyst. Bituminous coals contain fewer crosslinks, so the requirement for radical capping with hydrogen supplied via the catalyst is lower relative to subbituminous coals. Therefore, molybdenum catalyst can function to hydrogenate generated asphaltenes to oils.

CONCLUSIONS

When coal liquefies, there are competing reaction mechanisms of coal depolymerization to asphaltenes, repolymerization of generated radicals to char, and the formation of oils from asphaltenes. It appears that molybdenum sulfide catalyst, during temperature-staging and low severity conditions, primarily intervenes in liquefaction for subbituminous coals to provide atomic hydrogen to cap depolymerized coal fragments that form asphaltenes. This is because subbituminous coal contain a relatively high crosslink density compared to higher ranks of coals, and the catalyst remains very busy generating asphaltenes. For bituminous coals, conversions without catalyst tend to be relatively high, so molybdenum catalyst primarily intervenes to provide atomic hydrogen to help crack asphaltenes to oils. Because the crosslink density in bituminous coal is lower than in subbituminous coal, the catalyst is not as involved in capping radicals and can be effective as a hydrogenation vehicle to generate oils. Repolymerization is reduced as the activity in the other processes increases, therefore, less char is produced. For the coals DECS-1,6, work is still in progress to include temperature-staging and to evaluate various methods of dispersing catalyst. These results will be reported at future meetings. Since the sample set is coals is quite small, similar experiments on a larger set of coals would provide more insight into the role rank plays with molybdenum catalyst and low severity coal liquefaction.

ACKNOWLEDGEMENTS

Various portions of this work have been supported by the U.S. Department of Energy, The Pennsylvania Research Corporation, and The Pennsylvania State University Mining and Mineral Resources Research Institute. The authors are pleased to acknowledge this support.

REFERENCES

1. Donath, E.E and Hoering, M. *Fuel Proc. Tech.*, **1**, (1), 3, 1977.
2. Weller, S. and Pelipetz, M.G. *Ind. Eng. Chem.*, **43**, (5), 1243, 1951.
3. Garg, D. and Givens, E. *Preprints, Amer. Chem. Soc., Div. Fuel Chem*, **28**, (5), 200, 1983.
4. Epstein, M.J. M.S. Thesis, The Pennsylvania State University, 1987.
5. Derbyshire, F.J., Davis, A., Lin, R., Stansberry, P.G., and Terrer, M-T. *Fuel Proc. Tech.*, **12**, (7), 127, 1986.
6. Garcia, A.B. and Schobert, H.H. *Fuel*, **68**, 1613, 1989.
7. Burgess, C.E. and Schobert, H.H. *Preprints, Amer. Chem. Soc., Div. Fuel Chem*, **35**, (1), 31, 1990.
8. Davis, A., Schobert, H.H., Mitchell, G.D., and Artok, L. "Catalyst Dispersion and Activity Under Conditions of Temperature-Staged Liquefaction", DOE-PC-89877-1,2,3, Progress Reports, 1989-1990.
9. Burgess, C.E. and Schobert, H.H. *Fuel* (Special Edition from Coal Structure and Reactivity Conference Sept. 1990). Accepted for publication Nov 1990.
10. Hirsch, P.B. *Proc. Roy. Soc., (London)*, **A 226**, 143, 1954.
11. Stock, L.M., in *Coal Science* (Eds. M.L. Gorbaty, J.W. Larsen, and I. Wender) Academic Press, N.Y., 248, 1982.
12. Mastral, A.M. and Rubio, B. *Fuel*, **68**, 80, 1989.
13. Calkins, W.H. *Energy and Fuels*, **1**, 59, 1987.

Table 1: Liquefaction Conversion Data Comparing the Use of Molybdenum Catalyst to Using No Catalyst - Data from Weller and Pelipetz [7]

Authors	Weller and Pelipetz [7]	
Coal	Rock Springs - Sub B - C-73.9, H-5.0, N-1.5, S-0.8, O-13.6	
Conditions	450°C, 1 hr, 1000 psi H ₂	
Conversion	No Catalyst	AHM ^c
Tot Conv (Benzene Insolubles) ^a	33.7	92.7
Oils (Hexane Solubles)	10.4	41.1
Asphaltenes (Benzene Sol/Hexane Insol)	2.8	27.2
O/A ^b	3.71	1.51

- a) Total conversion.
- b) Oil to asphaltene ratio.
- c) Catalyst is ammonium heptamolybdate.

Table 2: Liquefaction Conversion Data Comparing the Use of Molybdenum Catalyst to Using No Catalyst - Data from Garg and Givens [8]

Authors	Garg and Givens [8]	
Coal	Kentucky Elkhorn #2 -hvCb C-77.8 H-5.2, N-1.8, S-1.1, O-7.2	
Conditions	825°F, 35 min, 2000 psig, H ₂ 18.9 MCF/T	
Conversion	No Catalyst	AHM ^c
Tot Conv (THF Insolubles) ^a	85.3	86.8
Oils (Hexane Solubles)	12.2	21.7
Asphaltenes (THF Sol/Hexane Insol)	65.4	57.9
O/A ^b	0.187	0.375

- a) Total conversion.
- b) Oil to asphaltene ratio.
- c) Catalyst is ammonium heptamolybdate.

Table 3: Liquefaction Conversion Data Comparing the Use of Molybdenum Catalyst to Using No Catalyst - Epstein [2]

Author	Epstein [2]			
Coals	PSOC 1266-dmmf- hvAb - C-83.2, H-5.0, N-2.1, S-0.5, O-8.6			
	PSOC 1401-dmmf-Sub B - C-74.3 H-5.2, N-1.1, S-0.2, O-19.3			
Conditions	425°C, 10 min, 1000 psi H ₂			
Coal	PSOC 1266		PSOC 1401	
Conversion	No Cat ^d	SAM ^e	No Cat	SAM
Tot Conv (THF Insol)^a	58.1	72.6	42.5	66.7
Oils (Hex Sol)	13.7	4.8	28.8	17.6
Asph (THF. Sol/Hexane Insol)^b	42.8	66.7	4.7	41.8
Gas	1.6	1.1	9.0	7.3
O/A ^c	0.32	0.07	6.1	0.42

- a) Total conversion.
- b) Asphaltenes.
- c) Oil to asphaltene ratio.
- d) No catalyst.
- e) Catalyst is sulfided ammonium molybdate.

Table 4: Liquefaction Conversion Data Comparing the Use of Molybdenum Catalyst to Using No Catalyst - Epstein [2]

Author	Epstein [2]			
Coals	PSOC 1266-dmmf- hvAb - C-83.2, H-5.0, N-2.1, S-0.5, O-8.6			
	PSOC 1401-dmmf-Sub B - C-74.3 H-5.2, N-1.1, S-0.2, O-19.3			
Conditions	350°C, 1 h/425°C, 10 min, 1000 psi H ₂			
Coal	PSOC 1266		PSOC 1401	
Conversion	No Cat ^d	SAM ^e	No Cat	SAM
Tot Conv (THF Insol)^a	59.0	77.3	41.9	90.7
Oils (Hex Sol)	10.2	48.8	14.5 g	28.2 g
Asph (THF. Sol/Hexane Insol)^b	47.3	36.8	9.9	46.7
Gas^f	2.5	2.4	17.5	15.8
O/A ^c	0.22	1.33	1.46	0.60

- a) Total conversion.
- b) Asphaltenes.
- c) Oil to asphaltene ratio.
- d) No catalyst.
- e) Catalyst is sulfided ammonium molybdate.
- f) Gas a total of both stages.
- g) Corrected data.

Table 5: Liquefaction Conversion Data Comparing the Use of Molybdenum Catalyst to Using No Catalyst - Burgess and Schobert [5,9]

Author	Burgess and Schobert [5,9]		
Coals	PSOC 1488-dmmf-Sub B - C-76.6, H-5.2, N-1.0, S-0.5, O-17.2		
Conditions	425°C, 10 min, 1000 psi H ₂		
Coal	PSOC 1488		
Conversion	No Cat^d	SAM^e	STM^f
Tot Conv (THF Insol)^a	25.4	65.7	42.7
Oils (Hex Sol)	12.0	13.1	14.6
Asph (THF. Sol/Hexane Insol)^b	9.6	45.8	20.0
Gas	3.9	6.8	8.1
O/A^c	1.25	0.29	0.73

- a) Total conversion.
- b) Asphaltenes.
- c) Oil to asphaltene ratio.
- d) No catalyst.
- e) Catalyst is sulfided ammonium molybdate.
- f) Catalyst is sulfided tetrahydroquinolinium molybdate.

Table 6: Liquefaction Conversion Data Comparing the Use of Molybdenum Catalyst to Using No Catalyst - Burgess and Schobert [5,9]

Author	Burgess and Schobert [5,9]		
Coals	PSOC 1488-dmmf-Sub B - C-76.6, H-5.2, N-1.0, S-0.5, O-17.2		
Conditions	350°C, 1h/425°C, 10 min, 1000 psi H ₂		
Coal	PSOC 1488		
Conversion	No Cat^d	SAM^e	STM^f
Tot Conv (THF Insol)^a	30.8	78.5	80.1
Oils (Hex Sol)	11.7	16.2	25.2
Asph (THF. Sol/Hexane Insol)^b	13.9	57.7	49.5
Gas	5.2	5.5	5.5
O/A^c	0.84	0.28	0.52

- a) Total conversion.
- b) Asphaltenes.
- c) Oil to asphaltene ratio.
- d) No catalyst.
- e) Catalyst is sulfided ammonium molybdate.
- f) Catalyst is sulfided tetrahydroquinolinium molybdate.

Table 7: Liquefaction Conversion Data Comparing the Use of Molybdenum Catalyst to Using No Catalyst - Burgess and Schobert [5,9]

Author	Burgess and Schobert [5,9]		
Coals	PSOC 1488-dmmf-Sub B - C-76.6, H-5.2, N-1.0, S-0.5, O-17.2		
Conditions	350°C, 1h 1000 psi H ₂		
Coal	PSOC 1488		
Conversion	No Cat ^d	SAM ^e	STM ^f
Tot Conv (THF Insol) ^a	18.3	47.8	48.5
Oils (Hex Sol)	6.8	10.2	11.1
Asph (THF. Sol/Hexane Insol) ^b	7.1	33.9	33.8
Gas	4.4	3.8	3.6
O/A ^c	0.96	0.30	0.33

- a) Total conversion.
- b) Asphaltenes.
- c) Oil to asphaltene ratio.
- d) No catalyst.
- e) Catalyst is sulfided ammonium molybdate.
- f) Catalyst is sulfided tetrahydroquinolinium molybdate.

Table 8: Liquefaction Conversion Data Comparing the Use of Molybdenum Catalyst to Using No Catalyst - Data from Davis et al. [6]

Authors	Davis, Schobert, Mitchell, and Artok [6]			
Coals	DECS 1-dmmf - Sub C - C-76.1, H-5.5, N-1.5, S-1.1, O-15.8			
Conditions	DECS 6 -dmmf - hvB b - C-80.8, H-6.1, N-1.6, S-0.5, O-11.0			
Conditions	275°C, 30 min, 1000 psi H ₂			
Coal	DECS - 1		DECS - 6	
Conversion	No Cat ^e	ATM ^f	No Cat	ATM
Tot Conv (THF Insol) ^a	6.6	9.0	17.7	25.0
Oils (Hex Sol) + Gas	1.6	1.5	4.9	6.9
Asph (Tol. Sol/Hexane Insol) ^b	2.2	3.6	2.1	3.0
Preasph.(THF Insol/Tol. Sol) ^c	2.8	3.9	10.7	15.1
O/A (where A=Asph+Preasph) ^d	0.32	0.2	0.38	0.38

- a) Total conversion.
- b) Asphaltenes.
- c) Preasphaltenes.
- d) Oil to asphaltene ratio.
- e) No catalyst.
- f) Catalyst is ammonium tetrathiomolybdate.

CHARACTERIZATION OF MARTIN LAKE LIGNITE AND ITS RESIDUES AFTER LIQUEFACTION

S. M. Fatemi-Badi, A. J. Swanson, N. K. Sethi and R. T. Roginski

Amoco Corporation and Amoco Oil Company
Amoco Research Center, P. O. Box 3011, Naperville, Illinois 60566

Keywords: coal liquefaction, coal/residue characterization, coal conversion

ABSTRACT

Martin Lake, Texas lignite typically gives 90-93% conversion in two-stage thermal/catalytic (T/C) liquefaction and 85-90% conversion in two-stage catalytic/catalytic liquefaction (C/C), as demonstrated at Amoco and at the Advanced Coal Liquefaction Facility in Wilsonville, Alabama. To identify the chemical and physical phenomena that underlie this low conversion, Martin Lake lignite and two of its residues, from C/C runs at Amoco, were analyzed by several analytical methods.

The atomic H/C ratio in the solids went through a minimum from 0.86, to 0.78, to 0.90 as conversion increased from 0%, to 64%, and 89%, respectively. Oxygen (wt.%, dry) was lowest in the high-conversion residue, giving 21.2%, 14.3%, and 11.4% at 0%, 64%, and 89% conversion, respectively. X-ray photoelectron spectroscopy (XPS) showed a similar trend of more carbon-oxygen bonds on the surface of unconverted lignite particles. XPS also showed surface enrichment of Ca and Mg with increase in conversion, whereas bulk Ca and Mg remained a constant fraction of the mineral matter. Carbonyl, aliphatic, and aromatic phenol/ether carbons were converted more rapidly than protonated aromatic, substituted aromatic, or bridgehead aromatic carbons, as shown by ^{13}C NMR. Volatile matter remained quite high, 26% (dry), in the high-conversion residue. Petrographic analysis showed a decrease in vitrinites, near-depletion of lipinites, and a sharp increase in the ratio of fusinite to semi-fusinite as conversion increased.

Overall, Martin Lake lignite showed a decrease in the most reactive components as conversion increased, which may explain why conversion slows down at 85-90%. The remaining residue is not totally unreactive, however, suggesting that higher conversion may be possible with the proper process or pretreatment.

INTRODUCTION

Work at Amoco and at the direct coal liquefaction pilot plant facility, operated by the Southern Company Services for the U.S. Department of Energy in Wilsonville, Alabama, has shown that typical conversion for Martin Lake, Texas lignite is in the range of 90-93% for two-stage liquefaction when the first stage reactor is operated at about 825 °F. However, when supported hydrogenation catalyst is used in the first stage, temperatures are kept below 810 °F to preserve catalyst activity. In these cases, coal conversion is only 85-90%. To identify the chemical and physical phenomena that underlie this low conversion, Martin Lake lignite and two of its residues, from runs at Amoco, were characterized using several analytical methods. Our main objective was to investigate the chemical and physical differences between the unreacted, unconverted Martin Lake lignite and converted residue samples after liquefaction. The specific objectives of this work were to find some reasonable answers to the questions of "what are the chemical functionalities involved in the liquefaction of low rank coals" and "why does conversion of low rank coals stop at 85-90% during catalytic/catalytic (C/C) liquefaction."

Three samples were used in this investigation, an unconverted Martin Lake lignite (0% conversion), a residue product from the low conversion process (64% conversion) and a residue product from the high conversion process (89% conversion). The samples were analyzed for elemental analysis (C, H, N, S, and O), proximate analysis (moisture, ash, volatile matter and fixed carbon), bulk

metals by Inductively Coupled Plasma (ICP) spectroscopy, surface minerals by X-ray Photoelectron Spectroscopy (XPS), Scanning Electron Microscopy (SEM), solid state ^{13}C NMR, and IR spectroscopy. Petrographic analysis was also performed.

EXPERIMENTAL

The two Martin Lake lignite residues were obtained from Amoco's AU-51L pilot plant and were the products of the two stage catalytic/catalytic (C/C) liquefaction process with Amocat-1CTM catalyst. Stage 1 and stage 2 process temperatures for low conversion residue were 100 and 740 °F and for the high conversion residue were 790 and 740 °F, respectively. Both residues and unconverted Martin Lake Lignite samples were washed with 40 volumes of THF prior to the analytical work.

The organic carbon, hydrogen and nitrogen content of the samples were measured by a Leco CHN-600 elemental analyzer. Total sulfur and oxygen content of the samples were determined using a Leco SC-132 sulfur analyzer and a Leco RO-478 oxygen determinator, respectively. The values for moisture, ash, volatile matter and fixed carbon of the samples were determined using a Perkin Elmer TGA 7 thermogravimetric analyzer.

The NMR data were obtained on a Chemagnetic M100 solid state NMR spectrometer operating at ^{13}C resonance frequency of 25.15 MHz. Cross-Polarization/Magic Angle Spinning (CP/MAS) technique was used to obtain solid state ^{13}C NMR spectrum. Based upon our previous studies of similar systems, cross-polarization contact time of 1 msec with 1 sec recycle delay were chosen as the best experimental parameters to obtain a quantitative ^{13}C spectrum. Dipolar Dephasing/Magic Angle Spinning (DD/MAS) technique was used to provide quantitative differentiation between quaternary and tertiary aromatic carbons. For the DD/MAS technique a period of 40 μsec was inserted between the end of the cross-polarization sequence and the beginning of the data acquisition, during which the high power proton decoupling field was turned off. In order to avoid linear phase distortions in the spectrum, rotational synchronized spin-echo procedure was used for both CP/MAS and DD/MAS techniques.

Diffused reflectance technique was used to obtain the IR data. Samples for diffuse reflectance infrared spectra were prepared by weighing 0.020 g sample and 0.980 g of KBr into a metal vial and shaking them for one minute on a Wig-L-Bug apparatus. The samples were transferred to the sample holder of a Harrick "Praying Mantis" diffuse reflectance apparatus. Spectra were obtained at 8 cm^{-1} resolution on a Mattson Cygnus 100 spectrometer using an MCT-A detector. A total of 1000 scans were co-added to obtain the final spectra.

A Perkin Elmer model 5400 Small Spot X-ray Photoelectron Spectrometer was used for XPS data collection. The data were obtained using an unmonochromatized radiation source from Mg K_{α} at 1253.6 eV on about 600 μm analysis area. The samples were pressed into pellets before analysis. The SEM data were obtained on a JEOL 840 A Scanning Electron Microscope equipped with a secondary and a Back Scatter Electron (BSE) detector. In addition, a TRACOR NORTHERN 5500 Energy Dispersive X-ray (EDX) system was used to obtain elemental composition of elements with atomic number of 11 or greater. The samples were prepared for SEM analysis by sprinkling them onto a sticky covered SEM stub and then coating them with Au/Pd (60/40) in vacuum evaporator. To expose cross sectional areas of the particles for detailed analysis, the samples were also embedded in a crystal bond compound and then grounded and polished before examination. SEM micrographs were obtained at 100, 500, and 5000 magnification. For microscopic examination of petrographic constituents, the samples were pelletized and polished according to the ASTM D 2797 procedure. The microscopic examinations were carried out at a magnification of 500 diameters, under oil immersion in reflected light illumination.

RESULTS AND DISCUSSION

Process conditions, percent conversion and product quality of Martin Lake lignite after liquefaction are shown in Table 1. Increasing the temperature of the first stage of the process from 100 to 740 °F, the lignite conversion (wt.%) was increased by more than 39% (from 64 to 89%). Most of this increase was in the lighter products such as C1-C3 and C4-360 °F distillate, which increased by 250%, and 360-640 °F distillate, which increased by more than 59%. The amount of product in the 650-975 °F range did not change significantly, and resid (975+ °F) was nearly eliminated.

Proximate analysis (wt.%, dry) and elemental analyses (wt.%, dry-ash-free) of the Martin Lake lignite and its two residues are shown in Table 2. As conversion of the lignite increased, a significant increase was observed in the ash content. This was followed by substantial decreases in the volatile matter (VM) and fixed carbon. Although oxygen content, determined by direct analysis, did not show a significant decrease with increasing lignite conversion, a considerable decrease was observed in the oxygen content calculated by difference, Table 2. The high values for direct oxygen of the residues reported here are believed to be distorted by the oxygen from the water present as moisture in these samples. In any case, the elemental oxygen data suggests a reduction in the oxygenated components during the process. As expected, the atomic H/C ratio was lower for the residue from the 64% converted sample (0.78) compared to the unconverted lignite (0.86). The atomic H/C ratio of the residue from the 89% converted sample, however, did not follow the same trend and increased (0.90). Although it is difficult to explain the increase in atomic H/C ratio, one explanation could be that some solvent is trapped in the residue from high conversion.

Solid state ^{13}C NMR data are shown in Table 3. The structural parameters, assuming 100 carbons per cluster, were derived by using combined CP/MAS and DD/MAS data following the method of Solum et al.¹ In this procedure, linear integration over selected chemical shift ranges of the CP/MAS spectrum provides the relative concentration of different carbon types. Magic angle spinning generates high and low field spinning sidebands from SP^2 carbons. Sideband intensity is appropriately distributed for all SP^2 carbon types. The use of DD/MAS technique permits quantitative differentiation of protonated and bridgehead aromatic carbons. In the 40 μsec time period, for which the proton decoupling field is turned off, all the signal from protonated aromatic carbons is lost while quaternary aromatics lose only about 10% of their signal.² Thus, from the difference in aromatic band intensity between CP/MAS and DD/MAS spectra and accounting for 10% loss in intensity of quaternary carbons, relative concentration of protonated aromatic is calculated. Finally, simple mass balance provides the relative concentration of bridgehead aromatic carbons.

In general, solid state ^{13}C NMR data, in Table 3, indicate that as the lignite conversion increased, the carbon aromaticity increased and the carboxyl groups decreased. The size of condensed aromatic clusters is directly related to the ratio of bridgehead aromatic to ring aromatic carbons, i.e., the fraction of aromatic carbons in the bridgehead position.^{1,3} As an example, for the original lignite (0% conversion), the ratio of bridgehead carbons (12.7) to total ring carbons (54.9) is 0.23, which corresponds to an aromatic cluster slightly bigger than naphthalene. The same ratios for 64% and 89% conversion residues are 0.25 and 0.27, respectively, which corresponds to an aromatic cluster slightly smaller than anthracene. NMR data also indicated an increase in total SP^2 carbons, aromatic carbons, protonated and bridgehead carbons with increasing conversion. Although the data did not show any significant changes in substituted aromatic carbons with increasing conversion, there was a significant decrease in oxygenated functional groups. This clearly suggests that decarboxylation and reduction of phenols/ethers had taken place in the liquefaction process. It should be mentioned that the decrease in oxygenated functional groups was also seen in the data obtained from elemental analysis, IR and XPS spectroscopies.

The carbonyl and C-H stretch regions were analyzed using diffused reflectance IR spectroscopy. IR spectra for the original lignite (0% conversion) and the low conversion (64%) residue are shown in Figure 1. The specific band assignments are based on spectral information compiled by Painter

et al.⁴⁻⁷ A comparison of spectra clearly shows that, while there is very little change in the C-H stretch region with treatment, there is clearly a loss in intensity for the bands in the 1740-1690 cm^{-1} region corresponding to oxygen-containing functional groups. Second derivative analysis of the spectra also indicates an intensity loss in the 1650-1560 cm^{-1} region, this loss is not obvious from the untreated spectra. While the bands near 1740 cm^{-1} and 1720-1690 cm^{-1} region may be attributed to an ester, ketone, aldehyde or carboxyl functional group, the bands in the 1650-1630 and ~ 1600 cm^{-1} are due to the highly conjugated C=O and highly conjugated hydrogen bonded C=O. The band at ~ 1600 cm^{-1} could also be attributed to aromatic ring breathing. The band in the 1590-1560 cm^{-1} is due to the carboxyl group in salt form (COO^-). Figure 2 compares the spectra for the original lignite (0% conversion) and the high conversion (89%) residue. In this case, a change in intensity of the C-H stretch band was seen. Of particular note are the relative decreases in intensity of the aliphatic CH_3 asymmetric stretch near 2960 cm^{-1} and aliphatic CH_2 and CH_3 symmetric stretch near 2850 cm^{-1} ; and the increases in the intensity of aliphatic CH_2 and CH_3 asymmetric stretch near 2925 cm^{-1} and aromatic C-H stretch in the region of 3100-2990 cm^{-1} . Here again, the loss in the intensity of the bands corresponding to the loss of oxygen-containing functional groups can also be observed.

Surface composition (wt.%, relative) obtained by XPS and bulk metal composition obtained by ICP analyses are shown in Tables 4 and 5, respectively. The bulk analysis of the samples by ICP indicated that the major elements in the samples were Si, Fe, Al, Ca, Mg, Na, K and Ti. As was expected, the concentration of these elements increased as the lignite conversion increased. Two important pieces of information were obtained from XPS surface analysis. First, while the relative surface concentration (wt.%) for most of the elements (C, Si, Al, S, N, and Fe) did not change with increasing lignite conversion, the relative surface concentration of two elements (Ca and Mg) increased significantly with increasing conversion. There is some evidence in the literature that cations like Na^+ , K^+ and Ca^{++} are inhibitors in coal pyrolysis^{8, 9}, but are promoter catalysts in coal steam gasification^{10, 11}. Therefore, in coal liquefaction, it is possible that the increase in Ca and Mg at the surface of the reacting lignite particles slows down significantly, or stops, conversion at 85-90%. Second, the electron binding energies obtained from XPS show significant loss of oxygen-containing functional groups during the liquefaction process supporting the data from NMR and IR spectroscopy. Therefore, as the lignite conversion approaches 90%, the remaining residue is a highly aromatic material, hence the conversion slows down considerably.

Maceral compositions obtained from petrographic analysis are shown in Table 6. The data are presented on a mineral-matter-free basis to allow the comparison between the macerals groups vitrinite, inertinite and liptinite. The inertinite maceral group can be subdivided into fusinite, semifusinite, micrinite, macrinite and sclerotinite and the liptinite maceral group can be subdivided into sporinite, resinite and cutinite. Vitrinites and liptinites are considered to be the potentially most reactive macerals. Inertinites, on the other hand, are considered to be unreactive macerals with the exception of semifusinite which may be partially reactive. As expected, the vitrinite macerals (wt.%, mmf) decreased from 58.2 to 51.4 and then to 41.2 as the lignite conversion increased from 0% to 64% and to 89%, respectively. Liptinite macerals also showed the same trend, dropping from 10.0 for the original lignite to 3.5 for the 64% conversion residue and almost to zero (0.4%) for the high conversion residue. Decreases in vitrinite and liptinite macerals were offset by increases in inertinites. However, for the high conversion (89%) residue the relative increase in fusinite was much higher than the increase in semifusinite. This could mean that some of the semifusinite had reacted at high conversion conditions. Petrographic analysis indicated a significant increase in the mineral matter (13.9, 26.4, 52.4%) with increasing lignite conversion. This was expected, due to the disappearance of the reactive macerals with increasing conversion.

SEM also showed changes in morphology of the samples with increasing conversion. The sample from high conversion (85%) is composed of smaller and more porous particles than unconverted

or low conversion (64%) samples. Also, the unconverted and low conversion samples consisted of large organic particles decorated with mineral particles. Large organic particles are not seen in the high conversion sample; mineral and organic phases are intimately mixed.

SUMMARY AND CONCLUSIONS

The NMR data clearly suggests that the main structural transformations during liquefaction of Martin Lake lignite are aliphatic sidechain cracking, decarboxylation, and deoxygenation. Some of the NMR data from Table 3 are shown graphically in Figure 3 to suggest answers for the two questions asked earlier, "what are the chemical functionalities involved in the liquefaction of low rank coals" and "why does conversion of low rank coals stop at 85-90% during catalytic/catalytic (C/C) liquefaction." As the lignite conversion approaches 90%, aliphatic and carbonyl functional groups are depleted. The remaining residue is a highly aromatic material, therefore, the conversion slows down considerably. IR data confirmed the increase in aromatic C-H groups and decrease in aliphatic C-H functional groups. IR also indicated a significant loss of reactive carbonyl functional groups, which may cause slow conversion. Data from XPS analysis indicated that the relative surface concentration of two elements (Ca and Mg) increased significantly with increasing conversion, which could also decrease the reaction rate, and hence, reduce the conversion. The electron binding energies from XPS also showed a decrease in C-O and C=O functional groups during the liquefaction process. Petrographic analysis showed a significant decrease in the reactive macerals (vitrinites and liptinites), sharp increase in the unreactive macerals (inertinites) and partial conversion of semifusinite as conversion increased.

Overall, Martin Lake lignite showed a decrease in the most reactive components as conversion increased, which may explain why conversion slows down at 85-90%. The remaining residue is not totally unreactive, however, suggesting that higher conversion may be possible with the proper process or pretreatment.

REFERENCES

1. Solum, M. S., Pugmire, R. J., and Grant, D. M., *Energy and Fuels*, 3, 1989, 187.
2. Alemany, L. B., Grant, D. M., Pugmire, R. J., Alger, T. D., and Zilm, K. W., *J. Am. Chem. Soc.*, 105, 1983, 2142.
3. Sethi, N. K., Facelli, J. C., Pugmire, R. J., and Grant, D. M., *Analytical Chemistry*, 60, 1988, 1574.
4. Painter, P. C., Coleman, M. M., Jenkins, R. G., and Walker, P. L., Jr., *Fuel*, 57, 1978, 125.
5. Painter, P. C., Coleman, M. M., Jenkins, R. G., Whang, P. W., and Walker, P. L., Jr., *Fuel*, 57, 1978, 337.
6. Painter, P. C., Snyder, R. W., Starsinic, M., Coleman, M. M., Kuehn, D. W., and Davis, A., *Applied Spectroscopy*, 35, 1981, 475.
7. Painter, P. C., Starsinic, M., and Coleman, M. M., "Determination of Functional Group in Coal by Fourier Transform Interferometry" in *Fourier Transform Infrared Spectroscopy*, Ferraro, J. R. and Basile, L. J., eds, vol. 4, 1985, Academic Press, N. Y.
8. Tyler, R. J., *Fuel*, 58, 1979, 680.
9. Tyler, R. J., and Schafer H. N., *Fuel*, 59, 1980, 487.
10. Hengel, T. D., and Walker, P. L., Jr., *Fuel*, 63, 1984, 1214.
11. Linares-Solano, A., Hippo, E. J., and Walker, P. L., Jr., *Fuel*, 65, 1986, 776.

ACKNOWLEDGEMENTS

The authors would like to thank Dr. K. Kuehn of Western Kentucky University for the petrographic analysis and interpretation of the petrographic data. We also would like to thank J. Schreiner and P. Hruskoci of Analytical Research and Services at Amoco Corporation for the XPS and SEM analyses. We are grateful to R. Lumpkin and J. Joseph for their helpful comments in reviewing this work. The contribution of D. Maciejewski and E. Hauber to this work are also greatly appreciated.

Table 1.

Process Conditions and Product Quality Data for Martin Lake Lignite

<u>Conditions and Products</u>	<u>Lignite Conversion</u>		
	<u>0</u>	<u>64</u>	<u>89</u>
Stage 1 Temperature, °F	Unreacted	100	790
Stage 2 Temperature, °F	Lignite	740	740
C1-C3, wt. %		3.4	10.1
C4-360 °F, wt. %		3.9	13.7
360-650 °F, wt. %		24.4	38.8
650-975 °F, wt. %		8.8	9.5
975+ °F, wt. %		9.8	1.0
H ₂ Consumption, wt. %		7.8	8.6

Table 2.

Proximate and Elemental Analyses Data Obtained for Martin Lake Lignite and the Converted Residues

<u>Proximate Analysis (wt.%, dry)</u>	<u>Lignite Conversion</u>		
	<u>0</u>	<u>64</u>	<u>89</u>
Moisture ^a	2.35	3.59	1.52
Ash	13.35	25.93	43.57
Volatile Matter	42.89	32.57	26.13
Fixed Carbon	43.76	41.50	30.30
<u>Elemental Analysis (wt.%, dry-ash-free)</u>			
Carbon	70.90	76.55	76.12
Hydrogen	5.11	5.03	5.76
Nitrogen	1.22	1.62	1.46
Sulfur	1.60	2.52	5.22
Oxygen (by difference)	21.17	14.28	11.44
Oxygen (direct)	21.76	18.20	17.98
H/C (atomic ratio)	0.86	0.78	0.90

^aMoisture values are on as-received basis.

Table 3.

Solid State ^{13}C NMR Data for Martin Lake Lignite and the Converted Residues

Structural Parameters	Lignite Conversion		
	<u>0</u>	<u>64</u>	<u>89</u>
Carbon Types (total = 100)			
Total SP ²	64.1	73.3	80.3
-- Carbonyl	9.0	6.0	6.0
-- Ring Aromatic	54.9	66.7	73.8
* Phenolic/Ethers	9.7	9.4	8.9
* Protonated	19.8	25.9	29.1
* Substituted	12.8	14.9	15.9
* Bridgehead	12.7	16.6	19.9
Total SP ³	35.9	26.7	19.7
# Bridgehead / # Rings	0.23	0.25	0.27
# Carbons / Cluster	10	11	12

Table 4.

Surface Composition (wt.%, Relative) Data from XPS Analysis of Martin Lake Lignite and the Converted Residues

Lignite Conversion	O	C	Si	Al	S	N	Fe	Ca	Mg
<u>0</u>	30.4	52.0	8.1	5.6	0.4	0.9	1.0	0.7	0.9
<u>64</u>	24.0	57.1	8.2	4.7	0.1	1.2	0.8	1.9	1.7
<u>89</u>	24.7	55.8	7.3	5.2	0.4	1.0	1.0	2.5	1.8

Table 5.

Metal Composition (Wt.%) Data from ICP Analysis of Martin Lake Lignite and the Converted Residues

<u>Lignite Conversion</u>	<u>Mg</u>	<u>Ca</u>	<u>Al</u>	<u>Si</u>	<u>Fe</u>	<u>Na</u>	<u>K</u>	<u>Ti</u>	<u>Sr</u>
0	0.26	1.08	1.16	2.91	1.23	0.07	0.06	0.08	0.03
64	0.51	2.34	2.43	5.40	2.70	0.13	0.11	0.15	0.07
89	0.71	3.80	3.81	7.60	4.70	0.19	0.18	0.22	0.10

Table 6.

Maceral Composition Obtained from Petrographic Analysis of Martin Lake Lignite and the Converted Residues

<u>Macerals (wt.%, mineral-matter-free)</u>	<u>Lignite Conversion</u>		
	<u>0</u>	<u>64</u>	<u>89</u>
Vitrinites	58.2	51.4	41.2
Inertinites	29.2	44.3	58.4
* Fusinite	2.3	3.8	16.7
* Semifusinite	22.7	36.4	32.8
* Micrinite	2.6	3.3	7.6
* Macrinite	1.4	0.8	1.3
* Sclerotinite	0.2	0.0	0.0
Liptinite	12.6	4.3	0.4
* Sporinite	10.0	3.5	0.4
* Resinite	2.1	0.8	0.0
* Cutinite	0.5	0.0	0.0

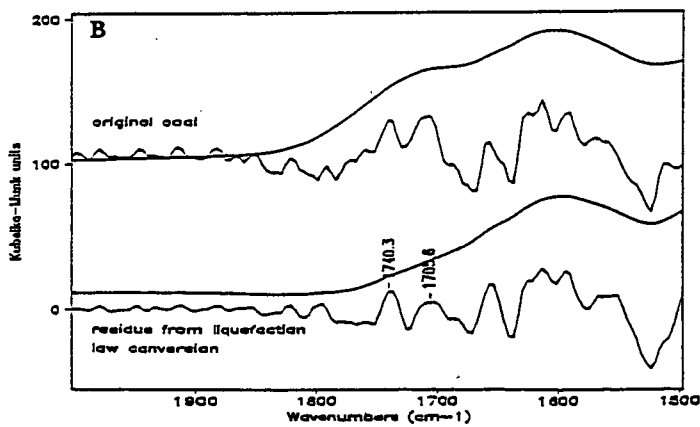
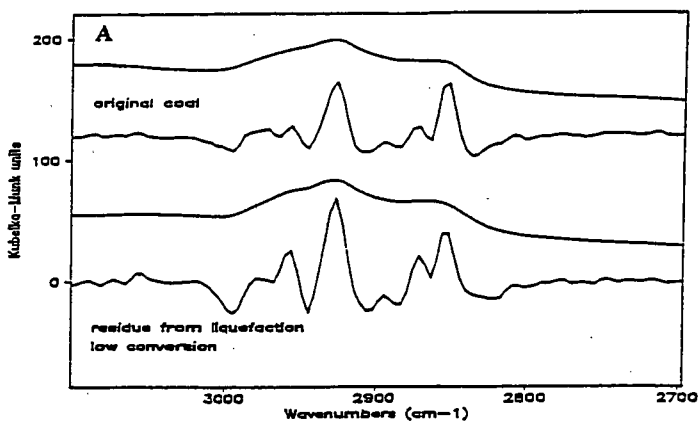


Figure 1. Infrared Spectrum for Martin Lake Lignite Coal and Low Conversion Residue. A) C-H Stretch; B) C=O Stretch.

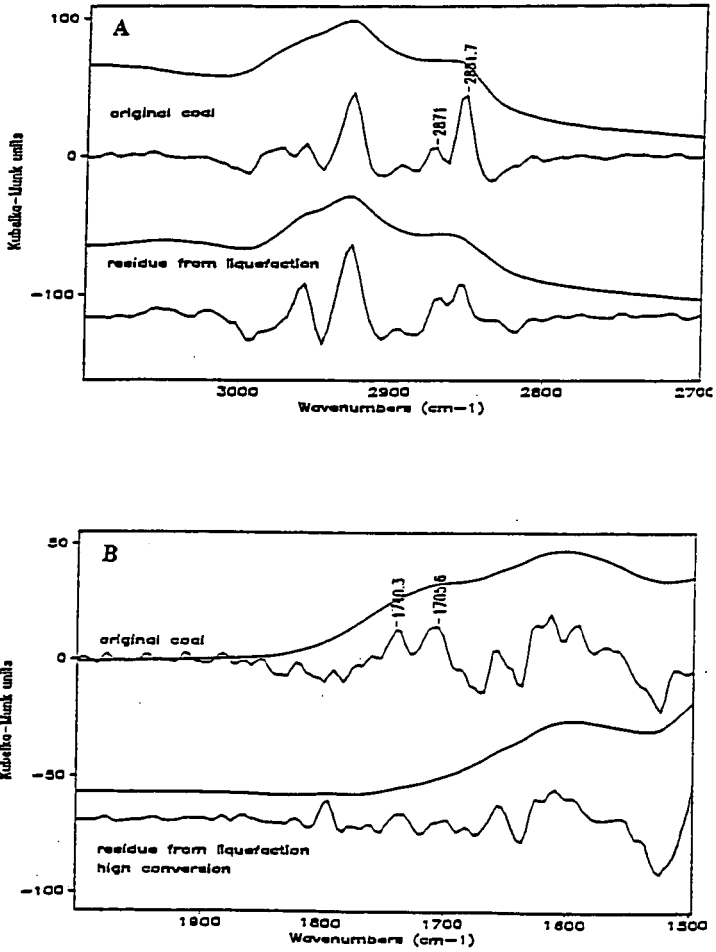
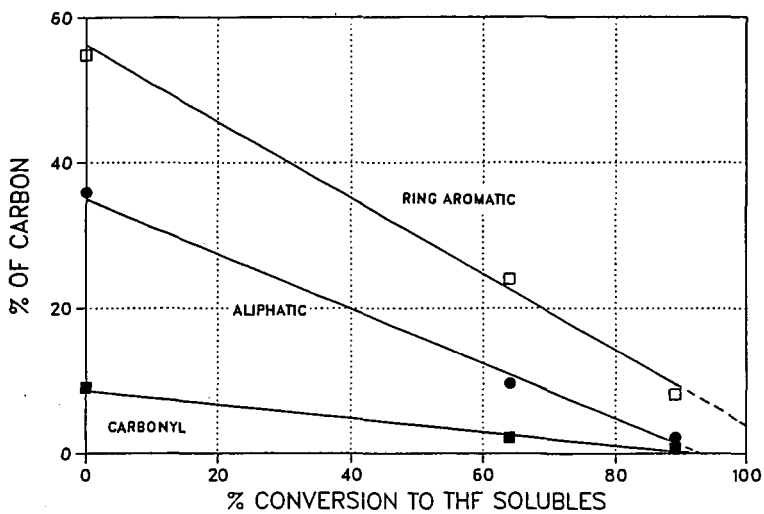


Figure 2. Infrared Spectrum for Martin Lake Lignite Coal and High Conversion Residue. A) C-H Stretch; B) C=O Stretch.

Figure 3. Carbon Types in Unconverted Martin Lake Lignite by C^{13} NMR



SOLUBILIZATION OF HIGH RANK POCAHONTAS NO. 3 COAL

Kuntal Chatterjee and Leon M. Stock
Chemistry Division
Argonne National Laboratory
9700 South Cass Avenue
Argonne, Illinois 60439.

INTRODUCTION

Reductive and non-reductive alkylation reactions are efficient methods of coal solubilization (1). C-Alkylation reactions using the strongly basic mixture of *n*-butyllithium and potassium *tert*-butoxide (called Lochmann's base) were successful for the near quantitative solubilization of Lower Kittanning coal (2). This contribution concerns the use of this reagent to promote C-alkylation of a high rank coal, Pocahontas No. 3, from the Premium Sample Program of Argonne National Laboratory. Evidence will also be presented to show that, apart from promoting C-alkylation, the basic reagent can alter the coal macromolecular structure by forming smaller fragments through hydrocarbon β -elimination reactions.

EXPERIMENTAL SECTION.

Materials. Pocahontas No. 3 coal, APCSP 5, was supplied by the Premium Sample Program of the Argonne National Laboratory (Anal. C, 91.1; H, 4.4;

N, 1.3; S, 0.5; O (by difference) 2.7; ash 4.7). The coal samples were dried at 110 °C under vacuum for 48 h prior to use.

n-Heptane (Aldrich) was shaken with concentrated sulfuric acid and subsequently distilled. The purified solvent was stored in the presence of molecular sieve 5A. Pyridine was purified by distillation over barium oxide. The alkyl iodides were obtained from Aldrich and were dried over molecular sieve 5A. The other chemicals such as *n*-butyllithium (1.6 M solution in hexane), potassium *tert*-butoxide, ammonium chloride and methanol were used as received from Aldrich Chemical Company.

Reaction Procedure for the Coal Sample. The C-alkylation reactions of the coal sample were carried out as reported earlier (2,3). *n*-Heptane (170 mL), potassium *tert*-butoxide (5.01g, 45 mmol) and *n*-butyllithium (30 mL, 1.6 M solution in hexane, 48 mmol) were added to a flame dried flask. The mixture was stirred at room temperature for 15 min, the coal sample (1g) was added, and the solution was refluxed for 6 h. The initial black solution turned brown when refluxing began. The alkyl iodide (55 to 60 mmol) was added dropwise to this coal anion suspension, after cooling the flask at 0 °C. The mixture was stirred for 48 h at room temperature to ensure complete alkylation of the coal anions. The residual base was quenched by adding ammonium-chloride and methanol. The solvents were removed by a rotary evaporator. The product was carefully collected and washed with an acidic solution of water and methanol (3:1 by volume), aqueous methanol (3:1, 20 L) and *n*-hexane (4L). The product was dried to constant weight at 110 °C under vacuum for 48 h. A portion of each of the product was subjected to Soxhlet extraction with pyridine.

In order to investigate bond cleavage reactions with bases, the coal anions were quenched with dilute acids instead of alkyl halides. The products thus obtained were washed and dried as usual and were subjected to pyridine extractions. In order to establish the optimum conditions for solubilization, the reaction conditions, the nature of base used, and the length of the alkyl group in the alkyl iodide were varied. The results are presented in the Tables.

RESULTS

The C-alkylation reaction of Pocahontas No. 3 coal (APCSP 5) with sodium amide in liquid ammonia was studied first. Previous work in our laboratory using sodium amide in liquid ammonia with another high rank coal, Lower Kittanning coal, PSOC 1197, gave significantly soluble alkylated products (4). As shown in Table I, the solubility of the products increased with an increase in length of the alkyl group. With 45 mmol of the base per gram of coal, the octylated product was about 38% soluble in pyridine. It should be mentioned that the raw coal is only 5% soluble in pyridine.

The solubility of the products increased when the base concentration was increased. With 15 mmol of sodium amide, the butylated product was only 13% soluble whereas with 200 mmol of the base, the butylated product was 46% soluble.

When a stronger base was used to alkylate this coal, better results were obtained. The results of Lochmann's base promoted C-alkylations of Pocahontas No. 3 are summarized in Table II.

When the coal was treated with Lochmann's base in refluxing heptane for 6 h and quenched with methyl iodide, the product was 45% soluble in pyridine (compared to only 12% with sodium amide). However, when the coal was butylated with *n*-butyl iodide, the solubility of the product remained at 45%. In addition, when the coal was refluxed with the base for 18 h instead of 6 h, a 10% increase in solubility was observed. Once again both the butylated and octylated products gave the same solubility (55%).

We next probed for the occurrence of carbon-carbon bond cleavage reactions with very strong bases. The results are shown in Table III. Use of sodium amide in liquid ammonia at -75 °C, *n*-butyllithium at 98 °C, potassium *tert*-butoxide at 98 °C and Lochmann's base at 98 °C show that only Lochmann's base provides any evidence for C-C bond cleavage.

DISCUSSION

Non-reductive C-alkylation reactions of Pocahontas No. 3 coal with sodium amide in liquid ammonia convert the 5% soluble coal to a material which is 46% soluble. The increase in solubility with the increase in the size of alkyl group is in agreement with our previous results (4). The larger groups can disrupt the intermolecular polarization forces thereby enhancing solubility. However, the fact that a higher concentration of the base enhances the solubility to a greater extent suggested that other factors are also important.

Lochmann's base appears to be a superior reagent for the conversion of the coal into soluble materials. The extent of solubilization is

virtually independent of the size of the alkyl group, and the methylated and butylated products are equally soluble. When the coal was treated with the base for 18 rather than 6 hours, there was a modest enhancement in the solubility of the product.

The results in Table III suggested that a prominent reason for the high solubility of the products obtained after Lochmann's base are due to carbon-carbon bond cleavage. When the coal sample was treated with Lochmann's base in refluxing heptane and quenched with dilute acid, the solubility of the coal increased from 5% to about 35% depending on the time of reaction. Thus base treatment alone can convert the coal to soluble materials. We infer that the strong base forms carbanions that can fragment via β -elimination as previously proposed (1(B), 5).

CONCLUSION

The Lochmann's base system is more effective than any other base system for the C-alkylation and solubilization of high rank Pocahontas No. 3 coal. Our results suggest that coal carbanions undergo fragmentation to reduce the molecular dimensions. The solubility realized by these fragmentation reactions is enhanced by C-alkylation reactions.

ACKNOWLEDGEMENT

We acknowledge the support of this work from the Office of Basic Energy Sciences, Division of Chemical Sciences, U. S. Department of Energy.

REFERENCES

1. (A) Davidson, R. M. *Coal Sci.*, 1982, **1**, 84-160; (B) Stock, L. M. *Coal Sci.*, 1982, **1**, 161-282.
2. Chatterjee, K.; Miyake, M.; and Stock, L. M. *Energy & Fuels*, 1990, **4**, 242-248.
3. Chatterjee, K.; Miyake, M.; and Stock, L. M. *Prep. pap. Am. Chem. Soc., Div. Fuel Chem.*, 1990, **35(1)**, 46-50.
4. Miyake, M. and Stock, L. M. *Energy & Fuels*, 1988, **2**, 815-818.
5. Chatterjee, K., Ph.D. Dissertation, The University of Chicago, 1990.

Table I. The C-alkylation of Pocahontas No. 3 coal with sodium amide in liquid ammonia.

reaction conditions: base, solvent, temperature, time	electrophile	solubility, wt% in pyridine
raw coal	-	5
coal ; NaNH ₂ (45 mmol / g), NH ₃ (l), -75 °C, 6 h	CH ₃ I	12
coal ; NaNH ₂ (45 mmol / g), NH ₃ (l), -75 °C, 6 h	<i>n</i> -C ₄ H ₉ I	21
coal ; NaNH ₂ (45 mmol / g), NH ₃ (l), -75 °C, 6 h	<i>n</i> -C ₈ H ₁₇ I	38
coal ; NaNH ₂ (15 mmol / g), NH ₃ (l), -75 °C, 6 h	<i>n</i> -C ₄ H ₉ I	13
coal ; NaNH ₂ (100 mmol / g), NH ₃ (l), -75 °C, 6 h	<i>n</i> -C ₄ H ₉ I	31
coal ; NaNH ₂ (200 mmol / g), NH ₃ (l), -75 °C, 6 h	<i>n</i> -C ₄ H ₉ I	46

Table II. The C-alkylation of Pocahontas No. 3 coal with Lochmann's base.

reaction conditions: base, solvent, temperature, time	electrophile	solubility, wt% in pyridine
raw coal	-	5
coal; <i>n</i> -BuLi + <i>Kr</i> -OBu (1:1), heptane, 98 °C, 6 h	CH ₃ I	45
coal; <i>n</i> -BuLi + <i>Kr</i> -OBu (1:1), heptane, 98 °C, 6 h	<i>n</i> -C ₄ H ₉ I	45
coal; <i>n</i> -BuLi + <i>Kr</i> -OBu (1:1), heptane, 98 °C, 18 h	<i>n</i> -C ₄ H ₉ I	55
coal; <i>n</i> -BuLi + <i>Kr</i> -OBu (1:1), heptane, 98 °C, 18 h	<i>n</i> -C ₈ H ₁₇ I	55

Table III. Base promoted solubilization reactions of Pocahontas No. 3 coal.

reaction conditions	product recovered, %	solubility, wt% in pyridine
raw coal	-	5
coal ; NaNH ₂ (45 mmol / g), NH ₃ (l), -75 °C, 6 h, protonation	92	5
coal ; NaNH ₂ (100 mmol / g), NH ₃ (l), -75 °C, 6 h, protonation	99	9
coal ; <i>n</i> -BuLi (45 mmol / g), heptane, 98 °C, 6 h, protonation	89	8
coal ; <i>Kt</i> -OBu (45 mmol / g), heptane, 98 °C, 6 h, protonation	91	10
coal ; Lochmann's base (45 mmol / g), heptane, 98 °C, 6 h, protonation	88	32
coal; Lochmann's base (45 mmol /g) heptane, 98 °C, 18 h, protonation	105	39

COAL LIQUEFACTION WITH MODEL SOLVENTS CONTAINING HYDROPHENANTHRENS AND/OR HYDROPYRENES

Kevin Bate* and Graham Harrison

Department of Applied Sciences,
Staffordshire Polytechnic,
College Road,
Stoke-on-Trent,
ST4 2DE UK.

*now at Point of Ayr, Coal Liquefaction Project,
Flynngroew, Clwyd, North Wales, CH8 9JJ

Keywords: H-donors, hydrophenanthrenes, hydropyrenes.

INTRODUCTION

The importance of the quality of the solvent in coal liquefaction is well known. Model solvent studies have helped to characterise and elucidate reactions occurring during coal liquefaction, particularly coal dissolution but have been limited in that the model solvents chosen have not been very representative of actual process solvents. Tetralin, the model solvent often used, is unlikely to be present in a significant concentration in recycle solvents which tend to contain mainly three and four ring compounds. Studies using hydroaromatic compounds with three and four rings are more representative but again hardly represent the complex nature of recycle solvents. Consequently, there is a need to undertake studies using more complex model solvents, particularly to evaluate the contribution from individual hydrogen donors to coal dissolution.

EXPERIMENTAL

Samples of hydrogenated phenanthrene and hydrogenated pyrene were obtained by hydrogenating the parent aromatic compound using a CoMo catalyst under a high hydrogen overpressure at elevated temperatures. Some variation in reaction conditions did apply but typical conditions were: 200 bar H₂ at 400°C for 2h, 100g of aromatic and 5g of 3% Co/15% Mo catalyst. All hydrogenations were conducted in a spinning/falling basket autoclave with the catalyst contained in a squat wire mesh basket as described previously (1).

Coal dissolution experiments were also carried out in the spinning/falling basket autoclave. The experiments used 300g of solvent and 150 g of air dried Point of Ayr coal (supplied by CRE), mainly at 420°C with variation in run times from 1 to 6h. The proximate (mass %, air dried) and ultimate (mass%, dmmf) analyses of the coal sample were: proximate - ash 15.9, moisture 3.5 and volatiles 27.8%; and ultimate - carbon 84.6, hydrogen 4.6, nitrogen 1.3, sulphur 1.3 and oxygen (by difference) 8.2%. The solvents used were denoted as follows: solvent A - hydrogenated phenanthrene; solvent B - 50 mass % hydrogenated phenanthrene plus 50 mass % phenanthrene; solvent C - 50 mass %, hydrogenated phenanthrene plus 50 mass % pyrene; solvent D - hydrogenated pyrene; and solvent E - 50 mass % hydrogenated pyrene plus 50 mass % hydrogenated phenanthrene.

After the dissolutions, undissolved material was removed by elevated pressure filtration (2 bar N₂ at 200°C) through a special unit described elsewhere(2). The filter cakes were washed with dichloromethane (DCM) to remove entrained solvent at a DCM cake ratio of 5:1; the solvent was removed by vacuum filtration and the cake was washed with further portions of

DCM until the washings were colourless. Samples of dried washed filter cakes were analysed for their ash contents using a Leco Proximate Analyser.

The filtered coal liquid was separated by solvent fractionation into toluene-insoluble, toluene-soluble/hexane insoluble and hexane-soluble materials. The hexane-soluble materials were analysed by gc using an OV101 capillary column contained in a Perkin-Elmer Sigma 3B Chromatograph equipped with 'on-column' injection. Similar gc analysis was carried out on the starting solvents dissolved in hexane.

RESULTS AND DISCUSSION

Analysis of Solvents

The results of the quantitative gc analysis of the five model solvents are shown in table 1. The contents of the various hydroaromatics of phenanthrene and pyrene, including the separate geometric isomers as well as peaks characterised as products from cracking reactions during the hydrogenations (butyltetralin and biphenyl) have been quantified. Characterisation of the chromatograms made use of marker compounds and gc.ms information supplied by CRE. Unfortunately the peaks for the two geometric isomers of H₆Py and H₁₀Py could not be attributed to the specific isomers and are referred to as H₆Py¹, H₆Py², H₁₀Py¹ and H₁₀Py².

In figure 1, the chromatogram of the most complex of the solvents (solvent E) is compared with that of a batch of recycle solvent (supplied by CRE). Although there was a difference in the ramp rates for the temperature programme for the two chromatograms (5°C min⁻¹ for the recycle solvent, 8°C min⁻¹ for solvent E), it is apparent that many of the peaks for the recycle solvent chromatogram were in common with those for the solvent E chromatogram, showing that solvent E would be very representative of an actual process solvent.

Coal Dissolution - Comparison of Solvent Performances

The solvents were compared in a series of coal dissolution experiments conducted at 420°C for different times. The results for solvents A, B, D and E are illustrated graphically in figure 2. For solvent C only 2h duplicate experiments were conducted, giving dissolutions (calculated by ash balance and expressed on 'daf' basis) of 69.2 and 69.4%; duplicate experiments were also carried out the solvent A for the 2h run and gave identical dissolutions of 72.4%. In spite of the excellent repeatability of the results, it is considered that the value for solvent D at 2h was abnormally high.

The total hydrogen donor contents of the starting solvents were evaluated from their gas chromatograms. For the recycle solvents fractions after dissolution, it was assumed that the hexane-soluble material contained the recycle solvent only and hence their hydrogen donor contents were determined from the chromatograms of the hexane-soluble fractions see (figure 3). This assumption was reasonable since the starting solvents were soluble in hexane (>99.5%) but most of the coal fragments produced during dissolution would not be and mass balance calculation on the solubility results indicated that the proportion extracted by hexane corresponded well with the mass of solvent in the dissolution.

After one hour, solvent A (hydrophenanthrenes) dissolved 62.4% of 'daf' coal and its H-donor content was reduced from 2.3 to 1.4% i.e. by 39%. For solvent D after one hour, the H-donor content was reduced by 61% from 1.8 to 0.7% for a dissolution of 72.4%. After 4h dissolution with solvent A, dissolution increased to 72.4% but donor depletion was only 57%. Hence hydrophenanthrenes induced a higher dissolution after 1h but used more of their H-donor content to produce the same dissolution, probably as a result of producing wasteful hydrogen gas through dehydrogenation without utilising the hydrogen for capping radicals.

Solvent E, which contained both hydrophenanthrenes and hydrophenyrenes, effected about the same dissolution as solvent D after 1h (71.9 vs. 72.4%) but utilised less of its H-donor content (49 vs 61%). Solvent B, which only has an initial H-donor content of 1.15%, showed the lowest dissolution (57.3% after 2h) whereas solvent C with the same initial H-donor content provided a dissolution of 69.2% after 2h. Therefore the addition of phenyrenes to hydrophenanthrenes induces a greater dissolution than the addition of phenanthrene, probable

because pyrene is more able to promote H-shuttling. The improved dissolution with solvent C was at the expense of a higher H-donor depletion (61 vs. 52%).

Coal Dissolution - Depletion of Individual Donors.

The variation of the contents of hydrophenanthrenes and phenanthrene with time is depicted in Figure 4 for solvents A and E. Figure 5 shows similar plots for the hydropyrenes and pyrene for solvents E and D. The general trends in figure 3 are: a gradual rise on the phenanthrene content becoming linear after the first hour; a rapid fall on the H₂P and s-HgP contents, particularly over the first hour, an initial rise in the content of H₄P (due to it being produced from the dehydrogenation of s-HgP more rapidly than it being lost by dehydrogenation to H₂P) followed by a gradual fall; an almost constant (solvent E) or small decrease (solvent A) in the content of a-HgP. The initial rapid decrease in the contents of s-HgP and H₂P corresponded with the initial increase in the phenanthrene contents and the decrease was more rapid for solvent A because of the absence of hydropyrenes which appear to have a larger contribution than hydropyrenes in the early stages of dissolution.

The general trends in figure 4 are: a rapid increase in the pyrene content over the first hour after which the pyrene content seemed to approach a constant value; a rapid decrease in the contents of H₄Py, the two H₆Py isomers and the two H₁₀Py isomers; and an initial decrease in the content of H₂Py after which there was a tendency to approach a constant value, mirroring the Py content and suggesting that an equilibrium ratio of H₂Py:Py was being approached.

Table 2 shows the percentage relative depletions of the various hydrogen donors for solvent E over 1h. It can be seen that, apart from H₂Py, the hydropyrenes were depleted by similar extents and to much larger extents than the hydrophenanthrenes. Therefore most of the hydropyrene contents in the recycle solvent fraction will be lost more readily than the hydrophenanthrene contents and, after the early stages of dissolution, the only hydropyrene remaining in a significant amount will be H₂Py. For the hydrophenanthrenes, the H₂P and s-HgP contents despite being reduced quite quickly will still be in sufficient quantities to provide a supply of donor hydrogen after most of the hydropyrene content has been used. The concentration of a-HgP was not reduced, indicating it has a higher stability towards dehydrogenation. However, its content might become important in the later stages of dissolution when its rate of dehydrogenation might be sufficiently fast to provide hydrogen for capping the radicals produced from cleavage of the more stable bonds bridging aromatic centres.

In a two-stage liquefaction process, bridging bonds surviving dissolution will be mainly catalytically cracked and stabilisation of the carbocations produced should come from the hydrogen held as hydrides at the catalyst surface not demanding any solvent H-donation. However, the second stage is often operated at higher temperatures and some thermally promoted cracking might take place in the bulk phase in which case the likely presence of the donors H₂Py and a-HgP could become important for further radical stabilisation.

CONCLUSIONS

The rate of coal dissolution is improved by the presence of hydropyrenes but these hydroaromatic compounds utilise more of their hydrogen donor contents than do hydrophenanthrenes for the same level of dissolution. The best solvent is one containing both hydrophenanthrenes and hydropyrenes and generally the contents of these compounds in actual process recycle solvent are high. Most of the coal is dissolved in the early stages and thereafter further dissolution becomes expensive in terms of consumption of hydrogen donors i.e. most of the donors are dehydrogenating at a much faster than the production of free radicals resulting in the generation of wasteful hydrogen gas. Therefore it might be economic to sacrifice some coal dissolution in order to maintain a better solvent quality.

Certain donors will be depleted more rapidly than others and, if dissolution starts to decrease with solvent recycle, it could be that the contents of the "faster donors" are not being properly made up during solvent rehydrogenation in the second stage rather than overhydrogenation of the solvent to saturates. Consequently it is important not only to monitor the total hydrogen donor content of the solvent but also to analyse the solvent for its content of the various

hydropyrenes and hydrophenanthrenes, a task that should be possible by gc analysis of the solvent. Based on these assessments it should be possible to control the second stage conditions to ensure the current balance between hydrogenation and hydrocracking.

References

1. Doughty, P.W., PhD Thesis, Staffordshire Polytechnic (CNA), April 1988
2. Bate, R., PhD Thesis, Staffordshire Polytechnic (CNA), September 1990.

Compound	Composition (mass %)				
	A	B	C	D	E
P	23.0	61.5	11.5		11.7
H ₂ P	2.2	1.1	1.1		1.1
H ₄ P	17.8	8.9	8.9		9.0
s-H ₈ P	27.9	14.0	14.0	2.1	14.8
a-H ₈ P	11.6	5.8	5.8		5.8
iso-H ₈ P	2.8	1.4	1.4		1.6
H ₁₄ P	3.6	1.8	1.8		2.0
Py			50.0	29.3	14.9
H ₂ Py				18.6	9.5
H ₄ Py				3.6	1.9
H ₆ Py ¹				18.7	9.5
H ₆ Py ²				13.4	7.0
H ₁₀ Py ¹				7.1	3.7
H ₁₀ Py ²				3.9	1.9
BT	2.8		1.4		1.3
BP	1.3		0.6		0.6
T	0.2		1.1		

Table 1. Composition of Model Solvents by G.C

P - phenanthrene, H₂P - dihydrophenanthrene, H₄P - tetrahydrophenanthrene
s - H₈P - sym - octahydrophenanthrene, a - H₈P - antisym - octahydrophenanthrene
iso-H₈P - isomerised octahydrophenanthrene, H₁₄P - perhydrophenanthrene
Py-pyrene, H₂Py - dihydropyrene, H₄Py - tetrahydropyrene, H₆Py¹, H₆Py² -
hexahydropyrene, H₁₀Py² - decahydropyrene, BT - butyltetralin, BP - biphenyl, T - tetralin.

Relative Depletion (%)

Hydrophenanthrenes				Hydropyrenes							
H ₂ P,	H ₄ P,	s - H ₈ P,	a - H ₈ P	H ₂ Py,	H ₄ Py,	H ₆ Py ¹ ,	H ₆ Py ² ,	H ₁₀ Py ¹ ,	H ₁₀ Py ²		
54.5	-3.3	50.0	0	51.6	89.5	85.3	88.7	89.2	89.5		

Table 2. Percentage Relative Depletions of Individual H-donors for Solvent E Over One Hour

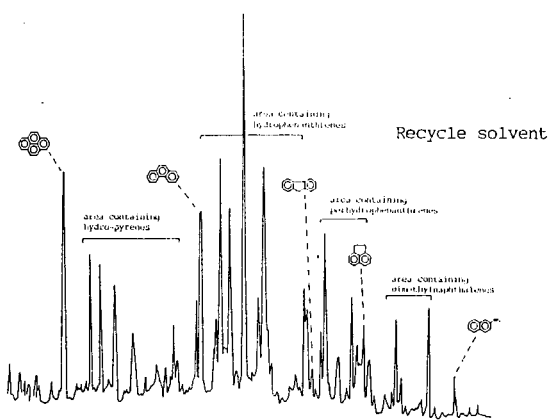
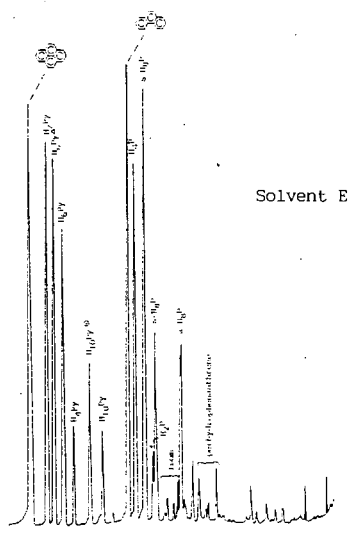


Figure 1. Gas chromatogram for solvent E (ramp rate $8^{\circ}\text{C min}^{-1}$) and a recycle solvent (ramp rate $5^{\circ}\text{C min}^{-1}$)

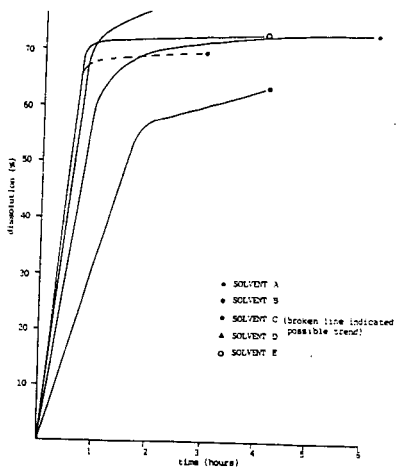


Figure 2. Plots of percentage dissolution vs time for the five model solvents A-E

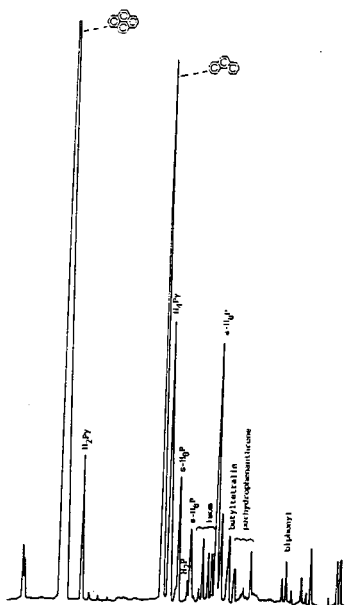


Figure 3. Gas chromatogram of a hexane-soluble material fraction of a coal liquid

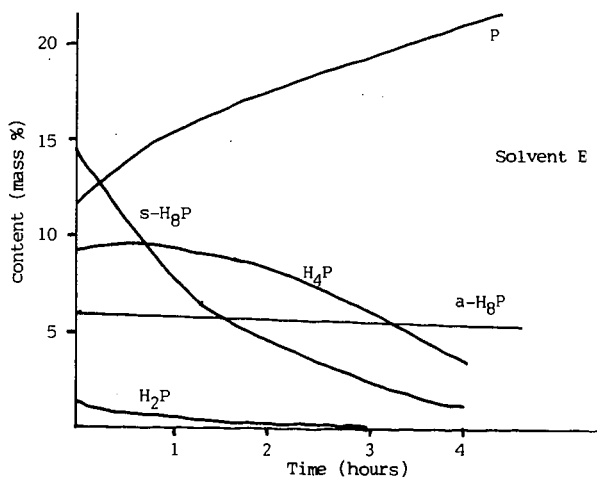
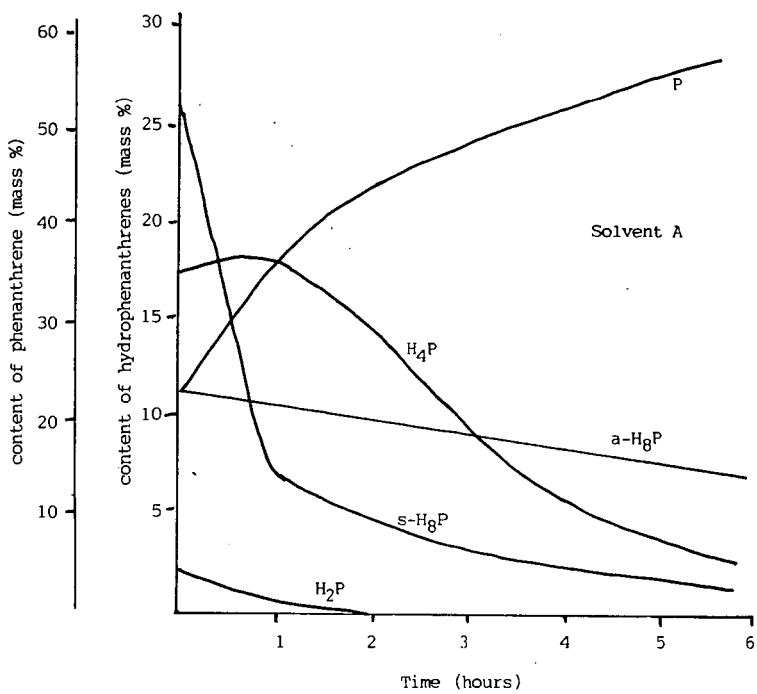


Figure 4. Variation of contents of phenanthrene and hydrophenanthrenes with dissolution time for solvents E (bottom) and A (top).

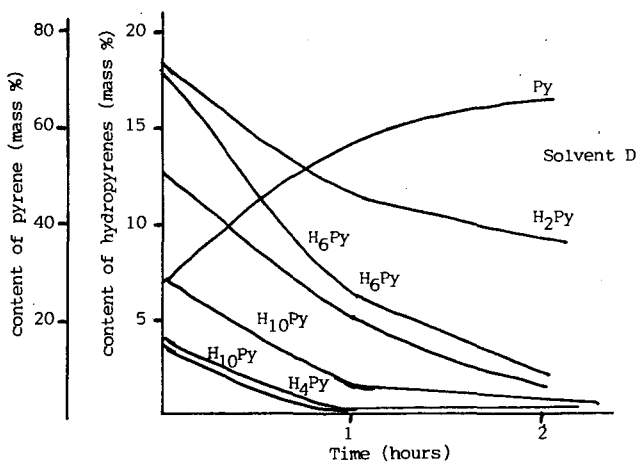
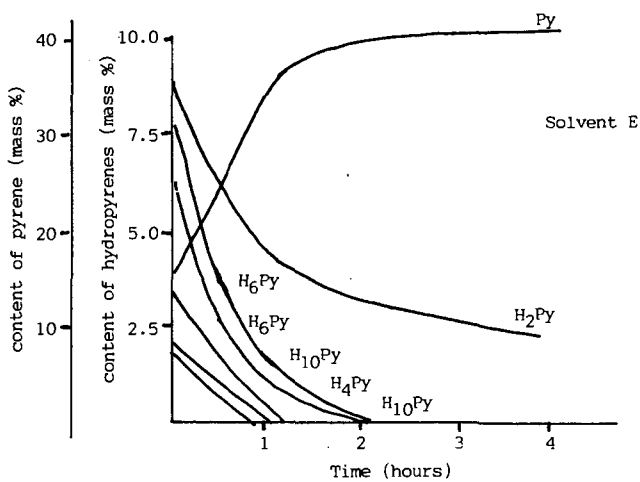


Figure 5. Variation of contents of pyrene and hydroxyrenes with dissolution time for solvents D (bottom) and E (top)

CLEAVAGE OF BENZYLAROMATICS AND THEIR RELEVANCE TO COAL CONVERSION

D. F. McMillen, R. Malhotra, and D. S. Tse
Chemical Kinetics Department, SRI International, Menlo Park, California 94025.

KEYWORDS: Mechanism, Liquefaction, Hydrogen-transfer, RHT, Bond-Cleavage.

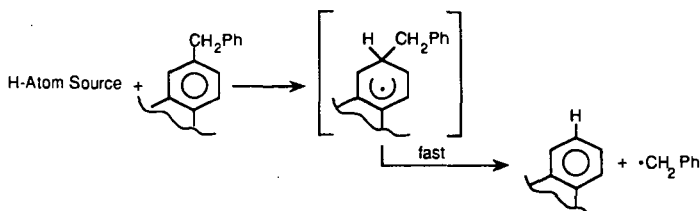
INTRODUCTION

The modes by which bonds are cleaved during coal liquefaction continues to be a subject of controversy, not only because the nature of the "critical" linkages in coals are not known with any certainty, but also because the detailed nature of some of the hydrogen-transfer reactions that lead to cleavage is still not fully understood. It is now fairly well agreed that ipso hydrogen displacement not involving free H-atoms can result in the cleavage of some coal-like structures under liquefaction conditions (1-8). However, it is still a matter of debate whether such cleavage is (a) general for linkages to aromatic rings, (b) significant for coal liquefaction, and (c) takes place by the radical hydrogen-transfer (RHT) process, as has been claimed (1). In this paper we present data that indicate that cleavage not involving free H-atoms (i.e., a solvent-mediated hydrogenolysis) is general for linkages to aromatic rings (though at rates which vary widely with the nature of the ring system). We also discuss, in the light of this recent data, some previously reported results that suggest such cleavages are indeed significant in coal liquefaction. Finally, we discuss those mechanistic alternatives to an actual RHT process that have not been eliminated by previous results. We defer all discussion of RHT itself or its specific mechanistic alternatives until the questions of generality of solvent mediated hydrogenolysis and its relevance to coal liquefaction have first been considered.

RESULTS AND DISCUSSION

Cleavage of Benzylaromatics. Figure 1 shows the measured rates of ipso-displacement of benzyl groups from arenes containing one to four aromatic rings in a 1:1 mixture of anthracene and 9,10-dihydroanthracene at 400°C. These experiments were performed in sealed fused-silica ampoules containing 10 wt% substrate in a 1:1 anthracene/dihydroanthracene mixture, and were analyzed by GC-MS. The measured rates are expressed as defined first-order rate constants. Displacement was observed in all cases, with the reaction becoming progressively more facile as the ΔH° for H-atom addition to the aromatics becomes more negative. While this cleavage is indeed extremely facile for alkyl-anthracenes and -pyrenes, as has recently been noted by several authors (4,6,7,11), it is clear from the data in Figure 1 that it is general for substituted aromatics, rather than unique to pyrene and anthracene type structures as has been suggested (6).

The defined first-order rate constants increase by almost four orders of magnitude (a factor of 6×10^3) in going from diphenylmethane to 1-benzylpyrene. This sensitivity is very similar to that observed by Futamura and coworkers (7) for reaction of diarylmethanes in tetralin, and is far greater than would result from addition of highly reactive free H-atoms to the respective arenes to give the cyclohexadienyl radical cleavage intermediates. Reported H-atom addition rates (9) give an Evans-Polanyi factor less than 0.2 and an anticipated rate increase of less than a factor of ten for free H-atom addition to benzylaromatics in this series. Thus, there is little doubt that some active H-donor other than H-atom itself is transferring hydrogen to the closed-shell reactants to generate the necessary cyclohexadienyl radical intermediate.



Scheme 1. Cleavage of Benzylaromatics by H-Atom Transfer.

Transfer of an H-atom directly from a dihydroaromatic (i.e., an RRD process) would certainly exhibit high selectivity (higher even than RHT). However, the rough similarity of cleavage rate constants observed in solvents having vastly different C-H bond strengths, such as dihydroanthracene and dihydrophenanthrene (1,2,11,22), and even tetralin (7), have already demonstrated that RRD cannot, in all cases, constitute the stoichiometric and rate-determining H-transfer step.

Significance for Coal Liquefaction. An explicit determination of the importance of cleavage by ipso-desubstitution in coal liquefaction, as noted above, is not possible at the present time, since the nature of the critical linkages broken during liquefaction cannot be determined with any certainty. However, as we have previously pointed out, (a) the ability of hydroaromatics to engender hydrogenolysis even in the absence of hydrogen pressures and catalysts, (b) the effectiveness of these known hydrogenolysis agents in coal liquefaction, and (c) the ineffectiveness of pure "scavengers", such as toluene, ethylbenzene and indane, together strongly suggest that hydrogenolytic cleavage of strong bonds is important in coal liquefaction (1,11,12-15). In addition to this descriptive evidence, we have shown several instances where the incorporation of strong-bond cleavage into the liquefaction mechanism pictures enables one to rationalize, and in some cases (15) even predict, coal liquefaction behavior that defies interpretation if one is limited to the traditional weak-bond scission picture of liquefaction. Studies by Zabransky and Stock (16) on coals with various structures grafted onto them very clearly showed that scission of strong bonds induced by the system was competitive with scission of the weak bonds.

The importance of hydrodealkylation has been questioned on the grounds that it is generally a very slow reaction and that other reactions, most notably H-abstraction-- β -scission, can also result in cleavage of strong bonds. Recently, Ceylan and Stock (17) have reported that demethylation of 1,3-dimethylnaphthalene in tetralin/coal mixtures occurs only to a minor extent (~1-4%) in two hours at 400°C, and is much slower than the H-abstraction-- β -scission cleavage of 1,3-diphenylpropane (~35% at 400°C in 30 min.). We do not disagree with these results. Indeed, we find the rates reported by Ceylan and Stock for demethylation of 1,3-dinaphthylmethane to be in good agreement with those we had reported for the decomposition of 1,2-dinaphthylmethane (1,12).

However, in trying to judge whether hydrodealkylation is a significant bond cleavage mode in liquefaction, we must remember that the H-abstraction-- β -scission chain decompositions cannot be the critical bond cleavages that occur during coal liquefaction. H-abstraction-- β -scission cleavages are recognized (5) to be very facile at 400°C, even under neat conditions, and are known not to benefit significantly from tetralin or other hydrogen donors. This type of bond cleavage makes the aliphatic portions of crude petroleum easy to thermally crack even in the absence of H-donors, but it does not lead to substantially increased distillate production rates in the presence of donors or other added sources of hydrogen (18,19). This behavior is of course in stark contrast to that of coals, whose liquefaction benefits enormously from "donor" solvents. Thus, while bond cleavages of the H-abstraction-- β -scission type may indeed be more facile than the typical hydrodealkylation reaction, they are not necessarily the important category of cleavage. By the very fact that ipso desubstitutions sometimes occur only at modest rates and primarily in the presence of favorable reagents, they might properly be judged to be more "critical" than those cleavages which are more facile, and occur anyway.

Furthermore, the rates of hydrodealkylation reactions are highly dependent on the nature of the aromatic ring system to which the linkage is connected, as shown in Figure 1. In addition to the effect of ring size, illustrated by the data in Figure 1, there are the steric and electronic effects of other substituents, notably alkyl and hydroxyl groups. In previous work involving hydroquinone-promoted dealkylation (20), we had observed that in dihydroanthracene the demethylation of 2-methyl-1-naphthol is ~10 times faster than that of 2-methylnaphthalene. Given the degree of phenolic substitution on aromatic ring systems in bituminous and lower rank coals, the cleavage of alkyl linkages to any given naphthalene ring system in a coal is very likely to be significantly higher than that of methylnaphthalene. For instance, had Ceylan and Stock used a methylnaphthol as their probe molecule, we anticipate they would have observed 20 to 30% demethylation in two hours at 400°C in their tetralin-coal-resid mixtures.

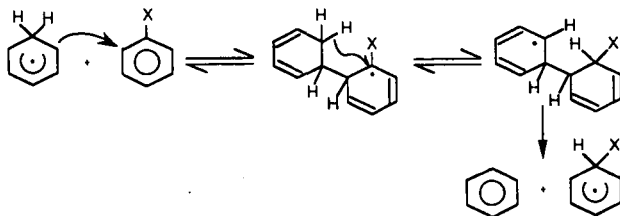
Finally, the cleavage rates for low molecular-weight model compounds are not necessarily indicative of how that same bond type will behave in a polymeric matrix such as coal. We have recently described (13) the "liquefaction" of a bibenzyl-type polymer, poly(1,4-dimethylenenaphthalene), in which the bond scission by hydrodealkylation was observed to be much faster than we had anticipated on the basis of monomeric model compound measurements. Furthermore, the net rate of spontaneous scission (homolysis) of the weak central bond was found to be much slower than one would anticipate from non-polymeric model compound measurements. We rationalized this latter observation by suggesting that the polymeric matrix provides an effective cage in which recombination of spontaneously produced benzylic radicals is drastically reduced. In contrast, bond scission by hydrodealkylation is a process not so easily reversed (since reversal involves an activated radical addition process to produce a highly unstable cyclohexadienyl radical). In fact, it appears that strong bond scission is enhanced in the polymeric system. Most likely, this is because every act of scavenging of polymer fragments by the donor dihydrophenanthrene produces a 9-hydrophenanthryl radical, which is capable of engineering hydrodealkylation, in the vicinity of the polymer. Regardless of the correctness of these explanations, the experimental result was that a hydrodealkylation expected to be some 300 times slower than a weak-bond homolysis had become, in the polymeric system, roughly as fast (13).

For all of the reasons cited in the above paragraphs, we assert that the fact that non-polymeric, unhydroxylated, two-ring probe molecules cleave at the rate of only a few percent per hour does not constitute convincing evidence that cleavages by ipso-substitution are unimportant in coal liquefaction. On the contrary, the other evidence reiterated above warrants the acceptance, at least as a working hypothesis, of the proposition that ipso-displacement by hydrogen constitutes an important part of coal conversion under liquefaction and coprocessing conditions. Given this conclusion, it becomes more than a mere academic exercise to determine in greater detail how the hydrogen transfer which induces this cleavage is taking place.

The Mechanism of Solvent-Mediated Hydrogenolysis. In the purely radical realm, several pathways for transfer of hydrogen leading to strong-bond cleavage have been considered (1,2,4,6,21,22). These pathways include radical hydrogen-transfer (RHT), reverse radical-disproportionation (RRD), also called "molecule-induced homolysis," concerted transfer of H₂, and a multi-step process in which the hydrogen atom source is the same cyclohexadienyl radical carrier species that would be the hydrogen atom donor in RHT itself. Another alternative that cannot be categorically excluded is an electron-transfer-proton-transfer sequence. Although we have been unable to find definitive evidence that would rule out this possibility, we consider it unlikely in systems where both the donor and acceptor are hydrocarbons.

Reverse radical-disproportionation has in some cases (i.e., those with 9,10-dihydroanthracene as the donor and high concentrations of substituted anthracenes as the acceptor) been shown (22) to constitute the stoichiometric hydrogen-transfer step, but with other common donor components, such as 9,10-dihydrophenanthrene and 4,5-dihydropyrene, RRD has been shown (1,2) not to be a major contributor. Similarly, thermodynamic requirements make a concerted transfer of H₂ much slower than sequential transfer in most cases of interest here (1,23). We have also previously presented evidence that a three-step indirect transfer process, such as that depicted in Scheme 2, is not responsible for the observed cleavage (1). However, recent experiments and calculations (6,8) have also raised additional questions (at least in the experimentally and computationally accessible systems) about the specific direct transfer route we

had previously invoked (RHT). Therefore, in the paragraphs below, we reexamine the principal remaining possibility, namely the indirect route.



Scheme 2. Three-Step H-Transfer Mechanism

H-transfer by a Multi-Step Process. This route is comprised of three known elementary reactions: radical addition, intramolecular H-atom abstraction, and β -scission. Because this was a reasonable alternative to the invoking of a new reaction in RHT, and because it had been previously suggested as a likely alternative (21), we discussed this possibility in detail in an earlier paper (1). At that time we ruled it out on the basis of two principal considerations. First, ipso H-transfer by an indirect route requires initial radical-addition at some position other than ipso, usually ortho or para to the ipso position, depending on whether the donor radical is of the 9-hydrophenanthryl type or the 9-hydroanthryl type. In some cases this addition would be extremely electronically unfavorable, because ortho or para is a fused ring position. Second, because reversal of the initial addition is expected to be many orders of magnitude faster than intramolecular H-abstraction (1), we would anticipate many initial additions to different sites (i.e., not just those o- or p- to the substituent), including ipso attack. Ipso attack should then lead to radical displacement products, which were often not observed. Since the recent experimental and theoretical work of Autrey and Franz (8), and of Freund et al. (6), have raised additional questions about the viability of the RHT pathway itself, we felt it was desirable to provide additional experimental evidence on the matter.

The most convincing evidence against the indirect route comes in fact from the displacement of 1-substituted pyrene derivatives -- ironically the same system whose reactions have caused Freund et al. (6) to invoke the indirect route. A feature of all indirect routes that commence with a radical addition is that subsequent intramolecular H-abstraction provides a set of linked aromatic systems in which the original donor framework again bears the free radical and the substrate portion has become a dihydro derivative. In other words, transfer of a single H-atom requires formation, as an intermediate, of a dihydro species. In the case of ultimate transfer of a hydrogen to the 1-position of pyrene, this intermediate would be a 1,2- or a 1,5-dihydropyrene. Both of these species are highly unstable (relative to the 4,5-dihydro species), since their formation requires destruction of the aromaticity of two of the rings of pyrene. Although there are no measured heats of formation available for these unstable dihydropyrenes, we can reliably estimate that the required intramolecular H-abstraction reactions would be more than three orders of magnitude slower for reaction of pyrene derivatives than for reaction of naphthalene derivatives (Table 1).

In contrast with these estimates, experimental results show that cleavage of pyrene derivatives is actually about two orders of magnitude faster than that of naphthalene derivatives. There is now not merely a quantitative mismatch between estimated and observed relative rates, but a qualitative inconsistency: those reactions which would have to be much slower, are actually much faster. Thus the increased susceptibility of pyrene linkages to ipso displacement that has been recently discussed (4,6) cannot be the result of a multi-step sequence of free radical reactions that has the same net result as the one-step RHT process.

CONCLUSIONS

The experimental evidence now makes it clear that cleavage induced by H-transfer is general for benzyl and alkyl linkages to aromatic ring systems. The substrate and positional selectivities of this cleavage show that it cannot simply result from displacement by free H-atoms, and relative rates in different solvent systems show it cannot result merely from reverse radical-disproportionation. Comparison of the response of coal liquefaction on the one hand and H-abstraction-- β -scission on the other to the presence of donor solvents is a strong indicator that the latter type of strong-bond cleavage, while probably important in resid conversion, does not constitute the "critical" cleavage that distinguishes between better and poorer liquefaction systems. Finally, a multi-step radical process for hydrogen transfer is ruled out by the sensitivity of linkages to the 1-position of pyrene, coupled with the marked instability of the 1,2- and 1,5-dihydropyrene intermediates that would be necessary in a multi-step process.

REFERENCES

1. McMillen, D. F.; Malhotra, R.; Chang, S. -J.; Fleming, R. H.; Ogier, W. C.; Nigenda, S. *E. Fuel* **1987**, *66*, 1611.
2. Bilmers, R.; Brown, R. L.; Stein, S. E. *Int. J. Chem. Kinetics* **1989**, *21*, 375.
3. Bockrath, B. C.; Schroeder, K. T.; Smith, M. R. *Energy and Fuels* **1989**, *3*, 268.
4. Smith, C. M.; Savage, P. E., "Reactions of Polycyclic Alkylaromatics, Part 1: Pathways, Kinetics, and Mechanisms for 1-Dodecylpyrene," *Ind. Eng. Chem. Res.* **1991**, *31*, XXX.
5. Poutsma, M. L. *Energy and Fuels*, **1990**, *4*, 114.
6. Freund, H.; Matturro, M. G.; Olmstead, W. N.; Reynolds, R. P.; Upton, T. H. *Am. Chem. Soc., Div. Fuel Chem. Preprints* **1990**, *35*(2), 496.
7. Futamura, S.; Koyanagi, S.; Kamiya, Y. *Fuel* **1988**, *67*, 1436
8. Autrey, T.; Franz, J. A. *Am. Chem. Soc., Div. Fuel Chem. Preprints* **1990**, *35*(2), 382
9. a. Tsang, W. J. *Amer. Chem. Soc.* **1985**, *107*, 2872.
b. Tsang, W. J. *Phys. Chem.* **1986**, *90*, 1152.
10. Bockrath, B. C.; Bittner, E.; McGrew, J. J. *Am. Chem. Soc.* **1984**, *106*, 135.
11. Malhotra, R.; McMillen, D. F. *Energy and Fuels* **1990**, *4*, 184.
12. McMillen, D. F.; Malhotra, R.; Hum, G. P.; Chang, S. -J. *Energy and Fuels* **1987**, *1*, 193.
13. Malhotra, R.; McMillen, D. F.; Tse, D. S.; StJohn, G. A. *Am. Chem. Soc.* **1989**, *3*, 465.
14. McMillen, D. F.; Malhotra, R.; Nigenda, S. E. *Fuel* **1989**, *68*, 380.
15. McMillen, D. F.; Malhotra, R.; Tse, D. S., *Energy and Fuels* **1991**, *5*, XXX.
16. Rose, G. R.; Zabransky, R. F.; Stock, L. M.; Huang, C.-B.; Srinivas, V. R.; Tse, K.-T. *Fuel* **1984**, *63*, 1339.
17. Ceylan, K.; Stock, L. M. *Fuel* **1990**, *69*, 1386.

18. Savage, P. E.; Klein, M. T.; Kukes, S. G. *Energy and Fuels* **1988**, *2*, 619.
19. Khorasheh, F.; Rangwala, H. A.; Gray, M. G.; Lana, I. G. D. *Energy and Fuels* **1989**, *3*, 716.
20. McMillen, D. F.; Chang, S. -J.; Fleming, R. H.; Laine, R. M.; Malhotra, R.; Nigenda, E.; Ogier, W., "Effect of of Amine Solvents and Oxygen Functionalities on Coal Liquefaction," *EPRI Research Project 2147-5*, **1985**.
21. Stein, S. E, "Free Radicals in Coal Conversion," in *Chemistry of Coal Conversion*, Schlosberg, R. H., Ed.; Plenum Press: N.Y., **1985**, 13.
22. Billmers, R.; Griffith, L. L.; Stein, S. E., *J. Phys. Chem.* **1986**, *90*, 517.
22. King, H.-H.; Stock, L. M. *Fuel* **1981**, *60*, 748.
23. Benson, S. W., *Thermochemical Kinetics*, 2nd ed; John Wiley and Sons: New York, **1976**.
24. Pedley, J. B.; Naylor, R. D.; Kirby, S. P., *Thermodynamics of Organic Compounds*, Chapman and Hall: New York, **1986**.

TABLE 1.

Comparison of Measured Rates of Cleavage with Estimated Rates of Multi-Step Components for Naphthalene and Pyrene Derivatives.

Benzylaromatic	exptl k _{cleavage} .s ⁻¹	Estimated Rate Constants ^a for Reaction of Three-Step Intermediate, s ⁻¹		ΔH ^o Intramol H-Abs ^b kcal/mol
		Reversal	Intramol H-Abs	
1-Benzyl-naphthalene	3 × 10 ⁻⁶	5 × 10 ⁻⁸	6 × 10 ⁻⁶	~-1
1-Benzylpyrene	5.4 × 10 ⁻⁴	5 × 10 ⁻⁸	<4 × 10 ⁻³	>+14

a. Rate constants estimated according to the regimen and data sources given in reference 11.

b. Estimated by group additivity procedures as described in reference 23, and by comparison with measured heats of formation for closest available analogs, as given in reference 24.

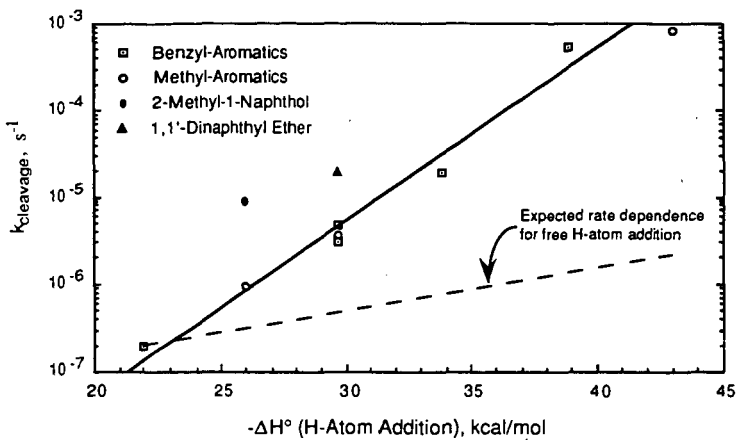


Figure 1 Measured rates of cleavage of benzyl- and methyl- aromatics in anthracene/dihydroanthracene at 400°C, as a function of the exothermicity of free H-atom addition.

Measured and estimated ΔH° (addition) are taken from reference 11. They are, in kcal/mol: phenyl, -22; 2-naphthyl, -26; 1-naphthyl, -27.9; 9-phenanthryl, -33.8; 1-pyrenyl, -38.9; and 9-anthryl, -43.

REACTIVITIES OF HYDROGENATED DI(1-NAPHTHYL)METHANES TOWARD THERMAL DECOMPOSITION AND HYDROCRACKING

Xian-Yong Wei, Eisuke Ogata, Shigeru Futamura,
Yoshio Kamiya, and Etsuo Niki
Department of Reaction Chemistry, Faculty of Engineering, The
University of Tokyo, 7-3-1, Hongo, Bunkyo-Ku, Tokyo, 113 Japan

Keywords: Hydrogenated Di(1-naphthyl)methanes, Thermal
Decomposition, Hydrocracking

INTRODUCTION

The decomposition mechanism of diarylmethanes has been extensively investigated [1-5], and it is generally accepted that the decomposition occurs via the ipso-addition of a hydrogen atom transferred from hydrogen donating solvent or gaseous hydrogen. It is noteworthy that the feasibility of the hydrogen transfer to the ipso-positions of diarylmethanes depends not only on the species of hydrogen donating solvent, hydrogen pressure and catalyst, but on aromatic ring sizes [4,5].

In the hydrogenolysis of di(1-naphthyl)methane(DNM) [5,6], hydrogenated di(1-naphthyl)methanes(H-DNMs) were formed in addition to naphthalene(Np) and 1-methylnaphthalene(1-MN). We previously reported that at low temperatures, the selectivities of H-DNMs were dependent upon the catalyst used to a large extent [7]. It is of significance to know how the reactivities of H-DNMs toward thermal decomposition or hydrocracking change with the degree of hydrogenation of H-DNMs.

EXPERIMENTAL

Materials

DNM was synthesized according to the methods described in the previous paper [5] and 1,2-di(1-naphthyl)ethane(DNE) according to the method of Buu-Hoi [8]. H-DNMs were prepared by hydrogenating DNM with Ni-Mo-S/Al₂O₃, stabilized nickel or ultra fine metallic iron catalyst, respectively, as shown in Table 1. DNM and H-DNMs prepared were identified by GC-MS. Table 2 shows the structures of these compounds. The other substrates such as diphenylmethane (DPM) and 1,2-diphenylethane(DPE), and solvent dodecane were purchased commercially and further purified if necessary by conventional methods.

Thermal decomposition and hydrocracking of the substrates

7.5 mmol of a substrate, 30 ml of dodecane were put into a 90 ml stainless steel, magnetically stirred autoclave. After being pressurized by hydrogen or nitrogen to 10 MPa, the autoclave was heated to a reaction temperature and kept for a prescribed period of time. Then, the autoclave was immediately cooled to room temperature in an ice-water bath. Thermal decomposition was usually carried out under nitrogen at 400°C, and hydrocracking in the presence of 0.5 g of FeS₂ catalyst with 0.05 g of sulfur under hydrogen at 300°C.

The products were identified by GC-MS and quantified by GC.

RESULTS AND DISCUSSION

Reactivities of DNM and H-DNMs toward thermal decomposition

Figure 1(a) shows the reactivities of DNM and H-DNMs mixture (MIX) toward thermal decomposition under nitrogen in the temperature range 300-430°C. At 300°C, the thermal decomposition does not proceed for any substrate. Ditetralylmethanes (8H-DNM and 8H'-DNM) slightly decompose at 350°C. At above 400°C, 4H-DNM begins to decompose with concurrent increase in the DNM concentration, suggesting the occurrence of dehydrogenation of H-DNMs. Figure 1 (a) shows that the reactivities of H-DNMs toward thermal decomposition decrease in the order: 8H'-DNM > 8H-DNM > 4H-DNM. Although the thermal decomposition of DNM and 4H-DNM were promoted under hydrogen (Fig.2(b)), the order of the reactivities did not change.

8H-DNMs(1) was thermally decomposed. Figure 2 shows that in spite of low initial concentration of 8H'-DNM, the molar ratio of 8H'-DNM to 8H-DNMs decreases steadily as the reaction proceeds, indicating that 8H'-DNM decomposes faster than 8H-DNM. As the reaction proceeds, the selectivities of the dehydrogenated products such as 4H-DNM and DNM, and that of a hydrogenated product, 14H-DNM increased, while those of the decomposed products such as tetralin (THN) and 5-methyltetralin (5-MT) decreased. These facts suggest that the disproportionation reaction concurs. The time profile of the product distribution for the thermal decomposition of 8H-DNMs(2) is illustrated in Fig.3. These results given in Fig.3 show that 8H-DNM is as reactive as 14H-DNM, but much lower than 8H'-DNM in reactivity.

To clarify the different reactivities of 8H-DNM and 8H'-DNM, the thermal decomposition of DPM and DPE were separately carried out under the conditions similar to those for 8H-DNMs. As shown in Table 3, in comparison with ca. 6% of conversion for DPE, DPM does not decompose at all. The bond dissociation energies of some diaryl hydrocarbons listed in Table 4 indicate that the aliphatic C-C bonds in DPE and DNE are thermally cleaved much more readily than the $C_{ar}-C_{alk}$ in DPM. By analogy of structural similarity between these compounds and octahydro-derivatives of DNM, the discrepancy in the reactivities of 8H-DNM and 8H'-DNM may be due to the different labilities of their breaking C-C bonds.

On the other hand, compared to 8H-DNM and 8H'-DNM, DPM and DPE are much less reactive, respectively. The difference should be attributed to the hydrogen donating effect of tetralyl groups in ditetralylmethanes. Table 3 indicates that DNM and DNE decompose more readily than DPM and DPE, respectively, but they are less reactive than 8H-DNM and 8H'-DNM, respectively. Because neither gaseous hydrogen nor hydrogen donating solvent was used, the hydrogen consumed in the thermal decomposition of DNM and DNE should result from dodecane used as a solvent. In decalin solvent, DNM does not decompose at all, but DNE decomposes much the same as in dodecane solvent. Two blank tests show that under the same reaction conditions (400°C, 10 MPa of N_2 , 1 h), ca. 1% of dodecane decomposes, but that decalin does not. These results indicate that the hydrogenolysis of DNM occurs in dodecane solvent. 20H-DNM derived from the complete hydrogenation of DNM shows even lower reactivity toward thermal decomposition than DNM. Compari-

son of the reactivities of the substrates listed in Table 3 suggests that the intramolecular hydrogen transfer plays a significant role in the cleavage of R-CH₂-R', where the R and R' denote aromatic or hydroaromatic rings. It could be also said that the thermal decomposition of H-DNMs, except for 20H-DNM, includes hydrogenolysis primarily induced by the intramolecular hydrogen transfer. The reactivities of DNM and H-DNMs toward thermal decomposition decrease in the order: 8H'-DNM > 8H-DNM > 4H-DNM > DNM > 20H-DNM.

Reactivities of DNM and H-DNMs toward hydrocracking catalyzed by FeS₂

The hydrocracking of a mixture of DNM and H-DNMs was carried out at 300°C in the presence of FeS₂ catalyst. Figure 4 shows that the reactivities of DNM and H-DNMs toward hydrocracking decrease in the order: DNM > 4H-DNM > 8H-DNM > 8H'-DNM, which is the reverse of that toward thermal decomposition (see above). The slight increase in the concentration of 8H'-DNM with the course of the reaction was observed, which may be due to the hydrogenation of DNM and 4H-DNM.

Fig. 5 shows the results of the hydrocracking of 8H-DNMs(1). In contrast to the relatively rapid hydrocracking of 8H-DNM, 8H'-DNM is hardly hydrocracked, partially because of its low concentration. Fig. 6 shows that in the hydrocracking of 8H-DNMs(2), the rate for the hydrocracking of 8H-DNM is above tenfold greater than that of 8H'-DNM. As is consistent with the low reactivity of 8H'-DNM toward hydrocracking, the yield of 1-methyltetralin(1-MT) is only small. As the hydrocracking of DNM and H-DNMs results principally from the ipso-addition of a hydrogen atom to an aromatic ring under the reaction conditions, the different reactivities of 8H-DNM and 8H'-DNM can be illustrated in Fig. 7. In the hydrocracking of 8H-DNM, the ipso-position of both tetralin rings can be attacked by H-atoms, and as an intermediate produced after the hydrocracking, tetralyl-5-methyl radical is much more stable than tetralyl-1-methyl radical. Hence, 8H-DNM is expected to decompose much more readily than 8H'-DNM after the ipso-addition of a hydrogen atom.

Table 5 shows the different reactivities of DPM and DPE, and those of DNM and DNE. DNE is mainly hydrogenated rather than decomposed. In general, hydrogen donating solvent scarcely shows its donating ability at a temperature as low as 300°C, especially in the presence of both gaseous hydrogen and an active catalyst [12-14]. Thus, the difference in the hydrocracking reactivities between 8H-DNM and DPM, and those between 8H'-DNM and DPE should be primarily due to the ring size effect. Under the same reaction conditions, 20H-DNM does not decompose at all. The order of the hydrocracking reactivities decreases: DNM > 4H-DNM > 8H-DNM > 8H'-DNM > 20H-DNM. The results may be explained on the basis of the hydrogen-accepting ability and adsorption ability [13,14] on the surface of catalyst used. They decrease in the order: naphthalene > tetralin > decalin. Because the hydrocracking proceeds mainly on the surface of FeS₂ catalyst via the attack (involving ipso-addition) on the substrates by H-atoms dissociated, the synergistic effect can be expected in the hydrocracking of DNM and H-DNMs.

Whitehurst et al. [15] have proposed that coal reactivity in liquefaction reactions is affected by its chemical structure. Takegami et al. [16] and Maekawa et al. [17] suggested that coal liquefaction proceeds through cleavage of ether and methylene bridges connecting relatively small structure units, such as polycyclic aromatic and hydroaromatic rings. According to our results, therefore, the severe hydrogenation of aromatic moieties in coal structure is likely to decrease the reactivity of the coal hydrogenated in the catalyzed hydroliquefaction, but the partial hydrogenation of aromatic moieties in coal structure forms precursors which are labile to thermal decomposition.

CONCLUSION

1. Mono- and di-tetrahydromethanes, which are afforded in the partial hydrogenation of DNM, are more reactive than DNM toward thermal decomposition. This fact suggests that the intramolecular hydrogen donation plays a significant role in the thermal decomposition of hydrogenated dinaphthylmethanes.
2. In hydrocracking with FeS_2 , di(1-naphthyl)methane decomposes rapidly, and the more fully it is hydrogenated, the more slowly its hydro-derivatives decompose.

REFERENCES

- 1 McMillen, D.F., Ogier, W.C., and Ross, D.S. *J. Org. Chem.*, **46**, 3322 (1981)
- 2 McMillen, D.F., Ogier, W.C., Chang, S.-J., Fleming, R.H. and Malhotra, R., *Proc., Int. Conf. on Coal Sci.*, Pittsburgh, p. 199 (1983)
- 3 McMillen, D.F., Malhotra, R., Chang, S.-J., Ogier, W.C., Nigenda, S.E., and Fleming, R.H. *Fuel*, **66**, 1611 (1987)
- 4 Kamiya, Y., Futamura, S., Mizuki, T., Kajioaka, M. and Koshi, K. *Fuel Process. Technol.*, **14**, 79 (1986)
- 5 Futamura, S., Koyanagi, S. and Kamiya, Y. *Fuel*, **67**, 1436 (1988)
- 6 Sakurai, A., Harada, Y., Oda, H. and Yokokawa, C. *Proc., 24th Coal Sci. Conf. Jpn. Soc. Fuel*, Tokyo, p. 2 (1987)
- 7 Ogata, E., Wei, X.-Y., Fukasawa, T. and Kamiya, Y. *Proc., Int. Conf. on Coal Sci.*, Tokyo, pp. 879-882
- 8 Buu-Hoi, Ng. Ph. and Hoan, Ng. *J. Org. Chem.*, **46**, 1023 (1949)
- 9 Vernon, L.W. *Fuel*, **59**, 102 (1979)
- 10 Hei, R.D., Sweeny, P.G. and Stenberg, V.I. *Fuel*, **65**, 577 (1986)
- 11 Malhotra, R., McMillen, D.F., Tse, D.S. and John G.A.S. *Energy & Fuels*, **3**, 465 (1989)
- 12 Ohe, S., Itoh, H., Makabe, M. and Ouchi, K. *Fuel*, **64**, 902-1111 (1985)
- 13 Ouchi, K. and Makabe, M. *Fuel*, **67**, 1536 (1988)
- 14 Ogata, E., Tamura, T. and Kamiya, Y. *Proc., Int. Conf. on Coal Sci.*, Maastricht, p. 243 (1987)
- 15 Whitehurst, D.D., Mitchell, T.O. and Farcasiu, M. In: *Coal Liquefaction, "The Chemistry and Technology of Thermal Processes"*, Academic Press, 1980, chap. 5
- 16 Takegami, Y., Kajiyama, S. and Yokokawa, C. *Fuel*, **42**, 291 (1963)
- 17 Maekawa, Y., Shimokawa, K., shii, T. and Takeya, J. *Fuel Soc. Jpn.*, **46**, 927 (1967)

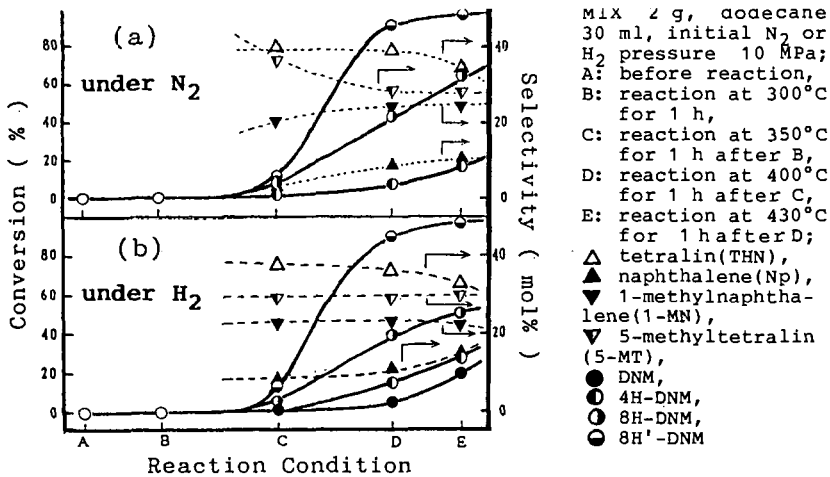


Fig. 1. Thermal decomposition of DNM and H-DNMs mixture (MIX)

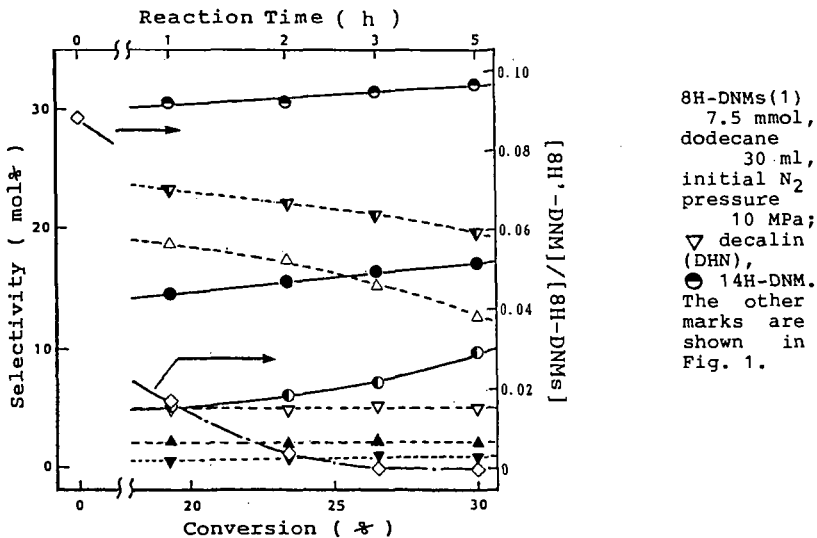


Fig. 2. Thermal decomposition of 8H-DNMs(1) at 400°C

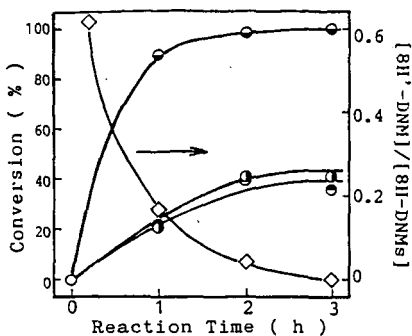


Fig. 3. Thermal decomposition of 8H-DNMs(2) at 400°C

8H-DNMs(2) 7.5 mmol, dodecane 30 ml, initial N₂ pressure 10 MPa. The marks are shown in Figs. 1 and 2.

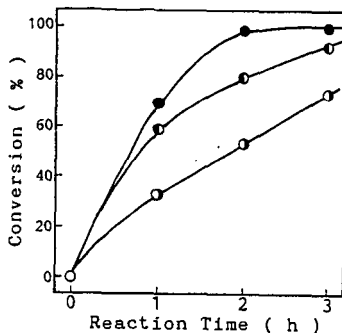


Fig. 4. Hydrocracking of MIX with FeS₂ catalyst at 300°C

MIX 2 g, dodecane 30 ml, FeS₂ 0.5 g, sulfur 0.05 g, initial H₂ pressure 10MPa. The marks are shown in Fig. 1.

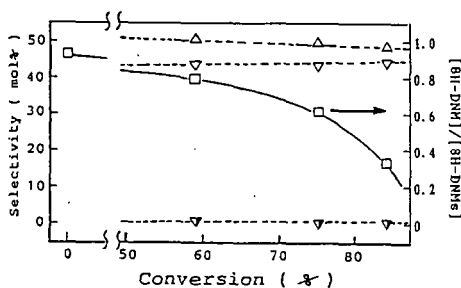


Fig. 5. Hydrocracking of 8H-DNMs(1) with FeS₂ catalyst at 300°C

8H-DNMs(1) 7.5 mmol, dodecane 30 ml, FeS₂ 0.5 g, sulfur 0.05 g, initial H₂ pressure 10 MPa, ▼ 1-methyltetralin (1-MT). The other marks are shown in Figs. 1 and 2.

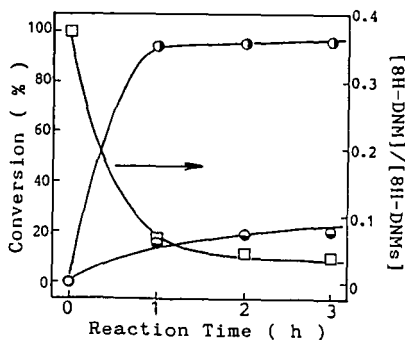


Fig. 6. Hydrocracking of 8H-DNMs(2) with FeS₂ catalyst at 300°C

8H-DNMs(2) 7.5 mmol, dodecane 30 ml, FeS₂ 0.5 g, sulfur 0.05 g, initial H₂ pressure 10 MPa. The marks are shown in Fig. 1.

Table 3 Thermal decomposition of H-DNMs and diarylalkanes at 400°C for 1 h

Substrate	Conv. (%)	Selectivity (mol%)							
		DHN	THN	Np	5-MT	1-MN	1-EN	Tol	Others
DNM	8.3 ^a	0	0	50	0	50	-	-	0
DNE	46.8	0	0	0.7	1.3	86.9	0.6	-	10.5
8H-DNMs(1)	19.3 ^b	5.1	18.6	2.2	23.1	0.6	-	-	50.4
	84.7 ^c								
8H-DNMs(2)	22.6 ^b	3.0	28.9	4.2	45.5	4.1	-	-	14.3
	89.5 ^c								
20H-DNM	~ 4	>90	-	-	-	-	-	-	-
DPM	0	-	-	-	-	-	-	0	-
DPE	6.0	-	-	-	-	-	-	15.9	84.10

substrate(s) 7.5 mmol, dodecane 30 ml, initial N₂ pressure 10 MPa; Tol: toluene, 1-EN: 1-ethylnaphthalene, ^a in decalin at 400°C, DNM does not decompose; ^b conversion of 8H-DNM; ^c conversion of 8H'-DNM; Others: including hydro- and dehydro-derivatives for DNE, 8H-DNMs(1), 8H-DNMs(2), and other alkylbenzenes for DPE.

Table 4 Bond dissociation energies(BDE) of some hydrocarbons

Bond	BDE(kcal/mol)	Reference
Ph-Ph	100	9
PhCH ₂ -Ph	84,89	9, 1
PhCH ₂ CH ₂ -Ph	97	10
PhCH ₂ -CH ₂ Ph	56,62	9, 1
NpCH ₂ -CH ₂ Np	50,55	9, 11

Np denotes naphthyl group.

Table 5 Hydrocracking of H-DNMs and diarylalkanes at 300°C for 1

Substrate	Conv. (%)	Selectivity (mol%)								
		THN	Np	5-MT	1-MN	1-EN	H-DNMs	H-DNEs	Bz	Tol
DNM	87.4	2.3	48.1	1.8	42.3	-	2.9	-	-	-
DNE	49.1	tr.	0.9	1.4	1.2	0.2	-	86.1	-	-
8H-DNMs(1)	59.1 ^a	50.2	0.5	48.0	0	-	0.2	-	-	-
20H-DNM	0	0	0	0	0	-	-	-	-	-
DPM	6.1	-	-	-	-	-	-	-	28.0	35.0
DPE	0	-	-	-	-	-	-	-	0	0

substrate(s) 7.5 mmol, dodecane 30 ml, FeS₂ 0.5 g, sulfur 0.05 g, initial H₂ pressure 10 MPa; Bz: benzene; H-DNMs: hydro-derivatives of DNE. The other abbreviations are defined in Figs 1, 2 and Table 3. ^a conversion of 8H-DNM. In the case of DNE, 8H-DNMs(1) and DPM, some unidentified products were obtained.

MECHANISMS FOR NONCATALYTIC AND CATALYTIC HYDROGEN TRANSFER PROCESSES UNDER COAL LIQUEFACTION CONDITIONS

Shigeru FUTAMURA, Seiya KOYANAGI, and Yoshio KAMIYA
Department of Reaction Chemistry, Faculty of Engineering, The
University of Tokyo, Hongo, Bunkyo-ku, Tokyo, 113 Japan

Keywords: hydrogen transfer, solvents, iron catalysts

INTRODUCTION

Recent progress in the chemistry of coal liquefaction has enabled us to envisage that radical-induced monohydrogen transfer is one of the key processes in the hydrogenolysis of strong bonds bridging aromatic units in coal [1-4]. We have succeeded in verifying that radical mechanism operates in the noncatalytic and Fe-catalyzed hydrogenolyses of reporter molecules such as trans-stilbene [5] and 9-benzylphenanthrene [6].

This paper intended to discuss 1) hydrogen transfer mechanisms for hydrogenolyses of the above compounds, 2) selectivities of benzylic radicals toward addition to aromatic nucleus and hydrogen abstraction in hydroaromatic hydrocarbon solvents, 3) catalysis of Fe compounds in solvent-mediated hydrogen transfer processes, and 4) reactant dependent catalytic activities of Fe compounds such as Fe_2O_3 , $\alpha\text{-Fe}$, and Fe_{1-x}S .

EXPERIMENTAL

Materials

9-Benzylphenanthrene (9-BP) and di(1-naphthyl)methane (DNM) were synthesized according to the method described in the previous paper [4]. trans-Stilbene and the solvents were commercially purchased and purified if necessary by conventional methods. $\alpha\text{-Fe}$ was prepared by reducing Fe_2O_3 in hydrogen streams at 450°C for 20 h. Its BET surface area was $14.2 \text{ m}^2\text{g}^{-1}$ (Shimadzu 2200). Fe_{1-x}S was prepared by reacting $\alpha\text{-Fe}$ with a small excess of elemental sulfur in tetralin under nitrogen at 380°C for 30 min. Its BET surface area was $10.4 \text{ m}^2\text{g}^{-1}$. The above catalysts were identified by X-ray diffraction analysis (Rigaku Denki RU-200A). After preparation, they were immediately immersed in 1-methylnaphthalene (1-MN) or in tetralin in a dry box under nitrogen and kept until use.

Batch experiments

A reaction solution consisting of a model compound and a hydrocarbon solvent with or without an Fe catalyst was put into a 90 ml SUS 316, magnetically stirred autoclave, pressurized by hydrogen or nitrogen. It was heated up to a reaction temperature and was kept there for 30 min. After the reaction, the autoclave was cooled by an electric fan to room temperature.

Product analysis

Benzyl(1-methylnaphthalene (BMN), 1-benzyl naphthalene (1-BN), and octahydrobinaphthalenes were identified by GC-MS (JEOL JMS-

DX300, equipped with a glass column (4mm diameter, 1m length) of 5 % OV-1 on Chromosorb W). 6-Benzyl-1,2,3,4-tetrahydronaphthalene (BTHN) and 6-(1,2-diphenylethyl)-1,2,3,4-tetrahydronaphthalene (DETN) were isolated by column chromatography and vacuum distillation, and they were identified by MS, $^1\text{H-NMR}$ (Varian EM 360A (60 MHz)), and $^{13}\text{C-NMR}$ (JEOL JMN-GX-400 (400 MHz)).

The reaction products collected with tetrahydrofuran were analyzed quantitatively by GC (Shimadzu GC-4C, equipped with a stainless column (4 mm diameter, 4 m length) of 10 % OV-17 on Chromosorb W (DMCS)).

RESULTS AND DISCUSSION

Reaction products

The spectral data of the reaction products obtained in the hydrogenolyses of trans-stilbene and 9-BP are as follows.

BMN m/z: 232 (100, M^+), 217 (68), 115 (13).

1-BN m/z: 218 (100, M^+), 217 (55), 141 (17).

BTHN m/z: 222 (62, M^+), 131 (100), 91 (36). $^1\text{H-NMR}$ δ in CCl_4 (ppm) 1.69 (4H, m), 2.62 (4H, m), 3.77 (2H, s), 6.80 (3H, bs), 7.09 (5H, bs). $^{13}\text{C-NMR}$ δ in CDCl_3 (ppm) 23.24, 23.30, 29.01, 29.39, 41.59, 125.89, 126.06, 128.36, 128.85, 129.17, 129.48, 134.74, 137.06, 138.10, 141.44.

DETN m/z: 312 (2.3, M^+), 221 (100), 91 (17). $^1\text{H-NMR}$ δ in CCl_4 (ppm) 1.39-2.12 (4H, m), 2.32-3.04 (4H, m), 3.21 (2H, d, $J=7.6$ Hz), 4.05 (1H, dd, $J=7.6$ Hz), 6.56-7.48 (13H, m). $^{13}\text{C-NMR}$ δ in CDCl_3 (ppm) 23.22, 23.24, 28.96, 29.44, 42.18, 52.75, 127.91, 128.06, 128.12, 128.30, 128.34, 128.49, 128.64, 128.92, 129.12, 134.82, 136.85, 140.46, 141.62, 144.63.

The regiospecific formation of DETN and BTHN was described in the previous paper [5].

1,1',2,2',3,3',4,4'-Octahydrobinaphthalenes m/z: 262 (22, M^+), 131 (100), 130 (68), 91 (32). 1,2,3,4,5',6',7',8'-Octahydrobinaphthalenes m/z: 262 (50, M^+), 130 (100), 104 (84).

Hydrogen transfer mechanism for the hydrogenolysis of trans-stilbene

trans-Stilbene can be a pertinent probe in order to verify hydrogen transfer mechanism and to characterize hydrogen donating abilities of solvents and activities of catalysts because the degree of stilbene isomerization can be a measure for mechanism determination, and dibenzyl cannot be dehydrogenated to trans-stilbene at 380°C.

Figure 1 shows the plot of the cis-stilbene content against the stilbene conversion. A fairly good linear correlation suggests that the stilbene isomerization cannot be ascribed to thermochemical equilibration of trans- and cis-stilbenes, supporting radical mechanism. A possible intermediate could be 1,2-diphenylethyl radical because the step from 1,2-diphenylethyl cation to dibenzyl is unlikely. In fact, the adduct of this radical to tetralin (DETN) was obtained in the hydrogenolysis of trans-stilbene in the presence of $\alpha\text{-Fe}$. These findings may suggest that 1,2-diphenylethyl radical is an intermediate in the

hydrogenation of trans-stilbene. Since the acidity of α -Fe is negligible [7], 1,2-diphenylethyl radical stabilized on the surface of α -Fe could be trapped by tetralin solvent.

Selectivities of benzylic radicals toward addition and hydrogen abstraction

Table 1 summarizes some data on selectivities of benzylic radicals toward addition and hydrogen abstraction, which are relevant to radical-induced monohydrogen transfer from solvents. Dibenzyl added in the system of DNM and a solvent (Reaction 1) thermally decomposes to selectively give benzyl radicals. Their relative reactivity of addition to hydrogen abstraction is 0.015 in tetralin and 0.033 in 1-MN. These findings are the first example of ipso-substitution by benzyl radicals, i.e., alkyl-dealkylation [8].

This type of benzyl radical addition to the aromatic nucleus is promoted by α -Fe in the hydrogenolysis of 9-BP (Reaction 2), where only a low concentration of the benzyl radical is present.

As described above, addition of 1,2-diphenylethyl radical to tetralin can be observed only in the presence of α -Fe, and the relative ratios of addition to hydrogen abstraction are around 0.2 at initial hydrogen pressure of 1.0 to 6.0 MPa (Reaction 3). On the other hand, $Fe_{1-x}S$ promoted further hydrogenation to give dibenzyl in higher selectivities. When tetralin was used as solvent, trace amounts of octahydrobinaphthalenes were obtained only in the presence of α -Fe.

In a binary solvent system of 9,10-dihydrophenanthrene (DHP) and 1-MN, only dibenzyl was obtained from stilbenes with no formation of 1,2-diphenylethylphenanthrene or benzylphenanthrene. This fact can be ascribed to the rapid capping of 1,2-diphenylethyl radical by DHP, which is a superior hydrogen donor.

The chemical behavior of 1,2-diphenylethyl radical could be affected by hydrogen donating ability of solvent and stability of solvent adduct itself.

These data confirm that monohydrogen transfer predominates from hydroaromatic radicals such as tetralyl and hydrophenanthryl.

Catalysis of Fe compounds in solvent-mediated hydrogenolysis of trans-stilbene

Table 2 shows the effects of Fe catalysts and hydrogen pressure on the hydrogenation of trans-stilbene in 1-MN. Comparison of Runs 1 and 3 shows that catalytic hydrogen transfer from 1-MN to trans-stilbene is negligible, and only about 2 % of 1-MN is consumed in these cases. Direct hydrogenation of trans-stilbene by molecular hydrogen is rather slow in the absence of α -Fe in 1-MN (see Runs 2 and 4). $Fe_{1-x}S$ showed a comparable catalytic activity, but it was more effective as hydrogenation catalyst than α -Fe. The differences in the trans-stilbene conversions and in the dibenzyl yields between Runs 1, 4, and 5 give the baseline increments caused by the α -Fe-catalyzed hydrogenation of trans-

stilbene, and comparison of Runs 1, 7, and 8 gives the corresponding increments for the $Fe_{1-x}S$ -catalyzed reactions.

Comparison of Runs 9, 11, and 14 (Table 3) clearly shows that intermolecular hydrogen transfer from tetralin to trans-stilbene is greatly promoted by α -Fe and $Fe_{1-x}S$. Dibenzyl yield increments at 6.0 MPa of hydrogen in the presence of α -Fe and $Fe_{1-x}S$ were 45 and 63%, respectively. The expected increment caused by catalytic incorporation of molecular hydrogen is not more than 25% for α -Fe (compare Runs 2 and 5) and 26% for $Fe_{1-x}S$ (compare Runs 2 and 8). Thus, in the system of H_2 -tetralin-Fe catalyst, trans-stilbene could be hydrogenated predominantly on the catalytic cycle.

Ogawa and coworkers have shown that the catalytic activity of $Fe_{1-x}S$ highly depends on H_2S pressure in the hydrocracking of diphenylmethane without solvent at 450°C [9]. At low pressures of H_2S , $Fe_{1-x}S$ is converted to FeS which is less active than $Fe_{1-x}S$. However, our results clearly show that both of α -Fe and $Fe_{1-x}S$ promote tetralin-mediated hydrogen transfer from gaseous hydrogen. Since dry coal liquefaction is not so feasible, catalyzed solvent-mediated hydrogen transfer could be a key reaction in coal liquefaction.

Reactant dependent catalytic activities of Fe compounds

As Table 4 shows, the catalytic activities of Fe compounds in the hydrogenolysis of 9-BP decreased in the order: α -Fe > $Fe_{1-x}S$ > Fe_2O_3 . The apparent catalytic activity of Fe_2O_3 can be ascribed to that of α -Fe partly produced in the deoxygenative reduction of Fe_2O_3 during the course of the reaction. The above order is different from that for the hydrogenolysis of trans-stilbene at 380°C. Almost the same product distributions with α -Fe and $Fe_{1-x}S$, and negligible surface area changes of both the catalysts suggest the catalyst dependent adsorption behavior of 9-BP, i.e., 9-BP is selectively adsorbed at its 9,10-position on α -Fe, while 9-BP is competitively adsorbed at its 1,2-, 3,4-, 5,6-, 7,8-, 9,10- positions on $Fe_{1-x}S$ [10]. For radical A in Scheme 1, a benzyl radical release is energetically more favorable than that of a hydrogen atom, promoting the hydrogenolysis of 9-BP. On the other hand, reversible hydrogen atom elimination predominates over subsequent hydrogenation for radicals $B \sim F$, which decreases the apparent conversion of 9-BP.

These data suggest that the regioselectivity of 9-BP adsorption is lost on $Fe_{1-x}S$ compared to α -Fe, and that radicals $B \sim F$ are competitively formed against radical A.

The lack of such catalyst dependence of trans-stilbene hydrogenolysis can be ascribed to the stronger adsorbing ability of the olefinic moiety in trans-stilbene.

Figure 2 shows the relationship between the 9-BP conversion and the yield of naphthalene derived from tetralin. A good linear correlation suggests that the bimolecular hydrogen transfer from tetralin to 9-BP is promoted by α -Fe and $Fe_{1-x}S$.

CONCLUSION

We have shown that in the noncatalytic and Fe-catalyzed hydrogenolyses of trans-stilbene and 9-benzylphenanthrene, radical mechanism operates, and that bimolecular hydrogen transfer from solvents is promoted by α -Fe and $Fe_{1-x}S$ without overhydrogenation of aromatic nuclei.

REFERENCES

1. Y. Kamiya, S. Futamura, T. Mizuki, M. Kajioka, and K. Koshi, *Fuel Proc. Technol.*, **14**, 79 (1986).
2. Y. Kamiya, E. Ogata, K. Goto, and T. Nomi, *Fuel*, **65**, 586 (1986).
3. D. F. McMillen, R. Malhotra, S.-J. Chang, W. C. Ogier, S. E. Nigenda, and R. H. Fleming, *Fuel*, **66**, 1611 (1987).
4. S. Futamura, S. Koyanagi, and Y. Kamiya, *Fuel*, **67**, 1436 (1988).
5. S. Futamura, K. Fujimoto, and Y. Kamiya, *Bull. Chem. Soc. Jpn.*, **63**, 2564 (1990).
6. S. Futamura, S. Koyanagi, and Y. Kamiya, *J. Fuel Soc. Jpn.*, in press.
7. K. Tanabe and H. Hattori, *Sekiyu Gakkaishi*, **29**, 280 (1986).
8. M. Tiecco and L. Testaferri in 'Reactive Intermediates', Vol. 3 (Ed. R. A. Abramovitch), Plenum Press, New York, 1983, p. 88.
9. T. Ogawa, V. I. Stenberg, and P. A. Montano, *Fuel*, **63**, 1660 (1984).
10. M. Minabe and K. Nakada, *Bull. Chem. Soc. Jpn.*, **58**, 1962 (1985).

Table 1 Selectivities of Benzylic Radicals toward Addition and Hydrogen Abstraction.

Reaction	Solvent	Catalyst	Radical	Addition/H abstraction
1	Tetralin	None	Benzyl	0.015 [b]
1	1-MN	None	Benzyl	0.033 [b]
2	Tetralin	Fe_2O_3	Benzyl	~ 0
2	Tetralin	α -Fe	Benzyl	0.057 [c]
2	Tetralin	$Fe_{1-x}S$	Benzyl	~ 0
2	1-MN	Fe_2O_3	Benzyl	~ 0
2	1-MN	α -Fe	Benzyl	0.14 [d]
2	1-MN	$Fe_{1-x}S$	Benzyl	~ 0
3	Tetralin	None	[a]	~ 0
3	Tetralin	α -Fe	[a]	0.21 [e]
3	Tetralin	$Fe_{1-x}S$	[a]	~ 0

Reaction 1: hydrogenolysis of DNM in the presence of dibenzyl (0.5-1.0 mol equiv.) under hydrogen (2.0 MPa) at 460°C.

Reaction 2: hydrogenolysis of 9-BP in the presence of Fe catalyst (0.5 mol equiv.) under hydrogen (6.0 MPa) at 450°C.

Reaction 3: hydrogenolysis of trans-stilbene in the presence of Fe catalyst under hydrogen (1.0 MPa) at 380°C.

a: 1,2-Diphenylethyl. b: [1-BN]/[toluene]; c: [BTHN]/[toluene]; d: [BMN]/[toluene]; e: ([DETN] + [BTHN])/[dibenzyl].

Table 2 Fe-Catalyzed Hydrogenolysis of trans-Stilbene in 1-MN.

Run	Gas phase (MPa)	Cat.	t-ST conv. (mol%)	Products (Selectivity/mol%)
				c-ST Dibenzyl Toluene
1	N ₂ (1.0)	None	6.9	43 44 tr.
2	H ₂ (1.0)	None	10	38 50 —
3	N ₂ (1.0)	α-Fe	7.4	53 36 3.6
4	H ₂ (1.0)	α-Fe	26	13 62 3.8
5	H ₂ (6.0)	α-Fe	44	6.6 68 3.0
6	N ₂ (1.0)	Fe _{1-x} S	7.9	48 37 3.8
7	H ₂ (1.0)	Fe _{1-x} S	21	18 71 3.3
8	H ₂ (6.0)	Fe _{1-x} S	40	7.7 78 2.9

trans-Stilbene 3 g (16.7 mmol), 1-MN 15 g (106 mmol), Fe catalyst 3.75 mmol of Fe, reaction temperature 380°C, reaction time 30 min.

c- and t-ST = cis- and trans-Stilbenes. tr.=trace.

Table 3 Fe-Catalyzed Hydrogenolysis of trans-Stilbene in Tetralin.

Run	Gas phase (MPa)	Cat.	t-ST conv. (mol%)	Products (Selectivity/mol%)
				c-ST Dibenzyl Toluene BTHN DETN
9	N ₂ (1.0)	None	24	18 39 — — —
10	H ₂ (1.0)	None	27	15 41 — — —
11	N ₂ (1.0)	α-Fe	41	8.3 51 5.6 4.1 5.6
12	H ₂ (1.0)	α-Fe	64	4.2 59 6.1 3.9 5.5
13	H ₂ (6.0)	α-Fe	95	— 71 9.5 7.8 6.4
14	N ₂ (1.0)	Fe _{1-x} S	51	6.7 69 — — —
15	H ₂ (1.0)	Fe _{1-x} S	61	4.6 70 2.1 — —
16	H ₂ (6.0)	Fe _{1-x} S	91	— 81 1.6 — —

trans-Stilbene 3 g (16.7 mmol), tetralin 15 ml (110 mmol), Fe catalyst 3.75 mmol of Fe, reaction temperature 380°C, reaction time 30 min.

c- and t-ST = cis- and trans-Stilbenes.

Table 4 Additive Effect of Fe Catalysts on the Hydrogenolysis of 9-BP in Tetralin (Tet).

Catalyst	Conv. of 9-BP	Selectivities of			
		Tol	BTHN	Phen	DHP
None	4%	100%	nd.	80%	3%
Fe ₂ O ₃	20	90	tr.	83	10
α -Fe	72	87	5%	92	8
Fe _{1-x} S	39	87	tr.	82	10

9-BP 7.5 mmol, Tet 75 mmol, Fe catalyst 3.75 mmol of Fe, initial hydrogen pressure 6.0 MPa, 450°C, 30 min.

Tol=Toluene, Phen=Phenanthrene.

Nd. and tr. denote 'not detected' and 'traces', respectively.

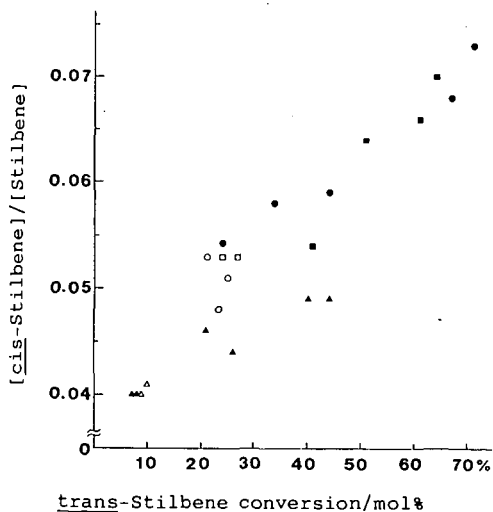


Fig. 1 Correlation of the trans-Stilbene Conversion and the cis-Stilbene Content in the Hydrogenolysis of trans-Stilbene at 380°C. ● DHP-1-MN, Fe cat. ○ DHP-1-MN, no cat. ■ Tetralin, Fe cat. □ Tetralin, no cat. ▲ 1-MN, Fe cat. △ 1-MN, no cat.

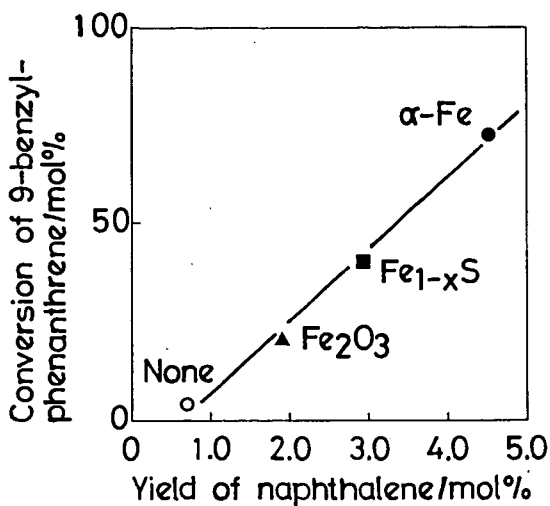
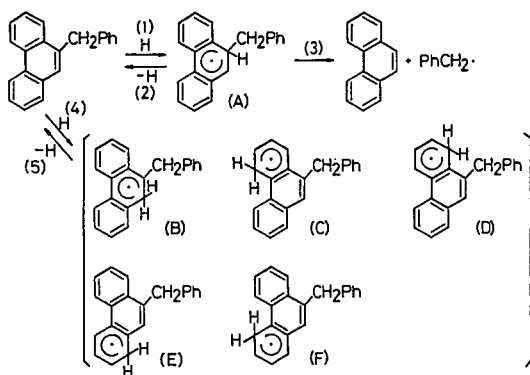


Fig. 2 Relationship between the 9-BP Conversion and the Naphthalene Yield in the Hydrogenolysis of 9-BP in Tetralin. 9-BP 7.5 mmol, tetralin 75 mmol, initial hydrogen pressure 6.0 MPa, 450°C, 30 min.



Scheme 1 Mechanism for the Hydrogenolysis of 9-BP.

A THEORETICAL AND EXPERIMENTAL STUDY OF UNIMOLECULAR
AND BIMOLECULAR RADICAL HYDROGEN TRANSFER REACTIONS

Tom Autrey, Gerald J. Gleicher, Donald M. Camaioni, Kim F. Ferris and
James A. Franz

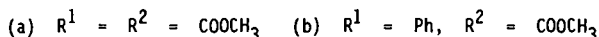
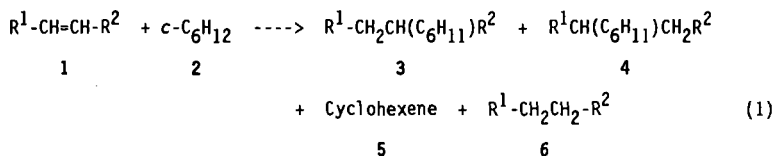
Pacific Northwest Laboratory(a)
P. O. Box 999 Richland, WA 99352

Keywords: Radical Hydrogen Transfer, RHT, AM1, Semiempirical Quantum Chemical Calculations

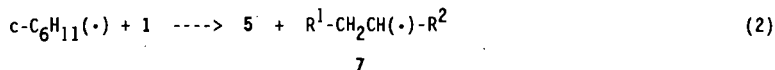
INTRODUCTION

The bimolecular transfer of hydrogen atom from an organic radical to an olefin or aromatic system, known as the radical hydrogen transfer (RHT) reaction, has been proposed as an important pathway for hydrogen transfer in liquid phase pyrolysis reactions and as an important pathway for selective bond cleavage in coal liquefaction.¹⁻⁵

Experimental observation of the RHT reaction was apparently first reported by Metzger,⁶ followed almost simultaneously by a study of Billmers et al.⁷ In Metzger's work, the radical addition of cyclohexane to dimethylfumarate and methyl cinnamate at 250 to 400 °C was examined:

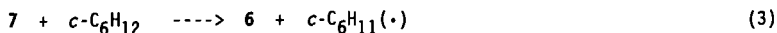


The reaction, which exhibits a chain length of 100, is initiated by hydrogen transfer from cyclohexane to 1. Reversible addition of cyclohexyl radical to 1 followed by abstraction from 2 leads to 3 and 4. The formation of reduced product 6 is suggested to occur via the RHT reaction of cyclohexyl radical with 1:



(a) Operated for the U. S. Department of Energy by Battelle Memorial Institute.

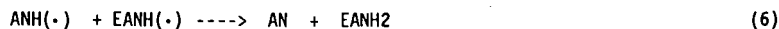
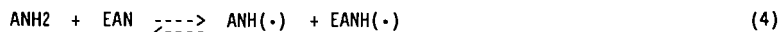
Chain propagation occurs by reaction of 7 with cyclohexane to produce the RHT product, 6:



Chain propagation also occurs by abstraction of hydrogen atom from cyclohexane by the adducts of cyclohexyl radical to 1. An alternate mechanism for formation of 6, the scission of hydrogen atom from cyclohexyl radical and addition of the H atom to 1, leading to 6, was ruled out, based on the observed first order dependence on 1 for the formation of 6. Unfortunately, hydrogen (H₂), which would have revealed the production of H·, was not analyzed in the reaction mixture. From the chain length of the reaction, the yield of 6 produced in the initiation step was suggested to be insignificant.

Metzger's results⁶ are indeed surprising, since they imply a very low barrier for the RHT reaction. The rate of β -scission of hydrogen from cyclohexyl radical is given by $k_\beta = 5 \times 10^{13} \exp(-36000/RT)$, or $k_\beta = 1.2 \times 10^2 \text{ M}^{-1}\text{s}^{-1}$ at 400 °C. For RHT transfer of hydrogen to the olefin, to occur 10 times faster than β -scission of free hydrogen at the $5 \times 10^{-3} \text{ M}$ concentrations of 1 employed, an RHT barrier of only 9.7 kcal/mole would be required. For RHT to occur 100 times faster than free hydrogen atom production requires an RHT barrier of only 6.6 kcal/mole. This assumes a typical bimolecular A-factor of $10^{8.5} \text{ M}^{-1}\text{s}^{-1}$ for RHT.

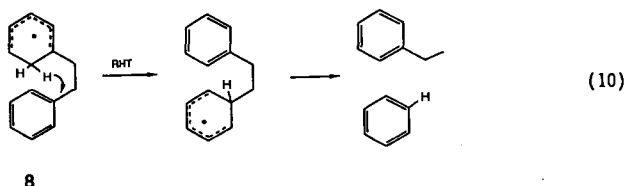
The study of Billmers et al.,⁷ examined the transfer of hydrogen from 9,10-dihydroanthracene (ANH₂) to 2-ethylanthracene (EAN) to form 9,10-dihydro-2-ethylanthracene (EAH₂) and anthracene (AN). The kinetic order of the non-chain reaction and the observed Arrhenius dependence were consistent with a mechanism involving rate-determining reverse radical disproportionation (RRD) (eq. 4). Other key steps include production of EANH(·) by RHT, eq 5, and formation of the product EANH₂ is by disproportionation (eq. 8) or abstraction (eq. 9).



Billmers et al.⁷ found that the rate of formation of EANH₂ was decreased by increasing the ratio AN/ANH₂ at fixed concentrations of ANH₂ and EAN in the initial reaction mixture. This is presumed to be due to the reverse of eq. 5. From an analysis of the reduction of the rate of production of EANH₂ with increasing AN/ANH₂, k_{-5} was estimated to be $120 \text{ M}^{-1}\text{s}^{-1}$ at 350°C, or $E_{-5} = 18.3$ kcal/mole.

In a related study of hydrogen transfer between 9,10-dihydrophenanthrene and anthracene, computer modeling of the observed kinetics led to an "RHT" rate constant $k = 7.5 \times 10^3 \text{ M}^{-1} \text{ s}^{-1}$ at 350 °C, corresponding to $E_a = 13.3$ kcal/mole. If correct, this is a surprisingly low activation barrier, since the barrier was lowered fully as much as the enthalpy change for the reaction compared to the thermoneutral transfer between anthracenes, -5 kcal/mole. This corresponds to an Evans-Polanyi factor of ca. 1 for the reaction, whereas hydrogen atom metathesis reactions usually exhibit Evans-Polanyi factors of 0.5 or less. The authors point out that the reaction kinetics are suggested to be equally well represented by a 3-step sequence of addition of hydrophenanthrenyl radical to anthracene, intramolecular hydrogen atom transfer, and radical scission to give phenanthrene and 9-hydroanthracenyl radical, without postulating the unconventional RHT reaction.

In recent work,⁹ we examined the intramolecular RHT reaction of the 2-(2-phenylethyl)cyclohexadienyl radical, **8**, (eq. 10). Intramolecular hydrogen shift from the cyclohexadienyl ring to the *ipso* position of the phenyl ring, followed by β -scission would have given benzene and ethylbenzene as products.



Competing with this reaction is β -scission to give benzyl radical and isotoluene, or hydrogen loss to give bibenzyl. No detectable RHT occurred at 235 °C for this near-thermoneutral reaction. The ratio of H• loss (or the isoenergetic β -scission) to RHT, determined by product detection limits, was greater than 100:1. The predicted A-factor for intramolecular RHT, $A_1 = 10^{10.8} \text{ M}^{-1} \text{ s}^{-1}$, and the predicted rate constant for H atom loss, $7.7 \times 10^2 \text{ M}^{-1} \text{ s}^{-1}$, results in a minimum barrier for the intramolecular RHT reaction of 23 kcal/mole for the slightly endergonic hydrogen transfer ($\Delta H^\circ = 0.5$ kcal/mole). In research currently under way, we are preparing exothermic analogues of intramolecular RHT to attempt to unambiguously observe, in a stereochemically restricted system, a "true" RHT reaction with no possibility of free H atom involvement.

In summary, studies to date suggest a barrier for thermoneutral hydrogen transfer in the RHT reaction between aromatic systems of ca. 18 kcal/mole. None of the studies of RHT or equivalent mechanisms have attempted to directly observe H₂, and direct determination of Arrhenius parameters and a detailed examination of the pathway of the hydrogen transfer process remains to be carried out.

To better understand the structural and energetic aspects of RHT, we have carried out a semiempirical molecular orbital study of bimolecular and intramolecular RHT reactions for a variety of aromatic systems. We also examined in detail the energetics of hydrogen transfer between ethyl radical

and ethylene via RHT, an addition/metathesis/scission pathway, and a hybrid "concerted" pathway.

RESULTS AND DISCUSSION

AM1/RHF¹⁰ transition states were located for hydrogen transfer reactions from the cyclohexadienyl radical to benzene, the *ipso* position of toluene, the 1-position of naphthalene, and the 9-position of anthracene. In addition, RHT transition states were located for thermoneutral hydrogen transfer between naphthalenes (1-positions) and anthracenes (9-positions), and the thermoneutral RHT reaction between ethyl radical and ethylene was examined. In each case, the hydrogen is caused to migrate to the olefinic or aromatic carbon.

Table I lists activation barriers for thermoneutral transfer of hydrogen between pairs of benzene, naphthalene, and anthracene rings. AM1 calculations often result in barriers that are higher than experimental values for reactions involving stretched bonds in open-shell systems. However, hydrogen abstraction barriers predicted by AM1 are often in good agreement with experimental values. For example, AM1/RHF predicts a barrier of 18 kcal/mole for the symmetric hydrogen abstraction reaction from cyclohexadiene by the cyclohexadienyl radical, in good agreement with thermoneutral abstraction reactions of alkyl radicals from alkanes, which, in the absence of steric effects, exhibit barriers of ca. 14 kcal/mole.¹¹ Thus, it was surprising to find that the nominally similar RHT reactions gave substantially higher barriers. Table II presents results for transfer of hydrogen from cyclohexadienyl to aromatic systems. For purposes of comparison, Table III gives calculated and experimental values of C-H bond dissociation energies and activation barriers for hydrogen loss from hydroaryl and ethyl radicals. Although a totally satisfactory calibration of the AM1 method for the present category of reactions is not possible, the overestimations of C-H bond dissociation energies for hydroaryl radicals suggest that the calculated AM1/RHF RHT barriers are 25 to 50% higher than the actual values. Finally, in Table IV, barriers for intramolecular RHT reactions are presented for 2-, 3-, and 4-carbon bridging linkages.

Although the AM1 method has obvious limitations, some interesting observations are possible: (1) RHT barriers for thermoneutral hydrogen transfer reactions are predicted to be closely spaced, with a slight increase in barrier going from benzene to anthracene. Thus, the hydroaryl radicals that have the strongest C-H bonds correspond to the aromatic systems best able to stabilize the liberated hydrogen atoms. (2) The predicted barriers drop dramatically as the hydrogen transfer reactions become more exothermic, such that the barrier for transfer between cyclohexadienyl and anthracene is low enough for the reaction to be observable at moderate (< ca. 250°C) temperatures. The dramatic drop is reminiscent of the drop in barrier for hydrophenanthrenyl H₂ transfer to anthracene vs. thermoneutral transfer between anthracenes.⁷ (3) In every case, the activation barrier for RHT is below that of free hydrogen atom production. Finally, (4) intramolecular RHT with 2-, 3- and 4-carbon bridges between the two benzenoid aromatic systems results in closely spaced activation barriers, higher by 2 to 4 kcal/mole than thermoneutral intermolecular RHT reactions. The question becomes whether RHT

will compete with free H₂ reaction or with the more conventional addition/transfer/scission pathway for hydrogen transfer.

The Addition/Transfer/Scission Pathway

The AM1/RHF barrier for the RHT reaction between ethyl radical and ethylene, 40.0 kcal/mole, is found to be less than the barrier for hydrogen scission, 52 kcal/mole, but remains a high energy pathway. To examine an alternative pathway to RHT, that of addition, metathesis, and scission, we examined the reaction of ethyl + ethylene. The results of a map of several possible surfaces is depicted in Figure 1. Throughout the calculation, the C4-C3 and C1-C2 bonds were constrained to be planar. The lower path shows the energy profile for addition of ethyl to ethylene to yield an eclipsed butyl radical (the *trans* conformer is calculated to be 5 kcal/mole more stable). The upper surface in Figure 1 shows the energy as a function of the C2-C3 distance, with equal C1-H-C4 distances at the position of maximum energy, corresponding to the energy barrier for hydrogen migration from C1 to C4. The energy gap labeled A shows the barrier for 1,4-hydrogen transfer, which is less than that of β -scission. The energy gap B corresponds to RHT via a cyclic transition state structure. It is calculated to be 1 kcal/mole lower than the acyclic transition state structure in which C2 and C3 do not interact. The energy gap C corresponds to H atom elimination. It is energetically the least favored reaction path. This calculation suggests that conventional addition/transfer/scission pathways may be favored by enthalpy over the direct RHT path, and that the RHT barrier is reduced (B in Figure 1) by the interaction of the two pi systems. Also, the position of the upper curve between 1.5 to 1.8 Å below the β -scission transition state energy raises the possibility that the addition/transfer/scission pathway might become concerted at suitably high temperatures. Further work to examine similar effects with RHT between aromatic systems is underway.

Finally, the lower predicted barriers for addition/metathesis/scission in this system may mean that intramolecular RHT reactions that are stereochemically precluded from the addition/metathesis pathways (and are true "RHT" reactions) may actually be significantly higher energy pathways. We are currently synthesizing model intramolecular RHT systems to observe exothermic RHT reactions to attempt to unambiguously observe and characterize RHT reactions.

REFERENCES

- 1) D. F. McMillen, W. C. Ogier, S.-J. Chang, R. H. Fleming and R. Malhotra, Proc. Intl. Conf. on Coal Science, Pittsburgh, PA 15-19 August, 1983, p. 199.
- 2) D. F. McMillen, R. Malhotra, S.-J. Chang, and S. E. Nigenda, Am. Chem. Soc., Div. Fuel Chem Preprints, 1985, 30(4), 297.
- 3) D. F. McMillen and R. Malhotra, Proc. 1987 Intl Conf. Coal Science, Maastricht, The Netherlands, 26-30 October, 1987.
- 4) D. F. McMillen, R. Malhotra, S.-J. Chang, W. C. Ogier, E. Nigenda and R. H. Fleming, Fuel, 1987, 66, 1611.

- 5) D. F. McMillen, R. Malhotra, G. P. Hum, and S.-J. Chang, Energy & Fuels, 1987, 1(2), 193.
- 6) J. O. Metzger, Angew. Chem. Int. Ed. Engl. 1986, 25, 80.
- 7) R. Billmers, L. L. Griffith and S. E. Stein, J. Phys. Chem. 1986, 90, 517.
- 8) R. Billmers, R. L. Brown, and S. E. Stein, Int. J. Chem. Kinetics, 1989, 21, 375.
- 9) Tom Autrey and James A. Franz "A Search for the Radical Hydrogen Transfer Pathway in Coal Liquefaction," Prepr. Fuel Div. Am. Chem. Soc. 1990, 35(2), 381.
- 10) MOPAC Molecular Orbital Program, Quantum Chemistry Program Exchange, Program No. 455, version 5.0, Quantum Chemistry Program Exchange, Department of Chemistry, Indiana University.
- 11) J. A. Franz, M. S. Alnajjar, R. D. Barrows, D. A. Kaisaki, D. M. Camaioni, and N. K. Suleman, J. Org. Chem. 1986, 51, 1446.

ACKNOWLEDGEMENT

The authors thank Dr. J. O. Metzger for useful discussions. This work was supported by the Office of Basic Energy Sciences, U. S. Department of Energy, under contract DE-AC06-76RLO 1830.

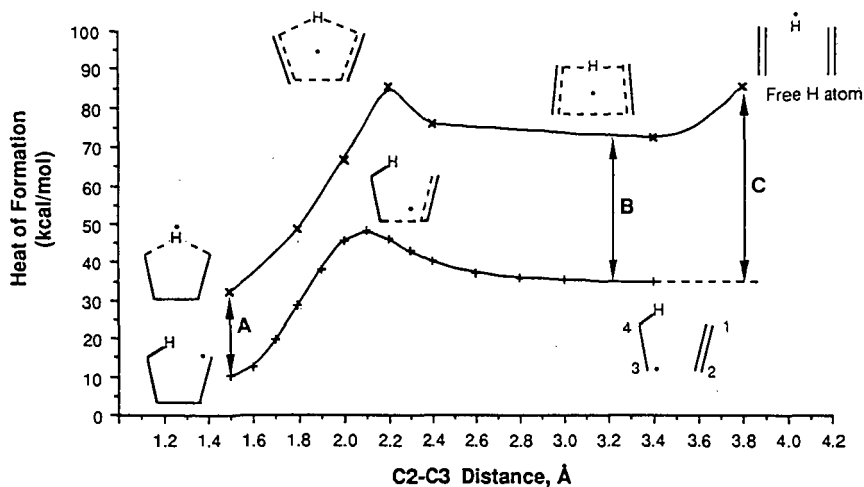


Figure 1. Reaction paths for ethyl radical + ethylene calculated with AMI/RHF. A: Barrier for 1,4-hydrogen atom shift from eclipsed butyl radical (*trans*-butyl radical conformation is 5 kcal/mole lower in energy). B: Barrier for radical hydrogen transfer (RHT). The Z-shaped or alicyclic TS structure with non-interacting termini is calculated to be 1 kcal/mole higher in energy. C: Barrier for H-atom elimination-addition reaction.

Table I. AMI/RHF Barriers for Thermoneutral Hydrogen Transfer From Hydroaryl Radicals to Aromatic Rings and the Ethyl + Ethylene Reaction

Reaction	ΔH^\ddagger , kcal/mole
Cyclohexadienyl + Benzene	32.7
1-Hydronaphthyl + Naphthalene	34.5
9-Hydroanthracenyl + Anthracene	36.6
Ethyl + Ethylene	40.0

Table II. AMI/RHF Barriers for Hydrogen Transfer From Cyclohexadienyl Radical to Aromatic Rings

Reaction	ΔH^\ddagger , kcal/mole ^a	ΔH° , kcal/mole ^b
Cyclohexadienyl + Toluene (<i>ipso</i> position)	36.4	0.4
Cyclohexadienyl + Benzene	32.7	0.0
Cyclohexadienyl + Naphthalene	25.6	-7.5
Cyclohexadienyl + Anthracene	16.4	-18.8

^aAMI/RHF calculation

^bExperimental heat of reaction for the hydrogen atom transfer reaction

Table III. Hydrogen Atom Scission from Hydroaryl and Ethyl Radicals

Reaction	ΔH^\ddagger , kcal/mole ^a		ΔH° , kcal/mole ^b	
	expt	calc	expt	calc
Cyclohexadienyl ---> benzene + H	28.7	44	25.7	34.8
1-Hydronaphthyl ---> naphthalene + H	37	--	35	39.9
9-Hydroanthracenyl ---> Anthracene + H	45	58	43	50.3
Ethyl ---> Ethylene + H	38	52	35.6	49.4

^aAMI/RHF calculation

^bExperimental heat of reaction for the hydrogen atom transfer reaction

Table IV. AMI/RHF Barriers for Intramolecular RHT Reactions^a

Ground State Radical	ΔH^\ddagger , kcal/mole
2-(2-phenylethyl)cyclohexadienyl, 8	38.2
2-(2-phenylpropyl)cyclohexadienyl	40.8
2-(2-phenylbutyl)cyclohexadienyl	39.4

^aThe hydrogen is transferred to the *ipso* position of the appended ring. See, e.g., eq. 10

THERMOLYSIS OF SURFACE-IMMOBILIZED PHENETHYL PHENYL ETHER

P. F. Britt, A. C. Buchanan, III, and V. M. Hitsman
Chemistry Division
Oak Ridge National Laboratory
P. O. Box 2008
Oak Ridge, TN 37831-6197

ABSTRACT

Our research has focused on modeling the constraints on free-radical reactions that might be imposed in coal as a consequence of its cross-linked macromolecular structure by covalently bonding diphenylalkanes to an inert silica surface. A surface-immobilized phenethyl phenyl ether ($\approx\text{PhCH}_2\text{CH}_2\text{OPh}$, or $\approx\text{PPE-3}$) has been prepared as a model for ether linkages in lignin by the condensation of *p*-HOPhCH₂CH₂OPh with the surface hydroxyls of a high purity fumed silica. Thermolysis of $\approx\text{PPE-3}$ at saturation surface coverage at 375 °C produces $\approx\text{PhCH}=\text{CH}_2$ and PhOH as the major products which are consistent with the proposed free-radical chain mechanism for the decomposition of fluid-phase phenethyl phenyl ether. However, significant quantities of $\approx\text{PhCH}_3$ and PhCHO (ca. 18% of the products) are produced indicating the emergence of a new reaction pathway on the surface. The mechanism for the decomposition of $\approx\text{PPE-3}$ will be discussed in light of this new information.

Keywords: thermolysis, model compounds, mechanisms, restricted diffusion

INTRODUCTION

Attempts to probe the fundamental chemical reactions responsible for the thermal conversion of coal into liquid products has been hampered by the complex heterogeneous macromolecular structure of coal. Our efforts have focused on modelling the impact of restricted diffusional mobility on the thermal reactivity of coal by covalently bonding model compounds representing structural features in coal to an inert silica surface. Thus far, our research has focused on the thermally induced free radical decomposition of α , ω -diphenylalkanes ($\text{Ph}(\text{CH}_2)_n\text{Ph}$ where $n=0-4$) at 345-400 °C.¹⁻⁵ The results have shown that significant perturbations can occur in free radical reaction mechanisms which can alter reaction rates and product selectivities compared to the corresponding fluid phase behavior. We now have initiated a study on the effects of restricted mass transport on the thermal decomposition of ether bridges which are prevalent in low rank coals and lignites. Although ether linkages are more thermally labile than the corresponding carbon analogues, it has been observed that

under liquefaction conditions optimized for bituminous coals, low rank coals and lignites afford low liquefaction yields.⁶ It has been proposed that cross-linking reactions associated with oxygen functional groups (-OH, -OCH₃, and -COOH) are responsible for the low yields.^{6,7} In order to better understand the chemical reactions leading to retrograde processes, the effects of restricted diffusion of the thermolysis of surface-attached phenethyl phenyl ether (\approx PhCH₂CH₂OPh, \approx PPE-3) has been studied. Although the thermal decomposition of phenethyl phenyl ether (PPE) has been previously studied in the gas phase,^{8,9a} liquid phase,^{9a} and in the presence of tetralin,^{8,10} hydrogen,^{10,11} and metal catalysts,¹¹ our results show that a previously undetected free radical decomposition pathway is available for the thermal cracking of \approx PPE.

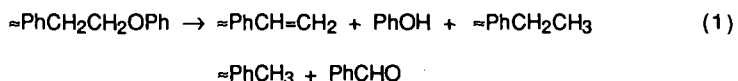
EXPERIMENTAL

Surface-immobilized phenethyl phenyl ether (\approx PPE-3) was prepared at saturation surface coverage by the condensation of *p*-HOC₆H₄CH₂CH₂OPh (2.25 equiv) with the surface hydroxyl groups of a high purity fumed amorphous silica (Cab-O-Sil, grade M-5, Cabot Corp., 200 m² g⁻¹, ca. 4.5 OH nm⁻²) at 222 °C for 30 min as previously described.¹⁻³ The excess phenol was sublimed from the sample by heating for 70 min at 254 °C under vacuum (3×10⁻³ Torr). The surface-attached PPE was liberated from the silica as the phenol by a base hydrolysis procedure, silylated to the trimethylsilyl ether, and analyzed by GC and GC/MS. The surface coverage was 0.562 mmol of \approx PPE-3 per gram of derivatized silica with the purity of recovered phenol >99.9% by GC. The starting phenol, *p*-HOC₆H₄CH₂CH₂OPh, was prepared in four steps from *p*-HOC₆H₄CH₂CH₂OH by selective benzylation of the phenol with K₂CO₃ and PhCH₂Br in dimethyl formamide, conversion of the alcohol to the tosylate with tosyl chloride in pyridine, base catalyzed alkylation of phenol with the tosylate using K₂CO₃ and PhOH in dimethyl formamide, and debenylation by catalytic hydrogenolysis using Pd/C in HOAc with 10 % H₂SO₄. Repeated crystallizations from benzene/hexanes afforded *p*-HOC₆H₄CH₂CH₂OPh in >99.9% purity by GC.

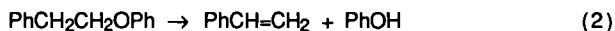
Thermolysis of \approx PPE-3 was performed at 375 ± 1 °C in T-shaped tubes sealed under high vacuum (ca. 10⁻⁶ Torr). The volatile products were collected as they formed in a cold trap (77 K), analyzed by GC and GC/MS, and quantitated by the use of internal standards with measured GC detector response factors. The surface-attached products were removed from the silica as the corresponding phenols by a base hydrolysis procedure, silylated to the trimethylsilyl ethers, and analyzed as above. All products were identified by the mass spectra and whenever possible, by comparison with an authentic sample.

RESULTS AND DISCUSSION

Thermolysis of \approx PPE-3 at 375 °C has been studied at saturation coverage from ca. 1-17 % conversion. At low conversion, \approx PPE-3 cracks to from approximately equal amounts of phenol plus surface-attached styrene (\approx PhCH=CH₂) as the major products (ca. 81 mol %) and benzaldehyde plus surface-attached toluene (\approx PhCH₃) as minor products (ca. 18 mol %). A trace amount of surface-attached ethylbenzene (\approx PhCH₂CH₃, ca. 1.5 mol %) was also detected. The conversion dependence of the products is shown in Figure 1.

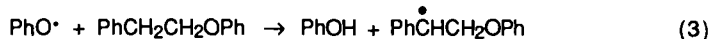


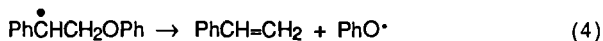
Thermolysis of phenethyl phenyl ether (PPE) in the gas or liquid phase at low conversions at 325-400 °C has been reported to yield PhOH and PhCH=CH₂ as



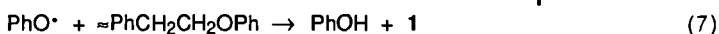
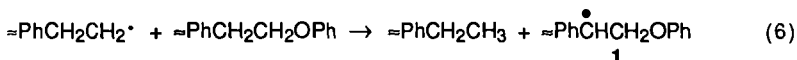
the major products (eq 2).^{8,9} Although minor amounts of PhCH₃ and PhCH₂CH₃ have been detected, they were attributed to secondary decomposition of PhCH=CH₂.⁸ However, benzaldehyde has not been reported from the thermal decomposition of PPE in the gas, liquid phase, or in the presence of hydrogen donors. In the thermolysis of \approx PPE-3, \approx PhCH₃ does not appear to be a secondary product formed at the expense of the surface-attached styrene as shown in Figure 1. The rate of decomposition of PPE in the liquid phase at 350-390 °C is similar to that of the carbon analogue 1,3-diphenylpropane (Ph(CH₂)₃Ph, DPP)⁹ and can be accelerated by the addition of benzyl phenyl ether. Likewise, the rate of decomposition of \approx PPE-3 at 375 °C (8.3 % h⁻¹) is similar to that of surface-attached Ph(CH₂)₃Ph (\approx DPP) at saturation coverage (7-9 % h⁻¹).² Since the rates of conversion of DPP and \approx DPP are similar, surface-attachment does not perturb the initial reaction behavior in the decomposition of \approx PPE-3.

The cracking of PPE is proposed to proceed by a free radical chain decomposition reaction, although a minor contribution from a concerted retro-ene reaction can not be completely ruled out.⁸ The decomposition reaction is initiated by homolysis of the weak C-O bond (bond dissociation energy estimated as ca. 63 kcal mol⁻¹)¹² to form 2-phenylethyl and phenoxy radicals. The radical chain propagation steps are shown in eq 3 and 4.

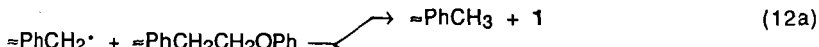
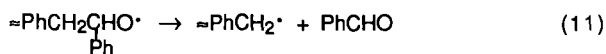
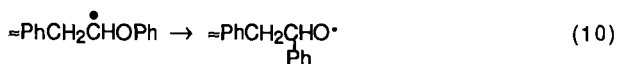
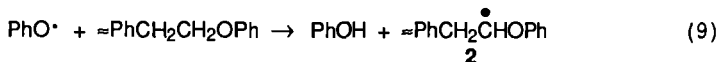




In the thermolysis of \approx PPE-3, a similar free radical decomposition reaction can be written to explain the formation of the products (eq 5-12). The reaction is initiated by the homolysis of the weak C-O bond. The resulting radicals can abstract hydrogen from \approx PPE-3 to form a surface-attached 1-phenoxy-2-phenyl-2-ethyl radical (1) which can undergo β -scission to yield surface-attached styrene and the chain carrying phenoxy radical.



Surface-attached PhCH_3 and gas phase PhCHO can be formed by a free radical chain process shown in steps 9-12. Hydrogen abstraction at the aliphatic site forms 1-phenoxy-2-phenyl-1-ethyl radical (2). Although radical 1 is estimated to be more stable than 2 by ca. 7 kcal mol⁻¹,¹² there is precedence for the competitive formation of products from the thermodynamically less stable radical of tetralin (2-tetralyl radical)¹³ and 1,4-diphenylbutane (1,4-diphenyl-2-butyl radical)¹⁴ at these temperatures.



Radical 2 can undergo a 1,2-phenyl shift from oxygen to carbon (eq 10). Analogous intramolecular 1,2-phenyl shifts have been reported in the thermal decomposition of phenetole ($\text{PhOCH}_2\text{CH}_3$)¹⁵ and anisole at 400 °C.¹⁶ β -scission of the rearranged radical affords benzaldehyde and the chain carrying surface-attached benzyl radical. Formation of $\approx\text{PhCH}_3$ from C-C homolysis of \approx PPE, producing $\approx\text{PhCH}_2\cdot$ and $\text{PhOCH}_2\cdot$, is predicted to be small

since the C-C bond is estimated to be ca. 7 kcal mol⁻¹ stronger than the corresponding C-O bond in PPE.¹² Furthermore, no anisole (from hydrogen abstraction by PhOCH₂·) or benzyl alcohol (from 1,2-phenyl shift and hydrogen abstraction by PhCH₂O·) was detected. Additional evidence for this previously undetected free radical pathway for the thermal degradation of PPE is found in the thermolysis of the ≈PhOCH₂CH₂Ph (≈PPE-1) at 375 °C in which ≈PhOH and PhCH=CH₂ are formed as the major products (ca. 80 mol %) and ≈PhCHO and PhCH₃ are formed as the minor products (ca. 20 mol %) indicating a similar free radical chain mechanism as described in steps 5-12 is occurring.¹⁷

At this point, it is unclear whether the additional mechanistic steps (eq 9-12) required to rationalize the product distribution from the thermolysis of ≈PPE are a consequence of restricted diffusion, or an undetected reaction pathway in the thermolysis of liquid phase PPE. However, these reactions may explain the formation of toluene at low conversions and the formation of 1,2-diphenylethane and benzyl phenyl ether at higher conversions (termination reactions of PhCH₂·) which are reported for the thermal decomposition of PPE.⁸ These steps may also be participating in the thermal decomposition of the homopolymers of 4-allylphenol and eugenol, which contain β-ether types linkages.^{18,19} The previous mechanism for the decomposition of PPE (steps 3 and 4)⁹ could not explain the formation of C₁-phenol and catechol (cresol, *m/e* 108 and 2-methoxy-4-methylphenol, *m/e* 138). However, by inclusion of reactions analogous to those in steps 9-12, a reasonable free radical chain pathway is available for formation of these products.

CONCLUSIONS

Covalent attachment of organic compounds to an inert silica surface has proven useful in modeling the effects of restricted substrate diffusion on free radical decomposition reactions which may occur in coal as a consequence of its cross-linked macromolecular structure. Thermolysis of surface-attached phenethyl phenyl ether, as a model for ether linkages in lignin, has shown a previously undetected pathway for the free radical chain decomposition of PPE which affords surface-attached toluene and gas phase benzaldehyde. Additional studies into the role of the radical rearrangements and the origin of this new decomposition pathway in the thermal decomposition of ≈PPE are currently under way.

ACKNOWLEDGEMENTS

This research was sponsored by the Division of Chemical Sciences, Office of Basic Energy Sciences, U. S. Department of Energy under contract DE-AC05-

840R21400 with Martin Marietta Energy Systems, Inc. VMH was supported by Oak Ridge Associated Universities Undergraduate Research Participation Program.

REFERENCES

1. Buchanan, III, A. C.; Dunstan, T. D. J.; Douglas, E. C.; Poutsma, M. L. *J. Am. Chem. Soc.* **1986**, *108*, 7703.
2. Buchanan, III, A. C.; Biggs, C. A. *J. Org. Chem.* **1989**, *54*, 517.
3. (a) Britt, P. F.; Buchanan, III, A. C.; Biggs, C. A. *Prep. Pap. -Am. Chem. Soc., Div. Fuel Chem.* **1989**, *34(2)*, 567. (b) Britt, P. F.; Buchanan, III, A. C., submitted for publication.
4. (a) Buchanan, III, A. C.; Britt, P. F.; Biggs, C. A. *Energy & Fuels* **1990**, *4*, 415. (b) Buchanan, III, A. C.; Britt, P. F.; Biggs, C. A. *Prep. Pap. -Am. Chem. Soc., Div. Fuel Chem.* **1989**, *34(4)*, 1317.
5. Buchanan, III, A. C.; Britt, P. F.; Poutsma, M. L. *Prep. Pap. -Am. Chem. Soc., Div. Fuel Chem.* **1990**, *35(1)*, 217.
6. Solomon, P. R.; Serio, M. A.; Deshpande, G. V.; Kroo, E.; Schobert, H.; Burgess, C. *Prep. Pap. -Am. Chem. Soc., Div. Fuel Chem.* **1989**, *34(3)*, 803.
7. Suuberg, E. M.; Lee, D.; Larsen, J. W. *Fuel* **1985**, *64*, 1668.
8. Klein, M. T.; Virk, P. S. *Ind. Eng. Chem. Fundam.* **1983**, *22*, 35.
9. (a) Gilbert, K. E.; Gajewski, J. J. *J. Org. Chem.* **1982**, *47*, 4899. (b) Gilbert, K. E. *J. Org. Chem.* **1984**, *49*, 6.
10. Korobkov, V. Y.; Grigorieva, E. N.; Bykov, V. I.; Senko, O. V.; Kalechitz, I. V. *Fuel* **1988**, *67*, 657.
11. Cassidy, P. J.; Jackson, W. R.; Larkins, F. P. *Fuel* **1983**, *62*, 1404.
12. (a) Benson, S. W. *Thermochemical Kinetics*, 2nd ed.; Wiley-Interscience: New York, 1976. (b) McMillen, D. F.; Golden, D. M. *Annu. Rev. Phys. Chem.* **1982**, *33*, 493.
13. (a) Franz, J. A.; Camaioni, D. M. *J. Org. Chem.* **1980**, *45*, 5247. (b) Benjamin, B. M.; Hagaman, E. W.; Raaen, V. F.; Collins, C. J. *Fuel* **1979**, *58*, 386.
14. Poutsma, M. L.; Dyer, C. W. *J. Org. Chem.* **1982**, *47*, 4903.
15. Collins, C. J.; Roark, W. H.; Raaen, V. F.; Benjamin, B. M. *J. Am. Chem. Soc.* **1979**, *101*, 1877.
16. Affi, A. I.; Hindermann, J. P.; Chornet, E.; Overend, R. P. *Fuel* **1989**, *68*, 498.
17. Britt, P. F.; Fox, Jr., J. B., unpublished results.
18. McMillen, D. F.; Malhotra, R.; Serio, M. A. *Prep. Pap. -Am. Chem. Soc., Div. Fuel Chem.* **1990**, *35(2)*, 430.
19. These polymers presumable contain the analogous C-C-O linkage; However, conclusive evidence for the structures of the polymers is not currently available.

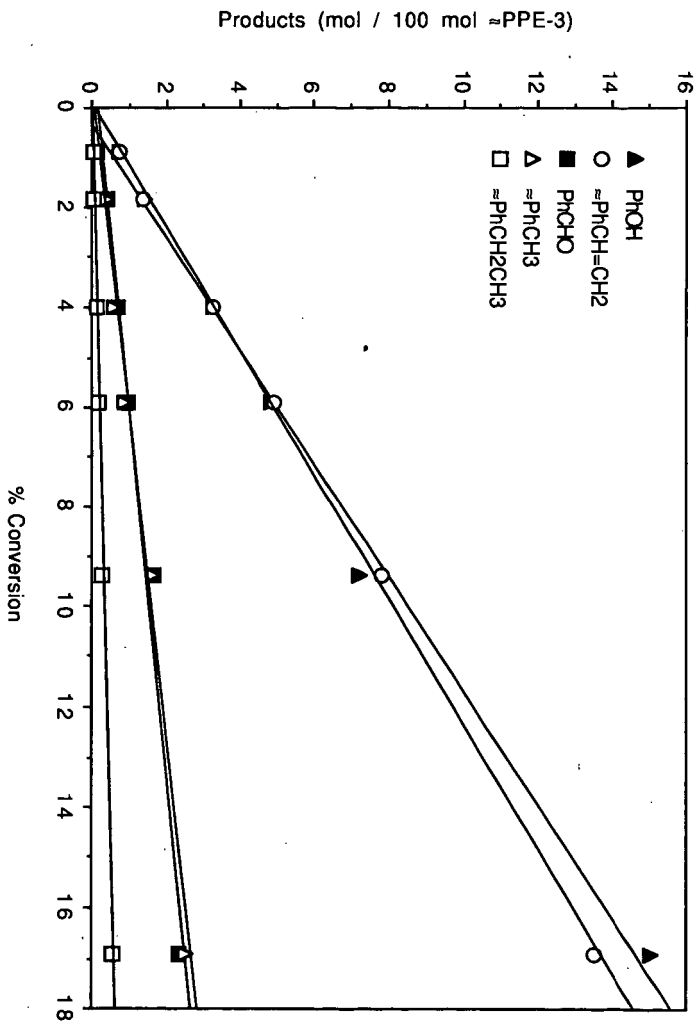


Figure 1. Product selectivities as a function of conversion for thermolysis of \approx PPE-3 at 375 °C at saturation coverage.

**ACID-CATALYZED CRACKING OF SURFACE-IMMOBILIZED
1,3-DIPHENYLPROPANE IN DISPERSED SOLIDS**

A. C. Buchanan, III, P. F. Britt, and C. A. Biggs
Chemistry Division
Oak Ridge National Laboratory
P.O. Box 2008
Oak Ridge, Tennessee 37831-6197

Keywords: acid catalysis, surface-immobilization, reaction mechanisms

ABSTRACT

We previously examined the impact of restricted mass transport on thermally induced, free-radical reaction pathways through the study of diarylalkanes covalently linked to an inert silica surface. We have now dispersed surface-attached 1,3-diphenylpropane (\approx DPP) with a low acidity SiO_2 -1% Al_2O_3 (surface area of 170 m^2/g) by solvent removal from a colloidal suspension of the components. Thermolysis studies at 310-375 $^\circ\text{C}$ under vacuum reveal a surprisingly efficient and selective acid-catalyzed cracking reaction for \approx DPP in the solid state. Even at 375 $^\circ\text{C}$, acid-catalyzed aromatic dealkylation of \approx DPP dominates over the normal free-radical decomposition path. The results indicate that significant solid-state interactions between catalyst and substrate can occur, which has significant implications for the use of dispersed catalysts in coal liquefaction and hydropyrolysis.

INTRODUCTION

There has been considerable recent interest in the development of unsupported, highly dispersed catalysts for improving the conversion and product selectivity in coal liquefaction^{1,2} and hydropyrolysis.³ This includes the study of sulfate-promoted metal oxide catalysts, which are reported to have strong surface acidity.^{2b} One potential advantage of such dispersed catalysts is the improved contact between the coal, solvent vehicle if present, hydrogen gas and the catalyst surface, particularly when catalysts with very small particle sizes can be generated. A significant mechanistic question still to be addressed is if, in the early stages of coal dissolution, significant activation of solid coal particles by solid catalyst can occur. In this paper we report initial results from model systems that begin to address this issue.

The cross-linked, network structure of coal may impose constraints on conventional reaction mechanisms as a consequence of restricted mass transport. We have examined this phenomenon for thermal reactions through the study of model compounds that are covalently anchored to an inert silica surface.⁴⁻⁷ In our current study, we employ surface-immobilized 1,3-diphenylpropane (\approx DPP) as the model compound. Thermolysis of \approx DPP has been studied in detail both by itself⁵ and in the presence of co-attached aromatics.⁶ The free-radical chain decomposition reaction that occurs for \approx DPP can be considered prototypical for

trimethylene (and longer) aliphatic groups that connect aromatic clusters in coal. In this study we examine the reactivity of solid \approx DPP dispersed in solid $\text{SiO}_2\text{-}1\% \text{ Al}_2\text{O}_3$ at 310-375 °C. Products that may be generated from potential acid-catalyzed reactions of \approx DPP will be easily distinguished from products of the thermal, free-radical reaction.

EXPERIMENTAL

Two-batches of \approx DPP were prepared with surface coverages of 0.532 and 0.320 mmol/g according to published procedures⁵ by the reaction of $p\text{-HOC}_6\text{H}_4(\text{CH}_2)_3\text{C}_6\text{H}_5$ with the surface hydroxyls of a fumed silica (Cabosil M-5, Cabot Corp., $200 \pm 25 \text{ m}^2/\text{g}$). The solid diluents, Aerosil 200 silica or Aerosil MOX 170 silica-alumina (Degussa Corp.), were dried in air at 200 °C for 4 h prior to use. The Aerosil 200 is an amorphous, fumed silica ($200 \pm 25 \text{ m}^2/\text{g}$; average primary particle size of 12 nm), while the Aerosil Mox 170 is a co-fumed oxide containing ca. 1% Al_2O_3 ($170 \pm 30 \text{ m}^2/\text{g}$; average primary particle size of 15 nm).⁸ Solid mixtures were prepared by making dilute slurries of \approx DPP and diluent in dry benzene, followed by solvent removal at 70 °C under vacuum. Analysis of aliquots of the diluted \approx DPP by standard procedures⁵ gave the expected amounts of \approx DPP within $\pm 5\%$.

Reactions were performed at 310-375 °C (± 1 °C) under vacuum (ca. 5×10^{-6} torr) in a controlled temperature tube furnace as previously described.^{4,5} Vapor-phase products migrated from the heated zone into a liquid nitrogen cold trap, and were analyzed by GC and GC-MS with the use of internal standards. Products on the surface were detached by digestion of the solid in aqueous base and, following workup, were analyzed by GC and GC-MS as phenols or the corresponding trimethylsilyl ethers.

RESULTS AND DISCUSSION

Thermolysis of \approx DPP (0.532 mmol/g) alone occurs readily at 375 °C by a free-radical chain pathway to afford the simple product mixture shown in Fig. 1a and Table 1. The origins of selectivity in product formation including the dependence on surface coverage and co-attached aromatics have been discussed.^{5,6} When \approx DPP is diluted with the Aerosil 200 silica (wt ratio of 1:2.8), the thermolysis products are the same but, as shown in Table 1, the rate of conversion of \approx DPP is reduced by a factor of four.

On the other hand, dilution of \approx DPP with the silica-alumina leads to a substantial rate acceleration as well as a remarkably different set of reaction products as shown in Table 1. Even at 375 °C, the products obtained are principally derived from aromatic dealkylation chemistry, which is characteristic of acid-catalyzed reactions over aluminosilicates involving carbocation intermediates.⁹ Another indicator of acid-catalyzed chemistry is the fact that the \approx PhCH₃ and \approx PhC₂H₅ products (isolated as the corresponding phenols) are isomerized to a mixture of ortho-, meta- and para- isomers with the meta-isomers formed in the largest amounts. Although numerous other products were detected in very small quantities, the acid-catalyzed cracking of \approx DPP is reasonably selective leading principally to surface-attached benzene (\approx PhH) and vapor-phase indan as the major products (Fig. 1b). Over the temperature range of 375-310 °C, these two products account for 67-74% of the total products (mass balances were $\geq 95\%$).

Large quantities of catalyst are not required to drive this reaction. Thermolysis of \approx DPP (surface coverage of 0.320 mmol/g) at 375 °C for 60 min with weight ratios of silica-alumina: \approx DPP of 0, 0.20, and 2.80 gave \approx DPP conversions of 5.5, 11.6, and 18.2%, respectively. Again, in the absence of the silica-alumina only thermally derived products are detected. However, even in the presence of the small quantity of catalyst, the product distribution is dominated by acid-catalyzed products and is similar to the distribution obtained when excess catalyst is employed.

The mechanism of acid-catalyzed cracking of liquid or vapor-phase organics over aluminosilicates is generally accepted to occur through the generation of carbocation intermediates at Brønsted and/or Lewis acid sites.⁸⁻¹¹ Although diarylalkanes have received little attention, alkylbenzenes exhibit products resulting from competition between cracking, transalkylation, and various isomerization reactions. Acid-catalyzed cracking of alkanes over aluminosilicates appears to proceed through a chain reaction involving hydride transfer from reactant molecules to chemically transformed (isomerized, cracked, etc.) carbocations.⁸⁻¹¹ For cracking of alkylbenzenes, a pathway is generally invoked involving protonation at the ipso position on the benzene ring followed by cleavage of the alkyl group as a carbocation, which generally leads to formation of an alkene.⁹ A similar path has been used to explain the hydrocracking at 350 °C of bibenzyl (to benzene and ethylbenzene) with zinc chloride supported on silica gel.¹² On the other hand, fluid-phase DPP has been shown to undergo selective acid-catalyzed cracking to benzene and indan at 100-130 °C in SbCl_3 and $\text{SbCl}_3\text{-AlCl}_3$ melts by a benzylic cation/hydride transfer chain mechanism.¹³ In the current study, cracking of \approx DPP to \approx PhH and indan (Fig. 1b) can be accommodated by either an ipso protonation path or a benzylic cation/hydride transfer chain path. Additional studies will be required to probe the involvement of these processes on the catalytic cracking of \approx DPP in dispersed solids.

It is interesting that the aluminosilicate employed in this study has a Si/Al atomic ratio of ca. 84, which indicates that a much smaller density of acidic sites is present than for typical amorphous aluminosilicate cracking catalysts whose corresponding ratio is 3-8.⁹ Furthermore, the substrate is a solid and the DPP moieties are subject to diffusional constraints as a result of surface attachment. Yet, the acid-catalyzed cracking of \approx DPP in this solid mixture is quite efficient. The small particle size of the fumed silica-alumina employed and the highly dispersed nature of the catalyst may be key factors in the observed efficiency of acid-catalyzed cracking of \approx DPP.

CONCLUSIONS

We have used surface-immobilized 1,3-diphenylpropane (\approx DPP) as a model system to investigate the potential role of acid-catalyzed cracking in dispersed solids. Initial results employing a small particle size, low aluminum content amorphous aluminosilicate demonstrate that efficient catalysis can occur in the dispersed solids at 310-375 °C. The product distribution is distinctly different from that obtained from a thermal free-radical process, and is consistent with the intermediacy of carbocations. The results indicate that significant interactions between the catalyst and substrate occur in the solid state. Hence, these results suggest that small particle size, highly dispersed catalysts may interact significantly with solid coal particles in the early stages of coal liquefaction/hydropyrolysis.

ACKNOWLEDGEMENT

This research was sponsored by the Division of Chemical Sciences, Office of Basic Energy Sciences, U.S. Department of Energy under contract DE-AC05-84OR21400 with Martin Marietta Energy Systems, Inc.

REFERENCES

1. (a) Utz, B. R.; Cugini, A. V.; Frommell, E. A. *ACS Symp. Ser.* 1990, 437, 289. (b) Dosch, R. G.; Stohl, F. V.; Richardson, J. T. *Ibid.* 1990, 437, 279.
2. (a) Herrick, D. E.; Tierney, J. W.; Wender, I.; Huffman, G. P.; Huggins, F. E. *Energy and Fuels*, 1990, 4, 231. (b) Pradhan, V.; Tierney, J. W.; Wender, I. *Prepr. Pap.-Am. Chem. Soc., Div. Fuel Chem.* 1990, 35(3), 793.
3. Snape, C. E.; Bolton, C.; Dosch, R. G.; Stephens, H. P. *Prepr. Pap.-Am. Chem. Soc., Div. Fuel Chem.* 1988, 33(3), 351.
4. Buchanan, III, A. C.; Dunstan, T. D. J.; Douglas, E. C.; Poutsma, M. L. *J. Am. Chem. Soc.* 1986, 108, 7703.
5. Buchanan, III, A. C.; Biggs, C. A. *J. Org. Chem.* 1989, 54, 517.
6. Buchanan, III, A. C.; Britt, P. F.; Biggs, C. A. *Energy and Fuels* 1990, 4, 415.
7. Britt, P. F.; Buchanan, III, A. C.; Biggs, C. A. *Prepr. Pap.-Am. Chem. Soc., Div. Fuel Chem.* 1989, 34(2), 567.
8. Degussa Corporation, Technical Bulletin.
9. (a) Pines, H. "The Chemistry of Catalytic Hydrocarbon Conversions"; Academic Press: New York, 1981; Chapter 1. (b) Corma, A.; Wojciechowski, B. W. *Catal. Rev.* 1985, 27, 29.
10. Guisnet, M. R. *Accts. Chem. Res.* 1990, 23, 392.
11. Rabo, J. A.; Gajda, G. J. *Catal. Rev.* 1990, 31, 385.
12. Sharma, R. K.; Diehl, J. W.; Olson, E. S. *Prepr. Pap.-Am. Chem. Soc., Div. Fuel Chem.* 1990, 35(2), 414.
13. Buchanan, III, A. C.; Dworkin, A. S.; Smith, G. P. *J. Am. Chem. Soc.* 1983, 105, 2843.

Table 1. Effect of Dispersed Solids on Thermolysis of \approx DPP (0.532 mmol/g)

Diluent ^a	None	A	B	B	B	B
\approx DPP (mmol)	0.255	0.0692	0.0644	0.0675	0.0437	0.0413
Temp ($^{\circ}$ C)	375	375	375	375	345	310
Time (min)	60	60	60	10	10	10
\approx DPP Conversion(%) ^b	10.3	2.6	23.5	17.4	11.8	4.8
Products						
(mol/100 mol \approx DPP)						
PhCH ₃	4.45	1.26	0.27	0.13	0.06	c
\approx PhCH ₃ ^c	5.85	1.34	2.61 ^e	1.60 ^e	1.00 ^e	0.36 ^e
PhCH=CH ₂	5.85	1.28	0.18	0.09	c	c
\approx PhCH=CH ₂	4.38	1.36	c	c	c	c
PhC ₂ H ₅	c	c	1.79	1.25	0.65	0.20
\approx PhC ₂ H ₅ ^e	c	c	0.88	0.70	0.44	0.24
PhH	d	d	5.17	3.47	1.95	0.73
\approx PhH	d	d	15.13	11.07	8.07	3.21
Indan	d	d	16.24	12.76	9.17	3.70
\approx Indan ^f	d	d	0.87	1.15	0.84	0.36
Indene	d	d	2.57	1.42	0.87	0.54
PhC ₃ H ₇	d	d	0.76	0.48	0.21	c
PhCH=CHCH ₃	d	d	0.30	0.14	c	c

^aA=Aerosil 200 SiO₂; B=Aerosil MOX-170 SiO₂-1%Al₂O₃; wt diluent: \approx DPP=2.80.

^bMass balances \geq 95%.

^c<0.05.

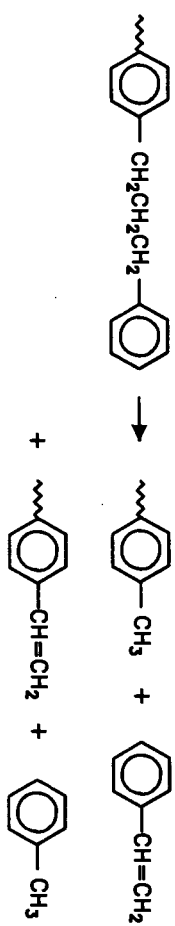
^dNot detected.

^eMixture of ortho-, meta-, and para- isomers in runs with silica-alumina.

^fMixture of two isomers.

Figure 1. Principal products from the reactions of surface-attached 1,3-diphenylpropane

(a) Thermolysis at 345–400 °C



(b) Acid-catalyzed cracking at 310–375 °C



EFFECT OF PORE STRUCTURE OF Ni-Mo CATALYSTS ON HYDROCRACKING OF ASPHALTENE AND PREASPHALTENE AND HETEROATOM REMOVAL

Chunshan SONG⁺*, Toshihiko NIHONMATSU[†], Kouji HANAOKA[†] and Masakatsu NOMURA[†]

⁺Fuel Science Program, Department of Materials Science and Engineering
The Pennsylvania State University, University Park, PA 16802, USA
[†]Department of Applied Chemistry, Faculty of Engineering, Osaka University
Yamada-oka 2-1, Suita, Osaka 565, Japan

Keywords: Catalyst pore size; Asphaltene conversion; Heteroatom removal

INTRODUCTION

Catalytic upgrading of coal liquids is an important step in two-stage coal liquefaction. This process is still confronted with the problem of achieving high catalyst performance for efficient conversion of heavy materials. A number of previous works showed the importance of catalyst pore structure in coal liquefaction (1-3) and in hydroprocessing of petroleum residues due to diffusional limitations (4-7). Several reports on hydrotreating of coal liquids (8-10) suggested that large pore catalysts are effective in converting 450°C+ fractions. Our preliminary results showed that the pore size of Mo catalysts supported on silica or alumina affects the conversion of asphaltene and preasphaltene (11-13).

The major purpose in upgrading primary coal liquids is to convert the heavy materials such as asphaltene and preasphaltene into oils (hexane solubles) with low heteroatom content, which can be used as feed for further refining by conventional petroleum processing technology. The knowledge on the catalyst pore size effect for converting coal-derived asphaltene and preasphaltene is still very limited. This work aimed at clarifying the effects of pore size of Ni-Mo catalysts on their performance in converting the heavy materials and in heteroatom removal. The results and mechanistic considerations are reported in this paper.

EXPERIMENTAL

The catalyst supports were cylindrical gamma-alumina extrudate prepared from boehmite gel (Table 1), which were provided by Sumitomo Metal Mining Co. (S-1), the Catalyst Society of Japan (S-2), and Chiyoda Chemical Engineering and Construction Co. (S-3 and S-4). The catalysts were prepared by co-impregnation of ammonium heptamolybdate and nickel nitrate from their aqueous solution, in which 25% aqueous ammonia was added to give a homogeneous solution, followed by evaporation under reduced pressure. The impregnated extrudates were then dried at 250°C for 2 h in a tube furnace (to remove adsorbed water) and calcined at 500°C for 5 h in an air flow. The catalysts were sulfided (11) and kept in hexane before use. Table 1 gives the physical properties, and Figure 1 shows the pore size distribution of the four Ni-Mo/Al₂O₃ catalysts prepared by using the same procedure. The pore size distribution was measured by using a Shimadzu AutoPore-9200 mercury porosimeter. A commercial KF-153S sulfided Ni-Mo/Al₂O₃ (14) catalyst (Cat-C) was also used in some experiments. The prepared catalysts have the same contents of Ni and Mo to those of the commercial Cat-C (NiO: 2.9, MoO₃: 15.8 wt%). The size of the available extrudates was 1.5 mm (d) for Cat-1, Cat-2 and Cat-C, and 0.8 mm for Cat-3 and Cat-4. In practice, the lowest catalyst sizes permitted in industrial fixed-bed operations are 0.8-1.6 mm.

Table 2 gives the sources and properties of the feed samples, in which Wan-SRC and Aka-SRC were produced from Wandoan subbituminous coal (at 440°C) and Akabira bituminous coal (at 420°C) in a coal liquefaction plant at Sumitomo Coal Mining Co. (11). The coal-derived asphaltenes, Aka-Asp and Wan-Asp (hexane-insoluble benzene solubles) and preasphaltene (Wan-Preasp) were separated from the corresponding SRC. The bitumen asphaltene (Aosb-Asp) was separated from Athabasca oil sand bitumen (12). The original asphaltenes were analyzed by using gel permeation chromatography, GPC (14-15) and ¹H NMR (16-17). The hydrocracking was carried out in a 60 ml rocking autoclave at 425°C for 1 h with 4.9 MPa H₂ (cold). Tetralin was used as solvent unless otherwise mentioned (5g feed/0.5g cylindrical catalyst/5g solvent). The products were separated into gases, oils (hexane solubles), asphaltene, and benzene insolubles, BI (15). The gases were analyzed by GC (Shimadzu 9A). The H₂S in gases were analyzed by using H₂S indicator tube (Kitagawa Indicator) at room temperature.

RESULTS AND DISCUSSION

Asphaltene Structure and Reactivity

Structure of Asphaltene. Table 3 gives the NMR results. As can be seen from Tables 2-3, the coal-derived asphaltenes, Aka-Asp and Wan-Asp have higher C, O and N contents, higher aromaticity and lower H/C atomic ratios, while the bitumen asphaltene (Aosb-Asp) has higher H and S contents, higher H/C ratio and lower aromaticity. Aka-Asp and Wan-Asp contain more aromatic hydrogens (Har), whereas Aosb-Asp is rich in aliphatic hydrogens present in long alkyl side-chains and naphthenic groups (Table 3). The size distribution of the asphaltenes was evaluated by GPC. Figure 2 shows the GPC results, in which the molecular size decreases with increase in elution (retention) time. The broad GPC curves of Aka-Asp and Wan-Asp show that they consist of various components ranging from relatively small to large molecules. The peak sizes correspond to a molecular weight (MW) range of about 200-1000. On the other hand, Aosb-Asp shows a sharp GPC peak in the range of much larger molecular sizes, corresponding to peak MW values of at least over 1000. The average MW values are in the range of 400-600 for Aka-Asp, Wan-Asp and other coal-derived asphaltenes (12,18), and 3000-6000 for Aosb-Asp and other bitumen and petroleum asphaltenes (12,19). These results showed that most coal-derived asphaltene molecules have smaller size and lower MW than bitumen and petroleum asphaltenes.

Reactivity of Asphaltene. Table 4 presents the data on asphaltene reactivity. The thermal run of coal-derived Aka-Asp in H₂-tetralin gave similar conversion to that of the bitumen asphaltene Aosb-Asp. However, the oil yield was lower, and the amount of BI formed from retrogressive reactions was higher with Aka-Asp. The run of Wan-Asp was also accompanied by considerable BI formation. The effect of tetralin in suppressing retrogressive reactions was evaluated by the runs using decalin. The BI from Aka-Asp increased from 9.7 to 12.2% when the solvent changed from H-donor tetralin to decalin, whereas there was little change in BI from Aosb-Asp (1.8 vs. 1.9%). These results showed that coal-derived asphaltenes have high thermal reactivity which also leads to remarkable retrogressive reactions to form BI. Probably the BI formation involved the crosslinking and condensation of reactive radicals and some unstable compounds, especially hydroxy compounds which are rich in coal-derived asphaltenes (18,20) and tend to undergo coupling reactions to form more refractory materials (21-22). As shown in Table 4, H₂S was also formed in the thermal runs, and considerable amounts of H₂S were produced from Aosb-Asp both in tetralin and in decalin. From these results, it seems that thermal decomposition of the bitumen asphaltene involved the cleavage of weak C-C and aliphatic C-S bonds (23), and the resulting radicals were readily stabilized in H₂-solvent systems to form oils, C1-C4 and H₂S.

Catalytic Conversion of Asphaltene and Preasphaltene

Catalyst Properties. With an attempt to examine the effects of catalyst pore size on a unified basis, we prepared four Ni-Mo catalysts using pure gamma-alumina supports. As can be seen from Figure 1 and Table 1, each of the four prepared Ni-Mo catalysts exhibits a unimodal distribution of pore sizes within a specific range. The median pore diameter (MPD) increases in the order of Cat-1 (120 Å) < Cat-2 (150 Å) < Cat-3 (290 Å) < Cat-4 (730 Å). The surface area, however, decreases as pore size increases. The unimodal pore structure and the significantly different pore sizes of Cat-1 through Cat-4 prepared by using the same procedure, enabled us to evaluate the pore size effects.

Asphaltene Hydrocracking. Figure 3 shows the distribution of products from hydrocracking of a coal-derived asphaltene, Aka-Asp. The catalysts significantly promoted Aka-Asp conversion and increased oil yields from 50.7% to more than 69%, without increase in gas yields. The catalysts also reduced BI from 9.7% to less than 3%. Figure 4 shows the conversions and product yields as a function of catalyst pore size (MPD). It is clear from Figure 4 that the conversions of Aka-Asp and oil yields increased remarkably with increase in catalyst MPD up to 290 Å, in spite of the decrease in catalyst surface area with increasing MPD. On the other hand, further increase in MPD from 290 to 730 Å did not offer any advantage. We also examined the solvent effect in the catalytic runs of Aka-Asp with Cat-1 and Cat-3. Using decalin instead of tetralin resulted in 1-2% more BI and slightly higher H₂ consumption. The amounts of BI formed in both cases were lower with large pore Cat-3 than with small pore Cat-1.

Figure 5 presents the results for hydrocracking of Aosb-Asp. The conversions and yields of oils plus gases increased with MPD up to 290 Å, while further increasing MPD to 730 Å decreased the conversion. In this case, catalysts also enhanced the formation of BI and gases. The amounts of H₂S formed in gas phase changed remarkably with different catalysts. The detected H₂S (ml at 25°C under ambient pressure) amounts were as follows: none (26.9) < Cat-1 (45.5) < Cat-2 (52.5) < Cat-3 (77.8) > Cat-4 (34.4). Because of the low S content of Aka-Asp (0.5%) as compared to that of Aosb-Asp (8.3%), the amounts of detected H₂S were much smaller, within 2-4 ml (Cat-1: 3.7; Cat-2: 2.0; Cat-3: 1.8; Cat-4: 1.9).

Since the sizes of the bitumen asphaltene molecules are very large (Figure 2), it might be expected that their conversion might be more sensitive to catalyst pore size. Nevertheless, the increasing extents of oil yields and conversions with MPD were higher with the coal-derived Aka-Asp (Figure 4). Moreover, the highest oil yield from Aosb-Asp with the largest-pore Cat-4 (69.4%) was still lower by 11% than that from Aka-Asp with Cat-3 (80.4%). This comparison suggests that the conversion of coal-derived asphaltene is sensitive to catalyst pore size although their molecular sizes are, on average, much smaller than bitumen and petroleum asphaltene. In addition, the catalytic runs of Aka-Asp consumed slightly more H₂ (2.1-2.3wt%) than the corresponding runs of Aosb-Asp (1.9-2.2wt% based on asphaltene). In both cases, H₂ consumptions with large pore Cat-3 were slightly higher than with small pore Cat-1.

Preasphaltene Hydrocracking. Preasphaltene is also a major fraction in primary coal liquids. Figure 6 presents the results for a coal-derived preasphaltene, Wan-Preasp using Cat-1, Cat-3 and Cat-4. The yields of asphaltene and recovered benzene insolubles were 24.8 and 41.2% with Cat-1, 30.1 and 34.4% with Cat-3, and 33.1 and 29.5% with Cat-4. Apparently, asphaltene yields increased with increasing catalyst MPD from 120 Å (Cat-1) up to 730 Å (Cat-4), rather than a decreasing trend as would be anticipated from the results with the asphaltene fraction as feed (Figure 4). These results suggest that the effect of catalyst pore size on product distribution also depends on the feed used.

SRC Hydroprocessing. Figure 7 presents the results for the unfractionated Wan-SRC, which contained each of the following fractions: oils (35.7%), asphaltene (33.1%) and preasphaltene (31.2%). In this case, we also used a sulfided commercial KF-153S Ni-Mo catalyst (Cat-C, Table 1), which has a MPD value similar to that of the well known Shell 324M Ni-Mo (90 vs. 86 Å). It should be noted that Cat-1 though Cat-4 is alumina-supported catalyst, while Cat-C contains 4.5wt% SiO₂. Figure 8 shows the results for Aka-SRC which contained more preasphaltene (41.5%) and less asphaltene (27.0%) and oils (31.5%) as compared to Wan-SRC. As can be seen from Figures 7 and 8, the yields of preasphaltene decreased with increasing MPD. The oil yields from both SRC increased with MPD up to 290 Å. The gas yields were nearly constant in the runs of Wan-SRC (3.6-4.6%) and Aka-SRC (4.3-5.0%).

Figure 9 shows the effect of catalyst pore size on the net conversion of the heavy materials during SRC hydroprocessing. For runs of both Wan-SRC and Aka-SRC, increasing catalyst pore size significantly promoted preasphaltene conversion. This is consistent with the results shown in Figure 6 for runs of the isolated preasphaltene fraction. It is interesting to note that increasing MPD above certain sizes caused decrease in asphaltene conversion during the runs of the whole SRC (Figure 9). This is considerably different from the trend observed in the runs of isolated asphaltene fraction, where increasing MPD remarkably promoted asphaltene conversion and oil yields (Figure 4). The net conversion of the heavy fractions, especially asphaltene, also appeared to be lower in the runs of unfractionated SRC.

Combination of the results in Figures 3-4 and in Figures 6-9 revealed that in SRC upgrading, when the catalyst pores exceeded certain sizes, more preasphaltene molecules which have larger sizes than asphaltene will diffuse into pores and react on catalyst surface, producing more asphaltene. There is no doubt that increasing pore size also facilitates the diffusion and reaction of asphaltene fractions (Figures 3-5), but the first step of catalytic conversion is adsorption. As the pore sizes become large enough to allow the diffusion of larger molecules, preasphaltene tend to adsorb on the catalyst surface in preference to asphaltene, probably because of the higher aromaticity and higher polarity of the former. The present results were obtained with cylindrical extrudate catalysts. Previous works showed that the change in the extrudate size within the range of 1.6 to 0.8 mm does not have any significant effect on initial activity, while the <100 mesh fine particles generally afford higher conversions than extrudates (24), which is another indication of the diffusional limitations occurring during SRC hydroprocessing.

Heteroatom Removal

Relative to the thermal runs, the Ni-Mo catalysts increased H contents and H/C ratios, and decreased heteroatom contents; the oils from coal-derived materials have lower H/C ratios (1.01-1.05) than those (1.36-1.39) from the bitumen asphaltene (24). Using the catalysts with different pore sizes caused considerable differences in O contents of the products from coal-derived materials and the recovered asphaltenes from Aosb-Asp, and in S contents of both oils and asphaltenes from Aosb-Asp, indicating the importance of catalyst pore size in hydrodeoxygenation (HDO) and hydrodesulfurization (HDS).

Figure 10 shows the O contents of products from Aka-Asp and Wan-SRC and those of recovered asphaltenes from Aosb-Asp as a function of catalyst MPD. There is little or no literature information relating to the effect of catalyst pore size on HDO of coal liquids and bitumen or petroleum. In this work, the analytical results for Aka-Asp and Aosb-Asp were confirmed by repeated analyses of samples from duplicated runs. The maximum HDO degree of given products corresponds to the lowest O contents. As can be seen from Figure 10, the MPD values of 120 Å (Cat-1) and 150 Å (Cat-2) correspond to higher HDO degree of oils, while the latter was superior (to the former) for HDO of asphaltenes where a maximum HDO was achieved in the cases of both Aka-Asp and Aosb-Asp. When SRC was the feed (Wan-SRC), the MPD range corresponding to higher HDO degrees of asphaltenes appeared to become wider or larger. Combining the results in Figures 1 and 10 suggests that 80-160 Å pores with a peak around 120 Å are effective for HDO of oils, while 100-200 Å (MPD: 150 Å) pores are preferable for HDO of asphaltenes.

In Figure 11 the S contents of oils and asphaltenes as well as the amounts of H₂S formed from the sulfur-rich Aosb-Asp were plotted against the catalyst MPD. Unlike HDO of Aosb-Asp, its HDS degree reached a maximum at catalyst MPD of 290 Å (Cat-3), which corresponds to the lowest S contents of products and the highest H₂S amount in gas. Sulfur is also the major heteroatom in petroleum, and there are many reports on HDS of petroleum crudes and heavy oils including the effect of pore size (4-7). In the catalytic runs of the coal-derived sulfur-less Aka-Asp, no difference in HDS was apparent, because all the catalysts completely removed sulfur from the products (24). Bertolacini et al.(1) showed that in the liquefaction of a high-sulfur coal using Co-Mo catalysts (60-100 mesh), the higher activities for HDS and coal conversion correspond to MPD of 100-120 Å and about 200 Å, respectively.

The HDO and HDS results can be explained in terms of relation between pore size and surface area, and competitive adsorption and reaction on catalyst surface. It is considered that there are two main paths for heteroatom removal: simultaneous asphaltene conversion and heteroatom removal, and HDO/HDS of formed or originally present oils and asphaltenes. By applying the molecular size distribution concept as suggested by GPC (Figure 2), one anticipates that the smaller pores contribute to HDS and HDO of small molecules, and larger pores promote the reactions of large molecules. Large pores facilitate the diffusion of large molecules, whereas the large pore catalysts possess lower surface area which lower the activity on catalyst weight basis. The results for runs of coal-derived materials (Figures 4,6,9) suggest that pore size change also affects the competition between adsorption of different compounds/fractions, and heavier molecules such as those in preasphaltene tend to adsorb in preference, which partially inhibit the conversion of less heavier asphaltene molecules. As long as the molecules can diffuse fast enough into the interior of the pores and can adsorb on the active sites, the degrees of HDO and HDS are then determined mainly by the area and intrinsic activity of the catalysts. Therefore, the existence of different ranges of preferable pore sizes for different reactions and for different feed materials is due to the interdependence between pore size, surface area, and competitive adsorption/reaction.

It is expected that there is difference in catalyst dispersion. With the chemically identical supports, the catalyst dispersion should increase with surface area. One can hardly see any effect in the observed trends with Cat-1, Cat-2 and Cat-3 that might be attributed to different dispersion. However, the generally lower HDS and HDO activities of the largest pore Cat-4 may be due in part to its lowest surface area, and poor dispersion of Ni-Mo active phase. On the other hand, there was little decrease in N content of products, probably because of the mild conditions (low H₂ pressure, 4.9 MPa). Stiegel et al.(8) reported that higher metal loadings and larger pores appear to yield some improvement in HDN. In addition, HDN over conventional Ni-Mo and Co-Mo catalysts is known to be more difficult than HDO and HDS, and requires extensive hydrogenation. Shabtai et al. (25) and Hirschon et al. (26) have found that adding Ru to alumina-supported Mo catalysts can improve HDN selectivity.

CONCLUSIONS

1. The performance of unimodal Ni-Mo catalysts for asphaltene and preasphaltene conversion and for oxygen and sulfur removal at 425°C with 4.9 MPa H₂ appeared to depend on their pore size distribution.
2. In the runs of isolated heavy fractions, the conversions increased with catalyst MPD up to 290 Å, and further MPD increase to 730 Å did not offer apparent advantage for converting coal- and oil sand bitumen-derived asphaltenes, but had positive effect in the runs of coal-derived preasphaltene.
3. Relative to the bitumen asphaltene, the sizes of most coal derived asphaltenes are much smaller, but their conversions are sensitive to catalyst pore size. The thermal conversion of coal-derived asphaltenes is accompanied by remarkable retrogressive reactions, even in the presence of H-donor solvent. When the large pore catalyst (MPD: 290 Å) was used, these materials can be converted into oils in high yields under mild conditions, while the oils have lower H/C ratios than those from the bitumen asphaltene.
4. In the hydroprocessing of unrefractionated primary coal liquids which contain preasphaltene in addition to asphaltene and oils (SRC), increasing catalyst pore size significantly promoted preasphaltene conversion, producing more asphaltene. In this case, the use of large pore catalysts seems to decrease the net conversion of asphaltene fraction.
5. The preferable pore size ranges, which may not be the optimum, appeared to be 80-160 Å with a peak MPD around 120 Å for HDO (oxygen removal) of oils, and 100-200 Å with a peak MPD around 150 Å for HDO of asphaltenes. Maximum HDS (sulfur removal) of the sulfur-rich bitumen asphaltene was observed at MPD of 290 Å which corresponds to a pore size range of 200-400 Å.

REFERENCES

1. Bertolacini, R.J.; Gutberlet, L.C.; Kim, D.K.; Robinson, K.K. *ACS Fuel Chem. Prepr.* 1978, 23, 1-10.
2. Ho, P.N.; Weller, S.W. *Fuel Processing Technol.* 1981, 4, 21-29.
3. Shimada, H.; Kuriita, M.; Sato, T.; Yoshimura, Y.; Kawakami, T.; Yoshitomi, S.; Nishijima, A. *Bull. Chem. Soc. Japan* 1984, 57, 2000-2004.
4. Ohtsuka, T. *Catal. Rev.-Sci. Eng.* 1977, 16, 291-325.
5. Green, D.C.; Broderick, D.H. *Chem. Eng. Prog.* 1981, 77, 33-39.
6. Takeuchi, C. *Kagaku Kogaku* 1986, 50, 598-603.
7. Onuma, K. *Shokubai* 1989, 31, 182-187.
8. Stiegel, G.J.; Tischer, R.E.; Polinski, L.M. *J. & EC Prod. Res. Dev.* 1983, 22, 411-420.
9. Tischer, R.; Narain, N.K.; Stiegel, G.J.; Cillo, D.L. *J. Catal.* 1985, 95, 406-413.
10. Yoshimura, Y.; Sato, T.; Shimada, H.; Nishijima, A. *Fuel Sci. Technol. Int'l* 1986, 4, 621-642.
11. Hanaoka, K.; Song, C.; Nomura, M. *Proc. 24th Japan Coal Sci. Conf.*, Tokyo, 1988, 222-225.
12. Song, C.; Nihonmatsu, T.; Nomura, M. *Proc. 24th Japan Coal Sci. Conf.*, Tokyo, 1988, 226-228.
13. Song, C.; Hanaoka, K.; Nihonmatsu, T.; Nomura, M. *Proc. 1989 Int. Conf. Coal Sci.*, Tokyo, 1989, 226-228. The catalyst pore size reported in this paper refers to the pore radius, not diameter.
14. Song, C.; Hanaoka, K.; Ono, T.; Nomura, M. *Bull. Chem. Soc. Japan* 1988, 61, 3788-3790.
15. Song, C.; Hanaoka, K.; Nomura, M. *Fuel* 1989, 68, 287-292.
16. Song, C.; Nomura, M. *Bull. Chem. Soc. Japan* 1986, 59, 3643-3648.
17. Song, C.; Hanaoka, K.; Nomura, M. *Energy & Fuels* 1988, 2, 639-644.
18. Schwager, I.; Yen, T.F. *Fuel* 1979, 58, 219-227.
19. Nakamura, M.; Shiroto, Y.; Takahashi, H. *Nippon Kagaku Kaishi* 1980, 1037-1046.
20. Herten, P.A.; Jackson, W.R.; Larkins, F.P. *Fuel* 1986, 65, 368-372.
21. McMillen, D.F.; Chang, S.-J.; Nigenda, S.E.; Malhotra, R. *ACS Fuel Chem. Prepr.* 1985, 30, 414-426.
22. Derbyshire, F.J.; Davis, A.; Lin, R. *Energy & Fuels* 1989, 3, 431-437.
23. Strausz, O.P. *ACS Petr. Chem. Prepr.* 1989, 34, 395-400.
24. Song, C.; Hanaoka, K.; Nihonmatsu, T.; Nomura, M., unpublished results.
25. Shabtai, J.; Guohe, Q.; Balsuami, K.; Nag, N.K.; Massoth, F.E. *J. Catal.* 1988, 113, 206-219.
26. Hirschon, A.S.; Wilson Jr., R.B.; Laine, R.M. *Appl. Catal.* 1987, 34, 311-316.

Table 1. Properties of Supports and Sulfided Ni-Mo Catalysts

Properties	Al ₂ O ₃ supports ^a				Ni-Mo/Al ₂ O ₃ catalysts ^b				
	S-1	S-2	S-3	S-4	Cat-1	Cat-2	Cat-3	Cat-4	Cat-C ^c
Median pore diam., Å	115	120	280	750	120	150	290	730	90
Surface area, m ² /g	203	174			152	128	126	80	255
Pore volume, ml/g	0.79	0.65	1.05	1.49	0.49	0.45	0.84	1.01	0.56

a) Data received; b) Measured for prepared catalysts; c) Commercial KF-153S-1.5E Ni-Mo/Al₂O₃; Metal loading in Cat-1 to Cat-4 and Cat-C, MoO₃: 15.8, NiO: 2.9 wt%.

Table 2. Elemental Analysis of Coal- and Bitumen-Derived Asphaltene and SRC

Asphaltene & SRC	Elemental (wt%)					Atomic H/C	Source and content		
	C	H	N	S	O ^a		Origin	Source	wt%
Aka-Asp	83.8	6.1	2.0	0.5	7.6	0.87	Akabira Coal	SRC	27.1
Wan-Asp	84.3	6.0	1.6	0	8.1	0.86	Wandoan Coal	SRC	33.1
Aosb-Asp	80.1	8.0	1.2	8.3	2.4	1.20	Ath. Oil Sand	Bitumen	15.0
Wan-Preasp	83.0	5.0	2.0	0	10.0	0.72	Wandoan Coal	SRC	31.2
Wan-SRC	85.7	6.1	1.5	0	6.7	0.85	Wandoan Coal	SRC	100.0
Aka-SRC	84.9	6.2	1.8	0.3	6.8	0.87	Akabira Coal	SRC	100.0

a) By difference.

Table 3. ¹H NMR Analysis of Coal- and Bitumen-Derived Asphaltenes

Asphaltene	H distribution per 100 C atoms ^a							Aromaticity f _a
	H _{ar}	H _{n-CH2} ^b	H _β CH2	H _α CH3	H _γ CH2	H _δ CH3 ^c	H _r ^d	
Aka-Asp	28.0	6.0	17.2	7.2	7.9	14.0	6.7	0.74
Wan-Asp	30.6	5.1	14.8	6.9	7.1	15.6	5.9	0.77
Aosb-Asp	9.6	5.5	15.1	7.3	11.9	41.1	28.6	0.58

a) Based on ¹H NMR and elemental analysis; b) Methylene H α to two aromatic rings; c) Includes β-CH₃ and methylene H γ or further from an aromatic ring; d) Methyl H γ or further from an aromatic ring.

Table 4. Reactivity of Asphaltenes in Non-Catalytic Hydrocracking

Solvent	Tetralin			Decalin	
	Aka-Asp	Wan-Asp	Aosb-Asp	Aka-Asp	Aosb-Asp
Asphaltene					
Products (wt%)					
Gas	5.7	4.8	4.2	4.9	6.5
Oil	50.7	49.0	59.4	50.6	58.2
Asphaltene	33.9	37.7	34.6	32.3	33.4
BF	9.7	8.5	1.8	12.2	1.9
H ₂ S in gas (ml)	2.7	1.1	26.9	1.0	20.1
Conversion (wt%)	66.1	62.3	65.4	67.7	66.6
H ₂ consumption (wt%)	0.5	0.6	0.9	0.9	1.1

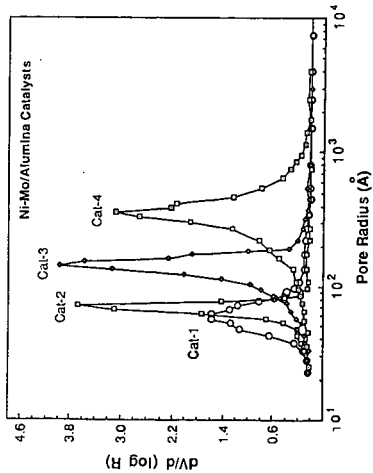


Figure 1. Pore size distribution of prepared Ni-Mo/Al₂O₃ catalysts

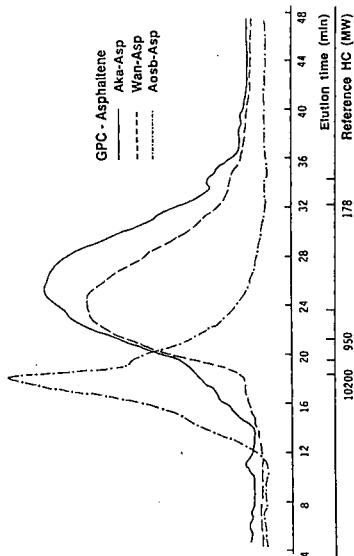


Figure 2. Gel permeation chromatograms of asphaltenes using CH₂Cl₂ as mobile phase

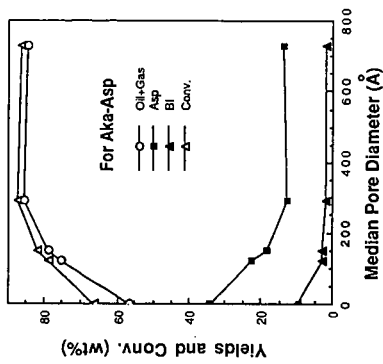


Figure 4. Effect of catalyst pore size on hydrocracking of coal-derived asphaltene

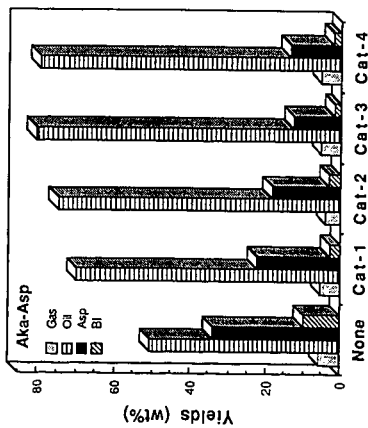


Figure 3. Effect of Ni-Mo catalysts in Aka-Asp hydrocracking

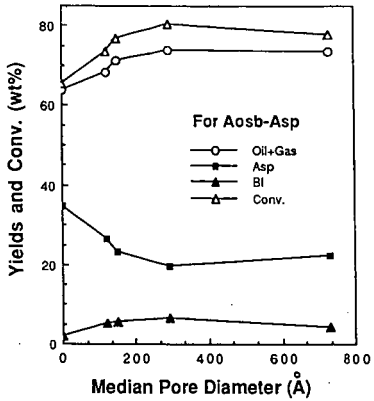


Figure 5. Effect of catalyst pore size on hydrocracking of oil sand bitumen-derived asphaltene

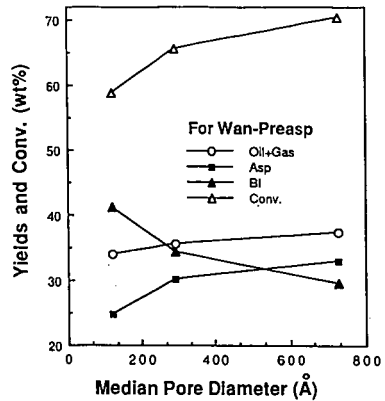


Figure 6. Effect of catalyst pore size on hydrocracking of coal-derived preasphaltene

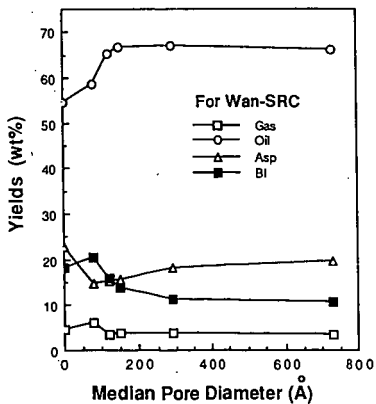


Figure 7. Effect of catalyst pore size on hydroprocessing of unfractionated SRC (Wan-SRC)

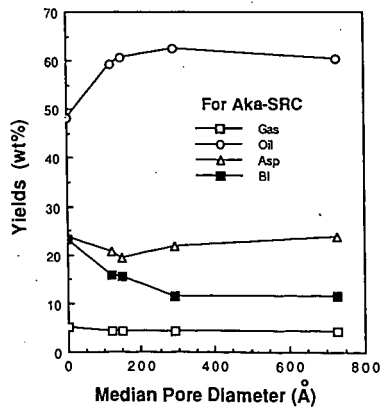


Figure 8. Effect of catalyst pore size on hydroprocessing of unfractionated SRC (Aka-SRC)

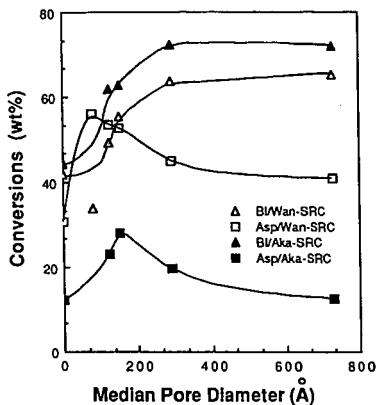


Figure 9. Effect of catalyst pore size on net conversion of asphaltene and preasphaltene in SRC hydroprocessing

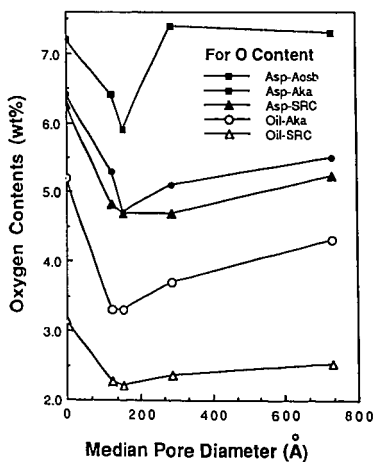


Figure 10. Effect of catalyst pore size on oxygen removal

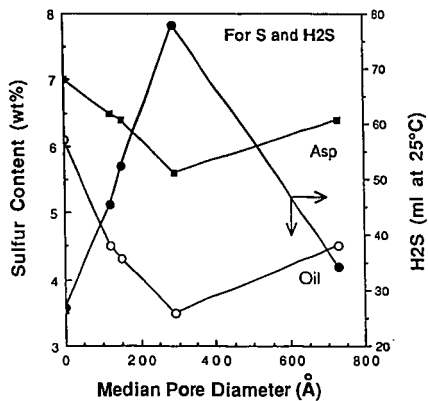


Figure 11. Effect of catalyst pore size on the removal of sulfur from the bitumen asphaltene

Ultrafine Iron Catalysts for Coal Dissolution

P.C. Eklund*, J.M. Stencel, Xiang-Xin Bi*,
R.A. Keogh and F.J. Derbyshire
University of Kentucky,
Center for Applied Energy Research,
3572 Iron Works Pike,
Lexington, KY 40511-8433
* Department of Physics and Astronomy

Keywords: Iron Catalysts, Ultrafine particles, Coal dissolution

Introduction

Over the last several years, developments in coal liquefaction technology have significantly lowered the estimated cost of producing coal liquids (1-3). Among the notable improvements and innovations have been the introduction of the ebullated bed reactor, the adoption of two-stage processing with the additional use of catalyst in the first as well as second stage, and the recycling of residual products to extinction with the production of higher yields of distillate liquids. Progress can be measured in terms of increased selectivity to distillates, improved hydrogen utilization and reduced operating severity.

At this time it is considered that further cost reductions could be realized through a combination of incremental measures rather than any single radical one (although there is always hope that this type of statement will prove to be hopelessly incorrect). One example of a physical process step which can benefit liquefaction economics is to use a cleaned coal feed (4). This would reduce the inventory of inert material in the reactor system, allowing a reduction in reactor size, decreased wear on engineering components and reducing the loss of valuable product with the rejection of these solids. Relatedly, more efficient methods for solid separation would be advantageous.

With regard to the chemistry of coal liquefaction, positive gains could be made by the development of supported catalysts with improved activity, selectivity and life. However, it is considered that a more fruitful approach lies in trying to achieve a greater degree of control over the initial

dissolution reactions through the use of highly dispersed catalysts (5). The specific objectives of research into the development and application of slurry phase catalysts are to increase the rate of conversion and to produce a solubilized product which can be upgraded with greater facility in the second stage. The anticipated outcome of successful research would be to alleviate the problems encountered by the supported catalysts in the second stage, increase throughput, and further improve selectivity to distillates. Moreover, the effective use of slurry phase catalysts can provide the means to liquefy efficiently low-rank coals. Subbituminous coals from the western US are much cheaper feedstocks than eastern bituminous coals. It has been shown that they can produce lower boiling and higher quality liquids (6-8), and that they cause less rapid deactivation of the second stage catalyst (2). The main problem is their lower rate and extent of conversion which causes inefficient use of reactor space and the loss of additional product on solids separation. If, as supposed, this is related to an imbalance between the rates of bond cleavage and hydrogenation, then it is possible that the situation can be redressed by the use of appropriate catalysts.

Molybdenum and iron are the most commonly investigated catalyst metals and both form an active sulfide under liquefaction conditions, or can be introduced after presulfiding. Although iron catalysts are less active, they are preferred for reasons of economy. A great deal of research has been spent in attempting to understand the chemistry of liquefaction in the presence of iron catalysts and the composition of the active phase. It has also been demonstrated that the use of powdered iron catalysts has allowed the liquefaction of subbituminous coals which could not otherwise be processed (see 8). Nevertheless, the activity of these catalysts is still much less than desired and means to enhance their activity are under investigation.

The catalyst activity is determined principally by its composition and the extent of its dispersion and intimate contact with the coal-solvent slurry. While it is generally considered that the active phase of Fe and Mo is a sulfide form, recent studies by Oyama and co-workers have shown that supported and unsupported Mo carbides and nitrides exhibit high activity for hydrodenitrogenation and hydrodesulfurization reactions (9-12), raising the possibility that the carbides and nitrides of Mo and other metals may be active liquefaction catalysts.

The catalyst dispersion is dependent upon the form and mode of addition of

the catalyst precursor. High activities are reportedly favored by catalysts introduced as oil-soluble organometallic precursors such as naphthenates and carbonyls (13-15). The results of some studies, however, indicate that even with these precursors, quite large crystallites or agglomerates can be formed during liquefaction and hence the potentially high dispersion is not maintained. There is some evidence to indicate that, if introduced as particulates, there is less tendency for agglomeration. Fine iron particles (50 nm mean diameter) synthesized by a flame pyrolysis technique appeared to have retained their particle size and shape during presulfiding and coal liquefaction (16,17). Other work has shown that FeS is more active as a colloid than in powder form (18).

The increase in catalytic activity that is expected with decreasing particle size may be due to a combination of effects: an increase in exterior surface and an associated enhancement of sulfiding kinetics; a radical departure from bulk properties, especially with regard to surface energetics as the particle size is reduced below about 10 nm. The synthesis of ultrafine catalyst particles could therefore provide a means to enhance the activity of dispersed iron (or other metal) catalysts.

To examine this proposition, a program of research has been initiated to synthesize ultrafine iron-based particles by a laser pyrolysis technique and to relate their composition, structure and other properties to their behavior as liquefaction catalysts. Later it is intended to investigate effect of the modifying their composition by the addition of promoters during synthesis. This paper describes some of the early findings of this research.

Experimental

Particle Synthesis

The technique for synthesizing ultrafine particles by laser pyrolysis appears to have first been performed by Haggerty and co-workers (19) whose interest was the preparation of silicon-containing ceramics. The method was utilized by researchers at Exxon to produce transition metal carbide particles for use as catalysts for synthesis gas reactions (20,21). One of the examples in the patents involved the synthesis of Fe₃C particles by the laser pyrolysis of vapor mixtures of Fe(CO)₅ and ethylene. This has been the starting point for the present program and the primary aim in the initial studies has been to produce reproducibly iron carbide particles of nanometer

size.

The apparatus used for synthesis has been described previously (22). The reaction cell is shown schematically in Figure 1.

The cell was fabricated from a six-way cross made from 3.8 mm diameter stainless steel tubing. The reactant gases ($\text{Fe}(\text{CO})_5$ and C_2H_4) flow vertically out of the tip of a ~ 1 mm dia. stainless tube and intersect the horizontal beam from a tunable cw CO_2 laser. The reactant gas mixture is heated in a small volume above the reactant gas nozzle by tuning the laser frequency to a strong rotational-vibrational band of C_2H_4 at $\sim 940 \text{ cm}^{-1}$. Thermal decomposition of $\text{Fe}(\text{CO})_5$ to Fe and CO occurs and the Fe reacts with the ethylene to produce ultrafine spherical particles which drift in a well-collimated stream vertically out of the cell. The particles are collected in a teflon membrane filter with average pore size 200 nm.

The reactant gases are confined near the vertical axis of the cross via a coaxial flow of argon which passes through a larger tube (~ 15 mm diameter) concentric with the much smaller reactant gas tube. Pre-heating the Ar flowing into the coaxial sheath to temperatures $T \sim 150^\circ\text{C}$, raised the pyrolysis temperature. Argon is also passed over the inside of NaCl windows to prevent the deposition of stray particles on the windows. Mass flow controllers were used to establish steady flows of Ar to the windows (~ 70 sccm) and coaxial sheath (~ 70 sccm). Another mass flow controller was used to regulate the flow of C_2H_4 (~ 4 -8 sccm) through a pyrex bubbler containing liquid $\text{Fe}(\text{CO})_5$. The relative concentrations of $\text{Fe}(\text{CO})_5$ and C_2H_4 in the reactant gas stream were determined from the cell pressure (measured by a capacitance manometer) and the equilibrium vapor pressure of the $\text{Fe}(\text{CO})_5$. Cell pressure was controlled by adjustment of a needle valve located between a rotary vacuum pump and the cross. To control the laser power density and the size of the "pyrolysis zone", a ZnSe lens was used to position the laser beam waist either directly above the reactant gas nozzle for maximum power density, or to one side of the nozzle or the other to reduce the power density. Approximately $\sim 5\%$ of the power was absorbed in the reactant gas mixture.

Liquefaction

The liquefaction experiments were conducted in 50 mL batch autoclaves using a reaction temperature of 658 K, a 15 minute residence time, tetralin

as the solvent and a hydrogen atmosphere (5.5 MPa, ambient). The reactor was charged with 5g of dry coal and 7.5 g of tetralin. Catalyst precursors, including $\text{Fe}(\text{CO})_5$, $\text{Fe}(\text{C}_5\text{O}_2\text{H}_7)_3$ and molybdenum naphthenate, were added to the reactor in concentrations required to produce equal amounts of metal sulfide during the liquefaction experiment. Two ultrafine, iron-containing catalyst preparations (referred as Fe1 and Fe2) produced by laser pyrolysis were added in 0.1g quantities. Dimethyldisulfide was added for all tests as the sulfiding agent. Coal conversion was obtained by determining the amount of pyridine insolubles (daf) after soxhlet extraction of the reactor products.

The coals used were a Western Kentucky #6 (bituminous) and a Wyodak coal (subbituminous). The analytical data for the two coals are given in Table 1.

Results and Discussion

Two preparations of spherical iron carbide particles were produced with diameters in the range 3 to 13 nm, both exhibiting the cementite (Fe_3C) structure as indicated by X-ray and electron diffraction. The two preparations are referred to as Fe1 and Fe2. They were prepared at laser power densities of about 1200 and 500 $\text{W}\cdot\text{cm}^{-2}$, respectively. The particles differed in that Fe1 was stable in air whereas Fe2 was not and spontaneously ignited. To allow their removal from the system for further study, the Fe2 particles were first slowly passivated in the reaction cell with an Ar/O_2 mixture (99%/1%). It is presently believed that Fe2 has a cementite core and a monolayer coating of Fe.

Examination by high resolution transmission electron microscopy showed that the particles were almost spherical in shape and confirmed their small particle size. Analyses of Fe1 particles by XPS, after exposure to air, were consistent with a surface stoichiometry of $\text{Fe}:\text{C}:\text{O}$ of 1:1:2. Hence a significant amount of oxygen is attached to the surface of these particles. The XPS spectra indicated that the surface iron was predominantly as Fe^{3+} in oxide form with about 10% as the carbide.

The conversions obtained in coal liquefaction experiments in the presence of the different additives are summarized in Table 2.

All of the catalysts enhanced the coal conversion over that obtained in the thermal case. For the bituminous coal, the highest conversions were obtained with Fe2 and molybdenum naphthenate. The other iron catalyst precursors

were significantly less effective.

For the subbituminous coal, the conversions tended to be lower. The highest was produced in the presence of molybdenum naphthenate and the iron catalysts all behaved similarly. In view of the high activity displayed by Fe₂ with the bituminous coal, the low conversion obtained with the lower rank coal is unexpected. The findings are preliminary and will be confirmed in future work.

At this point at least it may be concluded that the synthesis technique can satisfactorily produce nanometer size particles and that there are some indications that these iron carbides may possess moderate to high activity for coal conversion. Whether they also influence the product distribution and composition is yet to be determined.

Current work continues to focus on catalyst synthesis and on investigations of the catalyst phase after sulfiding and after liquefaction, and studies are being initiated of the catalyst functions through the use of model compounds.

References

1. Lumpkin R E, 1988, Science; **239**; 873-877
2. El Sawy A, Gray D, Talib A, Tomlinson G, 1986, Report SAND86-7103, Albuquerque, NM, USA, Sandia National Laboratories, 198pp.
3. Gray D, Tomlinson G, 1988, Report SAND87-7147, Albuquerque, NM, USA, Sandia National Laboratories.
4. Gray D, Tomlinson G, Wan, E, Moran D, Karlson F, Parsons T "Integrating Coal Cleaning and Pyrolysis with Two-Stage Direct Coal Liquefaction: Assessment of Technical and Economic Potential", presented at DOE Direct Liquefaction Contractors' Meeting, Pittsburgh, Pa, September, 1990.
5. Derbyshire F J, 1988, Catalysis in Coal Liquefaction, IEACR/08, London, UK, IEA Coal Research, 69pp.
6. Wu W R K, Storch H H, 1968, Hydrogenation of Coal and Tar. Bulletin 633, Washington, DC, USA, US Department of the Interior, Bureau of Mines, 195pp.

7. Derbyshire F J, Stansberry P G, 1987, *Fuel*; **66**; 1741-2
8. Tomlinson G C, Gray D, Neuworth M B, Talib A, Report SAND85-7238, Albuquerque, NM, USA, Sandia National Laboratories, 105pp.
9. Lee J S, Oyama S T, Boudart M, 1987, *J. Catalysis*; **106**; 125-133
10. Oyama S T, Schlatter J C, Metcalfe J E, Lambert J M, 1988, *I & EC Research*; **27**; 1639-1648
11. Schlatter J C, Oyama S T, Metcalfe J E, Lambert J M, 1988, *I & EC Research*; **27**; 1648-1653
12. Sajkowski D J, Oyama S T, American Chemical Society, Div. Petroleum Chemistry, Preprints, 35(2), 233-236, 1990
13. Hawk C O, Hiteshue R W, 1965, Hydrogenation of Coal in the Batch Autoclave. Bulletin 6322 Washington, DC, USA, US Department of the Interior, Bureau of Mines, 42pp.
14. Watanabe Y, Yamada O, Fujita K, Takegami Y, Suzuki T, 1984, *Fuel*; **63**; 752-755
15. Suzuki T, Yamada O, Then J H, Ando T, Watanabe Y, 1985. Proceedings - 1985 ICCS, Sydney, NSW, Australia, Pergamon Press, pp 205-8
16. Andres M, Charcosset H, Chiche P, Davignon L, Djega-Mariadassou G, Joly J-P, Pregermain S, 1983, *Fuel*; **62**; 69-72
17. Andres M, Charcosset H, Chiche P, Djega-Mariadassou G, Joly J-P, Pregermain S, 1983, Preparation of catalysts III (Eds. G Poncelet and P Grange), Elsevier, pp675-682
18. Nakao Y, Yokoyama S, Maekawa Y, Kaeriyama K, 1984, *Fuel*; **63**; 721
19. Haggerty J S, Cannon W R, 1981, in *Laser-Induced Chemical Processes* (Ed. J I Steinfeld), Plenum Press, New York, NY, USA
20. Fiato R A et al, 1987, US pat. 4,637,753
21. Rice G W et al, 1987, US pat. 4,659, 681

22. Bi X-X, Eklund P C, Stencel J M, Gonzalez R E, Srinivasan R, Derbyshire F J, Proceedings Materials Research Society Meeting, Boston, MA, 26th Nov - 1 Dec, 1990, pp. 167-170.

Table 1
Coal Properties

	<u>C(daf)</u>	<u>H(daf)</u>	<u>N(daf)</u>	<u>IS(daf)</u>	<u>O(daf)</u> ¹	<u>VM(daf)</u>
W.Ky.#6	82.87	5.42	1.72	5.15	4.8	43.10
Wyodak	71.02	5.42	1.37	1.00	21.2	59.92

¹ By difference

Table 2
Coal Conversion Data

Wt. Conversion (daf)

<u>Coal</u>	<u>None</u>	<u>Molybdenum</u>				
		<u>Naphthenate</u>	<u>Fe(C₅H₇O₂)₃</u>	<u>Fe(CO)₅</u>	<u>Fe1</u>	<u>Fe2</u>
Bituminous (W.Ky.#6)	47.1	80.3	62.7	70.4	n.d. ¹	80.9
Subbituminous (Wyodak)	45.0	73.7	64.6	66.5	61.5	65.0

¹ Not determined

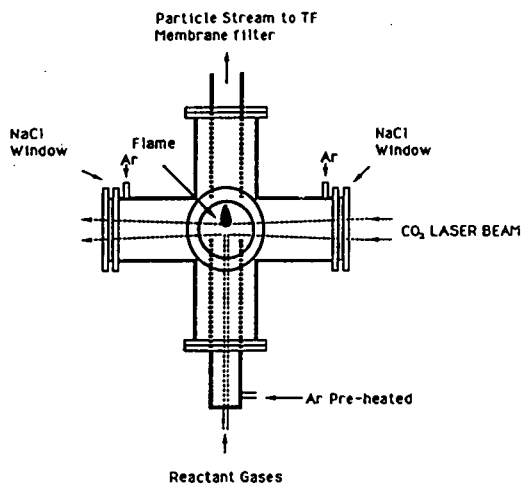


Fig. 1. Schematic Laser Pyrolysis Cell.

STRUCTURE AND DISPERSION OF IRON-BASED DIRECT COAL LIQUEFACTION CATALYSTS

G. P. Huffman, Bhaswati Ganguly, Mehdi Taghiei, F. E. Huggins and Naresh Shah
CFFLS, 233 Mining & Mineral Resources Bldg., University of Kentucky, Lexington, KY
40506-0107

Keywords: liquefaction, catalyst, iron, Mössbauer, XAFS.

Abstract

Mössbauer spectroscopy and X-ray absorption fine structure (XAFS) spectroscopy have been used to characterize the atomic structure and size dispersion of iron-based direct coal liquefaction (DCL) catalysts synthesized by a variety of methods. Samples investigated included a sulfated Fe_2O_3 catalyst, iron added to several coals by chemical impregnation, and iron added to lignite by cation exchange. In the as-dispersed state, all of these catalysts were in the form of superparamagnetic ferric oxides or oxyhydroxides. Size distributions were determined by measuring the percentages of iron contributing to magnetic hyperfine Mössbauer spectra at several temperatures between liquid helium and room temperature, and relating each temperature to a critical particle volume. Size information was also obtained from third and fourth nearest neighbor (nn) iron shell peak amplitudes in radial structure functions derived from the XAFS spectra.

Introduction

There has been much interest in recent years in the use of highly dispersed iron-based DCL catalysts. Several groups have developed methods of preparing such catalysts in very highly dispersed forms.⁽¹⁻¹⁴⁾ It is clearly of interest to develop methods for determining the structure and size of such catalysts. ^{57}Fe Mössbauer spectroscopy has been used by a number of researchers to characterize DCL catalysts.^(3,13-20) Yamashita et al.⁽²⁰⁾ have conducted complementary Mössbauer and XAFS spectroscopy studies on iron-based catalysts in coal.

In the current study, Mössbauer and XAFS spectroscopies have been used to characterize highly dispersed iron-based DCL catalysts prepared by several different research groups. The samples studied included Fe_2O_3 dispersed on carbon black,⁽²¹⁾ iron incorporated into coal by chemical impregnation with FeCl_3 ,⁽⁵⁻⁷⁾ a sulfated Fe_2O_3 catalyst,^(9,10) and iron added to lignite by cation exchange.

Experimental Procedure

Catalyst preparation and the efficacy of the various catalysts in DCL have been discussed elsewhere.⁽¹⁻¹⁴⁾ The iron cation-exchanged lignites were prepared in our own laboratory using procedures outlined by Walker and coworkers.⁽²²⁻²⁴⁾ A lignite from the Penn State sample bank (PSU 1482, Hagel seam) was used.

A standard constant acceleration Mössbauer spectrometer was used. Experimental and least squares analysis procedures are discussed elsewhere.^(25,26) Sample temperatures were varied between 12 and 295 K using a Displex cryogenic system.

The XAFS measurements were conducted on beamline X-19A at the National Synchrotron Light Source (NSLS) and beamline IV-1 at the Stanford Synchrotron

Radiation Laboratory (SSRL). X-ray energy was varied using Si(111) double crystal monochromators. All experiments were conducted in the fluorescent mode as described elsewhere.⁽²⁷⁾

Results and Discussion

Typical Mössbauer spectra are shown in Figures 1 and 2, which show the spectra obtained at room temperature and 12K from a Wyodak coal impregnated with Fe from an FeCl₃ solution⁽⁵⁻⁷⁾ and from an Fe₂O₃ on carbon black catalyst.⁽²¹⁾ All spectra were typical of superparamagnetic ferric oxides. As discussed in more detail elsewhere,⁽²⁸⁾ the spectra were least squares fitted a series of Lorentzian peaks constrained as quadrupole doublets or magnetic sextets. For most samples, the quadrupole doublet component of the spectrum was dominant at room temperature and exhibited Mössbauer parameters typical of a ferric oxide or oxyhydroxide (isomer shift \approx 0.34 to 0.39 mm/s, quadrupole splitting \approx 0.60 to 0.70 mm/s), while the magnetic component became dominant at low temperature and exhibited ferric isomer shifts (0.45 to 0.50 mm/s) and a range of magnetic hyperfine fields (450 to 540 kilogauss). For the samples prepared by Shabtai et al.⁽⁵⁻⁷⁾ and the cation-exchanged lignites, the Mössbauer parameters were consistent with a superparamagnetic iron oxyhydroxide, while those observed for the Fe₂O₃/SO₄²⁻ and Fe₂O₃ on carbon black were consistent with very fine particle hematite.

As discussed elsewhere,⁽²⁹⁻³¹⁾ when a magnetically ordered particle is small enough, thermal vibrations may cause the ordered spins of the particle to flip over the magnetic anisotropy energy barrier to a new orientation. To a first approximation, the frequency of spin flipping is given by

$$f = f_0 \exp\left(\frac{-K_a V}{kT}\right) \quad (1)$$

where K_a is the magnetic anisotropy constant, V is the volume of the particle, k is the Boltzman constant and T is the temperature. The frequency factor f_0 is given by Kundig et al.⁽²⁹⁾ as

$$f = K_a A / \rho N_L h \quad (2)$$

where A is the molecular weight, ρ is the density, N_L is Avogadro's number, and h is the Planck constant. For the magnetic anisotropy constants, we have used the values give by van der Kraan;⁽³¹⁾ $K_a = 0.55 \times 10^5$ joule/m³ for hematite, and $K_a = 1.67 \times 10^5$ joule/m³ for goethite. Eq. (2) then gives $f_0 = 4.2 \times 10^9$ sec⁻¹ for hematite and $f_0 = 8.7 \times 10^9$ sec⁻¹ for goethite. When f is small compared to the nuclear Larmor precession frequency of the ⁵⁷Fe nuclear magnetic moment ($f_L = 5 \times 10^7$ sec⁻¹), the particle will exhibit a well-resolved six line magnetic hyperfine spectrum. However, when f becomes comparable to or exceeds f_L , the magnetic spectrum collapses to a two peak quadrupole doublet. Putting f equal to f_L and rewriting Eq. (1), we obtain

$$V_c = \frac{kT}{K_a} \ln\left\{\frac{f_0}{f_L}\right\} \quad (3)$$

Eq. (3) can be viewed as defining a critical volume, V_c , for temperature T . At temperature T , to a first approximation, particles of volume $> V_c$ will give rise to a six-line magnetic hyperfine spectrum, while particles of volume $< V_c$ will exhibit a

paramagnetic quadrupole doublet.

The temperature variation of the magnetic and paramagnetic (quadrupole) percentages is then used with Eq. 3 to generate size distributions. The results are summarized in Figure 3 for all of the as synthesized catalysts investigated by size histograms that show the percentage of iron contained in ferric oxide particles as a function of particle diameter. Spherical particles are assumed in order to derive diameters from the volumes given by Equ. (3). The resolution of these size distributions depends, of course, on the number of temperatures at which spectra are obtained. As discussed in more detail elsewhere,⁽²⁸⁾ the error in the diameters indicated in these histograms is approximately $\pm 5 - 10 \text{ \AA}$, while the error in the iron percentages is about $\pm 5\%$.

It is seen that most of the catalyst particles in all of the catalysts examined are smaller than approximately $65 - 85 \text{ \AA}$ in diameter, with from 10 to 70% of the iron contained in particles less than $20-30 \text{ \AA}$ in diameter. Moreover, many of the particles in the smallest size bin may be of molecular dimensions. It is also seen that the samples prepared by the Shabtai FeCl_3 impregnation method⁽⁵⁻⁷⁾ exhibit the smallest size distributions. During the mild hydrotreatment (290°C , 1500 psig H_2 hot, 2 hours) used by Shabtai and coworkers,⁽⁵⁻⁷⁾ the iron remains in the form of a ferric oxide or oxyhydroxide and the particle sizes increase somewhat, as seen in Figure 5.

Fourier transformation of the extended X-ray absorption fine structure (EXAFS) of the XAFS spectrum produces a radial structure function (RSF) that is similar to a radial distribution function. Some typical RSFs from the current samples are shown in Figures 4-5. As discussed in detail elsewhere,⁽³²⁾ each peak represents a shell of atoms surrounding the central iron atom. The peak positions on the distance axis are shifted slightly downward by about 0.5 \AA relative to the true interatomic distances because of phase shifts, and the peak amplitudes are proportional to several factors, one of which is the shell coordination number.

In Figure 5, the radial structure function (RSF) of $\alpha\text{-Fe}_2\text{O}_3$ is compared to that of the $\text{Fe}_2\text{O}_3/\text{SO}_4^{2-}$ catalyst. It is seen that the amplitudes of the peaks arising from the third and fourth nearest neighbor (nn) iron shells in the catalyst are significantly reduced relative to those of the same shells in bulk $\alpha\text{-Fe}_2\text{O}_3$. For the cation-exchanged samples and for all of the Shabtai samples, before and after hydrotreatment, the RSFs are similar to that of goethite, but in most cases the third and fourth nn Fe shells are nearly undetectable. This is illustrated by Figure 4.

One explanation of the decreased amplitudes of the third and fourth nn iron shell peaks is that the iron atoms at or near the surfaces of these very small catalyst particles do not have their full complement of third and fourth iron nn. Since it may reasonably be expected that the first nn oxygen coordination of these iron atoms is unchanged, a convenient measure of the decrease in the average number of iron atoms in the third and fourth nn shells is the ratio of those peak heights in the RSF to that of the oxygen first nn shell. These peak height ratios are summarized for all catalyst samples and for the appropriate standard compounds in Table 1. Assuming that these ratios are proportional to the ratios of the coordination numbers, we can deduce the average iron coordination numbers for the catalysts by comparing their peak height ratios to those of the standard compounds for which the coordination numbers are known. These results are also indicated in Table 1. It is of interest to note that the third and fourth nn shell peaks are essentially absent from the RSFs of several of the Shabtai and cation-exchanged samples. However, because of the noise level of the RSFs, the lowest peak height ratio that can be reliably determined from the current data is approximately 0.2. Therefore, we can only put a lower limit on coordination numbers for these samples.

Table 1. Summary of peak height information from RSFs. H/H_{Ox} is the ratio of the height of the peak from the iron shell to that of the oxygen nn shell.

Sample	Peak No.	Shell type	Distance (Å)	H/H_{Ox} (± 0.1)	Coord. No. (± 1)	
Magnetite, Fe_3O_4	3	Fe	2.97	1.65	8	
	4	Fe	3.49	.169	12	
	PSOC 1482, ion ex. 0.5M $Fe(OOCCH_3)_2$	3	Fe		1.00	4.8
		4	Fe		1.07	7.6
Hematite, $2-Fe_2O_3$	3	Fe	2.88} <2.95>	1.74	1} 4	
			2.97}		3}	
	4	Fe*	3.70	1.27	6	
Fe_2O_3/SO_4^{2-}	3	Fe		0.91	2.1	
	4	Fe*		0.70	3.3	
Fe_2O_3 on carbon black	3	Fe		1.03	2.4	
	4	Fe*		0.58	2.7	
Goethite, $\alpha-FeOOH$	3	Fe	3.01} <3.28>	0.80	2} 8	
			3.21}		2}	
			3.42}		4}	
	PSOC 1482, ion ex., 0.02 M $Fe(OOCCH_3)_2$	3	Fe		0.43	4.3
PSOC 1482, ion ex., $FeCl_2$	3	Fe		<0.2	<2	
Blind Canyon [$FeCl_3$ treated - Shabtai]	3	Fe		<0.2	<2	

*Oxygen neighbor shells also contribute to this peak.

Summary and Conclusions

A variety of iron-based liquefaction catalysts have been investigated by Mössbauer and XAFS spectroscopy. Samples investigated included coals subjected to an $FeCl_3$ impregnation treatment described by Shabtai and coworkers,⁽⁵⁻⁷⁾ a highly dispersed Fe_2O_3 on carbon black catalyst,⁽²¹⁾ iron dispersed in a lignite by cation exchange, and a sulfated hematite catalyst (Fe_2O_3/SO_4^{2-}) prepared by Wender and coworkers,^(9,10). The results may be summarized briefly as follows:

1. Both Mössbauer and XAFS spectroscopies can determine the structure of the catalysts and provide information on their size. The Mössbauer technique is more accurate but is also a much slower measurement, typically requiring 10-20 hours, while the XAFS measurement normally requires about 30-60 minutes.
2. In all cases, the initial as-dispersed or as-prepared catalyst is in the form of a highly dispersed ferric oxide or oxyhydroxide.
3. Because of superparamagnetic relaxation effects, the Mössbauer spectra exhibit a

significant increase in the percentage of iron contributing to magnetic hyperfine patterns as the sample temperature is lowered. These magnetic hyperfine percentages may be converted into particle size distributions which indicate that the size of the as-dispersed ferric oxyhydroxides and oxides range from molecular to particles $\sim 20 - 100 \text{ \AA}$ in diameter.

A more detailed discussion of these results will be given elsewhere.⁽²⁸⁾

Acknowledgement

This research was sponsored by the U.S. Department of Energy under DOE Contract No. DE-FC22-90PC90029. The NSLS and SSRL facilities are also sponsored by the U.S. DOE. We are grateful to Dr. Joseph Shabtai of the University of Utah, Dr. Irving Wender of the University of Pittsburgh and Dr. Malvina Farcasiu of the U.S. DOE Pittsburgh Energy Technology Center for providing us with samples.

References

1. Suzuki, T.; Yamada, O.; Takehaski, Y.; Watanabe, Y. *Fuel Process. Technol.*, **1985**, *10*, 33-43.
2. Watanabe, Y.; Yamada, O.; Fujita, K.; Takegami, Y.; Suzuki, T. *Fuel* **1984**, *63*, 752-755.
3. Herrick, D. E.; Tierney, J. W.; Wender, I.; Huffman, G. P.; and Huggins, *Energy and Fuels*, **1990**, *4*, 231-236.
4. Herrick, D. E., Ph.D. Thesis, University of Pittsburgh, **1990**.
5. Shabtai, J. S.; Saito, I.; U.S. Patent, 4,728,418 (1988).
6. Shabtai, J. S.; Zhang, Y. *Proc. 1989 Internat. Confer. Coal Science*, Tokyo **1989**, Vol. II, 807-810.
7. Shabtai, J. S., Skulthai, T. *Proc. 1987 Internat. Conference Coal Science Maastricht*, The Netherlands, Elsevier, 761-764.
8. Marriadassou, D. G.; Charcosset, H.; Andres, M.; Chiche, P.; *Fuel*, **1986**, Vol. 62, pp. 69-72.
9. Pradhan, V. R.; Tierney, J. W.; Wender, I.; Preprints, Div. of Fuel Chem., *American Chemical Society*, August **1990**, vol. 35, No. 3, p. 793.
10. Pradhan, V. R.; Tierney, J. W.; Wender, I.; and Huffman, G. P.; **1991**, submitted to *Energy & Fuels*.
11. Tanabe, K.; Yamaguchi, T.; Hattori, H.; Sanada, Y.; Yuokoyama, S.; *Fuel Processing Technology*, **1984**, Vol. 14, pp. 247-260.
12. Tanabe, K.; Tamaguchi, T.; Hattori, H.; Matsuhashi, H.; Kimura, A.; *Fuel Processing Technology*, **1986**, Vol. 8, pp. 117-122.
13. Cook, P. S. and Cashion, J. D.; *Fuel*, **1987**, *66*, 661-668.
14. Cook, P. S. and Cashion, J. D.; *Fuel*, **1987**, *66*, 669-677.
15. Montano, P. A. and Granoff, F.; *Fuel*, **1980**, *59*, 214.
16. Montano, P. A.; Bommannavar, A. S.; and Shah, V.; *Fuel*, **1981**, *60*, 703.
17. Bommannavar, A. S. and Montano, P. A.; *Fuel*, **1982**, *61*, 523.
18. Ogawa, T.; Stenberg, V. I.; and Montano, P. A.; *Fuel*, **1984**, *63*, 1660-1663.
19. Montano, P. A.; Stenberg, V. I.; and Sweeny, P.; *J. Phys. Chem.*, **1986**, *90*, 156-159.
20. Yamashita, H.; Oksuka, Y.; Yoshida, S.; and Tomita, A.; *Energy & Fuels*, **1989**, *3*, 686.
21. Sample provided by Malvina Farcasiu, U. S. DOE Pittsburgh Energy Technology Center.
22. Walker, Jr., P. S.; Matsumoto, S.; Hanzawa, T.; Murira, T.; Ismail, I. M. K.; *Fuel*, **1983**, *62*, 140-149.
23. Jenkins, R. G.; Nandi, S. P.; and Walker, P. L.; *Fuel*, **1973**, *52*, 288.

24. Mahajan, O. P.; Yarzab, R; and Walker, P. L.; *Fuel*, **1978**, *57*, 643.
25. Huffman, G. P.; Huggins, F. E.; *Fuel* **1978**, *47*, 592-604.
26. Huggins, F. E.; Huffman, G. P. Mössbauer Analysis of the Iron-Bearing Phases in Coal, Coke, and Ash. *Analytical Methods for Coal and Coal Products*; Karr, Jr., C., Ed.; Academic Press: New York, 1979; Vol. III p. 371-423.
27. Lytle, F. W.; Greeger, R. B.; Sandstrom, D. R.; Marques, E. C.; Wong, Joe; Sprio, C. L.; Huffman, G. P.; and Huggins, F. E.; *Nucl. Instrum & Methods*, **1984**, *226*, 542-548.
28. Huffman, G. P.; Huggins, F. E.; Ganguly, B.; Taghiei, M.; and Shah, N., "Structure and Dispersion of Iron-Based DCL Catalysts," submitted to *Energy & Fuels*.
29. Kundig, W.; Bömmel, Constabaris, G.; Lindquist, R. H.; *Phys. Rev.*, **1966**, *142*, 327.
30. Wickman, H. H.; "Mössbauer Paramagnetic Hyperfine Structure," pp. 39-66, *Mössbauer Effect Methodology*, Ed. I. J. Gruverman, Plenum Press, NY, 1966.
31. van der Kraan, A. M.; *Phys. Stat. Sol.* **1973**, (a) *18*, 215.
32. Lee, P. A.; Citrin, P. H.; Eisenberger,; and Kincaid, B. M.; *Rev. Mod. Phys.*, **1981**, *53*, 769-806.

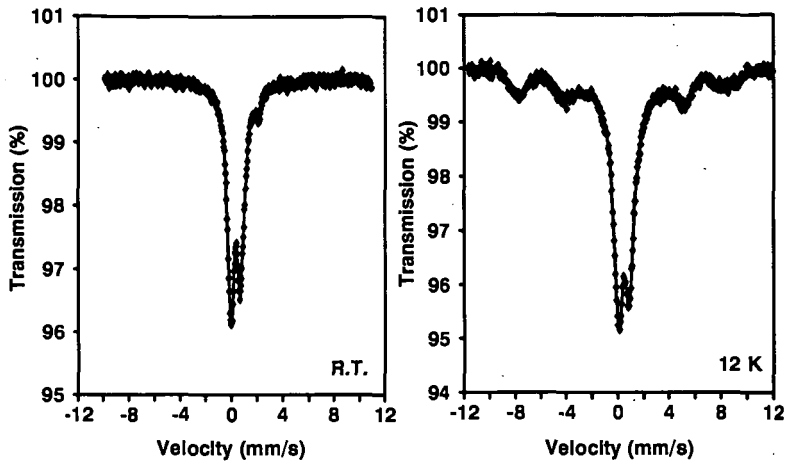


Figure 1- Room temperature and 12 K Mössbauer spectra of a Wyodak coal impregnated with iron by the Shabtal treatment.

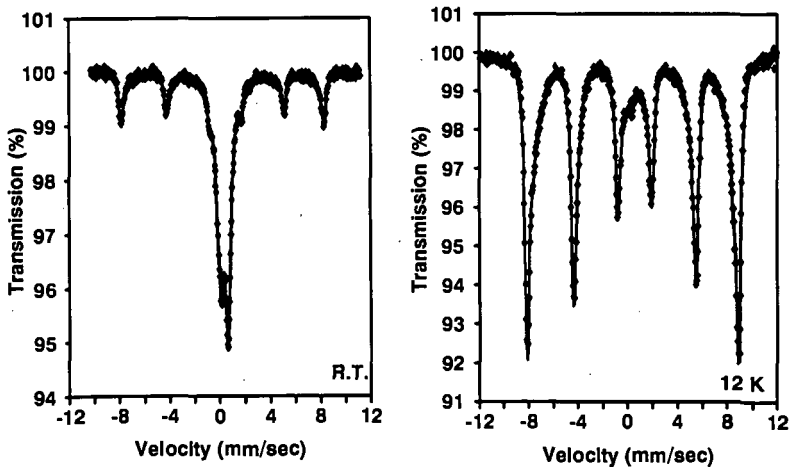


Figure 2- Room temperature and 12K Mössbauer spectra of an Fe₂O₃ on carbon black catalyst.

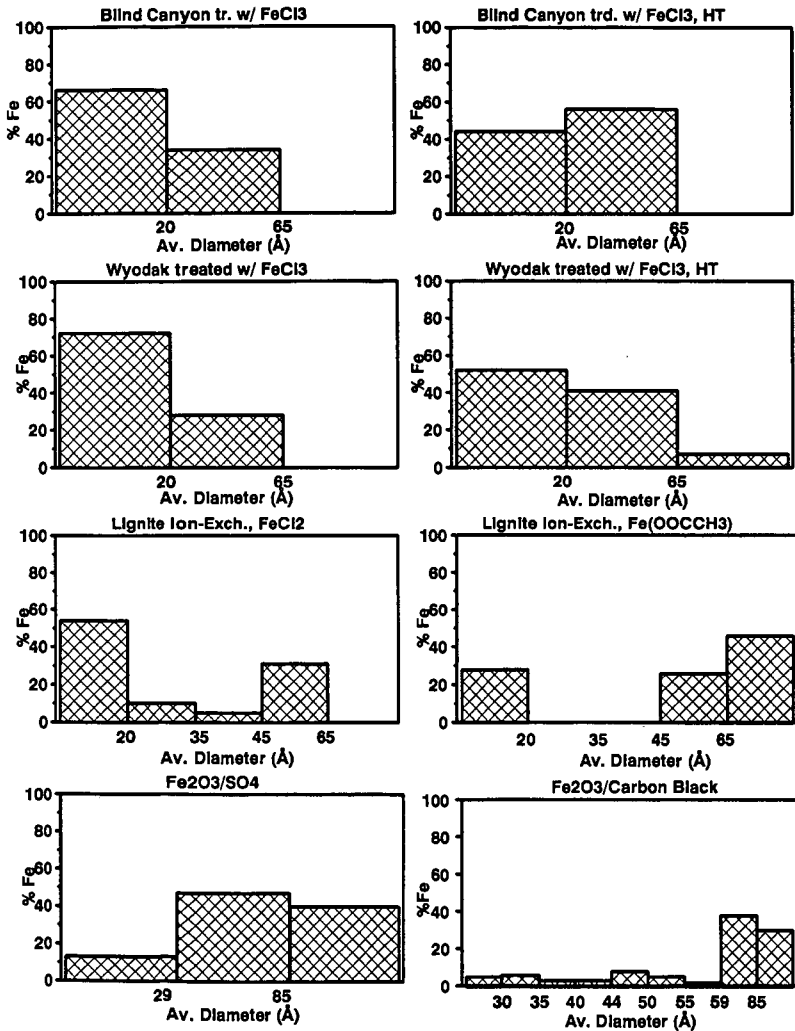


Figure 3- Size distribution for various as-dispersed iron DCL catalysts derived from Mössbauer data.

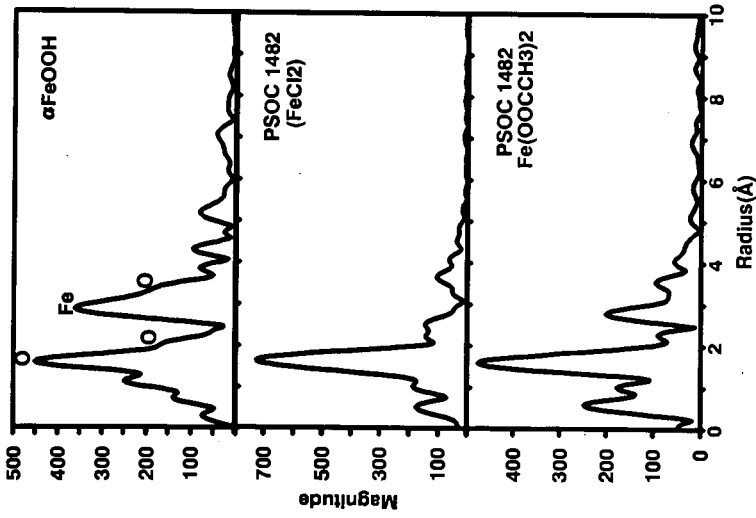


Figure 4. RSF's of goethite and two iron cation-exchanged lignites.

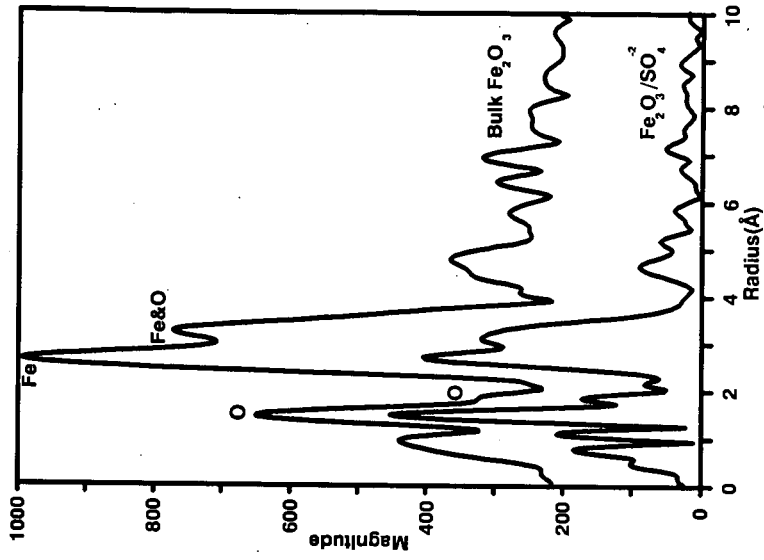


Figure 5. RSF's of hematite and $\text{Fe}_2\text{O}_3/\text{SO}_4$ catalyst.

HYDROTALCITE CATALYSIS OF HYDROTREATING REACTIONS

Ramesh K. Sharma, Daniel C. Stanley, Paul L. Holm,
and Edwin S. Olson,

University of North Dakota Energy and Environmental Research Center
Box 8213, University Station, Grand Forks, ND 58202

Key Words: Hydrotalcite, pillared, hydrotreating

Magnesium-aluminum hydrotalcites have been tested for hydrotreating coal liquids. To understand the mechanism of the reactions that are catalyzed by the hydrotalcites, model compounds have been reacted with various potential hydrogen donors in the presence of several forms of the hydrotalcites. Aryl-heteroatom bonds are easily cleaved by hydrogen at temperatures below 350°C, not only with terephthalate-pillared hydrotalcite, but also with hydrotalcite carbonate. Evidence favors a Lewis acid catalysis mechanism for this process. Although molecular hydrogen is required for heteroatom cleavage, no activation of molecular hydrogen or any hydrogen donor molecule occurs on the hydrotalcite. Thiomolybdate-exchanged pillared hydrotalcite is converted to an active hydrogenation catalyst at these temperatures. However, higher temperatures are required for hydrocracking activity.

INTRODUCTION

Novel supports for metallic sulfide catalysts have been under investigation for their potential use in coal liquefaction. Conventional supported hydrogenation catalysts have encountered difficulties in coal liquefaction due to deactivation and coking (1-4). New catalysts may require more dispersed forms of catalytic sites or greater micropore dimensions to improve accessibility to catalytic sites. Hydrotalcites have been utilized in catalytic processing of various types (5-10), and recently, pillared hydrotalcites with large micropores were utilized in oxidation reactions (11).

This paper describes recent efforts to understand the effects of the hydrotalcite structure during hydrotreatment processing. Model compounds were treated with hydrogen and hydrogen donors in the presence of various pillared and nonpillared hydrotalcites.

EXPERIMENTAL

The following reagents: bibenzyl, cumene, 1-methylnaphthalene, diphenyl sulfide, 9,10-dihydroanthracene, and neopentylbenzene were obtained from Aldrich Chemicals, Co., Milwaukee, Wisconsin.

Preparation of Catalysts:

Hydrotalcites and molybdenum-exchanged hydrotalcites were prepared as described earlier (11,12). Instead of ammonium molybdate, ammonium tetrathiomolybdate was used for exchange into hydrotalcite. For the preparation of formate-pillared hydrotalcite, 160 mL of carbon dioxide-free distilled water were placed in a three-necked round-bottomed flask fitted with nitrogen inlet and outlet tubes and a dropping funnel. The system was purged with nitrogen for 30 minutes. Sodium formate (21.77 g) and sodium hydroxide (57.66 g) were placed into the reaction flask and stirred. When the dissolution of sodium formate was complete, a solution of 41.04 g of magnesium nitrate hexahydrate and 30.0 g of aluminum nitrate nonahydrate in 128 mL of carbon dioxide-free water was added dropwise into

the flask. The addition was completed after about one hour. A gel-like white precipitate was formed. The dropping funnel was then replaced by a reflux condenser and the reaction mixture heated to 75-85°C and allowed to stir overnight. After 9 hours had elapsed, about one third of the water had escaped from the container, so additional carbon dioxide-free water was added to bring the volume back to its original level and the reaction stirred for 9 more hours. The crude product was isolated by vacuum filtration and purified by resuspending in carbon dioxide-free water and centrifuging. The pasty white material was dried by heating in vacuum at 65°C until all the moisture had been driven off. The infrared spectrum of the formate-hydrotalcite showed strong absorptions at 1593 and 1379-1406 cm^{-1} which are consistent with bands expected for the antisymmetrical and symmetrical vibrations of the COO^- structure (13).

Infrared spectra were obtained in KBr on either a Perkin Elmer Model 283 spectrometer or a Nicolet 20SXB FTIR spectrometer, equipped with a mercury cadmium telluride (MCTA) detector, and a Nicolet 1280 computer with a fast Fourier transform coprocessor. Quantitative GC/FID analyses were performed with a Hewlett Packard 5880A gas chromatograph equipped with Pectrocol column. Isooctane and n-octadecane were the internal standards. GC/MS was performed on a Finnigan 800 LTD ion trap detector with a HP 5890A gas chromatograph and a J&W 30-m x 0.32-mm (ID), 1.0-micron film of DB-5. A 15-m x 0.25-mm (ID), 0.25-micron DB-5 film capillary column was used for the analysis of high-boiling components. A Dupont Model 951 thermogravimetric analyzer module interfaced with a Dupont Model 1090 thermal analyzer was used to determine the thermal decomposition of the catalysts.

Hydrotreating Reactions:

In a typical run, 0.5 g of substrate and 0.25 g of catalyst were placed in a tubing bomb reactor. The reactor was sealed and pressurized with 68 atm of hydrogen or deuterium if needed, placed in a rocking autoclave heated to desired temperature, and heated for three hours. The reactor was cooled in dry ice-acetone slurry, degassed, and opened. The contents of the reactor were mixed with an appropriate internal standard and transferred into a centrifugation tube by washing with dichloromethane. The solid was separated by centrifugation. The liquid sample was analyzed by quantitative GC and GC/FTIR/MS. The solid was dried in vacuum at 110°C for 3 hours. The analytical data are given in Table 1.

RESULTS AND DISCUSSION

A thermogravimetric method was used to determine the thermal decomposition of hydrotalcite and supported-hydrotalcite catalysts. Heating terephthalate-pillared hydrotalcite to 100°C resulted in 3.8% weight loss. This can be assumed to be the loss of interstitial water. For the tetrathiomolybdate-exchanged terephthalate-pillared hydrotalcite, the weight loss continued to 240°C. The additional loss may be due to the removal of sulfur from MoS_2 moieties. In the 240-300°C range, rapid loss was observed, which could be due to further loss of sulfur to form MoS_2 moieties. When the temperature was increased further, the weight loss was more or less continuous until 466°C. A 25% weight loss occurred in this temperature regime, which may be attributed to the decomposition of terephthalate. The weight loss is not consistent with that expected for decomposition of the hydrotalcite layer structure. Thus the hydrotalcite layer structure is stable at temperatures used for hydrotreating reactions.

In order to identify the selectivity and reactivity of hydrotalcite catalysts, the reactions of model compounds such as bibenzyl, 1-methylnaphthalene, cumene, neopentylbenzene, and diphenyl sulfide were carried out with hydrotalcite, pillared

hydrotalcite, and molybdenum sulfide supported on hydrotalcite catalysts. Diphenyl sulfide was used as a test compound to investigate the catalytic activity of hydrotalcite catalysts for aryl-sulfur bond cleavages. The reaction of diphenyl sulfide with terephthalate-pillared hydrotalcite at 300°C for 3 hours in the presence of 68 atm of hydrogen gave 86.4% conversion of the substrate into products (Table 1). Reaction products were mainly benzene and H₂S, along with a small amount of benzenethiol. When the same reaction was carried out in the absence of catalyst, the conversion was very small (1%). A trace amount of benzene was the only product. The reaction of diphenyl sulfide with tetrathiomolybdate-exchanged terephthalate-pillared hydrotalcite at 300°C for 3 hours in the presence of 68 atm of hydrogen gave a high conversion (88.9%) of diphenyl sulfide. The major product from this reaction was benzene. Small amounts of cyclohexane, thiophenol, cyclohexanethiol were also formed. Nonpillared hydrotalcite (carbonate) gave conversion and product distributions

TABLE 1. CATALYTIC HYDROTREATING OF DIPHENYL SULFIDE (DPS)

Reaction Temp. = 300°C, Reaction Time = 3 hrs
Catalyst wt./Substrate wt. = 0.5, H₂ = 68 atm

Catalyst (g)	Substrate (mmol)	Conv. (%)	Major Products (mmol)
None	DPS (2.68)	1	Benzene (trace)
Mg-Al-HT (0.25)	DPS (2.73)	81.7	Benzene (4.5) Benzenethiol (0.13)
Zn-Cr-HT (0.25)	DPS (2.64)	60	Benzene (2.9) Benzenethiol (tr.)
PH-HT (0.25)	DPS (2.95)	86.4	Benzene (4.4) Benzenethiol (0.12)
F-HT (0.25)	DPS (2.71)	83.4	Benzene (4.0) Benzenethiol (0.2)
MgO (0.25)	DPS (2.67)	2	Benzene (trace)
Calcined Mg-Al-HT (0.25)	DPS (2.74)	40	Benzene (1.9) Benzenethiol (0.15)
Mo-PH-HT (0.25)	DPS (2.79)	88.9	Benzene (4.5) Cyclohexane (0.1)

Mg-Al-HT = Magnesium aluminum hydrotalcite carbonate

Zn-Cr-HT = Zinc chromium hydrotalcite nitrate

PH-HT = Terephthalate-pillared hydrotalcite

F-HT = Formate-exchanged hydrotalcite

Mo-PH-HT = Molybdenum-exchanged terephthalate-pillared hydrotalcite

similar to the terephthalate-pillared hydrotalcite described above. Thus neither the molybdenum (sulfide) nor the pillared structure are required for carbon-sulfur bond cleavage; the hydrotalcite itself is sufficient for catalysis of hydrogenolysis of these bonds. The active sites for this catalysis were hypothesized to be electron deficient aluminum sites in the hydrotalcite layer. The hydrotalcite-carbonate was calcined at 450°C to dehydrate and decompose carbonate. The hydrotalcite layer structure is significantly altered at higher temperatures. The calcined hydrotalcite was then used to catalyze the hydrogenolysis reaction of diphenyl sulfide. The conversion was low, but activity was not totally lost. Magnesium oxide was, however, completely inactive as a catalyst for diphenyl sulfide hydrogenation. These oxides are, of course, basic, but the calcined hydrotalcite may still contain active Lewis acid sites corresponding to trigonal Al atoms.

With zinc-chromium hydrotalcite (nitrate) as the catalyst, the conversion was significantly lower (60%). The product distribution was the same as that with magnesium-aluminum hydrotalcite carbonate. The conversion and product distributions from the reaction of formate-exchanged hydrotalcite were also comparable with that of terephthalate-pillared hydrotalcite. Unlike reactions with solid acid catalysts, no coking, oligomeric products, or dibenzothiin were observed in any of the reactions (14).

Reactions of diphenyl sulfide with terephthalate-pillared hydrotalcite (no molybdenum) in the absence of hydrogen gas indicated a very small conversion (3%) of diphenyl sulfide into products. A trace amount of benzene was the only product from this reaction (Table 2). Thus molecular hydrogen is required for carbon-sulfur bond cleavage in the hydrotalcite reactions. This was not the case in the reactions of various model compounds with strong acid catalysts, where products such as benzene were observed even when molecular hydrogen was not present. These products could be derived from proton addition to the ipso position of the benzene ring (Brønsted-acid mechanism) followed by cleavage of the substituent groups and probably hydride donation from Scholl intermediates. No condensation to oligomeric or polymeric material or coke was observed for any of the hydrotalcite reactions carried out in the absence of molecular hydrogen. This fact and the requirement for molecular hydrogen are inconsistent with a Brønsted acid mechanism for the hydrotalcite reaction.

When hydrogen was replaced by deuterium, the conversion of diphenyl sulfide was considerably smaller. The decreased conversion could be attributed to isotope effects. The majority of the benzene product was singly labeled, but multiple labeling was also observed. No deuterium was incorporated into the recovered diphenyl sulfide.

The reaction of molecular hydrogen with 1-methylnaphthalene was investigated with the hydrotalcite to determine if the hydrotalcite structure can catalyze the addition of hydrogen. The conversion of 1-methylnaphthalene was only 9% with the phthalate-pillared hydrotalcite, whereas the tetrathiomolybdate-exchanged phthalate-pillared hydrotalcite gave 95% conversion. Only a small amount of cracking to naphthalene occurred in either reaction. It is clear that the tetrathiomolybdate in the interstitial layer was converted to a form that was highly active for catalyzing the addition of molecular hydrogen to aromatics. It is not yet known what the form of molybdenum is: MoS₂ microcrystals, MoS cluster, or some monomeric form.

TABLE 2. REACTIONS OF DIPHENYL SULFIDE

Reaction Temp. = 300°C, Reaction Time = 3 hrs
Catalyst wt./Substrate wt. = 0.5

Catalyst (g)	Substrate (mmol)	Reduc. (psi/g)	Conv. (%)	Major Products (mmol)
PH-HT (0.25)	DPS (2.77)	None	3.0	Benzene (tr.)
PH-HT (0.25)	DPS (2.95)	Hydrogen 68 atm	86.4	Benzene (4.4) Benzenethiol (0.12)
PH-HT (0.25)	DPS (2.67)	Deuterium 68 atm	21.1	Benzene (0.4) Benzenethiol (tr.)
PH-HT (0.25)	DPS (2.75)	CO/H ₂ O 68 atm 0.22 g	10.2	Benzene (0.3) Benzenethiol (tr.)
PH-HT (0.25)	DPS (2.77)	DHA 1.00 g	9.0	Benzene (0.3) Benzenethiol (tr.)
PH-HT 0.25	DPS (2.83)	Methanol 1.00 g	7.1	Benzene (0.2)
F-HT (0.25)	DPS (2.79)	None	4.0	Benzene (tr.) Benzenethiol (tr.)

Thus, the hydrotalcite structure itself (no molybdenum) possesses significant capability for hydrodesulfurization. Since only minimal hydrogenation was observed with 1-methylnaphthalene, we conclude that hydrotalcite does not activate hydrogen, but hydrogen is required for the conversion of diphenyl sulfide with hydrotalcite. The question of how the C-S bonds are cleaved in the presence of hydrogen is very interesting and deserves further study. Since molecular hydrogen is evidently not activated directly by the hydrotalcite catalyst for addition to aromatics, the use of hydrogen sources other than molecular hydrogen was examined to determine whether the hydrotalcite catalyst could catalyze the transfer of hydrogen from these hydrogen sources to a sulfur-containing species, thereby catalyzing reductive cleavage of the C-S bond. The interlayer space of hydrotalcite contains basic species that could be involved in the formation of hydride-donor intermediates that would affect the reduction. Since carbon monoxide and water generate potential hydride donor species in the presence of a base, the reaction of diphenyl sulfide in this system was investigated (no molecular hydrogen added). Conversion was very small (10%). Hydrotalcite (formate) gave a similar poor conversion in the absence of hydrogen. Methanol has been shown to be an effective reductant in basic conditions, but it also gave a poor conversion of diphenyl sulfide in the reaction with hydrotalcite. A radical hydrogen transfer mechanism is another route for reduction of the C-S bond. The reaction of diphenyl sulfide was carried out in the presence of 9,10-dihydroanthracene. If the mechanism involved homolytic cleavage of the C-S bond to give a radical intermediate, this radical intermediate should be able to abstract hydrogen from dihydroanthracene. However, the conversion in the experiment was,

again, very poor (9%). Since the conversions in these experiments are a bit higher than in the case with no hydrogen or no reductant, there may have been some small amount of hydrogen generated in the experiments as a result of a water-gas reaction or dihydroanthracene decomposition to hydrogen.

No evidence for phenol was found in any reaction. The formation of phenol would have indicated that the basic species directly attacked the C-S bond. Catalysis of the C-S bond cleavage appears to be associated with the hydrotalcite layers, rather than basic species. Because of the aluminum atoms in the layer structure, many electron deficient sites (Lewis acids) are available for catalysis. The reactions observed with hydrotalcites are significantly different from reactions with other solid acid catalysts, however, since condensations and formation of dibenzodithiin were not found.

The hydrocracking activity of hydrotalcite and molybdenum supported on hydrotalcite was investigated by reacting bibenzyl, cumene, and neopentylbenzene with this catalyst. The reaction of bibenzyl with molybdenum supported on hydrotalcite at 300°C for 3 hours and in the presence of 68 atm of hydrogen gave a small percent conversion. Traces of benzene and toluene were the only products. Increasing the temperature (350 and 400°C) resulted in an increase in the percent conversion of bibenzyl (25 and 40%, respectively). Benzene, toluene, and ethylbenzene were major products of this reaction. Previous studies with solid acid catalysts gave mostly benzene and ethylbenzene via the Brønsted acid-ipso cleavage mechanism. The large amount of toluene formed from bibenzyl indicates that a major pathway for hydrocracking in the HT-catalyzed reaction is cleavage of the bond adjacent to the ring (α - β cleavage). A similar cleavage was observed for the reaction of cumene with HT catalyst, which gave ethylbenzene as the major product. Other products resulted from Lewis acid-catalyzed rearrangement and alkyl addition reactions of the cumene. Neopentylbenzene exhibited similar α - β cleavage to give toluene.

A mechanism involving the Lewis acid HT sites is shown in Figure 1. Al in the figure represents an electron deficient Lewis acid site that bonds to the aryl ring.

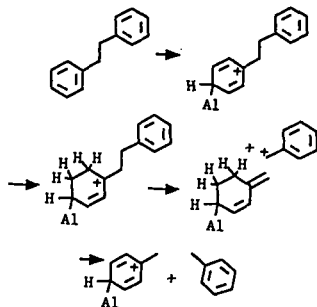


Figure 1. Hydrotalcite-catalyzed mechanism.

TABLE 3. CATALYTIC HYDROTREATMENT OF MODEL COMPOUNDS

Reaction Time = 3 hrs, Hydrogen = 68 atm
Catalyst wt./Substrate wt. = 0.5

Catalyst (g)	Substrate (mmol)	Temp. (°C)	Conv. (%)	Major Products (mmol)
PH-HT (0.25)	1-MENP (3.66)	350	9	Methyltetralins (0.1) Naphthalene (0.06)
MO-PH-HT (0.25)	(1-MENP) (3.67)	350	94.6	Methyltetralins (2.8) Decalin (0.2) Naphthalene (0.06) Tetralin (0.12)
PH-HT (0.25)	BB (2.69)	300	8	Benzene (tr.) Toluene (tr.)
Mo-PH-HT (0.25)	BB (2.76)	350	25	Benzene (0.04) Toluene (0.1) Ethylbenzene (0.2)
MO-PH-HT (0.25)	BB (2.75)	400	40	Benzene (0.2) Toluene (0.4) Ethylbenzene (0.2)
PH-HT (0.25)	Cumene (4.10)	400	14	Ethylbenzene (0.3) Benzene (0.1) n-Propylbenzene (0.1)
PH-HT (0.25)	NPB (3.40)	400	23.8	Benzene (0.13) Toluene (0.5)

PH-HT = Molybdenum-exchanged terephthalate-pillared hydrotalcite
DPS = Diphenyl sulfide
BB = Bibenzyl
NPB = Neopentylbenzene

CONCLUSIONS

Thiomolybdate-exchanged terephthalate-pillared hydrotalcite is converted to active hydrogenation catalyst during heating with the substrates. Effective hydrodesulfurization activity resides with the hydrotalcite portion of the catalyst. At higher temperatures, hydrocracking activity is also observed.

ACKNOWLEDGMENTS

This research was supported by contract No. DOE-FC21-86MC10637 from the U.S. Department of Energy. References herein to any specific commercial product by trade name or manufacturer does not necessarily constitute or imply its endorsement, recommendation, or favoring by the United States Government or any agency thereof.

REFERENCES

1. Derbyshire, F. ACS Div. of Fuel Chem. Preprints 1988, **33**, (3), 188.
2. Garg, D.; Givens, E.N. Fuel Proc. Technol. 1984, **9**, 29.
3. Kovach, S.M.; Castle, L.J.; Bennett, J.V.; Svrodt, J.T. Ind. Eng. Chem. Prod. Res. Dev. 1978, **17**, 62.
4. Mills, G.A.; Beodeker, E.R.; Oblad, A.G. J. Am. Chem. Soc. 1950, **72** 1554.
5. Reichle, W.T.; Warren, N.J. U.S. Patent 4 458 026, 1984.
6. Reichle, W.T. J. of Catalysis 1985, **4**, 547.
7. Reichle, W.T.; Kang, S.Y.; Everhardt, D.S. J. of Catalysis 1986, **101**, 352.
8. Rameswaren, M.; Dimotakus, E.; Pinnavaia, T.J. ACS Div. of Fuel Chem. Preprints 1988, **33**, (4), 942.
9. Kohjiya, S.; Sato, T.; Nakayama, T.; Yamashita, S. Makromol. Chem., Rapid Commun. 1981, **2**, 231.
10. Nakatsuka, T.; Kawasaki, H.; Yamashita, S.; Kohjiya, S. Bull. Chem. Soc. Japan 1979, **52**, 2449.
11. Drezdon, M.A. U.S. Patent 4 774 212, 1988.
12. Olson, E.S. "Quarterly Technical Progress Report for the Period July to September 1989," EERC.
13. Bellamy, L.J. The Infrared Spectra of Complex Molecules; 3rd Ed., John Wiley & Sons, Inc.: New York, 1975, 199.
14. Sharma, R.K.; Diehl, J.W.; Olson, E.S. ACS Div. of Fuel Chem. Preprints 1990, **35**, (2), 414.

MECHANISM OF HYDROTREATING REACTIONS: SOLID ACID CATALYSIS

University of North Dakota, Grand Forks, ND 58201
Energy and Environmental Research Center

by
Edwin S. Olson, John W. Diehl, and Ramesh K. Sharma

ABSTRACT

Acid catalysis of coal liquefaction has been extensively studied with both solid and liquid forms of catalysts. Zinc chloride has been utilized in the molten state, complexed with methanol, and supported on silica gel and other materials. This paper addresses the differences between the mechanistic pathways occurring in these various states. Thermal studies of the silica gel-supported zinc chloride demonstrate a change from Lewis to Bronsted acidity with increasing temperature. The major pathway for silica gel-supported zinc chloride is Bronsted acid catalysis, but some Lewis acid activity is found. Since hydrogen does not add directly to the primary carbonium ion intermediates involved in hydrodealkylation of alkylarenes, the role of hydrogen in driving the reaction to the cracked products rather than condensation is being investigated.

Key Words: Brønsted acidity, solid acid catalyst, oligomer

INTRODUCTION

Conversion of coal to a liquid product with an acid catalyst has been extensively investigated in the last quarter century. A liquefaction process which utilized molten zinc chloride as an acid catalyst was developed by consolidation Coal Company (1). Fundamental studies of the chemistry of zinc chloride-catalyzed liquefaction were pursued at Berkeley and other laboratories. Zinc chloride is a mild Lewis acid, and under anhydrous conditions was not able to effectively catalyze the cleavage of aryl-alkyl bonds at moderate temperatures (325°C) unless the rings were highly activated (2). Complexation of zinc chloride with methanol, water, or hydrogen halide gave catalysts with proton-donating potential (Bronsted acidity) that were able to catalyze hydrocracking more effectively (3). Reactions with dibenzylether at 325°C gave products that could have resulted from Lewis acid catalysis of cleavage of C-O bond (4); however, hydrogen chloride, which formed as a reaction product from the ether caused rapid cleavage of the ether when combined with the zinc chloride.

We have recently developed effective catalysts for coal hydrotreatment in which zinc chloride is complexed to solid supports. Zinc chloride bonded to silica gel or clay supports have been found to effectively catalyze cleavage reactions and remove heteroatoms from model compounds (5,6) as well as coal liquids (7,8).

This paper reports our work on the characterization of acidic sites of the silica gel-supported zinc chloride catalysts. Reactions with model compounds confirmed the mechanistic implications of these studies.

EXPERIMENTAL

Catalyst Preparation

Silica gel-supported zinc chloride catalysts, SZC-50 (50 wt.% zinc chloride-loaded silica gel) and SZC-16 (16 wt.% zinc chloride-loaded silica gel) were prepared as described earlier (5).

Characterization of Solid Acid Catalysts

Acidity Measurements

Surface acidity of the solid acid catalysts was determined by pyridine adsorption and desorption using infrared and thermogravimetric analyses.

Infrared Method

A small amount of sample (100 mg) was placed in a glass chamber attached to a vacuum pump, gas inlet, and a gas outlet. The chamber was evacuated, and argon saturated with pyridine was introduced into the chamber until the weight increase ceased. At this stage, the chamber was evacuated until the physisorbed pyridine was removed as indicated by the constant weight of the base absorbed sample. The infrared spectra of the pyridine-absorbed catalyst was obtained in KBr on a Nicolet 20SXB FTIR spectrometer with diffused reflectance cell, equipped with a mercury cadmium telluride (MCTA) detector, and a Nicolet 1280 computer with a fast Fourier transform coprocessor. The pyridine-absorbed catalyst was heated in vacuo at several temperatures, and infrared spectrum was recorded for the residue formed at each temperature.

Thermogravimetric Method

Approximately 20 mg of catalyst were placed on the sample pan of the DuPont 951 thermogravimetric balance module which was interfaced with a DuPont 1090 thermoanalyzer (controller and data station). The sample was purged at ambient temperature with argon until constant weight was achieved (several minutes). The argon flow was then stopped, and the sample chamber was evacuated. The vacuum pump continued to hold the partial vacuum until constant weight was once again achieved. The pump was then turned off, and a flow of pyridine-saturated argon at ambient temperature was introduced into the sample chamber. The pyridine-argon flow continued for 180 minutes at which time the weight gained by the sample had nearly ceased. The chamber was again evacuated, still at ambient temperature, and held under partial vacuum for 40 minutes. When constant weight was achieved, the temperature was increased at 20°C/min to 105°C where it was held for 30 minutes. The temperature was then increased at 2°C/min to 202°C and held there for 30 minutes, followed by a temperature increase at 20°C/min to 300°C where it was held for 60 minutes. Upon reaching constant weight, the experiment was terminated.

Hydrotreating Reactions

The details of experimental procedures used for the hydrotreating reactions are available in the reports published in the literature (5-9). The method of Vogel (10) was used for chlorine analysis.

RESULTS AND DISCUSSION

Elemental analyses of the zinc (II) chloride mixtures with silica gel obtained from the reaction in carbon tetrachloride and THF indicated that a small amount of chloride loss occurred during the heating procedure. Most of the salt (98%) was present, and only a small amount of chlorine was present as Si-O-ZnCl. The catalyst was a mixture of zinc chloride, zinc chloride complexed with silica gel, and oxyzinc salt.

Previous results from Hammett acidity studies at ambient temperature for SZC-50 indicated that highly acidic sites are present in this catalyst (6). Coordination of zinc chloride to surface silica hydroxyls on the silica gel-supported catalyst will be expected to generate new acidic sites of both Lewis and Brönsted types. The nature of these sites in the SZC-50 and SZC-16 catalysts at both ambient and higher temperatures is elucidated by the present study.

Infrared spectroscopy of the pyridine complex was used to determine the relative proportion of Lewis and Brönsted acid sites in the silica gel-zinc chloride catalysts. In the infrared spectrum of the pyridine-adsorbed catalyst, the bands around 1440 and 1536 cm^{-1} are assigned to the pyridine-Lewis acid coordination bond and the pyridine-Brönsted acid bond respectively. The relative intensities of these bands were converted to the concentration ratio by using the respective extinction coefficients. In the SZC-16 catalyst, very few Brönsted acid sites were present at ambient temperature. However, on heating the pyridine complex of SZC-16 at several temperatures (25-200°C) for 1 hour, the intensity of the band due to the pyridine-Brönsted acid bond increased (Table 1). The increase in the intensity of the Brönsted band must be due to creation of new strong Brönsted acid sites as the temperature increases. This process is accompanied by the loss of pyridine from that portion of the Lewis sites that are weakly acidic. Thus, there is a continuing decrease in the Lewis band, and corresponding decrease in the ratio of the concentration of Lewis sites to Brönsted sites with temperature. Table 1 also gives the calculated ratios from the absorbance data from the SZC-16 sample and extinction coefficients for the bands.

At ambient temperature, the ratio of the concentration of Lewis sites to Brönsted sites for the SZC-50 was 3.4. This lower ratio of Lewis/Brönsted acid sites in the SZC-50, which corresponds to a larger concentration of Brönsted sites, is likely due to increased electron-withdrawing effects of the greater number of zinc chloride moieties coordinated with the silica hydroxyls.

TABLE 1
INFRARED ABSORBANCE OF PYRIDINE-ADSORBED SZC-16

Temp (°C)	Absorbance		Lewis/Brönsted Sites
	1440 cm^{-1} Band (L-P Band)	1536 cm^{-1} Band (B-P Band)	
25	0.181	0.01	12.46
100	0.184	0.022	8.52
150	0.129	0.027	4.78
200	0.043	0.018	2.39

A thermogravimetric technique was also used to determine the total acid sites and stability of the catalyst. In the TGA experiment, the weight of the catalyst increased by 41.62 and 12.13 wt% for SZC-50 and SZC-16 catalysts respectively, upon pyridine absorption followed by evacuation at ambient temperature. The weight increase is due to the chemical reaction of the pyridine at both Lewis and Brönsted acid sites and, therefore, is a measure of the total acidity of the catalyst. The total acidity for SZC-50 and SZC-16 is 5.04 and 1.75 meq/g catalyst respectively.

Upon slowly heating the catalyst (2°C/min) to 300°C, all of the adsorbed pyridine could be removed. Heating above 300°C resulted in the loss of chlorine due to decomposition and or sublimation of zinc chloride from the catalyst surface.

Catalytic Hydrotreating of Model Compounds:

Reactions of model compounds such as bibenzyl, diphenyl sulfide, dibenzothiophene, cumene, 1-phenyldecane, n-hexadecane, and p-cresol with supported zinc chloride catalysts gave products indicative of a carbonium ion mechanism (5,6). The formation/conversion of acidic sites on the SZC catalyst to Bronsted acids at higher temperatures such as those useful in hydrotreating reactions has not yet been studied. However, we may speculate that at higher temperatures, significant numbers of Bronsted sites are present, and these sites are responsible for the majority of catalytic effects in cleavage of alkylarenes at temperatures between 300 and 400°C. Several experiments were carried out to identify whether Lewis or Bronsted catalysis is predominant at these temperatures with various related materials.

The reaction of bibenzyl in molten zinc chloride (ZC-melt) was carried out under conditions similar to those used for SZC catalysts, and a poor conversion was obtained (Table 2). This result is consistent with the earlier study of Bell (2), that demonstrated the poor catalytic ability of zinc chloride for hydrocracking when restricted to only Lewis acidity (no added hydroxy compound). A reaction conducted with silica gel (SG, no zinc chloride) gave a very poor conversion, consistent with the weak acidity of the silica hydroxyls. When the reaction was carried out with silica gel-zinc chloride (50% zinc chloride) catalyst, 85% of bibenzyl was converted into products. The major products were benzene, ethylbenzene and a small amount of toluene. The ratio of benzene to ethylbenzene was 3. In addition, 18% of the starting material was converted into oligomers. No coke formation occurred under these conditions. The conversion and product distribution from the reaction of bibenzyl with SZC-16 was comparable with that obtained from SZC (50% zinc chloride loaded silica gel). These results suggest that 16% zinc chloride loading on silica gel may be adequate for optimum catalytic activity.

The most likely mechanism for the reaction of bibenzyl with the SZC catalyst is the same as that proposed for the zinc chloride-hydroxyl or zinc chloride-hydrogen chloride complex suggested earlier (2) to account for the formation of ethylbenzene and benzene at temperatures in the 300°C regime. This mechanism proceeds via ipso protonation followed by cleavage of the aryl-alkyl bond to form the phenylethyl carbonium ion intermediate. The carbonium ion is then reduced to the alkyl group. Ethylbenzene is further cracked to benzene via the same steps, the extent depending on the activity of the catalyst.

The effect of molecular hydrogen on the conversion of bibenzyl and the product distribution was investigated by carrying out reactions both in the presence and absence of hydrogen. The percent conversion measured as the disappearance of the substrate was almost the same in both these reactions. However, the product distribution was significantly affected by the presence of hydrogen (Table 2). The reaction with no hydrogen produced 7% of coke which is formed due to retrograde condensation reactions. Also the amount of condensation products (substituted bibenzyls) increased from 18% to 27% in the absence of hydrogen. In the presence of hydrogen the amount of benzene was only slightly higher, but the amount of ethylbenzene increased considerably. In the reaction mechanism postulated above, the phenylethyl carbonium ion can undergo a variety of reactions (Figure 1) to give

TABLE 2
 CATALYTIC HYDROCRACKING OF BIBENZYL

Reaction Temp. = 350°C, Reaction Time = 3 Hrs, 5.49 mmols Bibenzyl

Catalyst (g)	Hydrogen (psig)	Conversion (%)	Major Products (mmols)
SG (0.25)	Hydrogen 1000	2	Benzene (tr.) Ethylbenzene (tr.) Toluene (tr.)
ZC-melt (0.25)	Hydrogen 1000	13	Benzene (0.08) Ethylbenzene (0.04) Toluene (0.02)
SZC-50 (0.5)	Hydrogen 1000	85	Benzene (3.54) Ethylbenzene (1.35) Toluene (0.15) Cond. Prod. (18%) Coke (0%)
SZC-50 (0.5)	None	83	Benzene (3.2) Ethylbenzene (0.8) Toluene (0.2) Cond. Prod. (27%) Coke (7%)
SZC-50 (0.5)	Deuterium 1000	64	Benzene (2.6) Ethylbenzene (1.1) Toluene (0.1) Cond. Prod. (24%) Coke (0%)
SZC-16 (0.5)	Hydrogen 1000	75	Benzene (3.12) Ethylbenzene (0.9) Toluene (0.2)

ethylbenzene product. The fact that ethylbenzene forms even in the absence of molecular hydrogen indicates that hydride transfer from Scholl intermediates or hydroaromatic condensation products is the major mechanism for formation of ethylbenzene. Hydrogen may be indirectly involved through reductions of these condensation products.

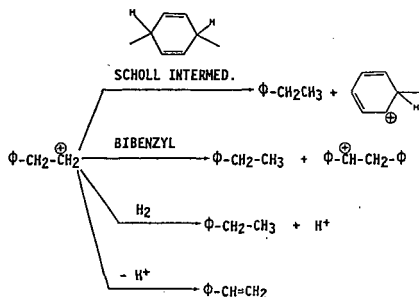


Figure 1. Reactions of Phenylethyl Carbonium Ion

When hydrogen was replaced with deuterium, the conversion was somewhat lower. This is very likely the result of an isotope effect that reduces the rate of hydrogenation of the Scholl intermediates or the rate of transfer of hydrogens from the hydrogenated Scholl intermediates to the carbonium ion intermediates.

1,3-Diphenylpropane (DPP) and neopentylbenzene (NPB) were also used to investigate the catalysis mechanism of silica gel-zinc chloride. The reactions were carried out at 350°C for 3 hours in the presence of 1000 psig of hydrogen. Major products and the percent conversion for these reactions are presented in Table 3. 1,3-diphenylpropane gave benzene and indan as the major products. The formation of these products requires no hydrogen or reduction, only the Brønsted acid catalyst. Ipso protonation of the aromatic ring, followed by aryl-methylene bond cleavage gives the phenylpropyl carbonium ion, that undergoes cyclization to give indan as the second major product. The minor products from this reaction were C₁-C₃ benzenes. These products probably result from other mechanism involving Lewis acid catalysis.

The conversion of neopentylbenzene was much lower than that of diphenylpropane, and a variety of products were obtained. The major product from this reaction was benzene, which again is formed by the ipso protonation of the aromatic ring followed by aryl-methylene bond cleavage. Neopentyl carbonium ion rearranged to produce 2-methylbutane (Figure 2). Toluene and 2-methylpropane may have been formed from the Lewis acid-catalyzed cracking of neopentylbenzene.

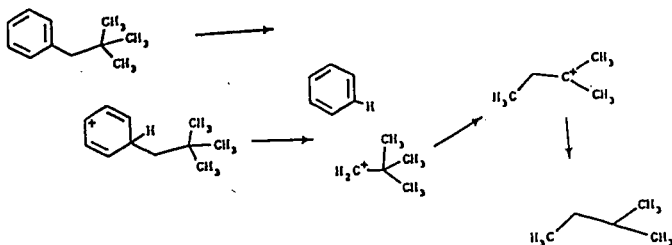


Figure 2. Brønsted Acid-Catalyzed Mechanism
TABLE 3

CATALYTIC HYDROCRACKING OF 1,3-DIPHENYLPROPANE AND NEOPENTYL BENZENE

Reaction Temp. = 350°C, Reaction Time = 3 HRS
Catalyst wt./substrate wt. = 0.5, H₂ = 1000 psig

Catalyst (g)	Substrate (mmols)	Conv. (%)	Major Products (mmols)
SZC-50 (0.25)	DPP (2.6)	76	Indan (1.39) Propylbenzene (0.08) Ethylbenzene (0.06) Toluene (0.05) Benzene (2.43) Cond. Prod. (0%) Coke (0)%
SZC-50 (0.25)	NPB (3.5)	26	Benzene (0.29) 2-Methylbutane (0.08) 2,2-Dimethylpropane (0.003) Toluene (0.06) 2-Methylpropane (0.04) Butane (0.003) Pentane (0.001) Ethylbenzene (0.03)

CONCLUSIONS

SZC catalysts contain fewer Brønsted acid sites at ambient temperature, but these sites increase at higher temperatures. At the hydrotreating temperatures, the cleavages of aryl-alkyl bonds are Brønsted acid-catalyzed. Hydrogen is not required for hydrocracking reactions, but prevents coking reactions.

ACKNOWLEDGEMENT

This research was supported by Contract No. DOE-FC21-86MC10637 from the U.S. Department of Energy. References herein to any specific commercial product by trade name or manufacturer does not necessarily constitute or imply its endorsement, recommendation, or favoring by the United States Government or any agency thereof. The assistance of Daniel Stanley is greatly appreciated.

REFERENCES

1. Zielke, C.W.; Struck, R.T.; Evans, J.M.; Costanza, C.P.; Gorin, E. Ind. Eng. Chem. Proc. Res. Dev., 1966, 5, 158-164.
2. Taylor, N.D.; Bell, A.T. Fuel, 1980, 59, 499-506.
3. Frederick, T.J.; Bell, A.T. J of Catalysis, 1984, 87, 196-204.
4. Frederick, T.J.; Bell, A.T. J. of Catalysis, 1984, 87, 226-237.
5. Sharma, R.K.; Diehl, J.W.; Olson, E.S. Processing and Utilization of High-Sulfur Coals III, Elsevier Science Publishers B.V., Amsterdam, 1990, 735-743.
6. Sharma, R.K.; Diehl, J.W.; Olson, E.S. ACS Div. of Fuel Chem. Preprints, 1990, 35 (2), 414-422.
7. Olson, E.S.; Diehl, J.W.; Sharma, R.K. ACS Div. of Fuel Chem. Preprints, 1990, 35 (2), 563-569.
8. Sharma, R.K.; Diehl, J.W.; Olson, E.S. ACS Div. of Fuel Chem. Preprints, 1990, 35 (3), pp.
9. Olson, E.S.; Diehl, J.W. Anal. Chem. 1987, 443-448.
10. Vogel, A. Textbook of Quantitative Inorganic Analysis, 4th edn., Longman Sci. and Tech. Group Essex, Eng., 1978, 434.

CATALYSIS OF MULTI-COMPONENT LEWIS ACIDS FOR COAL HYDROLIQUEFACTION AND MODEL REACTIONS

Chunshan SONG⁺*, Masakatsu NOMURA[†], and Tomohiro ONO[†]

⁺Fuel Science Program, Department of Materials Science and Engineering
The Pennsylvania State University, University Park, PA 16802, USA

[†]Department of Applied Chemistry, Faculty of Engineering, Osaka University
Yamada-oka 2-1, Suita, Osaka 565, Japan

Keywords: Lewis acids, Multi-component catalysts, Coal liquefaction

INTRODUCTION

Development of new catalysts is a promising approach to more efficient coal liquefaction. It has been recognized that dispersed catalysts are superior to supported catalysts for primary liquefaction, because the control of coal depolymerization or dissolution requires intimate contact between the catalyst and coal. The dispersed catalysts can be divided into metals and their oxides and sulfides (e.g. MoS₂), and acid catalysts such as ZnCl₂. An excellent review of coal liquefaction catalysts has been published recently by Derbyshire (1), which also incorporated many previous works on the catalytic effects of Lewis acids. In particular, the process development research conducted by Zielke and co-workers (2-4) at the Consolidation Coal Co. demonstrated the potential of using massive ZnCl₂ catalyst to liquify coals. The fundamental studies on model reactions by Bell and co-workers (5-8) at the University of California contributed to a mechanistic understanding of the catalytic effects of ZnCl₂ for coal liquefaction.

While ZnCl₂ and SnCl₂ have always been considered attractive because of their high activity and low cost, a considerable body of research at Osaka university has demonstrated that ZnCl₂ and SnCl₂ doped with alkali metal chlorides or transition metal chlorides are more effective for liquefaction of many bituminous, subbituminous and brown coals (9-13). One of the important observations from these works is that the addition of alkali metal chlorides to ZnCl₂ increases the yields of oils (hexane solubles) and decreases the gas yields and reduces H₂ consumption. This is desirable because hydrogen consumption is a major cost of coal liquefaction plant. With an attempt to develop new catalysts, we examined the catalytic effects of MCl_n-LiCl-NaCl-KCl and MCl_n-LiCl-KCl (MCl_n = CoCl₂, NiCl₂, MoCl₃, SnCl₂, ZnCl₂) for coal liquefaction. The results showed that NiCl₂- and MoCl₃-LiCl-KCl ternary salts are promising catalysts in view of high oil yields and coal conversions and lower heteroatom contents of oils (14-17), and they appeared to be superior to ZnCl₂-, SnCl₂- and CoCl₂-containing and other NiCl₂- and MoCl₃-containing salts (14,18). Little is known about the reaction chemistry, more specifically, the hydrogenation and cracking of polyaromatics and the cleavage of bridge structures during coal liquefaction using the NiCl₂- and MoCl₃-based catalysts. The purpose of this paper is to evaluate the catalysis of these two new catalysts based on coal liquefaction, pyrolysis, and model compound studies.

EXPERIMENTAL

The salts used are synthesized MoCl₃ (14), reagent grade NiCl₂, LiCl and KCl. The molar compositions of NiCl₂- and MoCl₃-LiCl-KCl and LiCl-KCl were 14:50:36,12:51:37 and 58:42, respectively, unless otherwise mentioned. The catalysts were impregnated on to coals from their methanol solution or suspension. The coals used are Morwell (C: 67%, daf basis) brown, Taiheiyō (C: 76%), Wandoan (C: 78%) and Yilan (C: 79%) subbituminous, and Akabira (C: 83%) bituminous coals (14-17). The temperature-programmed pyrolysis was conducted by using TGA in a nitrogen flow (14,19). The solvent-free coal liquefaction was carried out in a 200 ml shaking autoclave at 400°C for 1 hour with 9.8 MPa H₂ (14-15). The liquefaction in the presence of tetralin was conducted in 70 ml rocking autoclaves at 400°C for 1 h with 4.9 MPa H₂ (17). The products were separated into gases, oils (hexane solubles), asphaltene (hexane-insoluble benzene solubles), preasphaltene (benzene-insoluble pyridine or THF solubles), and residue (16). The gases were analyzed by GC for C₁-C₄, CO and CO₂; the oils and asphaltene were subjected to ¹H NMR (15,17) and elemental analyses. The model compounds tested are anthracene, phenanthrene, naphthalene, dibenzyl, benzylphenylether, and dibenzylether. Their reactions were performed in the 70 ml autoclaves under different conditions. The products were analyzed by GC, and GC-MS (20).

RESULTS

Temperature-Programmed Pyrolysis. The non-catalytic pyrolysis of the five coals in N₂ was conducted using two temperature programs: r.t. to 600°C at 5°C/min; and r.t. to 400°C at 5°C/min and then held at 400°C for 60 min. The second program was also used in catalytic pyrolysis in accordance with the temperature/time conditions in liquefaction (14). Figure 1 shows the pyrolysis results of the five coals up to 600°C. The yields of volatile products were calculated from the weight loss determined by TGA. The weight loss below 200°C is mainly due to adsorbed water and was not accounted as volatile materials. The amounts of volatile materials formed below 450°C decreased with increasing rank, *daf* C% of the coals. Figure 2 presents the results of catalytic pyrolysis of Akabira coal in N₂. Figure 3 shows the temperature-pressure profiles during heat-up and holding at 400°C for solvent-free liquefaction of Akabira coal with 9.8 MPa H₂. The NiCl₂- and MoCl₃-LiCl-KCl catalysts began to exert a measurable effect in enhancing coal pyrolysis in N₂ at the temperatures above 300°C (Figure 2). During the heat-up of the coal impregnated with these catalysts under pressurized H₂, the H₂ uptake became apparent at the same temperature region, indicating the onset of the catalytic reactions at the temperatures as low as about 300°C (Figure 3). The same trends were observed in the pyrolysis (14, 19) and t-p profiles in liquefaction of other coals. The t-p profiles for liquefaction of Akabira coal in the presence of tetralin were similar to those for the solvent-free runs, except that the evaporation of tetralin caused the pressure increase (below 300°C).

Solvent-free Liquefaction. In general, acids are used in massive amounts (1-9) as catalysts and reaction medium. In this work, the concentration of Lewis acids in ternary salts for liquefaction were below 15 mol%. Figure 4 shows the results of solvent-free liquefaction of Australian Wandoan subbituminous coal (400°C, 1 h, 9.8 MPa H₂) using various MCl_n-LiCl-NaCl-KCl and MCl_n-LiCl-KCl (MCl_n: 12-14 mol%, salts to coal: 1, wt ratio), where the yields of products are plotted against H₂ consumptions. It is clear from the product distribution that NiCl₂- and MoCl₃-LiCl-KCl afforded over 60% (*daf* coal basis) oils and showed higher selectivity to oils without remarkable increase in gas-make. The previous results for Wandoan coal (3 h runs, other conditions were the same) using ZnCl₂ and ZnCl₂-KCl (60:40, mol%) are also shown in Figure 4. Relative to ZnCl₂, ZnCl₂-KCl gave higher oil yield and lower gas yield with lower H₂ consumption, as has been observed for many other coals (9-11). Although the catalysts and reaction time were different, the results in Figure 4 showed that higher oil yields can be obtained with relatively lower H₂ consumption.

In order to examine the general effectiveness of the new catalysts, we conducted the solvent-free liquefaction of Australian Morwell coal, Japanese Taiheiyō and Akabira coals under the same conditions (400°C, 1 h, 9.8 MPa H₂). The results are summarized in Figure 5. Relative to the thermal runs, both NiCl₂- and MoCl₃-LiCl-KCl catalysts significantly enhanced coal conversion. More importantly, the oil yields of all the catalytic runs are almost three times that of non-catalytic runs of the bituminous, subbituminous and brown coals. These results established the general applicability of these two catalysts for liquefaction of coals, especially subbituminous coals (oil yields: ≥ 56%). ¹H NMR and elemental analyses revealed that the catalysts increased the contents of naphthenic CH₂ hydrogens (hydroaromatics) and decreased the O and N contents of oils.

Liquefaction in the Presence of H-Donor. In a previous work, addition of tetralin was found to further increase the conversion of coal, although this effect was substantially smaller in the catalytic runs than in the non-catalytic run (16). The NiCl₂- and MoCl₃-based catalysts played a key role in promoting oil production, while adding tetralin appeared to enhance the selectivity of the catalytic reactions, in view of increased conversion and decreased total hydrogen consumption. Based on these observations, we examined the catalyst performance at different loading levels for liquefaction of Chinese Yilan coal in the presence of tetralin under low H₂ pressure (400°C, 1 h, 4.9 MPa H₂; tetralin/coal: 5g/5g; metal to coal: Ni, 1.2-12 wt%; Mo, 1.7-17 wt%). Figures 6 and 7 show the effect of catalyst loading on the product distribution and hydrogen transfer, respectively. The loading of NiCl₂-LiCl-KCl to coal up to 20wt% (2.4wt% Ni to coal) significantly increased oil yields, coal conversions, enhanced gas-phase H₂ consumptions but decreased the net hydrogen-transfer from tetralin (Figure 6B). Further increase in its loading resulted in a little decrease in gas-phase H₂ and total hydrogen consumptions, in spite of the increase in oil yield. In the case of MoCl₃-LiCl-KCl, increase in its loading progressively increased oil yields and gas-phase H₂ consumptions and decreased the net hydrogen-transfer from tetralin (Figure 6A). In contrast to these trends, the use of LiCl-KCl, even at low loading, considerably suppressed the gas-phase H₂ consumption without any negative impact on the product distribution (Figure 6C).

Figure 7 shows the effect of catalyst loading on H-distribution of oils per 100 C atoms, as determined from NMR (17). The HCH_3 values indicate the contents of alpha-, beta- and gamma- CH_3 hydrogens and gamma- CH_2 hydrogens; the HCH_2 refers to the alpha- and beta- CH_2 hydrogens. As shown in Figure 7, the HCH_2 values increased, but HCH_3 decreased with catalyst loading, reflecting that loading the catalysts increased the contents of naphthenic CH_2 hydrogens present in hydroaromatic rings. These trends were also observed in the ^1H NMR analysis of oils from solvent-free liquefaction of the other four coals (15-16).

Model Compounds Studies. To gain a better understanding of the catalytic functions, the model reactions were undertaken using NiCl_2 , MoCl_3 , LiCl-KCl , and their combinations. Tables 1 and 2 present the results for anthracene and phenanthrene (400°C , 1 h, 9.8 MPa H_2), respectively, with constant molar ratio (0.3) of NiCl_2 or MoCl_3 to the reactant (3 g, 16.85 mmol). As shown in Table 1, both NiCl_2 - and MoCl_3 - LiCl-KCl considerably promoted the hydrogenation of anthracene to form tetra- and octahydroanthracene. In the runs of phenanthrene, which is known to have lower reactivity (20), the catalysts enhanced the formation of di- and tetrahydrophenanthrene. In the runs of naphthalene, these catalysts promoted hydrogenation to produce tetralin, but the conversions were within 15%. As shown in Tables 1-2, the use of LiCl-KCl gave nearly identical results to the thermal runs. However, adding LiCl-KCl to NiCl_2 and MoCl_3 , especially to MoCl_3 which exhibited very high cracking activity, significantly suppressed the extensive hydrogenation and ring-opening cracking. Figure 8 shows the effect of MCl_n content in the runs of anthracene. The yields of hydroaromatics and cracking products appeared to depend on the contents of Lewis acids MCl_n , especially in the case of MoCl_3 .

Table 3 is a summary of the bond dissociation energy of a number of C-O and C-C linkages. Various connecting linkages between aromatic rings are believed to be present in coals. We conducted model reactions of C-O linkage structures using benzylphenylether and dibenzylether at 350°C for 1 h with 4.9 MPa H_2 . As shown in Table 4, the presence of the salts significantly affected the reactions of the ethers. The use of NiCl_2 - and MoCl_3 - LiCl-KCl decreased the yields of simple products such as toluene, and increased the yields of the products from rearrangement and coupling reactions such as PhCH_2PhOH and $\text{PhCH}_2(\text{PhCH}_3)\text{CH}_2\text{Ph}$. The considerable formation of these products indicates that these catalysts promoted the C-O bond cleavage through acidic actions to produce benzyl cation, which underwent two main reactions: stabilization by hydrogenation; attacking other species to cause rearrangement or condensation. Table 5 shows the results for dibenzyl (C-C linkage) at 400 - 425°C for 1 h with 9.8 MPa H_2 . The NiCl_2 - and MoCl_3 - LiCl-KCl catalysts showed essentially no effect at 400°C for breaking this type of C-C linkage. It is to be noted that the use of LiCl-KCl has neither positive nor negative effect on hydrogenation of polyaromatics such as anthracene, phenanthrene (Tables 1-2) and dibenzyl, but it showed pronounced effect in the runs of the ethers especially dibenzylether. For comparison of catalytic functions, we also conducted the model reactions using a commercial Ni-Mo/ Al_2O_3 catalyst (Table 6), because it has high activity for hydrogenation of polyaromatics (20).

DISCUSSION

Catalytic Functions. In the earlier stage of this work, we inferred based on the high liquid yields in pyrolysis and in liquefaction of Wandoan coal that the NiCl_2 - and MoCl_3 - LiCl-KCl catalysts have higher hydrocracking ability (14). However, the model reactions using polyaromatics clearly showed that while they have hydrogenating ability, they do not possess high hydrocracking ability (Tables 1-2). In fact, their cracking ability is much lower than MoCl_3 or ZnCl_2 , and their hydrogenating ability is much lower than sulfided Ni-Mo commercial catalyst (20). The key question that arise is what are the key functions of the catalysts leading to high oil yields and coal conversions? The motivation of the later works on the pyrolysis, and model reactions presented in this paper comes from the desire to answer this question.

Analytical pyrolysis in N_2 is an useful technique for evaluating the coal reactivity and the effect of catalyst on the cleavage of bridge bonds. The pyrolysis showed that the NiCl_2 - and MoCl_3 - LiCl-KCl catalysts enhanced the formation of volatile materials from bituminous (Figure 2), subbituminous and brown coals in N_2 at the temperatures above 300°C (14,19). In fact, the yields of volatiles from non-catalytic pyrolysis up to 600°C can be obtained by the catalytic pyrolysis at 400°C (Figures 1-2). The fact that the temperatures for the appearance of catalytic enhancement in pyrolysis in N_2 correspond to the onset of H_2 uptake in the liquefaction of Akabira coal (Figures 2-3) and other coals indicates that the interactions between catalyst and coal and the participation of molecular H_2 begin to occur at the temperatures as low as about 300°C .

From the above results, it becomes clear that the NiCl₂- and MoCl₃-LiCl-KCl catalysts can promote the cleavage of connecting linkages in coal at low temperatures, followed by stabilization of the reactive fragments by transferable hydrogens in the internal (coal and its products) and external (H₂) hydrogen sources. The model reactions using the bridge-type compounds showed that they can promote the cleavage of C-O bond in ethers at low temperatures (Table 4). While the cleavage of C-C linkage in dibenzyl was not affected by the catalysts at 400°C (Table 5), there is a possibility that these catalysts can promote the C-C bond cleavage for the dinaphthylethane type C-C linkage, because the bond strength of the latter is lower than the former (210-235 vs. 255-258 KJ/mol, Table 3), and the latter is closer to that of bezylphenylether (221 KJ/mol, Table 3).

The liquefaction results showed that NiCl₂- and MoCl₃-LiCl-KCl significantly promote the production of oils without any significant increase in gas-make. The observed relationship between hydrogen consumptions and products distribution (Figures 4,6) suggests that the molecular H₂ was consumed mainly in producing oils in the catalytic runs. The results of model reactions in Tables 1-2 showed that adding LiCl-KCl to MoCl₃ and NiCl₂ suppressed extensive hydrocracking of polyaromatics, but retained their hydrogenation activity to produce partially hydrogenated species from 3- and 2-ring aromatics without remarkable ring-opening cracking. These results also confirmed the observation from ¹H NMR that the NiCl₂- and MoCl₃-based catalysts gave more hydroaromatic products in oils from both solvent-free (15,16) and tetralin-mediated coal liquefaction (Figure 7). The partially hydrogenated polyaromatics are also H-donors, which could be more effective than tetralin in terms of H-donation rate in coal liquefaction (17).

The cracking ability of the Lewis acid catalysts is determined mainly by their acid strength. When ZnCl₂ is used in coal liquefaction, it always increases the C1-C₄ gas yield and the ratio of iso-C₄ to n-C₄, which has been taken as an acidity measure (2-3, 10). NiCl₂- and MoCl₃-LiCl-KCl do not remarkably enhance C1-C₄ yields and the iso-C₄/n-C₄ ratio, because the ring-opening cracking and dealkylation were very limited. However, it is worthy while noting that *sym*-octahydrophenanthrene was also produced from anthracene in the catalytic runs (Table 1). Its yields increased with increasing MCln content, as shown in Figure 9. This is considered to be a result of acid-catalyzed isomerization of *sym*-octahydroanthracene. The extent of the isomerization shown in Figure 9 suggests that the acid strength of MCln-LiCl-KCl decreases with increasing LiCl-KCl content. We also observed some interesting trends in the case of ZnCl₂. It was found that adding KCl to ZnCl₂ enhanced H-D exchange in H₂-D₂ model reactions, which is indicative of the enhanced ability for activating molecular H₂ upon KCl doping. On the other hand, ZnCl₂-KCl afforded higher oil yield and coal conversion and lower gas yield with lower consumption of molecular H₂, indicating the lower cracking ability and higher oil selectivity of ZnCl₂-KCl relative to ZnCl₂ alone. This is a general trend in the solvent-free runs of many coals (9-11) including Wandoan coal (Figure 4).

The side reactions such as condensation (via benzyl cation) observed in model reactions (Table 4) seem to suggest that the hydrogenating ability of the NiCl₂- and MoCl₃-based catalysts is not sufficiently high. This trend is similar to that observed by Bell and co-workers for the reactions of ether compounds using ZnCl₂ (7-8), where the condensation reactions were more remarkable even at lower temperatures, 193-225°C. It should be noted that unsulfided and sulfided Ni-Mo/Al₂O₃ catalysts exhibited relatively similar activity in hydrogenating anthracene, phenanthrene (20) and dibenzyl, whereas the former also caused remarkable condensation in the reactions of the ethers (Table 6). On the other hand, the side reactions may be inhibited by H-donation during coal liquefaction. Apparently, the reactions of the bridge-type model compounds are far from the real situation, and the resulting data should not be over-emphasized.

The general implications from the above results are as follows: 1) To obtain high oil yields with catalysts, the extensive hydrocracking reactions such as those over MoCl₃ or ZnCl₂ are not necessarily required; such reactions will decrease oil yields and coal conversion and increase gas yields and H₂ consumptions; 2) It is critical to suppress the acidic cracking ability of the acid catalysts to achieve a better balance of hydrogenating ability with the cracking ability; 3) Selective reactions over dispersed catalysts, which begin to occur at low temperatures, can be more efficient in controlling coal depolymerization and promoting oil production. The target in primary liquefaction using multi-component catalysts is to obtain the products containing more oils and less asphaltene and preasphaltene with relatively lower H₂ consumption. The products should be derived under less-severe conditions and retain moderate reactivity for subsequent upgrading using supported catalysts.

Role of Catalyst Components and Retrogressive Reactions. The catalyst physical state and dispersion are also important factors, which have physical and/or chemical effect. Unlike $ZnCl_2$ or $SnCl_2$ which becomes molten salt at $313^\circ C$ or $255^\circ C$, $NiCl_2$ and $MoCl_3$ do not melt even at $600^\circ C$. However, from DTA analysis of various salts (18), we found that they become molten when a mixture of 58%LiCl:42%KCl was added. The DTA suggested the melting points of the two catalysts to be $360^\circ C$ and $387^\circ C$, respectively (14). The test using an electric furnace showed that at $400^\circ C$, $NiCl_2$ -LiCl-KCl is a homogeneous liquid, and $MoCl_3$ -LiCl-KCl exists in a semi-molten state. While the catalytic effects become measurable below their melting points (Figures 2-3), the molten state provides much better catalyst dispersion and more intimate contact with coal, which offers an advantage in controlling the depolymerization of solid coal. The addition of LiCl-KCl to $NiCl_2$ and $MoCl_3$ also causes the formation of some complex ions such as $NiCl_4^{2-}$ and $MoCl_6^{3-}$ at low and/or high temperatures (21). The decrease in the acid strength is probably associated with the formation of such complex ions. In addition, our preliminary tests showed that $NiCl_2$ can be reduced by H_2 at $400^\circ C$; $MoCl_3$ is not readily reducible even by using K (molten potassium) but it disproportionates at the temperatures above 420 - $450^\circ C$. They appeared to become stable upon the addition of LiCl-KCl at the reaction temperatures.

Figure 10 shows a H-transfer network model modified from previous reports (16-17), and Figure 11 presents a general reaction model (22). Recent research has revealed that coal reactivity is higher than had been thought previously, and the liquefaction of coals under conventional process conditions involves considerable retrogressive reactions, as illustrated in Figure 11 (PRIOM formation), especially in the cases of subbituminous coals and lignites (22-24). The use of $NiCl_2$ - and $MoCl_3$ -LiCl-KCl has been found to be especially effective for liquefying subbituminous coals. While the relative effectiveness of these two catalysts changes with the coals used, it appears that they can significantly stabilize the coal-derived fragments by interaction, direct and indirect hydrogenation (Figure 10) to suppress their retrogressive reactions (Figure 11). Although the model reactions using ethers did not provide positive support, this consideration is strongly supported by the fact that very high oil yields (56-65%, daf) were obtained from the subbituminous coals by using these catalysts in the absence of any solvent (Figure 5), and the fairly high conversions (82-92%) are also an convincing evidence. In the runs of Akabira bituminous coals (16), the addition of tetralin was found to further increase coal conversions in the catalytic runs (84-86% to 91-94%), indicating that the use of H-donor solvent is also beneficial. However, such an effect in the catalytic runs was much smaller than in the non-catalytic runs (46 to 92%). It is likely that in the catalytic runs both H_2 gas and the hydroaromatic products (Figures 6-7) contributed to H-transfer (Figure 10), in addition to the H-donation from solvent and from coal itself. In the non-catalytic runs at $400^\circ C$ (16,22), the effect of tetralin addition appeared to be smaller for converting subbituminous coals such as Wandoan coal (49 to 61%) than for bituminous coals. It is to be noted that McMillen, Malhotra and co-workers (27-28) proposed that hydroaromatics can induce the cleavage of some strong bonds through radical hydrogen transfer.

CONCLUSIONS

The liquefaction of five coals established the general effectiveness of the two new ternary catalysts, $NiCl_2$ - and $MoCl_3$ -LiCl-KCl both in solvent-free runs and in the runs with added tetralin. The catalysts begin to interact with coal and exert measurable effects on coal pyrolysis in N_2 and the participation of molecular H_2 in coal liquefaction at the temperatures as low as about $300^\circ C$. The desirable features of these catalysts in coal liquefaction are characterized by the high oil yields and high conversions, and that molecular H_2 is mainly consumed in producing oils without remarkable increase in gas-make. The active components in the ternary catalysts are $NiCl_2$ and $MoCl_3$, in which the LiCl-KCl acts to adjust (decrease) the acidity and to suppress the cracking ability, which contributes to balancing the catalytic functions. At the temperature of $400^\circ C$, $NiCl_2$ and $MoCl_3$ are solubilized and stabilized by LiCl-KCl, producing a chemically more stable, but mobile catalyst phase which is important for controlling coal depolymerization. LiCl-KCl binary salts are inactive for pure hydrocarbons but can interact with some heteroatom-containing structures such as ethers. In the presence of tetralin solvent, $NiCl_2$ - and $MoCl_3$ -LiCl-KCl increase the gas-phase H_2 consumption but decrease the net hydrogen transfer from tetralin; the use of LiCl-KCl remarkably reduces the H_2 consumption without any negative impact on product yields. The $NiCl_2$ - and $MoCl_3$ -based catalysts play a key role in promoting oil production from the coals, increasing the contents of hydroaromatics and decreasing O and N contents of oils, probably by enhancing the cleavage of some connecting linkages and selectively promoting the hydrogenation of polyaromatics (to create in-situ H-donors).

FUTURE RESEARCH

The present research contributes to an improved understanding of the key factors for developing novel multi-component, dual-functional catalysts. The catalysts examined and the conditions used, however, are not considered to be the best. Temperature-programmed pyrolysis and t-p profiles for liquefaction of coals suggest that coals can be liquefied at the temperatures below 400°C. The future work on the acid catalysts should be directed toward the low-severity liquefaction. Efforts should be made to minimize the catalyst loading, and achieve better balance of catalytic functions (suppressing the acid strength and/or increasing hydrogenating ability) by exploring novel formulations. For the effects of various catalysts, more attention should be given to liquefying low-rank coals, and to increasing oil yields (rather than the conversions to THF solubles). The coal pretreatment followed by low-severity liquefaction using novel acidic dispersed catalyst should be tested in the future work. An interesting two-stage coal depolymerization procedure involving the use of Lewis acid such as FeCl₃ (3-20 wt% on coal) in the first stage and a base in the second stage at the temperatures of 250-310°C has been proposed by Shabatai and co-workers (27-28). Their results and our results suggest that selective reactions of coals at low temperatures in the presence of specific acid catalysts can be very effective in promoting coal depolymerization and oil production. If more effective dispersed catalysts for primary liquefaction and the supported catalysts with proper pore structure (29) for upgrading coal liquids, can be developed and applied, further reduction in severity of the current two-stage liquefaction processes (400-460°C, 17-20 MPa) is practically possible.

REFERENCES

1. Derbyshire, F.J. *Catalysis in Coal Liquefaction*, IEA Coal Research: London, 1988, 69 pp.
2. Zielke, C.W.; Struck, R.T.; Evans, J.M.; Costanza, C.P.; Gorin, E. *I & EC Process. Res. Dev.* 1966, 5, 151.
3. Zielke, C.W.; Struck, R.T.; Evans, J.M.; Costanza, C.P.; Gorin, E. *I & EC Process. Res. Dev.* 1966, 5, 158.
4. Struck, R.T.; Zielke, C.W. *Industrial Conversion of Coal and Carbon to Gase, Liquid and High-Value Products*, Society for Chemical Industry: London, 1981.
5. Saïm, S.S.; Bell, A.T. *Fuel* 1982, 61, 745.
6. Saïm, S.S.; Bell, A.T. *Fuel* 1984, 63, 469.
7. Frederick, T.J.; Bell, A.T. *J. Catal.* 1984, 87, 210.
8. Frederick, T.J.; Bell, A.T. *J. Catal.* 1984, 87, 226.
9. Nomura, M.; Miyake, M. *J. High Temper. Soc.* 1982, 8, 138.
10. Nomura, M.; Kimura, K.; Kikkawa, S. *Fuel* 1982, 61, 1119.
11. Nomura, M.; Yoshida, T.; Morida, Z. *I & EC Prod. Res. Dev.* 1984, 23, 215.
12. Nomura, M.; Sakashita, H.; Miyake, M.; Kikkawa, S. *Fuel* 1983, 62, 73.
13. Nakatsuji, Kubo, T.; Nomura, M.; Kikkawa, S. *Bull. Chem. Soc. Japan* 1978, 51, 618.
14. Song, C.; Nomura, M. *Fuel* 1986, 65, 922.
15. Song, C.; Nomura, M. *Bull. Chem. Soc. Japan* 1986, 59, 3643.
16. Song, C.; Nomura, M. *Fuel* 1987, 66, 1225.
17. Song, C.; Hanoka, K.; Nomura, M. *Energy & Fuels* 1988, 2, 639.
18. Song, C.; Nomura, M. *Prepr. 50th Chem. Soc. Japan Ann. Meet.*, Tokyo, 1985, p.775.
19. Song, C.; Nomura, M. *Proc. 17th Japan Petr. Chem. Sym.*, Fukuoka, 1987, p.122.
20. Song, C.; Hanaoka, K.; Ono, T.; Nomura, M. *Bull. Chem. Soc. Japan* 1988, 61, 3788.
21. Song, C.; Ono, T.; Nomura, M. *Bull. Chem. Soc. Japan* 1989, 62, 630.
22. Song, C.; Hanoka, K.; Nomura, M. *Fuel* 1989, 68, 287.
23. US DOE COLIRN Panel, *Coal Liquefaction*, Final Report, DOE/ER-0400, 1989, p.3-10.
24. Derbyshire, F.J.; Davis, A.; Lin, R. *Energy & Fuels* 1989, 3, 431.
25. McMillen, D.F.; Malhotra, R.; Chang, S.-J. *Proc. 1987 Int. Conf. Coal Sci.*, Maastricht, 1987, p.197.
26. McMillen, D.F.; Malhotra, R.; Hum, G.P.; Chang, S.-J. *Energy & Fuels*, 1987, 1, 193.
27. Shabatai, J.; Skulthai, T. *Proc. 1987 Int. Conf. Coal Sci.*, Maastricht, 1987, p.761.
28. Shabatai, J.; Zhang, Y. *Proc. 1989 Int. Conf. Coal Sci.*, Tokyo, 1989, p.807.
29. Song, C.; Nihonmatsu, T.; Hanaoka, K.; Nomura, M. *ACS Fuel Chem. Prepr.*, paper in this issue.

Table 1. Hydrogenation and Cracking of Anthracene

Run No.	1	2	3 ^{a)}	4 ^{b)}	5	6
Catalyst	None	LiCl-KCl	MoCl ₅ - LiCl-KCl	NiCl ₂ - LiCl-KCl	MoCl ₅	NiCl ₂
Products ^{c)} (wt%)						
C ₁ -C ₄	0.1	0.2	0.9	0.2	2.6	0.2
C ₅ -C ₉	-	-	0.1	-	2.1	0.7
R ₁ ⊖R ₂	-	-	0.9	-	1.1	-
R ₁ ⊖R ₂ + ⊕R	0.1	0.1	3.0	0.8	40.2	1.6
R ₁ ⊖R ₂	0.2	0.1	0.6	0.1	1.8	0.1
⊕R ^{d)} + ⊕R	0.3	0.1	7.7	4.3	15.6	11.4
⊕R ^{e)}	-	-	10.4	8.0	9.7	15.8
⊕R	14.9	15.8	44.9	41.0	6.4	37.3
⊕R	69.3	66.4	19.9	30.2	-	21.0
⊕R ^{f)}	14.4	13.8	6.4	12.1	2.4	7.6
Conversion	-	-	2.1	1.6	8.7	4.0
	85.6	86.2	93.6	87.9	97.6	92.4

a-b) Molar contents of MoCl₅ (a) and NiCl₂ (b) are 12% and 14%, respectively; c) R₁ and R₂ mean alkyl groups or hydrogen; d) ungu-Octahydroanthracene; e) 4,9-Octahydroanthracene; f) 4,9-Octahydrophenanthrene

Table 2. Hydrogenation and Cracking of Phenanthrene

Run No.	9	10	11	12	13	14
Catalyst	None	LiCl-KCl	MoCl ₅ - LiCl-KCl	NiCl ₂ - LiCl-KCl	MoCl ₅	NiCl ₂
Products ^{a)} (wt%)						
C ₁ -C ₄	-	0.1	0.1	0.2	3.4	0.1
C ₅ -C ₉	0.2	-	-	0.1	10.4	0.3
R ₁ ⊖R ₂ b)	0.1	-	0.5	-	10.1	0.1
R ₁ ⊖R ₂ + ⊕R	0.4	-	-	0.1	27.1	0.2
R ₁ ⊖R ₂	-	-	-	-	1.1	0.1
⊕R ^{c)} + ⊕R	-	-	0.1	0.1	10.2	0.9
⊕R ^{d)}	-	-	-	0.8	5.3	1.6
⊕R	0.7	1.0	0.3	-	2.1	0.1
⊕R	0.8	0.9	1.5	6.0	4.6	9.7
⊕R	1.3	1.4	6.3	8.2	9.7	12.0
Conversion	96.3	95.4	90.9	83.4	13.9	74.1
	3.7	4.6	9.1	16.6	86.1	25.9

a) R₁ and R₂ mean alkyl groups or hydrogen; b) Including cyclohexyl phenyl ethane; c) ungu- and d) 4,9-Octahydrophenanthrene.

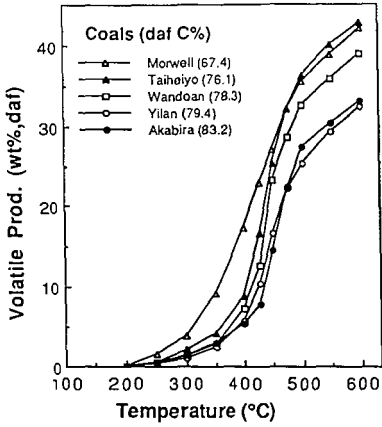


Figure 1. Coal pyrolysis in N₂ up to 600°C.

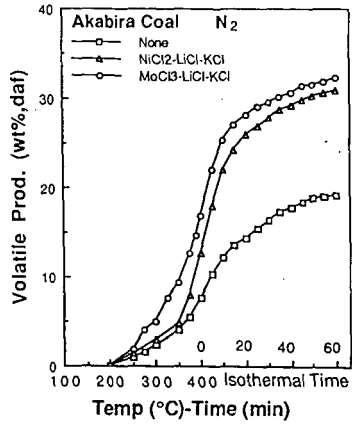


Figure 2. Pyrolysis of Akabira coal in N₂.

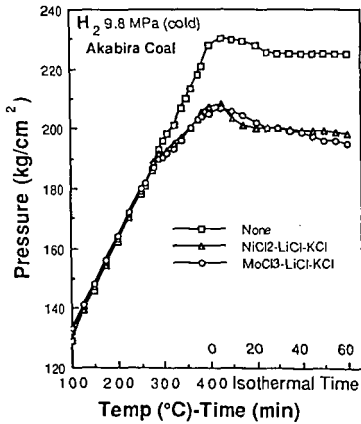


Figure 3. Reactor t-p profiles for liquefaction.

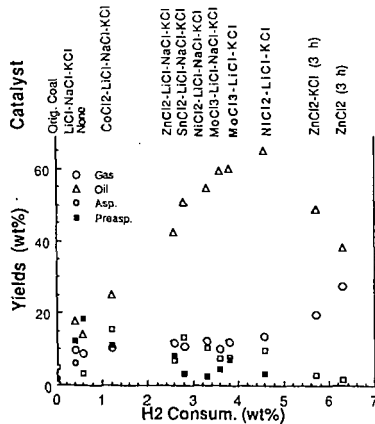


Figure 4. Dry liquefaction of Wandoan coal.

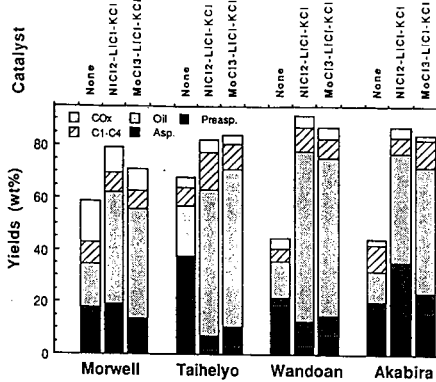


Figure 5. Dry liquefaction of coals.

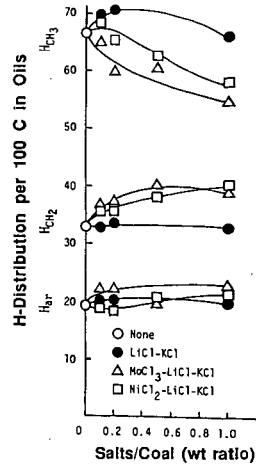


Figure 7. H-distribution of oils

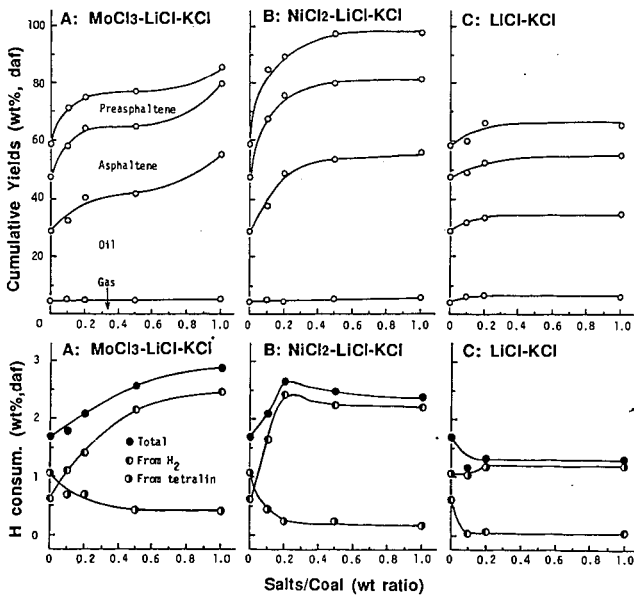


Figure 6. Effect of salt loading on coal conversion and H-transfer under low H_2 pressure

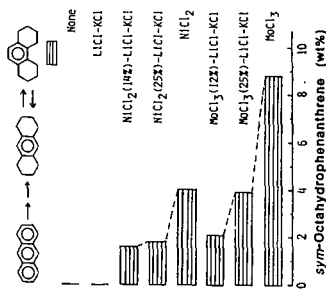


Figure 9. *sym*-octahydrophenanthrene from anthracene

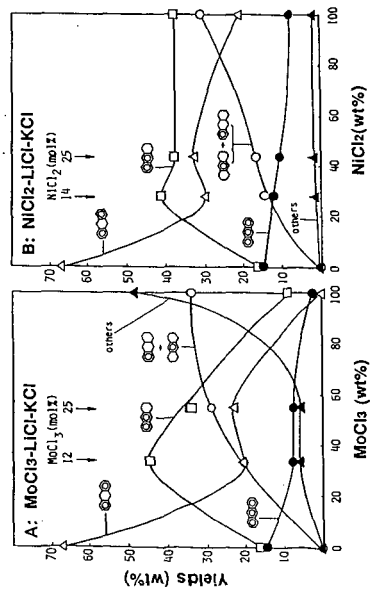


Figure 8. Effect of MoCl₅ content on hydrogenation of anthracene

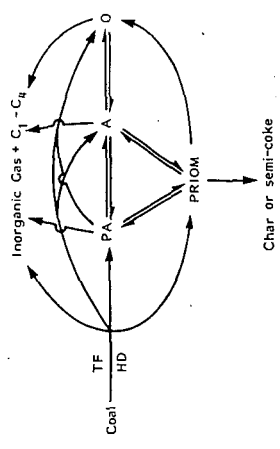


Figure 11. A reaction model for coal liquefaction
 TF: Thermal fragmentation; HD: Hydrogen donation by H in coal itself, vehicle and gas; PRIOM: Promlyt repolymerized or re-crosslinked insoluble organic materials; A: Asphaltene; PA: Preasphaltene; O: Oils including light distillate.

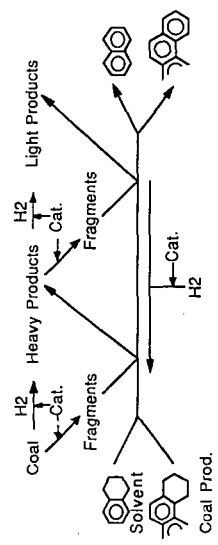


Figure 10. Hydrogen-transfer network in liquefaction

SULFATED METAL OXIDES AS CATALYSTS FOR COAL-OIL COPROCESSING

Vivek Pradhan, J. W. Tierney and Irving Wender
Department of Chemical and Petroleum Engineering
University of Pittsburgh, Pittsburgh, PA 15261

ABSTRACT

We recently reported on the investigation of the catalytic activities of iron and tin oxides treated with varying amounts of sulfate for the direct liquefaction of Argonne coals.^{1,2} This paper deals with the use of the same catalysts in addition to novel bifunctional, bimetallic catalysts such as $\text{Mo/Fe}_2\text{O}_3\text{SO}_4^{2-}$ containing about 0.5 to 2 wt% of Mo on the sulfate-promoted oxide (20-100 ppm Mo with respect to coal) for coprocessing of Argonne Illinois No.6 coal with Maya (650°F) ATB oil (20% coal+80% oil). The properties of these sulfate-promoted iron oxides before reaction and the types of active phases formed under liquefaction conditions (determined by XRD, electron microscopy, and Mossbauer spectroscopy) are correlated with their apparent activities for coprocessing carried out at 400°C. The sulfated bifunctional catalysts containing about 3500 ppm Fe and 50 ppm Mo with respect to coal are highly active for coprocessing, giving 80+% total coal conversion and 70 % yield of lighter oils with Illinois No. 6 coal and Maya ATB. These conversion values are higher than those obtained with ferric sulfate or carbonyl precursors such as $\text{Fe}(\text{CO})_5$ and $\text{Mo}(\text{CO})_6$. High catalyst dispersion and surface acidity are major factors that contribute to increased activity of these catalysts; Mo contributes a good hydrogenation function.

INTRODUCTION

The effects of catalytic activities of sulfate-treated iron and tin oxides and their relation to their catalytic activities in direct coal liquefaction have been reported.^{1,2,3} The high activity of these unsupported catalysts have been attributed mainly to their highly dispersed forms (available surface area per gm of catalyst) and to their enhanced surface acidity.

It is important to note that these sulfated oxides [$\text{M}_x\text{O}_y/\text{SO}_4^{2-}$] do not have real stoichiometric formulas but are a symbol for oxides which contain chemically attached surface species usually constituting a few percent of the total oxide. With $\text{Fe}_2\text{O}_3/\text{SO}_4^{2-}$, for instance, this could be considered as SO_3 chemisorbed on the Fe_2O_3 surface. We have found⁴ that the presence of a very small amount of moisture in the catalyst system helps maintain high acidic activity, likely due to transformation of the catalyst to its Bronsted acid form, responsible for generating carbocations.

The effects of various anions such as Cl^- , PO_4^{3-} , and SO_4^{2-} in the form of dopants added to metal oxides to decrease their particle size has been the topic of considerable interest in material science since the early eighties. It is known⁵ that the sulfate anion prevents sintering of ceramic oxide powders during calcination, thereby reducing the degree of crystallinity and

lowering the average crystallite size of these oxides. It has been shown that¹ the superacidic $\text{Fe}_2\text{O}_3/\text{SO}_4^{2-}$ forms a highly dispersed catalyst in the form of particles of about 30-100 Å units in diameter. It is this very property that also makes sulfated iron oxides good sensors for combustible gases.⁵

Addition of molybdenum to the sulfated iron oxide provides an excellent hydrogenation function to contribute to the catalytic action of the highly dispersed, superacidic $\text{Fe}_2\text{O}_3/\text{SO}_4^{2-}$.

EXPERIMENTAL

Catalyst Preparation and Characterization: The $\text{Fe}_2\text{O}_3/\text{SO}_4^{2-}$ and $\text{Mo}/\text{Fe}_2\text{O}_3/\text{SO}_4^{2-}$ catalysts consisting of varying amounts of molybdenum were prepared using homogeneous coprecipitation followed by an incipient wetness technique. Ammonium heptamolybdate was used as a starting salt for molybdenum impregnation. Conditions for the preparation of these catalysts are given in Table 1. The catalysts were characterized by BET-surface area analysis, sulfur analysis, thermal stability measurements, X-ray diffraction, and electron microscopy. A Phillips X-ray Diffractometer using $\text{Cu-K}\alpha$ radiation at 30 kV and 25 mA was used to obtain the powder diffraction patterns of the catalysts.

Average crystallite sizes of these catalysts were calculated from line broadening of the peaks, corrected for instrumental broadening. Transmission electron microscopy (TEM) and scanning electron microscopy (SEM) were carried out for structural investigation of the catalysts using JEOL 35 CX SEM and JEOL 200 CX TEM models. The residues of coal liquefaction experiments were also analyzed using X-ray diffraction and a JEOL 2000 FX STEM (100 kV beam) with an energy dispersive X-ray spectrometer (EDX) to determine composition and dispersion information about the catalytic phases formed under liquefaction conditions.

Reaction Studies: Coprocessing experiments were conducted in a 300ml stainless steel autoclave (Autoclave Engineers) agitated by a turbine impeller and heated by a tube furnace. Coal (10.0g), 40.0g Maya ATB residuum, and the desired catalyst precursors/sulfated catalysts were placed into the reactor, which was flushed with helium and stirred at 50°C for two hours to ensure mixing of the catalyst precursor in the viscous residuum. The reactor was pressurized with hydrogen to 6.9 MPa, heated to reaction temperature (400 or 425°C) in 30 minutes, and held there for 60 minutes while stirring at 1400 rpm. The reactor was then cooled to below 300°C in about five minutes. Soxhlet extraction with methylene chloride was used to determine conversion. Soluble products were recovered by rotary evaporation at 45°C under vacuum. Pentane solubles were determined by adding 40 volumes of n-pentane to the methylene chloride (CH_2Cl_2) solubles and then using Soxhlet extraction with n-pentane. Transmission electron microscopy was carried out using a JEOL 2000FX STEM (100kV beam) with an energy dispersive X-ray spectrometer.

RESULTS AND DISCUSSION

Catalyst Characterization: The iron and tin oxides treated with different amounts of sulfate were characterized by DTATGA to determine their thermal stability. For sulfated iron oxides promoted with small amounts of molybdenum, $\text{Mo}/\text{Fe}_2\text{O}_3/\text{SO}_4^{2-}$, decomposition of the sulfate group was found to occur above 600°C under an N_2 atmosphere. The effects of sulfate anion on reduction of grain sizes were published earlier.³ The average crystallite size

of the oxide particles had decreased upon treatment with 2 to 6 wt % of sulfate anion; this was accompanied by a corresponding increase in the specific surface area of these oxides, observed when liquid nitrogen physisorption was carried out using the BET method. A linear relationship was observed between the concentration of sulfuric acid used for sulfate treatment and the final amounts of SO_4^{2-} groups on the iron oxides up to about 8 wt% sulfate loading. From X-ray diffraction studies of the sulfated iron oxides, α - and γ - Fe_2O_3 were found to be the most abundant crystalline phases, while for tin oxides, the most abundant phase was crystalline SnO_2 . Catalyst characterization results are listed in Table 2. For $\text{Mo/Fe}_2\text{O}_3/\text{SO}_4^{2-}$ containing 20-100 ppm of Mo with respect to coal, no molybdenum was detected by X-ray diffraction; this could be due to the very fine dispersion of Mo apart from its small concentration on the $\text{Fe}_2\text{O}_3/\text{SO}_4^{2-}$ catalyst. Temperatures of the onset of liquefaction of Illinois No.6 coal using different sulfate-treated oxides as catalysts are listed in Table 2. These temperatures were determined using a high pressure, high temperature polarizing optical microscope with flowing H_2 at 300 psig pressure. $\text{Mo/Fe}_2\text{O}_3/\text{SO}_4^{2-}$ catalysts were also characterized by electron microscopy and found to have a grain size of about 10-15 nm. The amounts of Mo in the catalysts were determined by inductively coupled plasma analysis.

Reaction Studies: Initially a thermal (no added catalyst) run was carried out to determine the catalytic activities of the mineral matter (especially pyrite) inherent in coal. The coal conversion values listed in this paper are calculated based on weight of the final residue.

(I) Activities of the Sulfated Oxides

The sulfated iron and tin oxides were used in small concentrations for coprocessing of Illinois No. 6 with Maya ATB. Use of the $\text{Fe}_2\text{O}_3/\text{SO}_4^{2-}$ catalyst containing about 3.4 wt% of sulfate group, resulted in a coal conversion of 70 wt % with 72 wt % selectivity to oils at 400°C with about 3500 ppm iron with respect to the coal-oil mixture. When $\text{SnO}_2/\text{SO}_4^{2-}$ (3.9 wt% sulfate) was used as the catalyst with 3500 ppm of tin at 400°C, about 62 wt% conversion was obtained with about 76 wt% selectivity to oils. A reaction was carried out with a molybdenum containing catalyst precursor, $\text{Mo}(\text{CO})_6$, for comparison, using about 100 ppm Mo with respect to the mixture of coal and oil. This resulted in a 71 wt% coal conversion with 70 wt% selectivity to lighter oils. Use of a bimetallic, bifunctional catalyst, $\text{Mo/Fe}_2\text{O}_3/\text{SO}_4^{2-}$, consisting of 50 ppm Mo and 3500 ppm Fe with respect to the coal-oil mixture gave a coal conversion of 80 wt% with 80 wt% selectivity to lighter oils. The higher activity of this catalyst is attributed to the hydrogenation ability of Mo and, possibly, to the acid sites of the sulfated catalyst. Results of these catalyst activity comparisons and those obtained in the coprocessing reaction employing a bimetallic sulfated oxide of iron and tin, $\text{SnO}_2/\text{Fe}_2\text{O}_3/\text{SO}_4^{2-}$, (with 1750 ppm of each iron and tin) are shown in Figure 1(A).

Enhancement in total conversions as well as conversions to oils obtained with sulfated oxides are attributed mainly to enhanced "dispersions" (surface area/gm) with a possible contribution from the high surface acidity of these oxides upon sulfate treatment. It is likely that, with increase in the specific surface area and decrease in the average particle size of the oxides upon addition of small amounts of the sulfate group, conversion of the oxides to active catalytic sulfide phases, especially non-stoichiometric sulfides of iron, is facilitated.⁶ More of the active catalyst surface of these sulfides becomes available for reaction.

(II) Activity of $\text{Mo/Fe}_2\text{O}_3/\text{SO}_4^{2-}$ Catalysts at 400 and 425°C

Addition of small amounts of Mo to 0.5 to 2 wt% of the sulfated iron oxides (about 20-100 ppm Mo concentration with respect to the coal-oil mixture) resulted in substantial improvement in the selectivity to oils. A series of experiments were carried out to determine the coprocessing conversion of Illinois No. 6 with Maya ATB at two different reaction temperatures (400 and 425°C) and for different amounts of Mo loadings on $\text{Fe}_2\text{O}_3/\text{SO}_4^{2-}$. The results of experiments carried out at 400 and 425°C are shown in Figure 1(B).

Total coal conversions, as well as selectivities to lighter oils, increased for both temperatures with the amount of molybdenum in the sulfated iron oxide catalyst (0-100 ppm Mo with respect to the coal-oil mixture). Conversions as high as 84 wt% (maf coal) with selectivity values of higher than 80 wt% were obtained at about 100 ppm Mo + 3500 ppm Fe added in the form of $\text{Mo/Fe}_2\text{O}_3/\text{SO}_4^{2-}$. Surprisingly, we obtained slightly lower values for both coal conversion and selectivity to oils in almost all the reactions carried out at 425°C as compared to those at 400°C. This apparent decrease in coprocessing conversion is likely due to the extensive coking reactions occurring because of the presence of an acidic functionality in the catalyst. The coal liquefaction residues obtained in this case (425°C) had a rock-like appearance.

All of the aforementioned reactions were carried out without adding any external sulfur compound since Illinois No. 6 coal and the heavy oil (Maya ATB) together have enough sulfur to sulfide the added metals during reaction. Nevertheless, a run was made with addition of elemental sulfur (10% in excess of that required for complete sulfidation of both the Fe and Mo in the catalyst) to the coal-oil mixture prior to reaction at 400°C with 3500 ppm of iron and 100 ppm of Mo. No effect of the added sulfur was observed on either overall coal conversion (86 wt%) or the selectivity to lighter oils (82 wt%).

Product Characterization:

(I) Elemental Analyses of Methylene Chloride-Soluble Products

The methylene chloride solubles of the coprocessing product from using the Fe-Mo precursor were analyzed for C,H,N, and S contents. As seen from Table 3, an improvement in the H/C atomic ratios is obtained for the soluble products for the sulfated iron oxides containing small amounts of molybdenum as catalysts. At the same time, a significant degree of sulfur and nitrogen removal (75 to 80 % HDN and HDS) is obtained. With the $\text{Mo/Fe}_2\text{O}_3/\text{SO}_4^{2-}$ catalysts, this could be attributed to the enhanced acidic strength and high dispersions of the catalysts and the hydrogenative function contributed by Mo.

(II) X-Ray Diffraction and Electron Microscopy of Residues

X-ray diffraction (XRD) was performed on the methylene chloride-insoluble fraction of the coprocessing runs carried out with Illinois #6 coal with added iron catalysts. Transmission electron microscopy was employed to determine the size range of the iron- and molybdenum-containing particles produced from $\text{Fe}(\text{CO})_5$ and $\text{Mo}(\text{CO})_6$ precursors. To eliminate interference of the iron and other mineral matter in the coal, a model system was used which consisted of activated carbon with molybdenum or Fe-Mo deposited on it. This mixture was produced by heating a mixture of activated carbon (with a very low iron content), toluene (solvent), and $\text{Mo}(\text{CO})_6$ with or without $\text{Fe}(\text{CO})_5$ in an autoclave to decompose the precursor into small particles, some of which would end up on the carbon support. Similarly, for the electron microscopic studies, a $\text{Mo/Fe}_2\text{O}_3/\text{SO}_4^{2-}$ catalyst was deposited on an activated carbon matrix using tetralin as dispersion medium. These TEM images show the catalyst particles containing Fe and mo on active carbon with sizes ranging from 10-30 nm.

CONCLUSIONS

Sulfated iron and tin oxide catalysts were found to be active for the coprocessing of Argonne Illinois No.6 coal with Maya ATB (20:80 coal:oil) both at 400 and 425°C. For a bimetallic catalyst, $\text{Mo/Fe}_2\text{O}_3/\text{SO}_4^{2-}$, consisting of 50 ppm Mo and 3500 ppm iron, a 78 % coal conversion of Illinois No. 6 was obtained with an oil- selectivity of 80 % at 400°C. The sulfated iron oxide catalysts with small amounts of Mo(20-100 ppm) were more active than the soluble precursors of the same metals at 400°C. Significant HDN (~75 %) and HDS(~80%) were obtained with Mo-promoted sulfated iron oxide catalysts. We attribute the higher activity of the sulfated oxides to their fine grain size (30-100 Å) with increased catalyst dispersion and to increase in their acid strength. The comparison between the activities of sulfated oxides and the soluble precursors shows that finely divided solid catalysts could be as active as the catalysts produced from the soluble precursors of iron and molybdenum. Thus, the catalytic activity of the sulfated oxides are the result of several factors: the fine grain size is probably of the greatest importance, the superacidity of the starting catalysts may play a part during the initial phases of the reaction. In the case of $\text{Mo/Fe}_2\text{O}_3/\text{SO}_4^{2-}$, the hydrogenation ability of Mo certainly plays a part. However, there is still much to be learned about the mechanisms involved in these types of reactions. With these superacidic sulfated metal oxides as catalysts, the chemistry of the reactions in coal liquefaction could be different from what is known so far (such as possible involvement of radical ion intermediates). These finely divided solid catalyst-precursors therefore show great promise for application in hydroprocessing reactions

ACKNOWLEDGMENTS

The authors gratefully acknowledge the contributions of the Argonne coal sample bank for providing the coal samples, C. van Ormer and J.R. Blachere for the transmission electron microscopy, the donation of Maya crude by CITGO, and funding support from the U.S. Department of Energy under grant number DE-FC22-88PC8806.

References

1. Pradhan, V. R., Tierney, J. W., Wender, I., Preprints, Div. of Fuel Chem., *American Chemical Society*, August, 1990, Vol. 35, No. 3, p. 793
2. Pradhan, V. R., Tierney, J. W., Wender, I., Paper Presented at the 'Direct Liquefaction Contractors' Review Meeting (DOE)' Pittsburgh, 1990
3. Pradhan, V. R., Huffman, G.P., Tierney, J. W., Wender, I., *submitted to Energy and Fuels for Publication*
4. Wen, M. Y., Wender, I., Tierney, J., *Energy and Fuels*, Vol.4, 1990, pp.392-397
5. Nakatani, Y., Sakai, M., Matsuoka, M., *J. of Appl. Physics*, Vol. 21, 1982, pp. L758
6. Montano, P.A., Bommanavar, A. S., Shah, V., *Fuel*, 1981, Vol. 60, P. 703

Table 1. Preparation Conditions of Sulfated Iron and Tin Oxides

Catalyst	Catalyst Designation	Starting Salts	Norm. H ₂ SO ₄	Calcination, T°C
Fe ₂ O ₃ /SO ₄ ²⁻	I	Fe Alum ^a	--	500
Mo/Fe ₂ O ₃ /SO ₄ ²⁻	II	Fe Alum ^a	--	500
Mo/Fe ₂ O ₃ /SO ₄ ²⁻	III	Fe Alum ^a	--	500
Mo/Fe ₂ O ₃ /SO ₄ ²⁻	IV	Fe Alum ^a	--	500
SnO ₂ /SO ₄ ²⁻	V	SnCl ₄ /5H ₂ O	6.0	600
SnO ₂ /Fe ₂ O ₃ /SO ₄ ²⁻	VI	Chloride Salts ^b	6.0	500

^a Urea was used as the precipitating agent whereas ammonium heptamolybdate was used to impregnate small amounts of Mo on sulfated iron oxide before calcination.

^b The ferric and tin chloride salts were used here with 28 % ammonia water as a precipitation agent.

Table 2. Physicochemical Properties of the Sulfated Oxide Catalysts

Catalyst	Wt % Mo	S _p , m ² /g	XRD: D _{avg}	TEM :D _{avg}	Onset T°C ^a
Catalyst I	0.0	81.72	16 nm	20-25 nm	410
Catalyst II	0.4	81.50	12 nm	20-30 nm	nd
Catalyst III	1.0	88.00	9 nm	15-20 nm	400
Catalyst IV	2.0	92.21	9 nm	10-15 nm	400
Catalyst V	--	146.23	5 nm	10-15 nm	385
Catalyst VI ^b	--	320.00	5 nm	5-10 nm	nd

^a Onset coal liquefaction temperature for a non-catalytic liquefaction run for Argonne Illinois No.6 coal was 450°C as determined using a high temperature, high pressure polarizing microscope.

^b This catalyst consisted of equal weight percents of SnO₂ and Fe₂O₃.

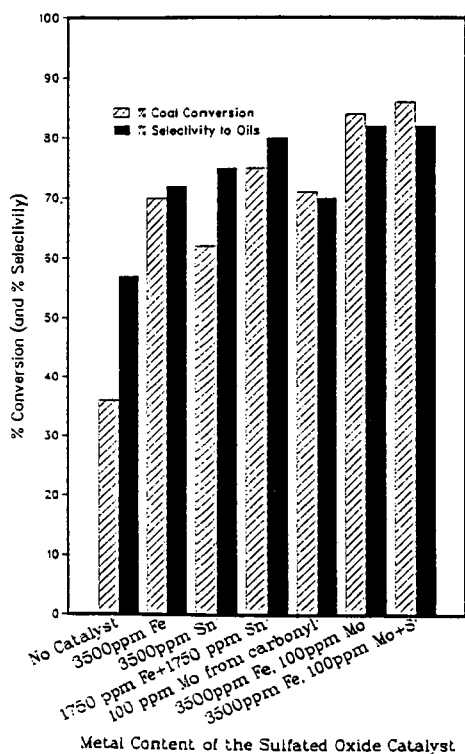
Table 3. Elemental Analysis of CH₂Cl₂ Solubles Obtained from Coprocessing of Illinois No.6 and Maya with Different Catalysts

Amount of Catalysts vs. Analysis : Wt %							
Catalyst	ppm Mo	ppm Fe	% C	% H	% N	% S	{H/C}atom
None	--	--	83.00	10.30	0.25	3.18	1.49
Catalyst III	50	3500	47.58	5.83	0.55	2.01	1.47
Catalyst IV	100	3500	66.99	8.52	0.72	2.13	1.53
Fe(CO) ₅	--	5000	83.83	10.45	0.33	3.01	1.50
Carbonyls	500	5000	82.53	10.79	0.43	2.94	1.57
Mo-naph. ^b	500	5000	83.07	10.50	0.40	2.89	1.52

^a All runs were made with Illinois No.6, 425°C, 1000 psig cold H₂, 60 minutes, 20 wt% coal/80 wt% Maya ATB.

^b Fe(CO)₅ was used in this run with Mo-naphthenate.

A



B

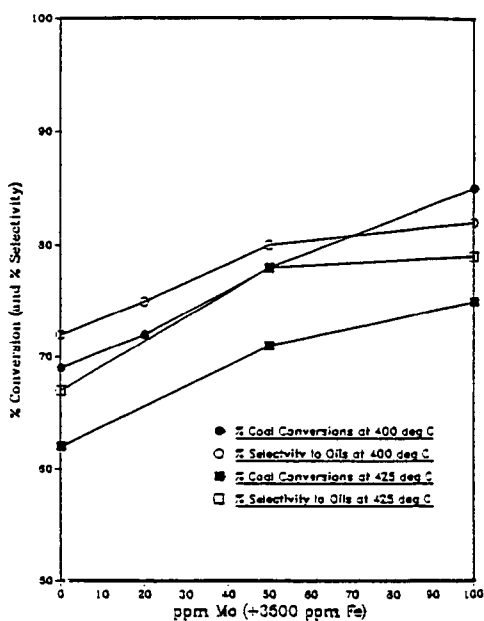


Figure 1. (A) Activity of Sulfated Metal Oxides for Coprocessing of Illinois No.6 Coal at 400°C, 1000 psig cold H₂, 1h and (B) Activity of Mo/Fe₂O₃/SO₄²⁻ Catalysts for Coprocessing at 400 and 425°C, 1000 psig cold H₂, 1h

DIHYDROQUINONE FOR ENHANCING COAL LIQUEFACTION YIELDS

J. H. Penn', Y.-Q. Liu, and P. Yassini
Department of Chemistry
West Virginia University
Morgantown, WV 26506

Keywords: Dihydroquinone, Coal Liquefaction, THF extractables

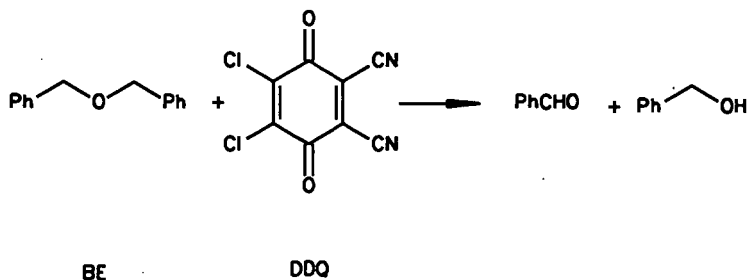
Abstract

Finding reagents and/or catalysts to enhance liquefaction of coal continues to be an area of active interest. During our studies directed towards the use of PI-acceptor induced bond cleavage reactions, we have found that 1,4-dihydroquinone enhances the yield of THF-extractables for a series of coals ranging from low rank sub-bituminous to high volatile bituminous. In certain cases, benzoquinone can also enhance the yields of THF extractables from coal. These reactions take place at surprisingly low temperatures (*i.e.*, 200°C).

Introduction

As part of our on-going effort to develop new ways to cleave bonds (1) through the use of electron transfer chemistry, we have been particularly interested in the reactions of quinones and their ability to cleave ether bonds (2). Representative of our work to date is the reaction of benzyl ether (BE) with 2,3-dichloro-5,6-dicyano-1,4-quinone (DDQ) which yields benzaldehyde and benzyl alcohol when heated together at 200°C in acetonitrile (CH₃CN) (2) as shown in eq (1).

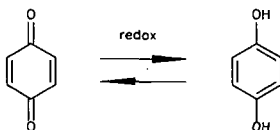
(1)



Although the use of quinones proved to be useful to bond

cleavage in model compounds, quinones proved to have only a small effect on enhancing liquid yields liquids from coal under similar conditions to those used in model compound studies. Interestingly, small quantities of quinones did appear to have a small positive effect on achieving greater quantities of THF-extractables. One rationale for this lack of enhancement arises from the oxidizing nature of these compounds. Since the major goal for liquefaction seems to involve the addition of hydrogen to the molecular framework of the coal polymer as it unravels, we reasoned that dihydroquinones, as the redox couples of quinones (note eq (2)), might prove effect in increasing liquid yields. Although dihydroquinones have been used as part of a complex mixture for enhancing coal liquefaction, we report here that **DHQ** by itself is sufficient to enhance the amount of THF-extractable material from a number of coals.

(2)



Experimental

Samples of coal were obtained from the Argonne Premium Coal Sample Bank. Bakerstown coal and Sewell coal were obtained from the West Virginia Coal Sample Bank.

A given weight of coal and a given weight of the added reagent were added to 5 mL of acetonitrile (CH_3CN , freshly distilled from NaH) in a 10 mm glass tube. Oxygen was removed from the solution via 3 freeze-pump-thaw degassing cycles and the sample tube was then sealed *in vacuo*. The sample tube was placed in a tubing bomb reactor to which excess CH_3CN was added to equalize the pressure on the outside and inside of the glass. The tube was then placed in an oil bath at the indicated temperature for the indicated length of time. After removal from the oil bath, the contents of the glass tube are placed in a Soxhlett extractor and refluxed with THF for 24 h. After evaporation of the THF *in vacuo*, the weight of the extract and the weight of the insolubles were determined.

Results and Discussion

In order to evaluate the effect of a reagent on liquefaction of coal, control experiments were performed with no added reagent to establish the amount of extractables without reagent. In all

cases, the coal was heated at 200°C for 48 h in the indicated solvent. Not surprisingly, the choice of solvent does have an effect upon the amount of THF-extractables obtained in these experiments. The results of these experiments are given in Table I. As expected, there is a solvent dependence on the amount of THF-extractability as evidenced by the effects shown on the Bakerstown coal. These experiments were mandated by the high mass balances afforded by acetonitrile (CH₃CN). Since all other solvents yielded mass balances less than 100%, we conclude that incorporation of CH₃CN into the insolubles and into the THF extractables occurs similarly in all experiments.

The results of adding a 1:1 weight ratio of dihydroquinone (DHQ) to the coal are shown in Table II. In these experiments, the coal and the DHQ have been heated together in the indicated solvent for 48 h at 200°C. In this table, the effects of the reagent are given by a Liquefaction Enhancement (L.E.) which has been defined by eq (3). In this equation, THF_{coal} and THF_{DHQ} are the amounts of extractables when either the coal or DHQ are treated alone. Normalization to the starting amount of coal is performed to enable comparison of one coal to another coal.

$$L.E. = \frac{(Total\ THF\ extract) - (THF_{coal} + THF_{DHQ})}{starting\ weight\ coal} \times 100\% \quad (3)$$

As can be seen in Table II, reasonable enhancements in the liquid yields are obtained. These results are made more remarkable when one considers that these LEs were obtained for temperatures as low as 200°C. A solvent dependence is noted for this effect, with only CH₃CN and cyclohexane (C₆H₁₂) showing positive enhancements.

Although these results are still preliminary in nature, we speculate that DHQ serves primarily as a hydrogen donor. In support of this hypothesis, DHQ gives a greater LE than tetralin (L.E. = -12%) for Bakerstown coal under similar conditions. Since a limited amount of 1,4-benzoquinone (BQ) shows a small positive L.E., the use of DHQ offers the possibility that a catalytic cycle may be opened up, making the product(s) of DHQ (i.e., BQ) effective for more liquefaction activity.

References

1. (a) Penn, J.H.; Lin, Z.; Deng, D.-L. *J. Am. Chem. Soc.*, **1991**, in press. (b) Penn, J.H.; Lin, Z.; Deng, D.-L. *Tetrahedron Lett.*, **1988**, *29*, 3635.
2. (a) Penn, J.H.; Lin, Z. *J. Org. Chem.*, **1990**, *55*, 1554. (b) Penn, J.H.; Deng, D.-L.; Aleshire, S.K. *J. Org. Chem.*, **1988**, *53*, 3572. (c) Penn, J.H.; Smith, R.S. *Tetrahedron Lett.*, **1986**, *27*, 3475.

Table I
Coal Extractability Without Added Reagent

Coal	Coal Rank	Solvent	%THF Extractable
Bakerstown		CH ₃ CN	19.9
		THF	25.9
		C ₆ H ₆	21.7
		C ₆ H ₁₂	4.8
Sewell		CH ₃ CN	19.5
Pittsburgh #8	HV Bituminous	CH ₃ CN	34.4
Blind Canyon	HV Bituminous	CH ₃ CN	26.4
Upper Freeport		CH ₃ CN	12.7
Beulah-Zap	Lignite	CH ₃ CN	5.4

Table II
Enhancements Using DBQ as a Co-reagent

Coal	Coal Rank	Solvent	L.E.
Bakerstown		CH ₃ CN	20.5
		THF	1.0
		C ₆ H ₆	2.3
		C ₆ H ₁₂	10.0
Sewell		CH ₃ CN	-1.9
Pittsburgh #8	HV Bituminous	CH ₃ CN	41.7
Blind Canyon	HV Bituminous	CH ₃ CN	7.8
Upper Freeport		CH ₃ CN	3.4
Beulah Zap	Lignite	CH ₃ CN	45.4

EVALUATION OF CATALYTIC ROLE OF VANADIUM IN COAL-OIL PROCESSING USING MODEL SYSTEMS

H. Kim and C. W. Curtis
Department of Chemical Engineering
Auburn University, AL 36849

Keywords: vanadium, coal-oil processing, model systems

ABSTRACT

The catalytic activity of vanadium for hydrogenation and heteroatom removal reactions occurring in coal-oil processing was evaluated using model systems. Two-ring aromatics, hydroaromatics and heteroatomic species containing S, N and O were selected as the models representing typical species in coal and oil. Vanadium catalysts generated *in situ* from organic vanadium complexes, such as vanadium acetylacetonate and vanadylacetylacetonate, were activated in the presence of sulfur. Their activity increased as the amount of sulfur present increased. The vanadium catalysts were active for partial saturation of two-ring aromatics to hydroaromatics but far less active for the further saturation to alicyclic compounds. The vanadium catalysts were severely poisoned by organic nitrogen compounds, showing lower activity for N removal than for S and O removal and achieving low amounts of hydrogenation and heteroatom removal of other reactants when nitrogen compounds were present.

INTRODUCTION

Vanadium (V) is one of the most abundant trace metals in petroleum and is more concentrated in the petroleum residuum than in the crude. (1) V sulfides, which are generated from their organic precursors such as V naphthenate, octoate or acetylacetonate in the presence of sulfur, have been used as hydrodesulfurization catalysts in petroleum refining. (2-5) The V indigenous to residuum may form V sulfide and be catalytic under coal-oil processing conditions. These species may influence the reaction pathways and product slates involved in the processing.

The objective of this study is to evaluate the catalytic activity of V sulfide for hydrogenation and heteroatom removal reactions occurring in coprocessing. The activity and selectivity of *in situ* generated V sulfide were evaluated by reacting model hydrocarbon and heteroatomic systems with V precursors, vanadium acetylacetonate and vanadylacetylacetonate, and excess sulfur under coal-oil processing conditions. The activity and selectivity of *in situ* generated V sulfide for the reactions of model compounds were also compared to those of a Mo sulfide catalyst generated *in situ* from Mo naphthenate and sulfur.

EXPERIMENTAL

Chemicals

The model reactants used were naphthalene (99%), indan (97%), indene (99%), benzothiophene (97%), o-cresol (99%), benzofuran (99.5%), quinoline (99%) and indole (99%). n-Hexadecane (99%) was used as a solvent. All of these chemicals were obtained from Aldrich. The V precursors were vanadium(III) acetylacetonate (VAcAc) and vanadyl(IV)acetylacetonate (VOAcAc). VAcAc was obtained from Shepherd Chemical and Aldrich, and VOAcAc was obtained from Aldrich.

Reactions and Analyses

Hydrogenation reactions were conducted in 20 cm³ batch tubing bomb microreactors. Four grams of hexadecane solution containing 2 wt% naphthalene and/or 1 wt% of

each of other reactants were charged to the reactor. The V precursor was introduced at a level of 2850 to 2950 ppm V while always keeping a constant weight ratio of V to reactant. Excess elemental sulfur, 0.034 g S which was three times the stoichiometric amount of sulfur to form V_2S_3 from V precursors, was added to the reaction. Prior to the reaction, 1250 psig H_2 was introduced at ambient temperature. The reactions were conducted at 380°C for 30 minutes with horizontal agitation at 550 cpm. The liquid products were analyzed by gas chromatography using a 30 m fused silica DB-5 column (J & W Scientific) and FID detection with p-xylene as the internal standard. Some of the reaction products were identified by GC/MS equipped with a VG 70EHF mass spectrometer and a Varian 3700 gas chromatograph.

RESULTS AND DISCUSSION

The catalytic activity of V generated *in situ* from VAcAc and VOAcAc was investigated in hydrogenation reactions of hydrocarbons and heteroatomic species individually or in combination under coprocessing conditions. In addition, the effect of sulfur on the activity of V species was determined.

The degree to which hydrogenation and heteroatom removal occurred in each reaction is reported in terms of percent hydrogenation (% HYD), percent hydrodesulfurization (% HDS), percent hydrodeoxygenation (% HDO), and percent hydrodenitrogenation (% HDN). The % HYD is defined as the number of moles of hydrogen used to achieve the final liquid product distribution as a percentage of the moles of hydrogen required to achieve the most hydrogenated liquid product. The % HDS, % HDN and % HDO are the summations of the mole percents of products not containing sulfur, nitrogen and oxygen, respectively. In the calculation of % HYD, the most hydrogenated liquid products defined for the systems used were decalin for naphthalene and tetralin; cyclohexane for indan, indene, benzothiophene, o-cresol, benzofuran, and indole; and n-propylcyclohexane and n-butylcyclopentane for quinoline.

Catalytic Activity of V for Aromatic Ring Saturation

The activity of V generated *in situ* from VAcAc and VOAcAc in the presence of excess sulfur was evaluated for hydrogenation of aromatics and alkyaromatics: naphthalene, tetralin, n-butylbenzene, n-propylbenzene, ethylbenzene and toluene. The result was compared to the activity of *in situ* generated Mo sulfide at the same metal loading level for the same systems. The V species from both precursors showed high activity for partially saturating two-ring aromatics to hydroaromatics, but low activity for fully saturating the two-ring aromatics or single-ring alkyaromatics to alicyclics and alkylalicyclics as did the Mo sulfide; only 2-5% of aromatic ring in alkyaromatics was saturated to alkylalicyclics with VAcAc, and only 3-9% was saturated with VOAcAc. However, the V sulfide catalysts showed a slightly higher activity for both the aromatic ring saturation and the ring hydrogenolysis than the Mo sulfide catalyst.

Activity and Selectivity of V Catalyst for Hydrogenation and Heteroatom Removal

The catalytic activity and selectivity of *in situ* generated V for reactions involving hydrogenation, hydrogenolysis and heteroatom removal were evaluated by using individual model systems. The major products and the degree of hydrogenation and heteroatom removal achieved with V catalysts were compared to those from comparable systems reacted with *in situ* generated Mo sulfide at equivalent reaction conditions (Tables 1).

Naphthalene and Tetralin. With V sulfide, both naphthalene and tetralin produced a partially saturated hydroaromatic, tetralin, as the primary product, as the same product with Mo sulfide. V sulfide, especially from VOAcAc, produced more decalin from both reactants, hence achieving higher % HYDs, than did Mo sulfide.

The V sulfide also produced various hydrogenolyzed products.

Indan and Indene. V sulfides showed low activity for saturating the aromatic ring of indan as did Mo sulfide. Indene was completely converted to indan with V catalysts, but only less than 12% of indan was converted further to fully saturated hexahydroindan, predominantly to *cis*-hexahydroindan. Compared to Mo sulfide, V catalysts were relatively more active for saturating the aromatic ring and for hydrogenolyzing the five-membered ring, showing a higher % HYD.

Benzothiophene. VAcAc and VOAcAc without sulfur was nearly inactive for hydrogenation of benzothiophene. But in the presence of excess sulfur, both V precursors almost completely hydrodesulfurized benzothiophene, producing ethylbenzene and ethylcyclohexane as the primary and secondary products, respectively. When compared to Mo sulfide, V sulfides were more active for producing ethylcyclohexane; the mole ratio of ethylcyclohexane to ethylbenzene produced was 6:90 with MoNaph, 23:72 with VAcAc and 23:66 with VOAcAc. Hence, V sulfides yielded higher % HYD than Mo sulfide.

***o*-Cresol.** In the absence of sulfur, VAcAc and VOAcAc did not catalyze the deoxygenation of *o*-cresol. But, in the presence of excess sulfur, *o*-cresol was completely deoxygenated with both precursors. When compared to Mo sulfide, V sulfides removed more oxygen and produced more alkylalicyclics, such as methylcyclohexane, ethylcyclopentane and their isomers, and less alkylaromatics such as toluene, hence yielding higher % HYD.

Benzofuran. With VAcAc and VOAcAc in the absence of sulfur, no oxygen was removed from benzofuran. But in the presence of excess sulfur, both VAcAc and VOAcAc completely converted benzofuran and achieved a high level of oxygen removal, producing ethylcyclohexane and ethylbenzene as the primary and the secondary products, respectively. V catalysts were more active for hydrogenolyzing the five-membered ring and removing oxygen from benzofuran than Mo sulfide.

Quinoline. VAcAc and VOAcAc in the presence of excess sulfur showed a relatively low activity for the hydrodenitrogenation of quinoline. With the *in situ* generated Mo sulfide, quinoline was completely converted, achieving 90% HDN. Propylcyclohexane and butylcyclopentane were the major products. By contrast, only 31% HDN and 36% HDN were achieved with VAcAc and VOAcAc, respectively, and 1,2,3,4-tetrahydroquinoline was the major product. The low activity for nitrogen removal and, thus, the low % HYD achieved suggested that the V sulfides, which were highly active for hydrogenation of aromatics and removal of S and O, might be severely poisoned by organic nitrogen compounds. In the absence of sulfur, V precursors were nearly inactive for quinoline denitrogenation.

Indole. With VAcAc and VOAcAc in the presence of excess sulfur, indole was completely converted, yielding *o*-ethylaniline as the primary product and ethylcyclohexane as the secondary product. V sulfides were less active for nitrogen removal compared to Mo sulfide. This low activity for indole denitrogenation again suggested that the activity of V catalysts might be severely inhibited by organic nitrogen compounds. Without sulfur, VOAcAc did not catalyze the nitrogen removal from indole.

Reaction Pathway of Heteroatom Removal. Because V sulfides did not actively catalyze the direct hydrogenation of ethylbenzene to ethylcyclohexane (only up to 3-4%) and toluene to methylcyclohexane (5-9%), the large amounts of ethylcyclohexane produced from the hydrogenation of benzothiophene (23% with VAcAc and VOAcAc), benzofuran (66% with VAcAc, 58% with VOAcAc) and indole (26% with VAcAc, 32% with VOAcAc) and methylcyclohexane from *o*-cresol hydrogenation (60% with VAcAc, 55% with VOAcAc) appeared to be produced from heteroatom-

containing intermediates: octahydrobenzothiophene and 2-ethylcyclohexanethiol for benzothiophene, octahydrobenzofuran and 2-ethylcyclohexanol for benzofuran, perhydroindoline and 2-ethylcyclohexylamine for indole, and methylcyclohexanol for o-cresol. Therefore, heteroatom removal with V sulfides was simultaneously achieved through two different pathways as with Mo sulfide. (6) For removal of the heteroatom from benzothiophene, benzofuran and indole, one pathway proceeded through the hydrogenation to dihydro-products, followed by heteroatom removal, producing ethylbenzene, and the other pathway proceeded through the aromatic ring saturation, thereby producing the heteroatom-containing saturated intermediates that later released heteroatoms, producing ethylcyclohexane. For o-cresol, one pathway proceeded through direct oxygen removal from o-cresol, producing toluene, and the other proceeded through aromatic ring saturation, producing methylcyclohexanol, and then followed by oxygen removal, producing methylcyclohexane. When compared to Mo sulfide, V sulfides catalyzed the heteroatom removal principally through the second pathway, which utilized the heteroatom-containing saturated intermediates to produce alkylalicyclics. Hence, the % HYD achieved with V sulfides was higher than that with Mo sulfide in all cases except for the systems containing nitrogen compounds.

Effect of Combined Reactants

The effect of additional hydrocarbon and heteroatomic species on the hydrogenation of other reactants was tested with VOAcAc in the presence of excess sulfur (Table 2). In this experiment, two compounds of naphthalene, indan, benzothiophene, o-cresol, benzofuran, quinoline, indole or pyridine were mixed.

Effect on Naphthalene Hydrogenation. The activity of V sulfide for naphthalene hydrogenation was not affected much by other hydrocarbons, sulfur-compounds or oxygen-compounds. The slightly reduced % HYD of naphthalene was because of possible competitive reactions occurring on the same active sites of the catalyst. When nitrogen-containing compounds were mixed, the activity of V sulfide was tremendously reduced, indicating that organic nitrogen compounds inhibited the activity of V sulfide for hydrogenation of aromatics.

Effect on Benzothiophene Hydrodesulfurization. Nitrogen-containing reactants and products severely inhibited the activity of VOAcAc for sulfur removal from benzothiophene, while hydrocarbons and oxygen-compounds reduced % HYD in a small amount by competitive reactions on the same catalyst.

Effect on the Hydrodeoxygenation of o-Cresol and Benzofuran. The extent of hydrodeoxygenation catalyzed by V sulfides was slightly reduced by additional sulfur-compounds, while not being greatly affected by other hydrocarbons and oxygen-compounds. When quinoline was added, the activity of the V sulfide catalyst for HDO was severely inhibited. Therefore, nitrogen compounds appeared to be the most detrimental to V sulfide catalysts not only for the hydrodenitrogenation of nitrogen-containing reactants but also for other hydrogenation and heteroatom removal reactions.

Effect of Sulfur Amount on the Activity of V Catalyst

The activity of V species was generated in the presence of sulfur. The effect of the amount of sulfur on the activity of *in situ* generated V species was examined using naphthalene hydrogenation (Table 3). Without sulfur, neither V precursors showed any activity for naphthalene conversion. When sulfur was added, catalytic activity of the V species was observed. Addition of more sulfur induced higher conversion of naphthalene to decalin, indicating that the activity of the *in situ* generated V catalyst strongly depended on the amount of sulfur present.

The effect of sulfur amount on the activity of V catalysts for hydrogenation of aromatics and heteroatom removal was also tested by introducing more sulfur in combined reactions (Table 4). Two different levels of sulfur, three times and

nine times the stoichiometric amount of sulfur required to form V_2S_3 (0.034 g and 0.102 g S, respectively), were added in each reaction set. In the hydrogenation of combined sets of naphthalene-indan, naphthalene-benzothiophene and naphthalene-indole, the higher sulfur amount achieved higher % HYDs of all reactants and also markedly increased the extent of nitrogen removal from indole. However, in the combined reaction of naphthalene and o-cresol, more sulfur increased naphthalene hydrogenation, but it decreased o-cresol deoxygenation and thereby decreased o-cresol hydrogenation. These results indicated that the addition of more sulfur could enhance the activity of V sulfide for aromatic hydrogenation, sulfur removal and nitrogen removal, but that excessive sulfur might reduce the activity of V sulfide for oxygen removal.

SUMMARY

The activity of V sulfide generated *in situ* from VAcAc and VOAcAc was strongly dependent upon the amount of sulfur present. The characteristics of V sulfides in the model hydrogenation and heteroatom removal reactions were somewhat similar to those observed with the *in situ* generated Mo sulfide. In the hydrogenation of aromatics and alkylaromatics, V sulfide was active for the partial saturation of an aromatic ring in multiring aromatics but far less active for the further saturation to alicyclics and for the saturation of single-ring alkylaromatics. The heteroatom removal with V sulfide simultaneously occurred through two pathways as did with Mo sulfide: one pathway for heteroatom removal prior to saturation of the aromatic ring, producing alkylaromatics and the other for heteroatom removal following the saturation of the aromatic ring, producing alkylalicyclics. When compared to Mo sulfide, the V sulfide was more active for the hydrogenation of aromatic rings adjacent to the heteroatom before the heteroatom was removed, producing more heteroatom-containing alkylalicyclics as the intermediates and thus more alkylalicyclics in the final product slates. Therefore, V sulfide achieved higher % HYDs in the hydrogenation of oxygen and sulfur-containing compounds than did Mo sulfide. V sulfide was more active for O removal but less active for N removal than Mo sulfide.

In combined reactions, the activity of V sulfide for hydrogenation and heteroatom removal was only slightly affected by other aromatics, hydroaromatics, organic sulfur compounds, and organic oxygen compounds, but it was severely inhibited by organic nitrogen compounds. A higher content of sulfur enhanced the activity of V sulfide for the hydrogenation of aromatics, hydroaromatics and sulfur- and nitrogen-containing compounds and for the removal of S and N. However, this excessive sulfur slightly inhibited the activity of V sulfide for O removal.

Because coprocessing feed materials contain several percents of indigenous sulfur, the V indigenous to residuum may be converted to V sulfide *in situ* and show a catalytic activity for the aromatic hydrogenation and heteroatom removal reactions involved in coprocessing. However, because the activity of V sulfide can be inhibited by organic nitrogen components indigenous to the feed materials, V sulfide can be far less catalytic in coprocessing than that shown in the model hydrogenation reactions.

REFERENCES

1. Speight, J.G. "The Desulfurization of Heavy Oil and Residua"; Marcel Dekker: New York, 1981; Chapters 1 and 2.
2. Herbstman, S. U.S. Patent 4,125,455, 1978.
3. Gleim, W.K.T.; Lake, I.; Gatsis, J.G.; Plaines, D, III. U.S. Patents (a) 3,165,463, 1965, (b) 3,161,585, 1965, and (c) 3,252,895, 1966.
4. Hutchings, L.R.E. U.S. Patent 4,139,453, 1979.
5. Gatsis, J.G. U.S. Patent 3,915,842, 1975.
6. Kim, H; Curtis, C.W. Energy Fuels 1990, 4, 206-14.

Table 1. Comparison of the Hydrogenation Activity of In Situ Generated V sulfide from VOAcAc and VOAcAc and Mo sulfide from MoNaph in Model Systems^a

Reactant	Hetero atom (A)	Major Products		% H ₂ O ^b		% H ₂ O ^c	
		V sulfide	Mo sulfide	V sulfide VAcAc	Mo sulfide VAcAc	V sulfide VAcAc	Mo sulfide MoNaph
Naphthalene	-	tetralin	tetralin	42.9±0.8	50.8±3.0	42.6±0.4	-
Tetralin	-	tetralin	tetralin	15.3±0.3	26.9±0.8	4.7±0.3	-
Indene	-	indan	indan	17.2±1.3	18.0±0.6	16.0±0.3	-
Indan	-	indan	indan	3.6	6.8±0.2	3.4±0.3	-
Benzothioephene	S	ethylbenzene	ethylbenzene	47.6±1.4	50.3±0.6	40.7±0.7	99.6±0.8
o-Cresol	O	methylcyclohexane	toluene	74.2±0.4	71.6±0.2	36.2±0.2	100.0±0.0
Benzofuran	O	ethylcyclohexane	ethylbenzene	67.4±0.6	69.1±0.2	46.3±0.7	92.4±0.8
quinoline	N	1,2,3,4-THQ ^d	propylcyclohexane	51.9±1.8	54.9±0.1	90.6±1.5	31.0±2.4
Indole	N	o-ethylaniiline	ethylcyclohexane	38.8±0.3	43.8±0.0	70.4±2.2	33.8±0.7

^a The reactions were conducted at 360°C for 30 minutes with 3000 ppm metal loading in the presence of excess sulfur, three times the stoichiometric sulfur to form V₂S₅ and MoS₂ (0.094 g for V, 0.024 g for Mo). Most reactions were at least duplicated, and the amount of hydrogenation and heteroatom removal was summarized as the average value and standard deviation of $\bar{x} \pm \sigma$.

^b The most hydrogenated liquid products used in calculating % H₂O were: decalin for naphthalene and tetralin, and cyclohexane for indan, indene, benzothioephene, benzofuran and o-cresol.

^c % H₂O: Percent heteroatom removal of S, N and O.

^d 1,2,3,4-tetrahydroquinoline.

Table 2. Effect of Multiple Compounds on the V Sulfide-Catalyzed Hydrogenation of Naphthalene, Benzothiophene, o-Cresol and Benzofuran^a

(A) Naphthalene

Additional Compound ^b	Naphthalene % HYD
None	50.8±3.0
Indan	43.5±1.2
Benzothiophene	50.1
Benzofuran	49.0±2.5
o-Cresol	48.8±3.9
Quinoline	5.7±0.6
Indole	9.1±0.1
Pyridine	14.4±1.6

(B) Benzothiophene

Additional Compound ^b	Benzothiophene	
	% HYD	% HDS
None	50.3±0.6	100.0±0.0
Naphthalene	48.2	100.0
o-Cresol	46.7±0.5	100.0±0.0
Quinoline	19.8±0.5	32.3±1.4

(C) o-Cresol and Benzofuran

Additional Compound ^b	Reactant			
	o-Cresol		Benzofuran	
	% HYD	% HDO	% HYD	% HDO
None	71.6±0.2	100.0±0.0	69.1±0.2	98.6±0.1
Naphthalene	69.3±2.3	97.1±2.9	67.4±1.9	95.5±3.5
Benzothiophene	66.0±0.7	92.5±1.2	-	-
Benzofuran	72.7	100.0	-	-
o-Cresol	-	-	69.9	100.0
Quinoline	7.3±0.3	12.8±0.6	26.0±0.1	5.2±0.2

^a Most of the reactions were performed two or three times with VOAcAc and 0.034 g S and the % HYD, % HDS and % HDO were expressed as an average value and a standard deviation in the form of $X \pm \sigma_n$. In calculating % HYD, the most hydrogenated liquid products determined were decalin for naphthalene and cyclohexane for benzothiophene, o-cresol and benzofuran.

^b Each reactant except for naphthalene (2 wt%) was added at 1 wt% level in the hexadecane solution.

Table 3. Effect of Sulfur Amount on the Activity of *In Situ* Generated Vanadium Catalysts in Hydrogenation of Naphthalene

Product, mole %	Sulfur Amount ^a					
	0	1	2	3	5	10
VAcAc % HYD ^b	0.9	5.3±1.5	35.7±1.4	42.9±0.8	50.2±0.8	61.3
t-D/c-D Ratio ^c	-	-	-	1.09±0.08	1.14±0.03	1.37
VOAcAc % HYD ^b	0.7	21.2	40.4	50.8±3.0	57.3±1.1	NP ^d
t-D/c-D Ratio ^c	-	-	-	1.10±0.02	1.13±0.01	

- ^a Multiples of the stoichiometric amount of sulfur required to form V₂S₃.
^b % HYD calculated using decalin as the most hydrogenated liquid product.
^c Approximate ratio of trans- to cis-decalin.
^d NP: not performed.

Table 4. Effect of Sulfur Amount on the V Sulfide-Catalyzed Hydrogenation of Model Compounds^a

Sulfur Amount ^b	Reactants ^c		
	Naphthalene % HYD	Indan % HYD	
Naphthalene/Indan			
	3	43.5±1.2	3.0±0.5
9	55.8±0.3	10.0±0.2	
Naphthalene/Benzothiophene			
	3	50.1	48.2
9	54.8±0.5	53.9±0.1	100.0
			100.0±0.0
Naphthalene/o-Cresol			
	3	48.8±3.9	69.3±2.3
9	52.4±3.2	63.7±2.5	97.1±2.9
			89.7±2.9
Naphthalene/Indole			
	3	9.1±0.1	41.9±0.1
9	15.7±0.3	55.3±0.6	37.1±0.3
			58.0±3.6

- ^a Combined reactions of 2 wt% naphthalene and 1 wt% of other compounds were performed with VOAcAc.
^b The sulfur amount was expressed as multiple times the sulfur required to form V₂S₃.
^c In calculating % HYD, the most hydrogenated liquid products used were decalin for naphthalene and cyclohexane for the other reactants.

RETROGRESSIVE REACTIONS IN COAL/PETROLEUM CO-PROCESSING

Jasna Tomic and Harold H. Schobert
Fuel Science Program,
Department of Materials Science and Engineering,
The Pennsylvania State University,
University Park, PA 16802

Key words: co-processing, model compounds, retrogressive reactions

INTRODUCTION

Co-processing is the simultaneous reaction of coal and petroleum resids to produce distillable liquids. It can be viewed as a new approach to direct liquefaction where the petroleum resid takes the role of the traditional liquefaction solvent [1]. The co-processing system is somewhat more complex from a chemical standpoint because of the predominantly aromatic character of the coal and mainly aliphatic nature of the petroleum products. The variety of hydrocarbons present in such a system determine the chemical reactions. One of the major undesirable reaction products is coke (or semi-coke) which causes problems in the co-processing technology. The formation of coke diverts carbon into unwanted by-products, reducing yields of the more desired products, and can upset heat and mass transfer processes in the reactor.

The intention of this study is to examine the chemical interactions and process conditions that contribute to retrogressive reactions during co-processing. We studied only thermal reactions (that is, reactions without added catalyst) since the aim is to focus on the retrogressive reaction chemistry that takes place between the different organic components of the system, and not to optimize the system for maximum liquids yields. The main objectives of this project are: 1) to determine the groups of chemical components originating from the coal and the petroleum that are responsible for initiating coke formation; 2) to identify the optimum reaction conditions that decrease the amount of insoluble coke; and 3) to rank pairs of coal/petroleum feedstock that minimize the amount of coke formed during co-processing reactions.

EXPERIMENTAL

Five coal samples from the Penn State Coal Sample Bank were used in this project, ranging in rank from subbituminous B through high volatile A bituminous. Data on the elemental composition on these coals is given in Table 1. The selected coal samples were first reacted with five model compounds representative of petroleum resids: eicosane, 1-phenyldodecane, 1,4-diisopropylbenzene, durene, and pyrene. The model compounds were obtained from Aldrich and were used as received. These model compounds were chosen on basis of their aromaticity and H/C ratios, to provide a set of compounds having a reasonably wide range of both properties. Real co-processing reactions were conducted with three vacuum feed resids. Analyses of the petroleum feedstock are presented in Table 2. Two of the petroleum feedstock were obtained from Amoco Co. (West Texas FHC-470 and Blend FHC-571) and one from Unocal (Hondo).

All of the reactions were conducted in a 20ml stainless steel vertical tubing bomb (microautoclave) reactor. Each reaction was conducted with 2.5g of coal and 5g of model compound or resid. The coal was dried to a 1% moisture under vacuum and was stored under a nitrogen blanket. The starting pressure (cold) was 3.5MPa (500 psi) of nitrogen or hydrogen. The reaction temperatures were 350° C, 400° C, 450° C and the time was fixed at 30 min.

The contents of the reactor were rinsed with tetrahydrofuran (THF) and the products were separated to THF-solubles and THF-insolubles. The Soxhlet thimble containing the insoluble matter was then extracted under a nitrogen atmosphere for 24 h. Excess THF was removed by rotary evaporation and the solid residue was dried under vacuum for 12 h before weighting. The degree of

retrogressive reactions occurring was defined by the yield of tetrahydrofuran insolubles which was calculated on a percent basis dividing the weight of the THF-insolubles by the weight of the coal (daf).

In order to assess the influence and contribution of the model compounds to the formation of solid residue during these reactions, blank runs of the model compounds (in the absence of coal) were performed. Similarly coal was reacted alone under the same reaction conditions in order to obtain the information on the products resulting directly from the coal itself and baseline data for thermal stability of the resids was obtained.

Solid state ^{13}C NMR and Fourier transform (DRIFT) spectroscopy was performed on the unreacted coal. These spectra were used as a baseline to be later compared with the spectra obtained on the THF-insoluble residue in order to examine the structural changes occurring during the reactions. Some of the solid products were analyzed by elemental analysis in order to determine the H/C ratios which in a very crude way can give indications about the aromaticity.

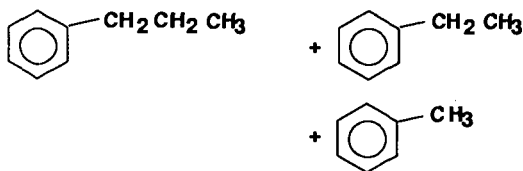
RESULTS AND DISCUSSION

Some results from the reactions of the five coals with the five model compounds under nitrogen and hydrogen are presented in Table 3. The most obvious observation is that the yield of THF-insolubles is the lowest in the reactions with pyrene. Also the values obtained for reactions with coal/eicosane and coal/1-phenyldodecane are very close to each other, as well as are the ones for coal in reaction with 1,4-diisopropylbenzene and durene. This was also verified when the H/C atomic ratios of the solid residue were plotted as a function of reaction temperature. Figure 1 shows that coal reacts with eicosane and 1-phenyldodecane in a similar fashion and that coal also reacts similarly in the presence of 1,4-diisopropylbenzene and durene. Pyrene reacts in a way notably different than the other four model compounds.

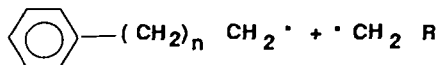
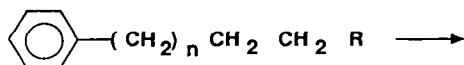
Eicosane and 1-phenyldodecane have in common the long paraffin chain. Thermal cracking of eicosane will lead to the production of 1° radicals by C-C bond cleavage, as for example:



A similar reaction path for alkylated benzene compounds (1-phenyldodecane) is supported by a collateral study in our laboratory [2] where it was shown that n-butylbenzene decomposes to:

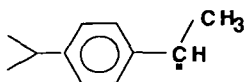


In other words, the alkylated benzene compound tends to crack at every possible position along the chain. This process also gives rise to primary radicals via:



Therefore, 1-phenyldodecane will form similar radicals to eicosane because most probably the cracking of bonds will take place along the dodecyl chain.

On the other hand, cracking of durene and 1,4-diisopropylbenzene will lead to benzyl radicals like the one shown below:



Pyrene, being a polyaromatic hydrocarbon, is very stable and does not easily form radicals by thermal cracking. In the literature pyrene has been described as a good "hydrogen shuttler" [3]. While transferring the hydrogen the pyrene most likely transforms to a hydroaromatic structure. Therefore, the similar chemistry of eicosane and 1-phenyldodecane arise from the fact that both crack to 1° radicals, and the similar behavior of durene and 1,4-diisopropylbenzene arises from the formation of the benzylic radicals from the two compounds. Pyrene would do neither. The expected thermal behavior of the 1° radical-forming compounds, benzylic radical-forming compounds, and pyrene is reflected both in the relative yields of THF-insolubles from a given coal and the variation of H/C ratio (Figure 1) as a function of temperature.

The reactions were performed under a nitrogen and hydrogen atmosphere. Under the given conditions of these experiments, namely 3.5MPa overpressure, the differences in degree of coal conversion calculated on basis of THF-insoluble are not significant. Comparisons of coal conversions under a nitrogen and hydrogen atmosphere at a given temperature are shown in Figure 3. Although it might be expected that the conversions would increase in the presence of hydrogen gas under the given reaction conditions the effect of the chemical nature of the coal and model compound (or petroleum resid) override the effects of the gas atmosphere. Furthermore, it should be recalled that these reactions are conducted without a hydrogenation catalyst being present.

Three temperatures of reaction were used in these experiments; 350°, 400°, and 450° C. Overall, the lowest yield of insoluble matter was recorded at 400° C. The lowest temperature is probably not enough for significant radical generation by fragmentation to take place while at 450° extensive cracking of the model compounds (and resids) takes place. In cases of severe cracking reactions it was not possible to maintain a good material balance. The effect of the reaction temperature is dependent on the rank of coal. For the two lower rank coals used, subbituminous B (PSOC 1488) and hvC bituminous (PSOC 1498) the coal conversion increases with increasing temperature of reaction. The three remaining project coals (hvB and hvA bituminous) achieve their highest conversion to THF-solubles at 400° C. Alternatively, it can be said that retrogressive reactions are at a minimum at 400° C. These optimum temperatures seem to coincide with the maximum fluidity temperatures of the coals. The three higher rank coals have temperatures of maximum fluidity above 400° C while the two lower rank coals do not pass through a fluid phase (with FSI's of 0 and 0.5). The temperature dependence of the coal conversion for the five project coals is shown on Figure 2.

Thermal stability tests on the petroleum resids (that is in the absence of coal) showed that considerable insoluble matter was formed only at the highest reaction temperature of 450° C. For West Texas FHC-470 the maximum insoluble is 17% of the total weight, for Blend FHC-571 the maximum is 3.73%, and for Hondo resid 5.77%.

The resids were reacted with the five project coals under the identical conditions as the model compound reactions. The yield of THF-insolubles was the lowest at 400° C. This agrees with the results reported by Moschopedis et al. [4]. When the temperature is increased to 450° C a drastic increase in solid residue is observed. This is attributed to extensive cracking taking place at higher reaction temperatures, with the high population of radicals thus increasing opportunities for retrogressive reactions. This observation is consistent with the results from the reactions with some of the model compounds, namely the ones containing the long side chains. When the coal conversion for the reactions with the model compounds and with the petroleum resids are compared (Figure 4), it is found that conversion in the presence of the resids is comparable to that achieved in the presence of pyrene. For reaction temperatures less than 450° C, the petroleum resids are as good a solvent for coal particles as pyrene. At higher reaction temperatures the interactions between the coal particles and petroleum resids seem to favour retrogressive reactions and the formation of insoluble matter.

CONCLUSIONS

The coal/model compound reactions showed that the reactivity of the vehicle is based on radical generation: eicosane-like, durene-like, and pyrene-like. The yield of THF-insolubles, therefore the degree of retrogressive reactions, is the lowest in the presence of pyrene. Coal/resid co-processing reactions at 400°C give coal conversions comparable to those in the presence of pyrene. The optimum temperature for minimizing retrogressive reactions in co-processing reactions is around 400° C. In addition, the maximum fluidity temperature of the coal defines the optimum temperature for coal conversion under co-processing reaction conditions.

ACKNOWLEDGMENT

The authors are pleased to acknowledge the financial support for this research provided by the U.S. Department of Energy. We are also grateful for the assistance of Dr. O.P. Mahajan of Amoco Corporation and Dr. G.E. Dolbear of Unocal in obtaining the resid samples. We have also enjoyed useful discussions with; Drs. Bruce Utz and Karl Schroder of the Pittsburgh Energy Technology Center (DOE).

REFERENCES

- [1] Curtis, C.W., and R.A. Winschel. in "Coal Liquefaction: A Research Needs Assessment Technical Background" DOE/ER-0400 UC-108, Final Report, Vol II, February 1989.
- [2] Eser, S., C. Song, H.H. Schobert and, P.G. Hatcher. "Compositional Factors Affecting the Thermal Degradation of Jet Fuels", U.S.D.O.E. Report, No. 42-3462-TPR-Annual, 1990.
- [3] Derbyshire, F.J. and, D.D. Whitehurst, *Fuel*, 60, p.655, 1981.
- [4] Moschopedis, S.E., R.W. Hawkins, and J.G. Speight, *Fuel Processing Technology*, p.213, 1982.

Table 1. Analyses of Project Coals.

Coal (rank)	PSOC-1488 subB	PSOC-1498 hvCb	PSOC-1501 hvBb	PSOC-1504 hvAb	PSOC-1448 hvAb
%C (dmmf)	76.56	78.24	81.17	82.88	85.20
%H	5.27	5.50	5.32	5.86	6.12
%N	0.95	1.83	1.56	1.77	1.86
%O	17.22	14.43	11.95	9.49	6.81
FSI	0.0	0.5	2.0	5.5	8.0
max fluid.T, °C	n/a	n/a	421	433	438

Table 2. Analyses of Petroleum Feedstock.

	Hondo.	W. Texas FHC-470	Blend FHC-571
Oils (wt.%)	43.9	39.4	21.4
Resins	40.2	59.1	62.8
Asphaltenes	15.9	0.5	14.8
%C	83.40	86.39	83.91
%H	11.80	11.23	10.26

Table 3. Yields of THF-insolubles for PSOC 1488 with model compounds at three different temperatures under hydrogen.

	Yield THF-insoluble, %		
	PSOC 1488 (350° C, H ₂)	PSOC 1488 (400° C, H ₂)	PSOC 1488 (450° C, H ₂)
Eicosane	94.41	84.06	80.12
1-Phen	94.13	82.32	79.42
1,4-Diiso	95.90	81.77	81.68
Durene	96.07	85.01	84.30
Pyrene	83.25	73.47	74.24

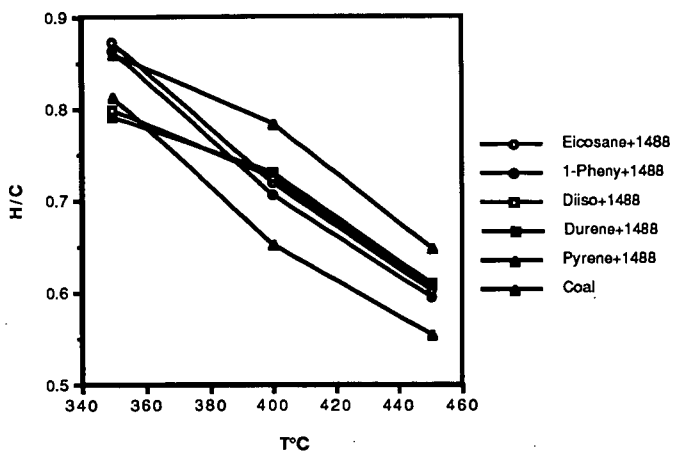


Figure 1: H/C atomic ratios of the THF-insolubles as a function of reaction temperature for different feed combinations for PSOC 1488

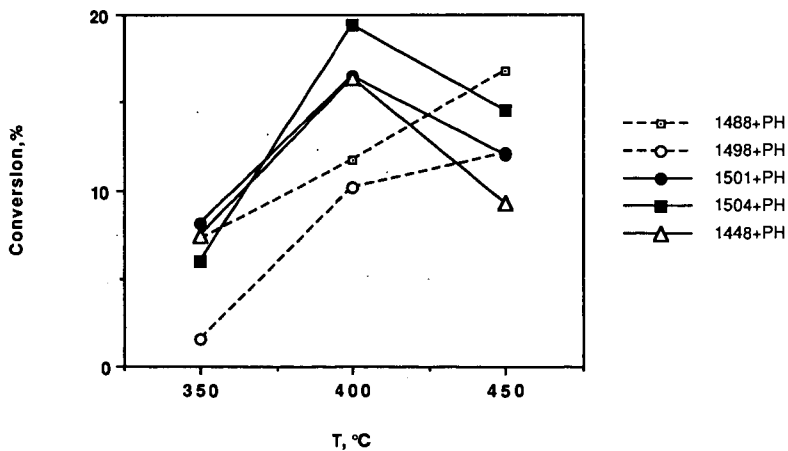


Figure 2: Temperature dependence of coal conversion for the five project coals.

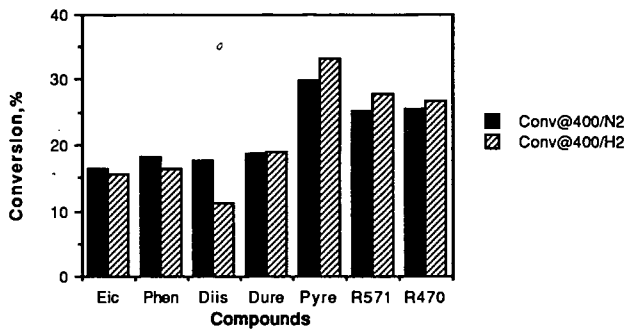


Figure 3: Conversion for PSOC 1501 at 400° C under N₂ and H₂.

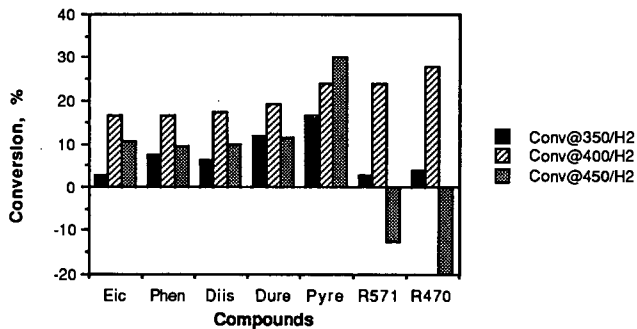


Figure 4: Conversion for PSOC 1448 at three reaction temperatures under H₂.

RETROGRESSIVE ARYL-ALKYL BOND FORMING REACTIONS
FACILITATED BY REACTIONS OF SULFUR-CENTERED FREE RADICALS

Mikhail S. Alnajjar and James A. Franz

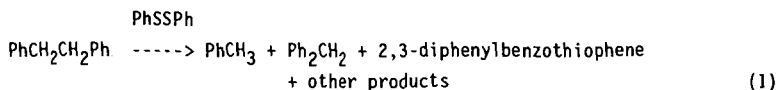
Pacific Northwest Laboratory
Battelle Memorial Institute
P. O. Box 999, Richland, WA 99352

Keywords: Sulfur, C-C Bond Cleavage, Rearrangements

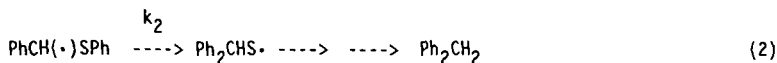
INTRODUCTION

It is well known that additives such as elemental sulfur, pyritic minerals and thiols play a significant role in structural reorganization during the thermal degradation of coals.¹⁻⁴ Studies have shown that the rates for hydrogen atom transfer reactions between benzylic positions of model compounds and coals are increased significantly with higher sulfur content.^{5,6} Displacement reactions of aromatic substituents by thiyl radicals and abstraction reactions by sulfur-centered radicals have long been recognized,⁷⁻¹⁰ and are thought to be important in coal liquefaction. However, the mechanistic aspects of C-C and C-S bond formation and the rearrangement of organic structure in coal facilitated by thiyl radicals is less well understood.

Recently, we have demonstrated the importance of thiyl radicals in the enhancement of the cleavage of strong C-C bonds and in the formation of inert thiophene structures (eq. 1).^{11,12} Products from the pyrolysis of bibenzyl in the presence of PhSSPh are shown in eq. 1. Diphenylmethane is formed in



a sequence of reactions involving the key step of phenyl migration from sulfur to the carbon-centered radical (eq. 2)¹³. Thus, at coal

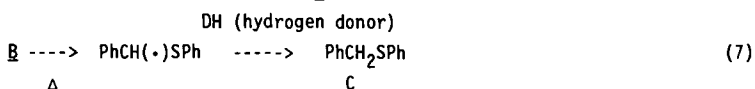
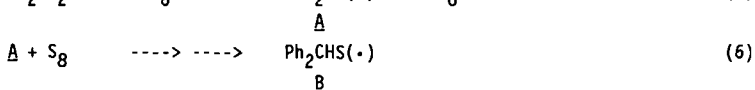
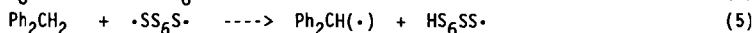


liquefaction temperatures (450°C), reaction (2) proceeds very rapidly and the rate constant of the phenyl migration (k_2) approaches $1.5 \times 10^4 \text{ s}^{-1}$.¹³

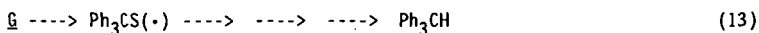
In this paper, we present preliminary results of high-temperature reactions of elemental sulfur with diphenylmethane and triphenylmethane. These results demonstrate the complete reversibility of reaction (2) and provide direct evidence of thiyl radical participation in the cleavage of strong carbon-carbon bonds through a series of abstraction and migration reactions.

RESULTS AND DISCUSSION

Pyrolysis of diphenylmethane in the presence of excess elemental sulfur at $380 \pm 3 \text{ }^\circ\text{C}$ gave toluene, thiophenol and triphenylmethane as the major products along with lesser amounts of PhCH_2SPh , PhSPh , PhSSPh and higher molecular weight products (Table I). The near unity ratio of toluene to thiophenol demonstrates the elementary free radical reactions in eqs. 3-10.



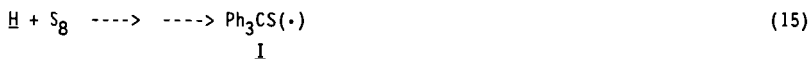
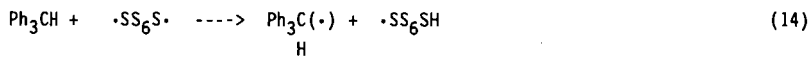
Triphenylmethane is formed via the termination reaction of diphenylmethyl and thiophenoxy radicals followed by hydrogen atom abstraction and phenyl migration reactions (eqs. 11-13). The formation of



The minor products show the origin of termination, displacement, abstraction, and oxidation reactions.¹²

As noted in Table I (compare entries 4 and 2), triphenylmethane was more abundant at low sulfur concentration. Rapid phenyl migration in eq. 13 and the low concentration of thiol donors provide an explanation for the observed result.

Table II gives the product distributions of the pyrolysis reaction of triphenylmethane with elemental sulfur at $380^\circ\text{C} \pm 3$. The formation of thiophenol and diphenylmethane is a consequence of phenyl migration from carbon to a sulfur-centered radical, eqs. 14-19. The production



of toluene and diphenyldisulfide is the result of further reactions of diphenylmethane with sulfur and the termination of thiophenoxy radical respectively. A similar interpretation explains the high yield of Ph_2CH_2 in the presence of low concentration of sulfur (Table II, entry 4). Rapid phenyl

migration, eq. 16, followed by abstraction and further reduction produced the desired product.

SUMMARY

These observations show that the cleavage of strong alkyl-aromatic carbon-carbon bonds can become completely reversible under the influence of thiyl radicals, via a rapid sequence of 1,2-phenyl migration, or neophyl-like rearrangements of thiyl radicals.^{12,13}

EXPERIMENTAL

General. Diphenylmethane, triphenylmethane, and sulfur were purchased from the Aldrich Chemical Co. and used as received. Products were identified by gas chromatography by coinjection with authentic samples. Gas chromatography was carried out using a Hewlett-Packard Model 5890A equipped with an on-column injector and flame-ionization detection. Analyses were performed on a 25-m, 0.32 mm i.d. J&W Scientific DB-5 capillary column.

General procedure for Thermolysis Reactions. To a 0.01-0.05g of diphenylmethane or triphenylmethane was added an appropriate amount of sulfur. The mixture was mixed, freeze-thaw degassed in liquid nitrogen, and sealed under high vacuum. The tubes were introduced to a fluidized sand bath at $380^{\circ}\text{C} \pm 3$ for intervals of 5 and 20 minutes, cooled immediately in tap water, open under nitrogen, and transferred to a degassed solution of CH_2Cl_2 containing naphthalene as an internal G.C. standard.

ACKNOWLEDGEMENT

This work was supported by the Office of Basic Energy Sciences, U. S. Department of Energy, under contract DE-AC06-76RLO 1830. Pacific Northwest Laboratory is operated for the U. S. Department of Energy by Battelle Memorial Institute.

REFERENCES

- 1) A. Attar, Fuel 1978, 57, 201.
- 2) R. F. Yarzab, P. H. Given, W. Spackman, and A. Davis, Fuel 1980, 59, 81.
- 3) H. H. King and L. M. Stock, Fuel 1980, 59, 447.

- 4) P. A. Montano, Y. C. Lee, A. YeYe-Odu, and C. H. Chien, "Iron Sulfide Catalysis in Coal Liquefaction" in Mineral Matter in Coal, Ed. K. Vorres, American Chemical Society Symposium, Series 301 (1986), 416.
- 5) C. B. Huang, and L. M. Stock, Prepr., Div. Fuel. Chem., Am. Chem. Soc. 1982, 27(3-4) 28.
- 6) J. A. Franz, and D. M. Camaioni, Fuel 1984, 63, 990.
- 7) C. Walling, "Free Radicals in Solution", Wiley-Interscience, New York, NY, 1957.
- 8) M. L. Poutsma, "Free Radicals", (Ed. Kochi, J.), Wiley, New York, NY, Vol. II, 1973.
- 9) H. B. Glass and D. E. Reid J. Am. Chem. Soc., 1929, 51, 3428.
- 10) S. Oae and S. Kawamura, Bull. Chem. Soc. Jap. 1963, 36, 163.
- 11) M. S. Alnajjar, and J. A. Franz, Am. Chem. Soc., Prepr., Div. Fuel. Chem., Am. Chem. Soc. 1986, 31, 287.
- 12) M. S. Alnajjar and J. A. Franz, Proceedings International Conference Coal Chemistry. Eds. J. A. Moulin, K. A. Nater, and H. A. J. Chermin, Elsevier Science Publisher, Amsterdam, The Netherlands, 1987, 273.
- 13) M. S. Alnajjar, J. A. Franz, Proceedings International Conference on Coal Science, Tokyo, 1990, Vol. I, p. 181.

Table I

Effect of Sulfur on Product Distributions from Diphenylmethane
Thermolysis at 380 ± 3 °C.^{a,b,c}

$[\text{Ph}_2\text{CH}_2]/[\text{S}]^{\text{d}}$	Time (min)	PhCH_3^{e} ($\times 10^{-3}$)	PhSH^{e} ($\times 10^{-3}$)	$\text{Ph}_3\text{CH}^{\text{e}}$ ($\times 10^{-4}$)
0.55	5	0.86	0.68	1.32
0.55	20	1.42	1.40	1.80
0.22	20	0.82	1.10	0.80
10.0 ^f	20	1.60	1.75	8.9

a) In the control experiment, the absence of sulfur, Ph_2CH_2 produced trace amounts of PhCH_3 , $\text{PhCH}_2\text{CH}_2\text{Ph}$, Ph_3CH and tetraphenylethane under the reaction conditions. b) % Conversion of $\text{Ph}_2\text{CH}_2 = 10\text{-}20\%$. c) PhCH_2SPh , PhSSPh , PhSPh and higher molecular weight materials were also produced in small amounts. d) Ratio of diphenylmethane to sulfur. e) In mmoles. f) $\text{PhCH}_2\text{CH}_2\text{Ph}$ and Stilbene were also produced.

Table II

Effect of Sulfur on Product Distributions from Triphenylmethane
Thermolysis at 380 ± 3 °C.^{a,b,c}

$[\text{Ph}_3\text{CH}]/[\text{S}]^{\text{d}}$	Time (min)	PhCH_3^{e} ($\times 10^{-4}$)	PhSH^{e} ($\times 10^{-3}$)	$\text{Ph}_2\text{CH}_2^{\text{e}}$ ($\times 10^{-3}$)	PhSSPh^{e} ($\times 10^{-3}$)
0.55	5	0.30	1.0	3.63	0.45
0.55	20	9.7	3.38	6.55	1.2
0.22	20	7.15	2.20	4.03	0.20
10.0	20	3.0	3.20	17.7	1.75

a) In a control experiment in the absence of sulfur, Ph_3CH produced no detectable products. b) % conversion of $\text{Ph}_3\text{CH} = 10\text{-}20\%$. c) Higher molecular weight materials were also produced. d) Ratio of triphenylmethane to sulfur. e) In mmoles.

**REACTION PATHWAYS DURING COPROCESSING.
THE REACTION OF ILLINOIS NO. 6 COAL WITH
LLOYDMINSTER RESID UNDER MILD CONDITIONS**

Kadim Ceylan and Leon M. Stock*
Department of Chemistry
The University of Chicago
Chicago, Illinois 60637

Keywords: Coprocessing, Hydrogen Transfer

INTRODUCTION

Over the past few years a number of processes have been developed for the direct liquefaction of coal. Typically, these processes involve thermal degradation of the macromolecular structure of coal, and are followed by hydrogenation to stabilize the degraded material and to increase the hydrogen-to-carbon ratio of the distillable products. In conventional coal liquefaction, a hydrogenated coal derived solvent is used as a vehicle for the transfer of hydrogen to the coal components. Coprocessing of coal with petroleum resid is an alternative technology in which the petroleum resid replaces the donor solvent. Coprocessing of petroleum resid with coal is a bridge between coal liquefaction and hydrocracking that simultaneously upgrades coal and resid. Consequently, coprocessing may offer some special advantages.

It has been observed that a better understanding of the chemistry of coprocessing might yield improvements in the technology (1). Therefore, coprocessing has received recent attention and new effort has been directed to elucidate the reaction pathways (2-6). The coprocessing of Illinois No. 6 and Wyodak coals with Lloydminster and Hondo resid has been thoroughly investigated (7,8), and other studies have discussed the hydrogen atom exchange, hydrogen atom transfer, and carbon-carbon bond cleavage reactions that may occur during coprocessing (9-14).

It seemed appropriate to establish more securely the relationship between the basic work and the reaction pathways that are involved in coprocessing. Accordingly, we have studied the coprocessing reactions of Illinois No. 6 coal with Lloydminster resid under the same reaction conditions that were used to investigate the influence of these fossil materials on hydrogen atom transfer and carbon-carbon cleavage reactions.

EXPERIMENTAL

Materials and equipment. The coals, resids, and the reference catalyst were supplied by John G. Gatsis of the Allied Research Center.

Illinois No. 6 coal was prepared by the Kentucky Center for Energy Research (KCER) and used as received (Anal. %C, 68.60; %H, 4.51; %N, 1.39; %S, 3.04; %O, 9.65; %H₂O, 3.15; %Ash, 9.65). Wyodak Coal was obtained from the Pennsylvania State University program and was prepared by KCER, and was dried prior to use (Anal. %C, 63.01; %H, 4.50; %N, 0.90; %S, 1.08; %O, 16.73; %H₂O, 1.78; %Ash, 12.00). Lloydminster Resid (Anal. %C, 83.6; %H, 11.5; %S, 4.77) and Hondo Resid (Anal. %C, 82.3; %H, 10.3; %S, 6.08; %N, 1.24) were obtained by UOP Research Center and used as is. The catalyst was a UOP proprietary material. The other chemicals were available commercially and they were purified as necessary.

The reactions were carried out in a SBL-2 fluidized sand bath equipped with Techne TC-8D temperature control unit. Three types of reactors were used. The glass capillary reactors were 2.4 mm (i.d.) × 20 cm, the glass tubular reactors were 5 mm (i.d.) × 20 cm, and the stainless steel (SS) reactors had an internal volume of 4.5 ml.

Nuclear magnetic resonance spectroscopy for ^1H was performed with the University of Chicago 500 MHz system and ^2H analysis was performed with a Varian XL-400 system. Infrared spectra were recorded with a Nicolet 20 SX spectrometer.

Procedures. The procedures for coprocessing were closely parallel to the procedures that were used in the previous study (11). The total quantity of material in the reactors were approximately 75 mg for the glass capillary, 500 mg for the glass tubular reactors, and 1.2 g for the stainless steel reactors. A mixture of the fossil fuel material, in which the resid and coal were combined in a 2:1 ratio (maf basis), was placed into the reactor, and it was carefully sealed under an atmospheric pressure of argon or pressurized with argon or dideuterium. The starting cold argon or dideuterium gas pressure in the stainless steel reactors was approximately 500 psig. The reaction vessels were then immersed into the sand bath which had been preheated at 400 °C. The reactor was vigorously shaken during the reaction. At an appropriate time, the reactor was removed from the sand bath and cooled immediately by immersing it in water. The glass reactors were cut and the stainless steel reactors were carefully vented to the atmosphere and then opened. The reactor contents were extracted into tetrahydrofuran, filtered, and the residue was Soxhlet extracted with tetrahydrofuran. The soluble product was fractionated into asphaltenes (n-heptane insoluble), resins (n-heptane soluble, n-pentane insoluble), and oils (n-pentane soluble) by successive extractions with n-heptane and n-pentane, according to the procedure suggested by Speight and co-workers (15).

RESULTS AND DISCUSSION

Illinois No. 6 coal was coprocessed with Lloydminster resid. The earlier coprocessing work with these materials was carried out at 420 °C in 2 hrs with a high pressure of dihydrogen, 3000 psi (7,8). Under these conditions, Gatsis and his co-workers achieved very high conversions of the coals into tetrahydrofuran soluble products. We elected to examine the same fossil materials under much milder conditions so that the conversion of the coal would be less complete, and the influences of selected reaction parameters on the product yield and distribution could be investigated. Accordingly, the reaction temperature was decreased to 400 °C, and the reaction time was decreased to 1 hr. Dideuterium was used in some experiments, but at 500 psi. The results are summarized in Table I.

Coal conversion was the principal parameter that we used to evaluate the results. The conversion values were calculated on the basis of the transformation of the insoluble coal into tetrahydrofuran soluble materials. As expected, the conversions that are presented in Table I are considerably less than the conversions that were reported by Gatsis and co-workers (7,8).

The reaction time is an important variable. An increase in the reaction time for the coprocessing of Illinois No. 6 coal and Lloydminster resid from 60 to 90 min in an inert atmosphere increased the conversion from 44 to 54%. Similarly, an increase in the reaction time for the coprocessing of the same substances from 15 to 60 min in a dideuterium atmosphere increased the conversion from 28 to 52%. These findings are in accord with the results and conclusions of Gatsis and his co-workers who also pointed out that the incremental increase diminished after the first 60 min (7,8). The observations for Illinois No. 6 coal and Lloydminster resid indicate that the use of dideuterium increases the conversion from 44 to 52%, the use of a catalyst increases the conversion from 44 to 50% and the incorporation of both a catalyst and dideuterium increases the conversion to 53%. The oil yields are not impacted in the same way. The addition of the catalyst in the absence of dideuterium actually reduces the oil yield from 27 to 22%. Indeed, the highest oil yield was observed when the reaction was carried out with dideuterium but in the absence of the catalyst.

Additional experiments were carried out with Wyodak coal and Hondo resid. It was found that coprocessing of these fossil fuels without the catalyst at 400 °C for 1 hr produced the following reactivity patterns.

For Coal Conversion and Oil Yield

Wyodak
Lloydminster > Wyodak
Hondo > Illinois No. 6
Lloydminster > Illinois No. 6
Hondo

The order of reactivity for coprocessing without a catalyst is exactly inverse to the order of reactivity of the same pairs of fossil materials in the exchange of hydrogen atoms with tetralin-d₁₂ under the same experimental conditions (11).

For Exchange of Hydrogen with Tetralin-d₁₂ at 400 °C

Wyodak < Wyodak < Illinois No. 6 < Illinois No. 6
Lloydminster < Hondo < Lloydminster < Hondo

The order of reactivity in the molybdenum-promoted coprocessing reaction is also essentially inverse to the reactivity pattern for exchange with tetralin-d₁₂.

Previous work with 1,3-diphenylpropane suggested that Illinois No. 6 coal was the most effective initiator as well as the most effective hydrogen atom donor among the four fossil materials and that Lloydminster resid was the least effective initiator as well as the least effective hydrogen atom donor. Although it is difficult to provide a comprehensive interpretation of the observations for the complex coprocessing system, it is relevant to consider the chemistry of the thermolytic reactions of the coals and resids. Success in coprocessing depends upon facile initiation reactions and the occurrence of uninterrupted chain propagation sequences that redistribute hydrogen atoms, fragment the large coal and resid molecules, and enhance the solubility through adduction. Parallel heteroatom removal reactions are also essential.

Free radical decomposition reactions of the coal macromolecule must proceed in order to initiate the free radical propagation reactions that are necessary to convert it and the resid into lower molecular weight fragments and eventually into n-pentane soluble products. The resids that we have examined are much less effective initiators than the coals. They are also less effective hydrogen atom donors than the coals. Indeed, the observations for the coprocessing of the resid with Illinois No. 6 coal, which is simultaneously the best initiator and best hydrogen donor, suggest that its donor properties interfere with its successful coprocessing because hydrogen donation terminates the essential chain reactions and simultaneously increases the aromatic character of the coal macromolecules. The observations also suggest that blends of coals and resids may offer opportunities for enhanced conversion.

Dihydrogen addition clearly plays a major role in the liquefaction of coals (15,16). Evidence concerning the utilization of dihydrogen in coprocessing is more limited, but Curtis and Cassel have reported that the addition of hydrogen atom donors to the reaction system decreases the dihydrogen gas consumption (5). Their observations also imply that the hydrogen donor capacity of the collection of the fossil materials in the liquid phase can interfere with the desirable addition of dihydrogen to the initially highly aromatic coal molecules. We examined selected spectroscopic properties of the reaction products to gain further perspective on the course of the reaction. Representative nuclear magnetic resonance spectra are shown in Figure 1. Dideuterium was used to probe the role of dihydrogen in the reaction. Although the influence of the gas on the conversion and oil yields was modest, the spectroscopic information clearly establish that deuterium atoms were incorporated into the products. Weak absorptions near 2100 cm⁻¹ were observed in the infrared spectra of most products. Our preliminary results suggest that more deuterium is incorporated in the oil than in the other fractions, and the representative ²H NMR spectra indicate that the deuterium is abundantly incorporated into aliphatic structural elements with resonances between 1 and 2 ppm. Lesser amounts of deuterium appear in benzylic and aromatic positions. We estimate that 0.1 to 0.2 mmol of dideuterium is incorporated per gram of the reactants in these reactions at 400 °C and 500 psi dideuterium. These results prompted further study of the distribution of dideuterium among the reactions products. The work is discussed in the next paper.

CONCLUSION

The experimental results strongly suggest that hydrogen transfer processes occur very rapidly among all the constituents, and that dideuterium is added to the reaction products in the presence and absence of the molybdenum catalyst. The reactivity pattern for the four fossil materials suggest that the

hydrogen atom transfer reactions have a significant influence on the course of the reaction. In particular, the hydrogen donor properties of Illinois No. 6 coal appear to interfere with its conversion.

Acknowledgement. We are indebted to the Office of Fossil Energy of the U. S. Department of Energy for their support of this investigation and to John Gatsis for his very able assistance in the preparation and characterization of the fossil fuels.

REFERENCES

1. Cugini, A. V.; Lett, R. G.; Wender, I. *Energy Fuels* 1989, 3, 120.
2. Curtis, C. W.; Chung, W. J. *Energy Fuels* 1989, 3, 148.
3. Fouda, S. A.; Kelly, J. F.; Rahimi, P. M. *Energy Fuels* 1989, 3, 154.
4. Ohuchi, T.; Steer, J.; Muehlenbachs, K.; Carson, D. *Fuel Process Techn* 1988, 15, 429.
5. Curtis, C. W.; Cassel, F. N. *Energy Fuels* 1988, 2, 1.
6. Miller, R. L.; Giacomelli, G. F.; McHugh, K. J.; Baldwin, R. M. *Energy Fuels* 1989, 3, 127.
7. Gatsis, J. G.; Nelson, B. J.; Lea, C. L.; Nafsis, D. A.; Humbach, M. J.; Davis, S. P. "Continuous Bench-Scale Single Stage Catalyzed Coprocessing", Contractor's Review Meeting, Pittsburgh, October 6-8, 1987.
8. Nafsis, D. A.; Humach, M. J.; Gatsis, J. G. "Coal Liquefaction, Co-Processing", Final Report, DOE/PC/70002-TE, 1988.
9. McMillan, D. F.; Malhotra, R.; Hum, G. P.; Chang, S. J. *energy Fuels* 1987, 1, 193.
10. Bockrath, B. C.; Schroeder, K. T.; Smith, M. R. *Energy Fuels* 1989, 3, 268.
11. Ceylan, K.; Stock, L. M. *Fuel* 1990, 69, 1386.
12. Stock, L. M. "Hydrogen Transfer Reactions" in "The Chemistry of Coal Conversion", Schlosberg, R., Ed., Plenum Publishing Co., 1985, Chapter 6.
13. King, H. H.; Stock, L. M. *Fuel* 1984, 63, 810.
14. King, H. H.; Stock, L. M. *Fuel* 1982, 61, 257.
15. Speight, J. S.; Long, R. B.; Trowbridge, T. D. *Fuel* 1984, 63, 616.
16. Hayatsu, R. Unpublished research.

Table I. Coprocessing Reactions of Fossil Fuels^a

Entry	Coal and Resid	Reactor	Gas	Cat, % ^b	conv wt%	soluble product composition		
						asph	resin	oil
1	Illinois No. 6 + Lloydminster	tubular	Ar	-	44.2	28.7	9.7	61.6
2	Illinois No. 6 + Lloydminster	tubular	Ar	-	53.9	21.7	11.2	67.1 ^c
3	Illinois No. 6 + Lloydminster	SS	D ₂	-	27.8	27.6	12.1	60.1 ^d
4	Illinois No. 6 + Lloydminster	SS	D ₂	-	51.5	33.5	3.3	63.2
5	Illinois No. 6 + Lloydminster	SS	Ar	1%	50.0	50.0	7.0	43.1
6	Illinois No. 6 + Lloydminster	SS	D ₂	1%	53.0	33.1	7.1	59.1
7	Illinois No. 6 + Lloydminster	capillary	Ar	-	40.8	22.0	-	78.0 ^c

^aThe reactions were carried out at 400 °C for 1 hr. The coal conversion is based upon the quantity of insoluble residue. ^bThe wt% catalyst concentration was calculated from 100 (molybdenum/coal (maf)). ^cThis reaction was carried out for 90 min. ^dThis reaction was carried out for 15 min. ^eThe yield of n-heptane soluble material is reported.

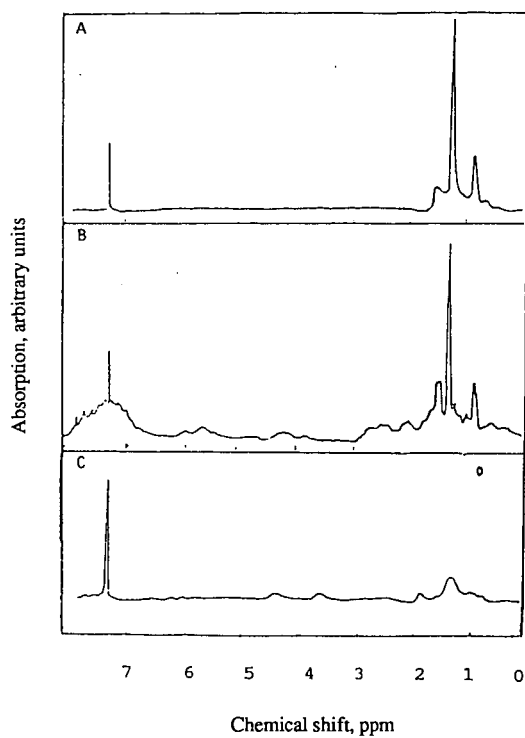


Figure 1. A. The ^1H NMR spectrum of the oil fraction of Lloydminster resid.
 B. The ^1H NMR spectrum of the oil produced in experiment 4.
 C. The ^2H NMR spectrum of the asphatene produced in experiment 4.

DETERMINATION OF DIDEUTERIUM UPTAKE IN COAL PETROLEUM RESID COPROCESSING

Michael D. Ettinger and Leon M. Stock
Department of Chemistry, University of Chicago, Chicago, Illinois 60637

John G. Gatsis, UOP Research Center, Des Plaines, Illinois 60017

Keywords: Coprocessing, NMR, Liquefaction

INTRODUCTION

Coal petroleum resid coprocessing is a novel application of direct coal liquefaction which has potential for practical applications. Several lines of argument suggest that a better understanding of the chemistry of the coprocessing reaction would lead to improvements in coprocessing technology. In order to gain insight into this problem, batch autoclave studies were carried out by using Illinois No. 6 coal with Lloydminster resid under a dideuterium atmosphere to study the deuterium incorporation in the products. Quantitative deuterium nuclear magnetic resonance methods were used to analyze the liquid products, and gas chromatography-mass spectrometry was used to analyze the gas products.

EXPERIMENTAL

Materials. The materials used were the same as those described in the accompanying article.

Coprocessing Reaction Procedure. Weighed amounts of Lloydminster resid and Illinois No. 6 in a two-to-one ratio (resid/MAF coal) and the catalyst (.02% wt) were added to an 1800 cc rocking autoclave. The autoclave was sealed and pressurized first with hydrogen sulfide and then with dihydrogen or dideuterium to give a 10 vol% hydrogen sulfide and 90 vol% dideuterium blend at 1470 psi. The autoclave was heated to 420 °C for a residence time of 2 hrs. At the reaction conditions, dideuterium was added automatically so that the desired reaction pressure (3000 psi at temperature) was maintained. After the desired time-at-temperature, the autoclave was cooled to room temperature, and then depressurized with the gas passing through a foam trap, caustic scrubbers, metering system, and then a sample was collected for analysis. To remove additional gas from the remaining reaction mixture, the material in the autoclave was stripped with dinitrogen.

This gas was also passed through the foam trap, caustic scrubber, metering system, and analyzed. Any slurry product in the foam trap was recovered with toluene and added to the toluene rinse solution. The slurry product from the autoclave was poured off. The material remaining in the autoclave was removed by rinsing the vessel with toluene until the autoclave was clean. The combined slurry product was solvent separated into four fractions according to the flow chart shown in Figure 1.

Deuterium spectra were obtained on a Varian XL 400 MHz spectrometer. One hundred to 200 scans were acquired using a 90° pulse and a 30-sec delay between pulses. Triphenylmethane-d₁ was used as a quantitative internal standard. Proton spectra were obtained similarly on the University of Chicago 500 MHz spectrometer by using tetrakis(trimethylsilyl)silane as a quantitative internal standard.

RESULTS

The autoclave reaction using a combination of Illinois No. 6 coal with Lloydminster resid mixed with a molybdenum based UOP proprietary catalyst was carried out at 420 °C for two hours under a dideuterium atmosphere at a constant pressure of 3000 psi. The results of the solvent separation of

the products are summarized in Table I. The oil, resin, asphaltene, and insoluble yields are based upon the starting amount of MAF coal and resid. As can be seen from Table I, approximately 23% of the starting material is unaccounted for. This portion represents the gas yield and the loss of a small amount of light material in the work-up procedure. The asphaltene conversion is calculated as the amount of asphaltene and unconverted coal (insolubles) in the autoclave product divided by the amount of starting MAF coal and asphaltene fraction of the starting resid. An asphaltene yield of 74% was obtained with Illinois No. 6 coal and Lloydminster resid. Coal conversion is calculated as the amount of starting MAF coal minus unconverted MAF coal (insolubles) divided by the starting amount of MAF coal. A coal conversion of 93% is obtained with Lloydminster resid and Illinois No. 6 coal. The elemental analysis of the oil, resin, asphaltene, and insoluble fractions are shown in Table II along with the fractional analyses of the starting resid. In all of the product fractions, the sulfur content significantly decreased even though hydrogen sulfide gas was present.

The deuterium incorporation into the different molecular fragments defines the paths of hydrogen transfer. In this first analysis of the results, the assignments are made according to the following chemical shift ranges. Deuterium resonances in the range of 6.3-10 ppm are assigned to aromatic deuterium atoms, while those found in the range of 4.2-0 ppm are assigned to aliphatic types. A further breakdown of the resonances in the ranges 4.2-2.0 ppm, 2.0-1.0 ppm, and 1.0-0 ppm was made by assigning resonances in those ranges to deuterium atoms alpha to aromatic rings, deuterium atoms beta to aromatic rings and in methylene and methine positions not alpha to aromatic rings, and deuterium atoms in methyl groups gamma or further from aromatic rings, respectively. Proton NMR characterization was also carried out to complement the results for deuterium. The proton NMR experiments use tetrakis(trimethylsilyl)silane as an internal standard. The NMR data from the coprocessing reaction products of Illinois No. 6 coal with Lloydminster resid are shown in Tables III and IV. In addition to the actual amount of deuterium incorporated into the products, Table III also shows the hydrogen content in each of the products. Thus, the percent deuteration of the aromatic and aliphatic regions was determined.

A relatively large amount of deuterium, 24.1 mmol g⁻¹, was incorporated into the aliphatic component of the oil. While the absolute amounts of deuterium uptake at the different structural positions vary from 2.9 mmol g⁻¹ to 24.1 mmol g⁻¹, the relative percentages of deuteration are high and not quite so varied indicating that significant exchange had taken place at all positions. These percentages are close to the initial deuterium to total hydrogen ratio of (H/H+D) = 0.25 at the start of the reaction. Some selectivity of the catalyst was observed between the solvent separated fractions with the extent of deuteration decreasing in the order asphaltene > resin > oil. In addition, aliphatic positions were slightly preferred in the asphaltene and resin fractions while the smallest amount and smallest percentage of deuterium incorporation occurred at the aromatic sites in the oil fraction.

CONCLUSIONS

Analysis of the deuterium NMR results clearly shows that the level of deuterium atom incorporation was significant at all positions. All components of the system are undergoing hydrogen transfer chemistry, and there are plentiful opportunities for fragmentation and addition reactions. The deuterium contents of the reaction products, (D/H+D), are only moderately different than the values expected for complete equilibration. The modest differences that do exist are compatible with the view that the weaker carbon-hydrogen bonds such as the alpha aliphatic group undergo reaction selectively even in the presence of the effective catalyst. The high deuterium incorporation at the other sites such as the methyl and methylene groups in paraffinic components, when coupled with the fact that the catalyst is essential for high conversions, suggests that the modest selectivity that is observed arises more from the differences in the way in which the organic molecules bind to the catalyst than to inherent differences in their thermal chemistry.

Acknowledgement. We are indebted to the Office of Fossil Energy of the U. S. Department of Energy for their support of this investigation.

Table I. Solvent Separation of Coprocessed Lloydminster Resid and Illinois No. 6 Coal with Dideuterium

Sample	Wt % MAF
Oil	62.32
Resin	3.91
Asphaltene	8.50
Insoluble	2.40
Coal Conversion	92.78
Asphaltene Conversion	74.08

Table II. Analysis of Original Resid Components and Solvent Separated Product

	Starting Material	Products
<u>Oil fraction</u>		
Wt.% MAF	73.50	62.32
Carbon, wt.%	82.86	84.88
Hydrogen, wt.%	10.82	13.67
Sulfur, wt.%	4.30	1.24
<u>Resin fraction</u>		
Wt.% MAF	10.41	3.91
Carbon, wt.%	82.68	86.16
Hydrogen, wt.%	8.76	8.66
Sulfur, wt %	7.44	1.73
<u>Asphaltene fraction</u>		
Wt.% MAF	16.09	8.50
Carbon, wt.%	82.82	87.70
Hydrogen, wt.%	8.51	7.09
Sulfur, wt.%	7.85	1.68
<u>Insoluble fractions</u>		
Wt.% MAF	-	2.40
Carbon, wt.%	-	24.03
Hydrogen, wt.%	-	1.71
Sulfur, wt.%	-	6.51

Table III. Hydrogen and Deuterium Content of Solvent Separated Coprocessing Products

	Hydrogen (mmol g ⁻¹)		Deuterium (mmol g ⁻¹)		% Deuteration	
	Aromatic (6.3-10 ppm)	Aliphatic (4.2-5 ppm)	Aromatic (6.3-10 ppm)	Aliphatic (4.2-0 ppm)	Aromatic (6.3-10 ppm)	Aliphatic (4.2-0 ppm)
Oil	14.5	86.8	2.9	24.1	16.7	21.7
Resin	16.7	45.6	5.3	14.6	24.1	24.3
Asphaltene	14.5	31.7	5.0	11.9	25.6	27.3

Table IV. Aliphatic Deuterium Content in Solvent Separated Coprocessing Products

Solvent separated fraction	Alpha-D 2.0-4.2 ppm (mmol g ⁻¹)	Beta-D 1.0-2.0 ppm (mmol g ⁻¹)	Gamma-D 0.0-1.0 ppm (mmol g ⁻¹)	% Alpha deuteration
Oil	6.2	15.6	2.3	31.6
Resin	7.5	6.0	1.1	29.1
Asphaltene	5.9	4.8	1.2	29.4

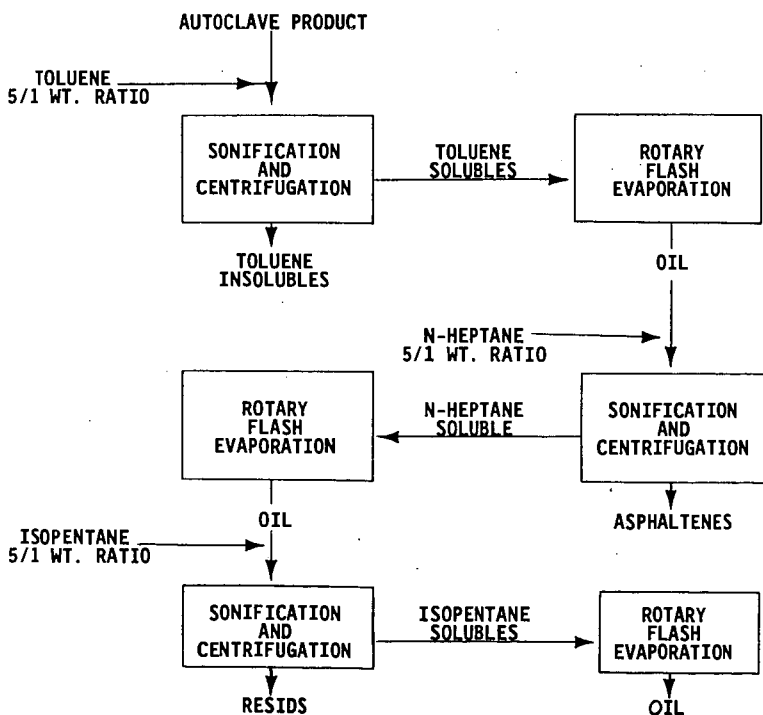


Figure 1. Solvent Separation of Coprocessing Product